ABSTRACT

MENG, JIAJIA. Converting Biomass into Renewable Fuel Intermediate – Bio-oil: Elucidating Torrefaction Effect on Bio-oil Quality and Study on Bio-oil Aging Mechanism. (Under the direction of Dr. Sunkyu Park and Dr. David C. Tilotta).

Converting biomass into liquid transportation fuel is of great importance for a secure energy supply. Though biomass pyrolysis offers a convenient avenue to produce a liquid fuel intermediate - bio-oil, a significant amount of effort is still demanded to overcome the poor oil properties towards its application as drop-in transportation fuel. These challenges include reducing bio-oil oxygen content, water content, acidity and improving its stability during storage and upgrading. The current research investigated the torrefaction effect on improving bio-oil physicochemical property and stability. In this study, fluidized-bed fast-pyrolysis was performed on torrefied loblolly pine with different torrefaction severities. The results showed that torrefaction pretreatment can significantly reduce the oxygen and water content and acidity of the bio-oil as well as varying bio-oil chemical composition with concentrated pyrolytic lignin and levoglucosan. A modified cellulose pyrolysis mechanism was proposed to explain the increased levoglucosan concentration in the torrefaction-based bio-oil. With regarding to the bio-oil stability, torrefaction based bio-oil showed less physicochemical and compositional variation than that of raw bio-oil. In addition, torrefaction based bio-oil could maintain a uniform oil phase for twelve-month storage. All these effects are attributed to the structural and compositional change of torrefied wood induced by the thermal pretreatment.

The unstable nature of the pyrolysis oil is one of the key issues that limits its upgrading and further application, as aged bio-oil typically shows increased water content, viscosity, and phase separation. The aging phenomena are explained by the polymerization of bio-oil components under acidic and thermal conditions catalyzed by the mineral compounds

contained in char particles in the bio-oil. Current research on bio-oil aging is focused on characterizing the aging behavior together with seeking methods to slow down the aging speed. However, only limited amount of research was reported on investigating the molecular-level polymerization mechanism of pyrolysis oil during the aging. Based on the results obtained from this study, the aging mechanism was proposed to be acid-catalyzed and free-radical condensation reactions which have temperature/time and acidity dependent. After aging, the bio-oil water content, viscosity and acidity increased; the aged bio-oil water insoluble fraction increased while the water soluble fraction reduced accordingly. Each bio-oil fraction reacted in similar manner as the water soluble fraction and pyrolytic sugar fraction of bio-oil generated high molecular weight solids after aging, and lignin fraction condensed significantly with the addition of acid catalyst. The reaction severity can be enhanced with high temperature heating in a low pH environment. Few types of aldehyde presented in the bio-oil could promote the condensation degree of pyrolytic lignin with selected acid catalyst. These results suggest a bio-oil aging reaction fashion involving individual bio-oil fraction aging and inter-reaction between different bio-oil fractions. For its first time, the electron paramagnetic resonance (EPR) study revealed the presence of free radicals in the bio-oil; further characterization of each fraction of the bio-oil showed that these radicals are all located in the pyrolytic lignin fraction. The EPR characterization of aged bio-oil together with using radical scavengers in accelerated aging showed that there is a weak correlation between the radical presence and bio-oil aging degree tentatively indicating the relative stable nature of bio-oil containing radicals. However, further research is needed to elucidating the radical reactivity when bio-oil is subjected to a high temperature upgrading conditions.

Converting Biomass into Renewable Fuel Intermediate – Bio-oil: Elucidating Torrefaction Effect on Bio-oil Quality and Study on Bio-oil Aging Mechanism

by
Jiajia Meng

A dissertation submitted to the Graduate Faculty of
North Carolina State University
in partial fulfillment of the
requirements for the degree of
Doctor of Philosophy

Forest Biomaterials

Raleigh, North Carolina

2013

APPROVED BY:

_____	_____
Dr. Sunkyu Park Co-Chair	Dr. David Tilotta Co-Chair
_____	_____
Dr. Stephen Kelley	Dr. Fanxing Li
_____	
Dr. Elon Ison	

BIOGRAPHY

Jiajia Meng was born on July 30th, 1983 in Wuxi, Jiangsu, China. He graduated from Nanjing Forestry University in June of 2006 with a Bachelor's degree in chemical engineering. In his junior year, he joined an international internship program launched by StoraEnso in Finland and worked as a research intern at Oulu Mill for 60 days. After graduation, he continued his graduate study at the same university and attained a Master's degree in Pulp and Paper Science in June 2009.

Followed by his research interest, Jiajia Meng applied the graduate school at North Carolina State University and successfully started his Ph.D. studies in August 2009 in the Department of Forest Biomaterials under the guidance of Dr. Sunkyu Park and Dr. David C. Tilotta as a Hoffman and NSF Fellow. His research at NC State focused on converting lignocellulosic materials into renewable transportation fuel using thermochemical conversion pathway.

ACKNOWLEDGMENTS

I would like to express my gratitude to Dr. Sunkyu Park and Dr. David C. Tilotta, co-chairmen of my advisory committee, for their encouraging guidance, exceptional advice in my research, and moral support through this dissertation process. I would also like to thank my committee members, Dr. Stephen Kelley, Dr. Fanxing Li and Dr. Elon Ison for their advice and assistance in my research.

Sincere thanks also go to Dr. Houming Chang, Dr. Richard Phillips, Dr. Hasan Jameel, Dr. Lucian Lucia, Dr. Ilona Peszlen, Dr. Tatyana Smirnova, Dr. Ewellyn Capanema, Dr. Hanna Gracz, Dr. Sudipta Dasmohapatra, Dr. Phillip Westmoreland, Dr. Xinlian Geng, Dr. Matthew Cooper, Dr. Douyong Min, Dr. Zhoujian Hu, Dr. Zhiying Yu, Dr. Junyeong Park, Michael Maltby, Barbara White, Melissa Rabil, Xueyong Ren, Andrew Moore, Brandon Jones and Peter Jin at NCSU and Dr. David Dayton, Dr. John Carpenter, Steve Mazzarelli, Matt von Holle, Joshua Herr, John Albritton at RTI International for their suggestions, discussions, and friendship.

More importantly, I give sincere thanks to my parents for supporting me throughout this process and for their patience in waiting for me to finish this chapter of my life.

TABLE OF CONTENTS

LIST OF TABLES

LIST OF FIGURES

CHAPTER 1

The Effect of Torrefaction on the Chemistry of Fast-Pyrolysis Bio-oil

1. Introduction

Thermochemical conversion of lignocellulosic biomass has received increasing attention as a strategy to produce biofuels from renewable resources. Fast pyrolysis, one of the promising thermochemical approaches, rapidly converts organic biomass into bio-oil, bio-char, and syngas in the absence of oxygen. With a residence time of less than two seconds, this simple and low-cost technology can transform various feedstocks such as agricultural and forest residues into value-added biofuels and chemicals. In addition, biofuels derived from renewable biomass contributes a positive effect on greenhouse gas emission as compared with petroleum-based transportation fuels [Reijnders, 2006]. Because of these advantages, fast pyrolysis is thought to have great potential as an avenue for replacing petroleum-based fuels and chemicals.

Although fast pyrolysis has been studied over the last few decades, several unfavorable properties of its liquid product hinder its application to the production of value-added fuels and chemicals [Czernik and Bridgwater, 2004]. First, owing to its high oxygen content (~40%) [Mohan et al., 2006], pyrolysis bio-oil has a relatively high chemical reactivity. For example, bio-oil components such as acids and aldehydes can engage in several types of reactions to form esters and other oligomers, resulting in higher molecular weights [Diebold, 2002]. Therefore, increased viscosity and phase separation often occur to the bio-oil during storage. Second, the bio-oil is also plagued by high acidity (pH~2) and

volatility, which also lead to numerous application challenges. In short, fresh bio-oil is not suitable for direct application without stabilization and reduction of oxygen concentration in it.

Several upgrading technologies have been proposed to reduce the oxygen content of bio-oil, usually involving catalytic hydrotreating and hydrocracking [Elliott and Hart, 2009; Sharma and Bakhshi, 1993]. Unfortunately, these approaches require high hydrogen consumption and their overall yield of high quality bio-oil is low [Elliott, 2007]. To reduce high hydrogen demand during catalytic upgrading, fast pyrolysis on biomass having low oxygen content is a promising alternative as it should produce bio-oil with low oxygen content.

A potential method of reducing the oxygen content of biomass feedstock is through torrefaction. A mild pyrolysis process, torrefaction occurs at 200–350 °C and is valued as an effective way to improve the thermochemical quality of biomass in its application with coal co-combustion [Prins et al., 2006a; Zwart et al., 2006; Couhert et al., 2009]. Most importantly, this mild thermal pretreatment reduces the oxygen content significantly by losing water, carbon dioxide, and carbon monoxide [Yan et al., 2009]. In addition, the removal of acidic components like acetic acid originating from acetoxy groups in the xylan side chain has been reported [Yan et al., 2010; Prins et al., 2006b; Bourgois and Guyonnet, 1988]. As another advantage, the specific grinding energy of torrefied pine chips can be reduced to 30 kW h/t compared to 260 kW h/t of untreated pine chips [Phanphanich and Mani, 2011]. It is also reported that torrefaction can reduce the size distribution of particles,

where evenly sized wood particles can be utilized for the process [Repellin et al., 2010]. All these advantages are potentially beneficial to the production and quality of pyrolysis bio-oil.

To the best of our knowledge, torrefaction as a pretreatment technology for fast pyrolysis to enhance bio-oil properties has not yet been reported. The work presented here puts forward an idea of integrated torrefaction and fast pyrolysis processes. It is expected that under suitable combinations of torrefaction and pyrolysis conditions, pyrolysis bio-oil with enhanced physical and chemical properties can be produced from thermally treated biomass. The objective of this study, therefore, was focused on comparing fast pyrolysis of torrefied wood with that of non-treated wood by examining the change of the bio-oil chemistry.

2. Materials and Methods

2.1 Torrefied biomass production

Loblolly pine chips (15 by 6 mm) containing bark were used as the raw material for torrefaction. A pilot-scale torrefaction system at North Carolina State University was operated to produce torrefied wood at three different severities, which were produced at 270, 300, and 330 °C for 2.5 min respectively and referred as TW-270T, TW-300T and TW-330T in this study. The wood without torrefaction was named raw wood and the torrefaction severity increases in the series from TW-270T to TW-330T. The severity of torrefaction is often indicated by the weight loss during the torrefaction process [Almeida et al., 2010] and the products used in this study have the weight loss of 16.5%, 24.1%, and 46.5% for TW-270T, TW-300T and TW-330T respectively, based on the original weight of non-torrefied dry wood.

2.2 Pyrolysis bio-oil production

A lab-scale reactor, presented in Fig. 1.1, was used for the fast pyrolysis operation. The reactor consists of a screw feeder, a fluidized-bed with a diameter of 43 mm, and a liquid collection system with two water-cooling condensers and one electrostatic precipitator.

Two round electric muffle furnaces were placed outside of the reactor to provide the heat source. Approximately 200 g of sand was deposited into the bottom of the pyrolysis reactor as the fluidizing and heat transfer medium. Two streams of nitrogen gas, one introduced from the bottom of the reactor and the other from the end of the feeding tube, were used as fluidizing gas. The nitrogen flow at the feeder facilitates the feeding procedure and prevents the blockage of biomass in the feeding channel. In addition, the reactor maintains an oxygen-free environment during the biomass pyrolysis.

Fast pyrolysis was performed at 500 °C with a nitrogen flow rate of 12 L/min and a biomass feeding rate of 150 g/h. The residence time was calculated to be 1.5 s. The produced pyrolysis aerosols were collected in the two condensers cooled with water at 5 °C, and the electrostatic precipitator (ESP) maintained at 12 kV. The pyrolysis bio-oils were collected at two locations, after the first condenser and after the electrostatic precipitator as shown in Fig. 1.1. These oils were named BOC (bio-oil after condenser) and BOP (bio-oil after precipitator), respectively. Also, the bio-oil originated from raw wood was labeled as LP-Raw (LP as liquid product) and the bio-oils made from torrefied wood were labeled as LP-270T, LP-300T and LP-330T respectively.

2.3 Characterization of torrefied wood and pyrolysis bio-oil

Compositional analysis. An air dried woody sample (40–60 mesh) was extracted with benzene-ethanol mixture (v/v = 2:1) according to Tappi Standard T204 cm-07 for 24 h. The extraction amount was calculated by the gravimetric method of the extraction liquid after vacuum drying. The amounts of structural carbohydrates and lignin of both torrefied wood and non-torrefied wood were measured by Klason lignin analysis [Dence, 1992] followed by HPLC sugar analysis [Sluiter et al., 2008].

Elemental and proximate analysis. Carbon, hydrogen, and nitrogen analyses of both the biomass and bio-oil were performed according to ASTM-D5291 using a Perkin Elmer CHN Elemental Analyzer (2400 Series II). A sample size of 7 mg was used for each test, and the analyses were performed in triplicate. The carbon, nitrogen, and hydrogen amounts were determined by this method and the oxygen contents were calculated by difference. The proximate analyses were performed with a muffle furnace according to ASTM-D1762-84.

Water content. The water content of the bio-oils was determined by Karl-Fischer titration according to ASTM E 203-08 using HYDRANAL Titrant 5E, HYDRANAL Solvent E and HYDRANAL Water Standard 10.0. The apparatus used was a Schott Automatic Volumetric Karl Fischer Titrator (WU-24907-00).

High heating value. The high heating value of both wood and bio-oil was measured according to DIN 51900 with 1108 oxygen combustion bomb (Parr Instrument Company). Prior to the analysis, the wood powder was pressed to make a tablet and 0.5 g of sample loading for both wood and bio-oil was applied for each analysis.

GC/MS analysis. Gas chromatographic/mass spectrometric (GC/MS) analyses of bio-oils were performed on a Finnigan Polaris Q Plus system. The MS detector was set at a full scan mode with a mass to charge range from 10 to 550 amu. Standard electron impact (EI) ionization at 70 eV was employed and the ion source temperature was 200 °C. The GC column used for separation was a DB-1701 column 60 m × 0.25 mm with 0.25 lm film thickness. The GC oven temperature was initially held at 45 °C for 4 min, then ramped at 3 °C/min to 280 °C, and held at 280 °C for 15 min. The injector and detector temperatures were set at 250 and 280 °C, respectively. The injector split ratio was fixed at 30:1. High purity helium was employed as the GC carrier gas at a flow rate of 38 cm/min, and the bio-oil sample was prepared as 6 wt.% solutions dissolved in acetone filtered through a 0.25 lm PTFE filter. 1 μL of bio-oil solutions were injected for each analysis and duplicate tests were performed for each analysis.

3. Results and Discussions

3.1 Torrefied wood characterization: compositional, proximate, and ultimate analyses

Loblolly pine derived torrefied wood is considered to have a similar composition as its original wood with respect to cellulose, hemicellulose, and lignin, but the amount of each component is expected to be different depending on the torrefaction conditions. To investigate the effect of torrefaction on the composition of loblolly pine, Klason lignin and sugar analysis were performed on the torrefied wood. However, Klason lignin and acid soluble lignin are named in Table 1.1 as acid insoluble residue and acid soluble residue, respectively, because the acid hydrolysis residues of torrefied wood may be chemically and

structurally different to conventional Klason lignin and it may also contain thermal degradation residues from carbohydrates. As shown in Table 1.1, a reduction of cellulose (represented by glucan) and hemicellulose (represented by xylan, galactan, arabinan and mannan) was noticed as the torrefaction intensity increased. The reduction rate of hemicelluloses is higher than that of cellulose. For the TW-300T sample, 51.3% of the hemicellulose loss (18.7–9.1%) is realized and the cellulose loss is identified as 11.4% (36.1–32.0%). While both the hemicelluloses and cellulose had an intense thermal degradation, it should be noted that lignin was relatively preserved. This result can be explained by the different thermal reactivity of the three major wood components.

According to thermogravimetric analysis of the isolated biomass components (data not shown here), hemicellulose (beech wood xylan from Sigma–Aldrich) is the most reactive compound and its major decomposition temperature resides around 275 °C. Followed by hemicellulose, cellulose (Avicel PH-101 from Sigma–Aldrich) mainly decomposes at 325 °C and lignin (alkali lignin from Sigma–Aldrich) has a very slow decomposition profile which peaks at 375 °C. The torrefaction temperature used in this study is in the range of 280–350 °C which exceeds the temperature where maximum hemicellulose decomposition occurs but also resides in the early decomposition range of cellulose.

The original extractives in the raw biomass are expected to be extensively removed during the torrefaction because of the intense thermal pretreatment. However, Table 1.1 shows an increasing amount of the extractable compounds for the torrefied wood. GC/ MS data of these extractives for torrefied wood (data not shown) indicates that they are different from the original extractives in raw wood but similar to the composition of bio-oils, i.e., their

major compositions are levoglucosan and lignin fragments. The generation of these distinct extractives originates from the torrefaction. Thermal decomposition of wood components destroys its matrix and increases the extractable fractions in the wood. Some of these heavy fractions (moderate molecular weights) with high boiling points resided in the wood and became extractable while others (compounds with lower boiling points) went to the vapor phase during torrefaction.

Table 1.2 shows the results of the proximate and ultimate analyses of the wood samples. These analyses are useful in gaining a better comprehension of how these feedstocks differ in terms of their fuel properties. It is worthwhile to state that, other than the conventional 'moisture content' expression in Table 1.2, the term 'highly volatile' content is applied because measuring the moisture content at 105 °C by using an oven drying method is not appropriate for torrefied wood. Simply, some of the extractives, as discussed above, will be released during the drying process. The weight loss of these condensates should not be significant; therefore the change of highly volatile content within the four samples can still be representable for the variance of moisture content among them. Fast pyrolysis usually requires the water content of the feedstock be typically less than 10% [Mohan et al., 2006]. As received however, biomass, being hydrophilic in nature, has a moisture content in the range of 50–60% (wet basis) [Demirbas, 2004] and requires extra energy and/or time to dry it prior to being fed into a pyrolysis reactor. Other than removing water from the biomass, it does not produce any valuable products and this amount of energy and time consumption could be costly in the industry production. Table 1.2 shows that the water content of the torrefied wood is under 10%, and this low moisture content can be maintained during storage

due to the change in hydrophobicity after the thermal pretreatment [Acharjee et al., 2011]. Therefore, the additional drying step for fast pyrolysis is not necessary when torrefaction is performed as a pretreatment. Indeed, torrefaction also consumes energy, however, it can result in high quality bio-oil and reduce the energy consumption in grinding process for fast pyrolysis; on the other hand, different from the simple drying process, torrefaction produces volatiles that can be collected as byproducts and the major composition of this condensates mainly contains acetic acid and small quantities of methanol, formic acid, lactic acid, furfural and hydroxyl acetone [Prins et al., 2006a,b]. Carbon dioxide and carbon monoxide with trance amount of hydrogen and methane was also detected from torrefaction gas products [Prins et al., 2006a,b]. The improved bio-oil quality, reduced energy consumption in the grinding process together with the potential value of collected torrefaction volatiles may compensate the energy consumption of torrefaction to some extent. In Table 1.2, the volatile matter content decreases from raw wood to TW-330T along with the increased fixed carbon content. This can be explained by the loss of volatiles during torrefaction treatment which make the torrefied wood more concentrated in thermally non-reactive carbon. These two indices show the theoretical yields of liquid and solid products from the fast pyrolysis operation. Considering the fact that highly torrefied biomass is less reactive, it is expected that TW-330T may give the lowest bio-oil yield under the identical pyrolysis conditions.

Similar to other work [Bourgois and Guyonnet, 1988], this study showed that torrefaction produces solid fuel with decreased oxygen and increased carbon contents. As shown in Table 1.2, the oxygen-to-carbon ratio is 0.64 for raw wood, followed by 0.53 for TW-270T, 0.48 for TW-300T, and 0.33 for TW-330T. Therefore, the quality of pyrolysis

feedstock has been improved by torrefaction pretreatment in terms of oxygen-to-carbon ratio. As a result, the high heating value increases with the reduced oxygen content in torrefied wood. In addition, the slightly reduced hydrogen content and increased nitrogen content were not significant after torrefaction pretreatment.

3.2 Fast pyrolysis operation and its mass balance

Bio-oil, bio-char and non-condensable gas (NCG) are the major products obtained from a fast pyrolysis process. In this study, the yield of bio-oil and bio-char was determined by weight and the gas yield was estimated by difference. All yield results shown in Table 1.3 were calculated based on the air-dry mass of biomass.

As shown in Table 1.3, as the torrefaction severity increases, the total bio-oil yield is reduced and the yield of bio-char is increased. Non-torrefied wood achieves the highest bio-oil yield; TW-270T and TW-300T attain similar capacity of bio-oil production. It is not surprising to see that the severely torrefied wood produces only 33.5% total bio-oil since some thermally-reactive components have been removed in the torrefaction process as confirmed by the lower amount of volatiles in the proximate analysis for TW-330T. To increase the bio-oil yield for TW-330T, different pyrolysis conditions such as a higher temperature with longer residence time might be necessary. The heating value of the bio-oil produced from torrefied wood is higher than that from raw wood materials. However, when comparing the heating value of bio-oil (dry base) to its pyrolysis feedstock, only TW-330T oil shows higher value than its starting material; while the heating value of the other two bio-oils are slightly lower than that of their torrefied raw materials. Clearly, BOC has a much

higher weight and water content than BOP as listed in Table 1.3. Also, bio-oils from torrefied wood generally have less water content than that from raw wood. Compared to that of TW-270T and TW-300T, the lower bio-oil yield from TW-330T can be explained by the loss of BOC since the amount of BOC for TW-330T is less than half of that collected from TW-270T and TW-300T. It is assumed that the condenser mainly collects the low molecular weight molecules, such as water and acids from the stream of the volatile gas. The electric-precipitator, however, is much more effective at collecting higher molecular weight molecules such as sugar and pyrolytic lignin. Those low molecular weight molecules in BOC may be the primary degradation products from the hemicelluloses and cellulose; therefore the low amount of BOC for TW-330T is reasonable.

Table 1.4 presents the results of the mass conversion for carbon and oxygen in fast pyrolysis of torrefied feedstocks based on elemental analysis. These results show how torrefaction affects the elemental distribution in pyrolysis products and discloses the reason as to why bio-oil, with a low oxygen-to-carbon ratio, can be produced via torrefaction. Of all of the carbon in raw wood, 57.9% went to bio-oil, 17.5% to bio-char and 24.6% to NCG. For torrefied wood, however, less carbon was converted into bio-oil components and most of it is retained in bio-char. The low carbon conversion to bio-oil for torrefied wood suggests that thermally treated wood is less reactive at the same pyrolysis conditions. The oxygen conversion in fast pyrolysis affects the oxygen content in bio-oil. As shown in Table 1.4, 74.2% of the oxygen went to bio-oil made from raw, while the pyrolysis of TW-270T and TW-300T gave 64.7 and 57.0% of oxygen resulted in the bio-oil respectively. In the case of fast pyrolysis of TW-330T, only 43.1% of oxygen in wood was transformed into bio-oil, but

a noticeably higher amount of oxygen went into bio-char and NCG compared to that for the mild torrefied sample. Both carbon and oxygen conversion from pyrolysis feedstock to bio-oil shows a decreasing trend from raw biomass to severely torrefied wood, and the reduction rate is higher for carbon conversion than that for oxygen conversion.

3.3 Bio-oil characterization: elemental and chemical analyses

Fig. 1.2 compares the oxygen-to-carbon ratio and the effective hydrogen-to-carbon ratio of bio-oils pyrolyzed from torrefied wood to those of non-torrefied wood. The definition of effective hydrogen-to-carbon ratio is expressed in Eq.1. Where, n_H, n_O and n_C are the mole numbers of hydrogen, oxygen and carbon respectively. This term eliminates the hydrogen contribution of water to the overall hydrogen to carbon ratio and it is a useful indicator in the field of bio-oil hydrotreating. [Vispute et al., 2010]

$$H/C_{eff} = (n_H - 2no) / nc \quad (1)$$

As shown in Fig. 1.2, there is clear evidence that the oxygen-to-carbon ratio decreases with effective hydrogen-to-carbon ratio as the raw wood materials go through more intense torrefaction. Similarly, the bio-oils such as BOC, BOP, and their combined mixture (MBO) inherit these features from their feedstocks. Additionally, the BOP not only preserves the reduced oxygen to carbon ratio from their starting wood materials, but also their absolute ratio is lower than that of the raw wood material. This is especially true for the BOP produced from the TW-Raw, TW-270T and TW-300T samples. The reason for this reduction of oxygen-to-carbon ratio in BOP might be due to the configuration of the bio-oil collection system. When volatile gases pass the cold condenser, most of the low molecular oxygenates

with high oxygen-to-carbon ratios will be retained in the BOC condenser; therefore fewer of them would flow into the ESP system. In addition, both BOC and BOP show improvement on the effective hydrogen-to-carbon effective ratio with an increasing torrefaction severity of the fast pyrolysis feedstock. This increase may suggest that lower hydrogen consumption during a hydrotreating process for bio-oil upgrading would be required.

Low molecular weight (<550 Da) compounds obtained from pyrolysis of wood are often easily identified by gas chromatography followed by mass spectroscopy (GC/MS) [Ralph and Hatfield, 1991]. Although GC/MS has a limitation in that only a portion of components in the bio-oil can be detected because of sample volatility requirements, this analysis is still accepted as a powerful technology for bio-oil characterization.

Due to the apparent differences between the two fractions of bio-oil as discussed above, the BOC and BOP samples were analyzed separately. Figs. 1.3 and 1.4 show total ion chromatograms for BOC and BOP produced from raw wood and TW-330T, respectively. More than one hundred components of the bio-oil were identified by searching the NIST 2008 MS library and were confirmed with standard chemical retention time and other references [Pouwels et al., 1989; Faix et al., 1991; Reeves and Galletti, 1993; Marsman et al., 2007; Mullen and Boateng, 2008; Nowakowski et al., 2010].

To visualize the changes of the functional group composition in bio-oil as a function of torrefaction severity, a summary of the relevant chromatographic peaks is presented in Fig. 1.5. In this figure, the chemicals have been classified into ten groups including esters, alcohols, aldehydes, ketones, acids, furanics, pyranics, anhydrosugars, phenolics and other unidentified oxygenates. For additional details, Tables 1.5 and 1.6 list the major compounds

and their area percentages obtained from the chromatograms for BOC and BOP, respectively. These chemicals are arranged in a decreasing order according to their peak area occupancy for each bio-oil species. It is worthwhile noting that about 95% of the total area of the chromatograms was identified. Generally, it was found that the difficulties in the identification were mainly due to overlapping peaks and low signal to noise ratios.

A distinct compositional variation can be noticed in BOC and BOP when comparing the bio-oils having the same feedstock origin. In BOC, esters, aldehydes, ketones, acids, furanics, pyranics, anhydrosugars and phenolics are the major components with relatively few alcohols. All of these chemicals are evenly weighted (10–20%). Conversely, furanics, anhydrosugars, pyranics, and especially phenolics (up to 50% for BOP from TW-330T) are abundant in BOP. When comparing the composition of torrefaction based bio-oil to that of the raw material, both BOC and BOP pyrolyzed from torrefied wood are generally rich in pyrolytic lignin and anhydrosugars but lack light oxygenates such as acids and aldehydes and the most consistent trend in Fig. 1.5 is the increasing amount of lignin oligomers and anhydrosugars from LP-Raw to LP-330T.

The varied composition of bio-oils from torrefied wood can be attributed to two aspects. On the one hand, torrefaction pretreatment alters the composition of torrefied wood, resulting in less holocellulose but more lignin residues. Therefore, after fast pyrolysis, a reduced amount of light oxygenates from cellulose and hemicellulose will be presented in bio-oil while pyrolytic lignin becomes more concentrated. On the other hand, the mild thermal pretreatment may modify the structure and chemistry of the wood components and change their reaction pathways in fast pyrolysis. These modifications may favor the

formation of certain bio-oil compounds. In addition, this may lead to the formation of certain chemical species that do not exist in bio-oil from non-treated biomass.

By comparing GC/MS data shown in Figs. 1.3 and 1.4, together with detailed GC/MS identification (partially shown in Tables 1.5 and 1.6), it is found that all of the major bio-oil compounds that have been identified in bio-oil from raw wood also exist in bio-oils pyrolyzed from torrefied wood. The only difference is the quantity of these species. Indeed, there are some minor components having unique peaks in the chromatograms of bio-oils pyrolyzed from torrefied wood which have not been identified. These peaks may be new bio-oil species resulting from the torrefaction pretreatment, but, the compounds are relatively insignificant due to their extremely low area occupancy in the chromatograms. Therefore, it may be concluded that torrefaction mainly change the bio-oil composition in terms of the quantities of same oil species rather than producing significant amount of novel bio-oil compounds.

However, it is worth noting that the detected species by GC/MS are only a portion of the bio-oil composition (GC-visible) and the newly created bio-oil compounds may exist in the GC-invisible portion. Therefore, the possibility of significant species difference within the composition of these bio-oils cannot be ruled out.

4. Conclusions

Pyrolysis bio-oils produced from torrefied loblolly pine feature reduced oxygen-to-carbon ratios and water content, which are beneficial for downstream processes such as hydrotreating and hydrocracking. However, these reductions are realized with the penalty of bio-oil yield due to the increased thermal resistance of torrefied biomass at the same pyrolysis conditions. Based on the GC/MS analysis, the chemical composition of bio-oils produced from torrefied biomass shows a high quantity of pyrolytic lignin compounds, which indicated that they have good potential for phenolic-based chemical production. In summary, torrefaction is considered as an effective pretreatment strategy for fast pyrolysis to produce high quality bio-oil.

5. Acknowledgements

The author would like to thank Chris Hopkins at North Carolina State University for torrefaction operation to produce torrefied wood and Steve Kelley for his valuable comments during the work. This work is supported by the National Science Foundation under Grant No. 0832498.

References

Acharjee, T.C., Coronella, C.J., Vasquez, V.R. 2011. Effect of thermal pretreatment on equilibrium moisture content of lignocellulosic biomass. Bioresource Technology, 102(7), 4849-4854.

Almeida, G., Brito, J.O., Perré, P. 2010. Alterations in energy properties of eucalyptus wood and bark subjected to torrefaction: The potential of mass loss as a synthetic indicator. Bioresource Technology, 101(24), 9778-9784.

Bourgois, J., Guyonnet, R. 1988. Characterization and analysis of torrefied wood. Wood Science and Technology, 22(2), 143-155.

Couhert, C., Salvador, S., Commandré, J.M. 2009. Impact of torrefaction on syngas production from wood. Fuel, 88(11), 2286-2290.

Czernik, S., Bridgwater, A.V. 2004. Overview of Applications of Biomass Fast Pyrolysis Oil. Energy & Fuels, 18(2), 590-598.

Demirbas, A. 2004. Effect of initial moisture content on the yields of oily products from pyrolysis of biomass. Journal of Analytical and Applied Pyrolysis, 71(2), 803-815.

Dence, C.W. 1992. The Determination of Lignin. in: Methods in Lignin Chemistry, (Eds.) S. Lin, C. Dence, Springer Berlin Heidelberg, pp. 33-61.

Diebold, J.P. 2002. A Review of the Chemical and Physical Mechanisms of the Storage Stability of Fast Pyrolysis Bio-Oils. in: Fast Pyrolysis of Biomass: A handbook, (Ed.) A.V. Bridgwater, CPL Press. Newbury, U.K., pp. 205-241.

Elliott, D.C. 2007. Historical Developments in Hydroprocessing Bio-oils. Energy & Fuels, 21(3), 1792-1815.

Elliott, D.C., Hart, T.R. 2008. Catalytic Hydroprocessing of Chemical Models for Bio-oil. Energy & Fuels, 23(2), 631-637.

Faix, O., Fortmann, I., Bremer, J., Meier, D. 1991. Thermal degradation products of wood. Holz als Roh- und Werkstoff, 49(5), 213-219.

Marsman, J.H., Wildschut, J., Mahfud, F., Heeres, H.J. 2007. Identification of components in fast pyrolysis oil and upgraded products by comprehensive two-dimensional gas chromatography and flame ionisation detection. Journal of Chromatography A, 1150(1–2), 21-27.

Mohan, D., Pittman, C.U., Steele, P.H. 2006. Pyrolysis of Wood/Biomass for Bio-oil: A Critical Review. Energy & Fuels, 20(3), 848-889.

Mullen, C.A., Boateng, A.A. 2008. Chemical Composition of Bio-oils Produced by Fast Pyrolysis of Two Energy Crops†. Energy & Fuels, 22(3), 2104-2109.

Nowakowski, D.J., Bridgwater, A.V., Elliott, D.C., Meier, D., de Wild, P. 2010. Lignin fast pyrolysis: Results from an international collaboration. Journal of Analytical and Applied Pyrolysis, 88(1), 53-72.

Phanphanich, M., Mani, S. 2011. Impact of torrefaction on the grindability and fuel characteristics of forest biomass. Bioresource Technology, 102(2), 1246-1253.

Pouwels, A.D., Eijkel, G.B., Boon, J.J. 1989. Curie-point pyrolysis-capillary gas chromatography-high-resolution mass spectrometry of microcrystalline cellulose. Journal of Analytical and Applied Pyrolysis, 14(4), 237-280.

Prins, M.J., Ptasinski, K.J., Janssen, F.J.J.G. 2006a. More efficient biomass gasification via torrefaction. Energy, 31(15), 3458-3470.

Prins, M.J., Ptasinski, K.J., Janssen, F.J.J.G. 2006b. Torrefaction of wood: Part 2. Analysis of products. Journal of Analytical and Applied Pyrolysis, 77(1), 35-40.

Ralph, J., Hatfield, R.D. 1991. Pyrolysis-GC-MS characterization of forage materials. Journal of Agricultural and Food Chemistry, 39(8), 1426-1437.

Reeves Iii, J.B., Galletti, G.C. 1993. Use of pyrolysis—gas chromatography/mass spectrometry in the study of lignin assays. Journal of Analytical and Applied Pyrolysis, 24(3), 243-255.

Reijnders, L. 2006. Conditions for the sustainability of biomass based fuel use. Energy Policy, 34(7), 863-876.

Repellin, V., Govin, A., Rolland, M., Guyonnet, R. 2010. Energy requirement for fine grinding of torrefied wood. Biomass and Bioenergy, 34(7), 923-930.

Sharma, R.K., Bakhshi, N.N. 1993. Catalytic upgrading of pyrolysis oil. Energy & Fuels, 7(2), 306-314.

Sluiter A., Hames, B., Ruiz, R., Scarlata, C., Sluiter. J., Templeton, D., Crocker, D. (2008). NREL Laboratory Analytical Procedure. NREL/TP-510-42618, 1-18.Retrieved from <http://www.nrel.gov/biomass/pdfs/42618.pdf>.

Vispute, T.P., Zhang, H., Sanna, A., Xiao, R., Huber, G.W. 2010. Renewable Chemical Commodity Feedstocks from Integrated Catalytic Processing of Pyrolysis Oils. Science, 330(6008), 1222-1227.

Yan, W., Acharjee, T.C., Coronella, C.J., Vásquez, V.R. 2009. Thermal pretreatment of lignocellulosic biomass. Environmental Progress & Sustainable Energy, 28(3), 435-440.

Yan, W., Hastings, J.T., Acharjee, T.C., Coronella, C.J., Vásquez, V.R. 2010. Mass and Energy Balances of Wet Torrefaction of Lignocellulosic Biomass†. Energy & Fuels, 24(9), 4738-4742.

Zwart, R.W.R., Boerrigter, H., van der Drift, A. 2006. The Impact of Biomass Pretreatment on the Feasibility of Overseas Biomass Conversion to Fischer−Tropsch Products. Energy & Fuels, 20(5), 2192-2197.

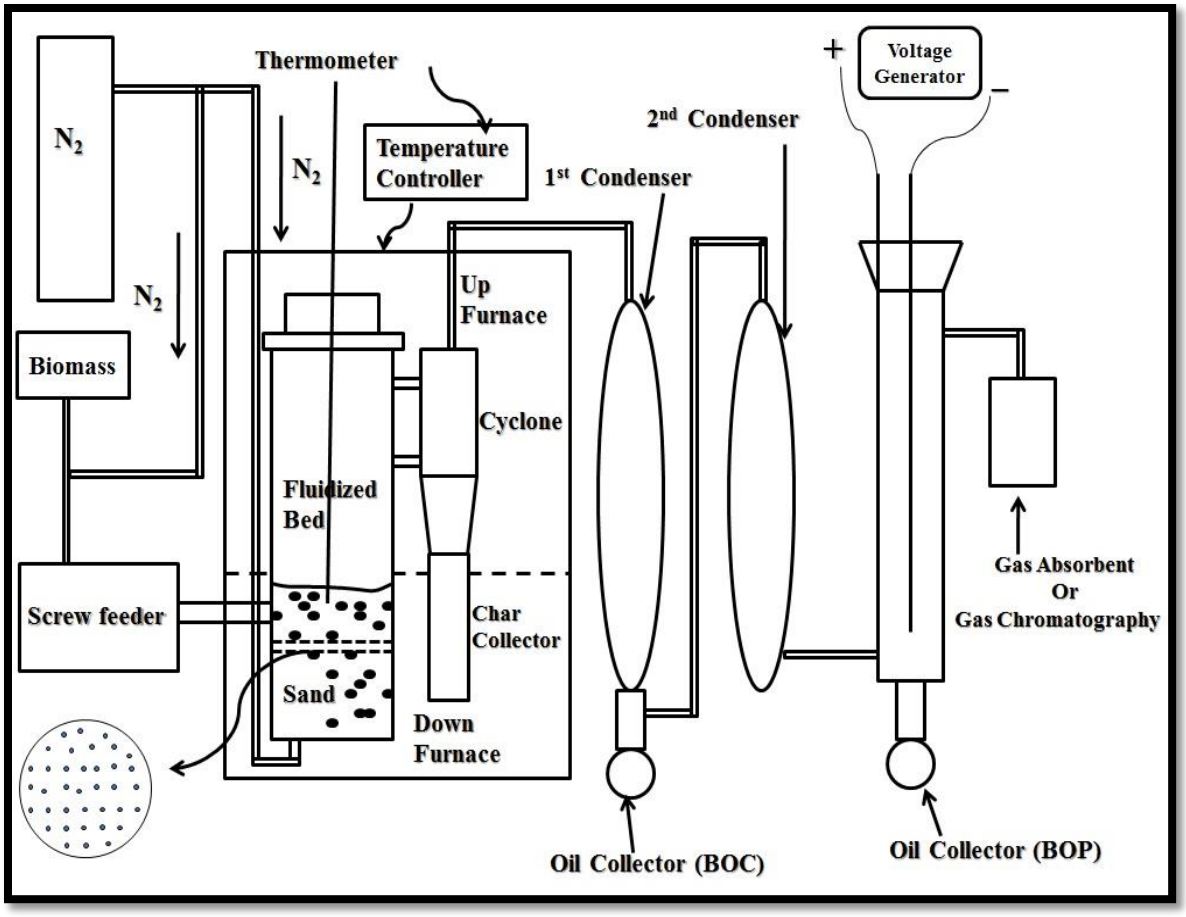

Figure 1.1 Schematic diagram of lab-scale fast pyrolysis reactor.

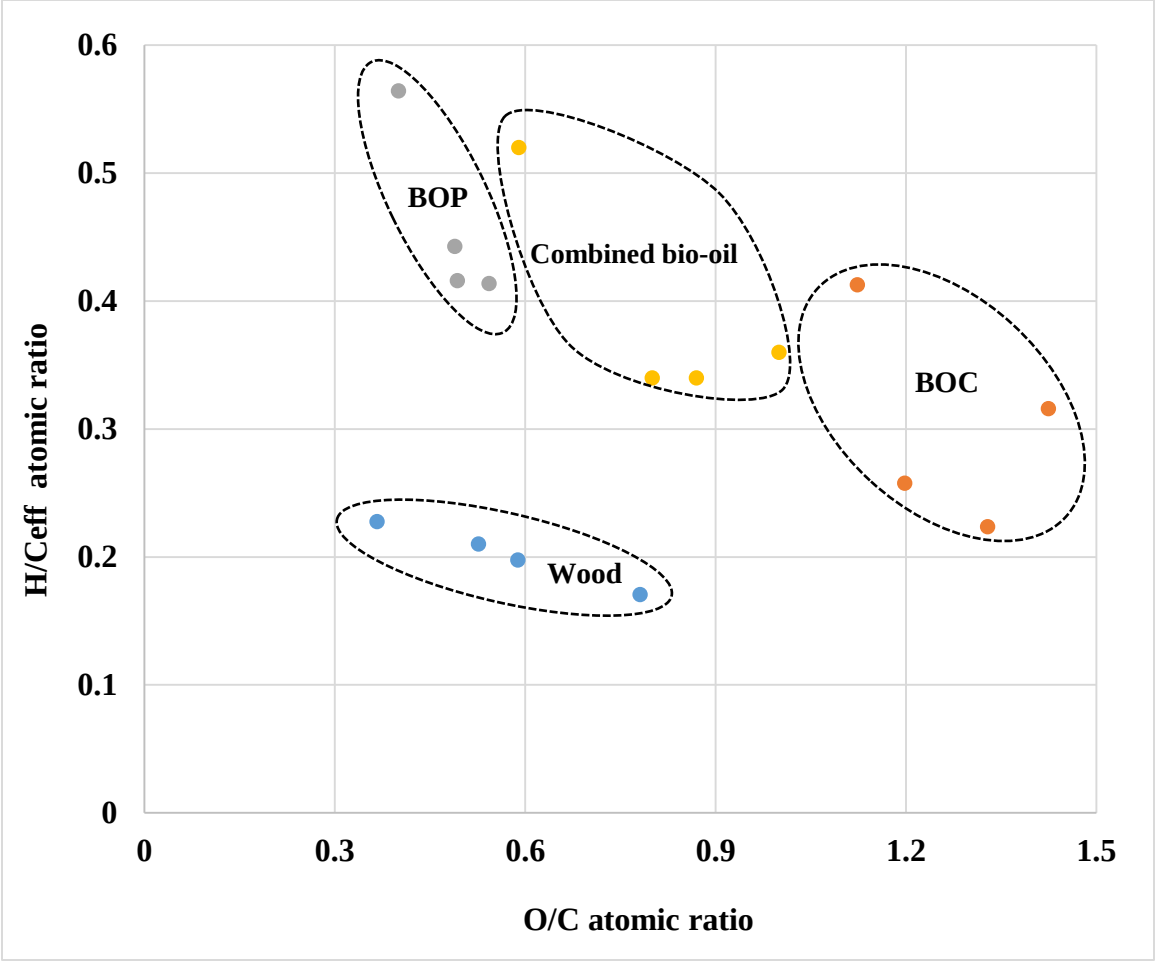

Figure 1.2 Elemental analysis of bio-oils and wood: oxygen-to-carbon ratio vs. hydrogen-to-carbon effective ratio. Within these groups, the four points from right to left represent bio-oils produced from raw wood, TW-270T, TW-300T and TW-330T. Combined bio-oil indicates the mixed BOC and BOP.

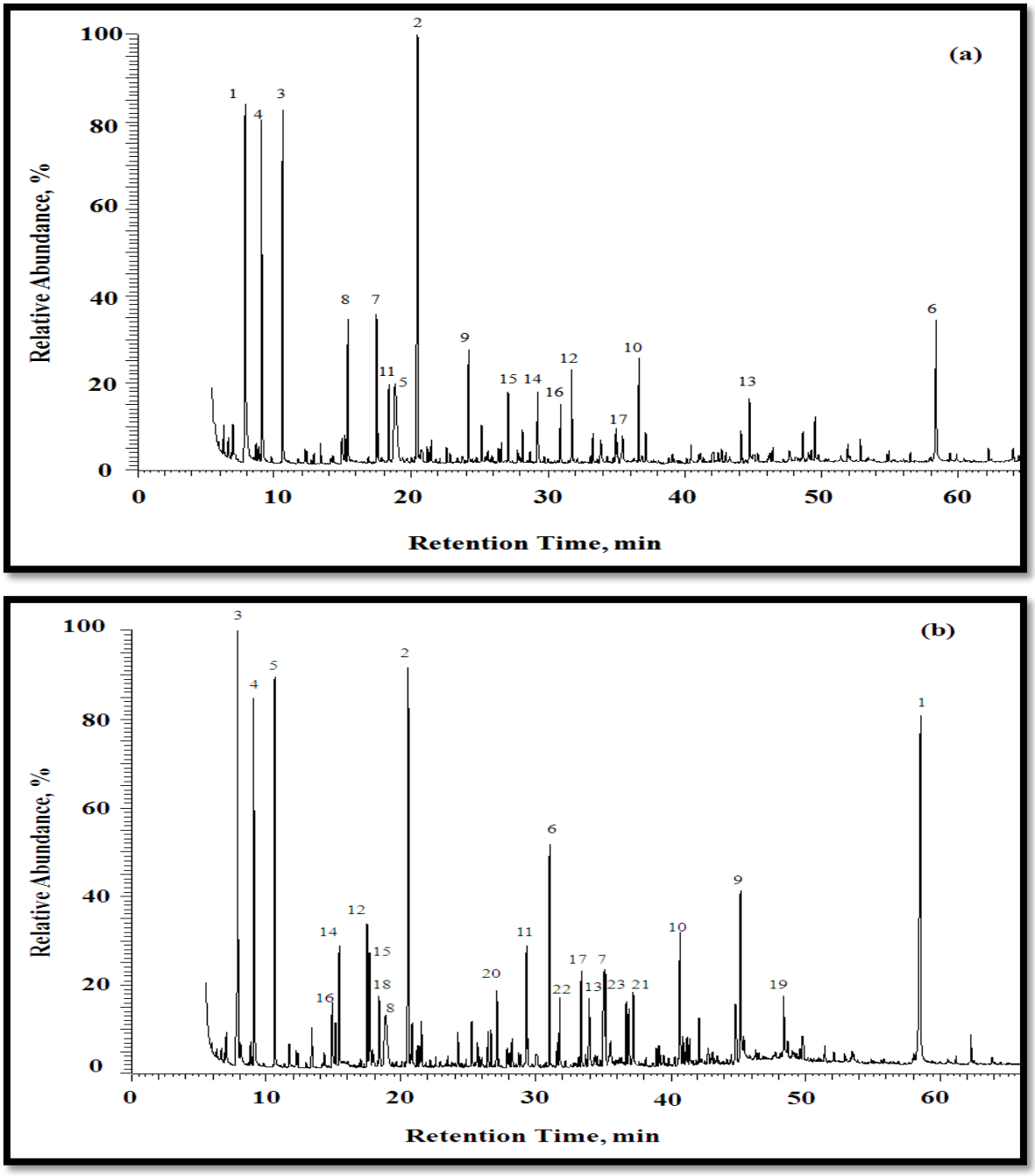

Figure 1.3 Total ion chromatograms for condenser collected bio-oil produced from (a) non-torrefied wood: BOC-LP-Raw and (b) severely torrefied wood: BOC-LP-330T. The chemical compounds (numbers above the peaks) are identified in Table 1.5.

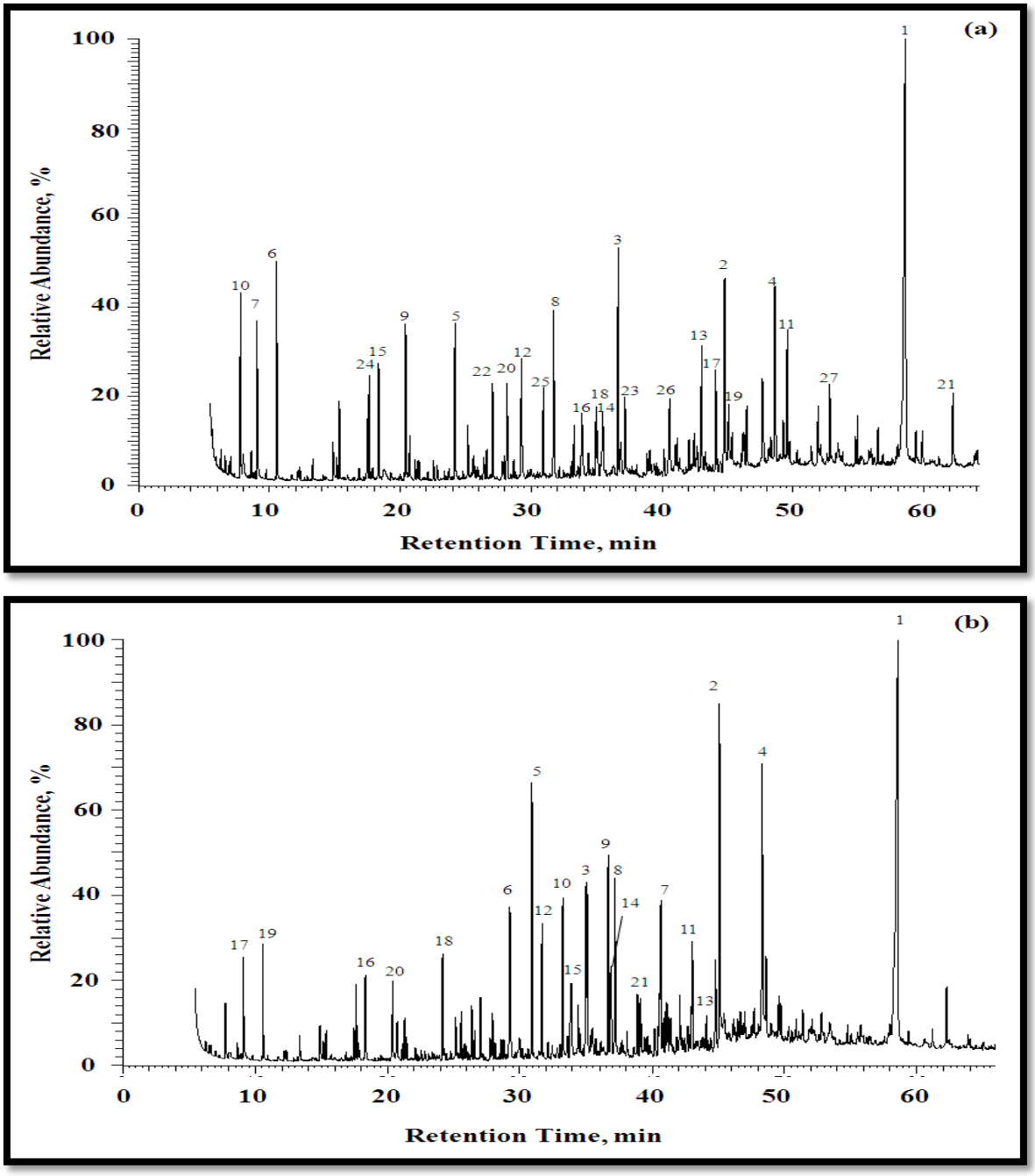

Figure 1.4 Total ion chromatograms for ESP collected bio-oil produced from (a) non-torrefied wood: BOP-LP-Raw and (b) severely torrefied wood: BOP-LP-330T. The chemical compounds (numbers above the peaks) are identified in Table 1.6.

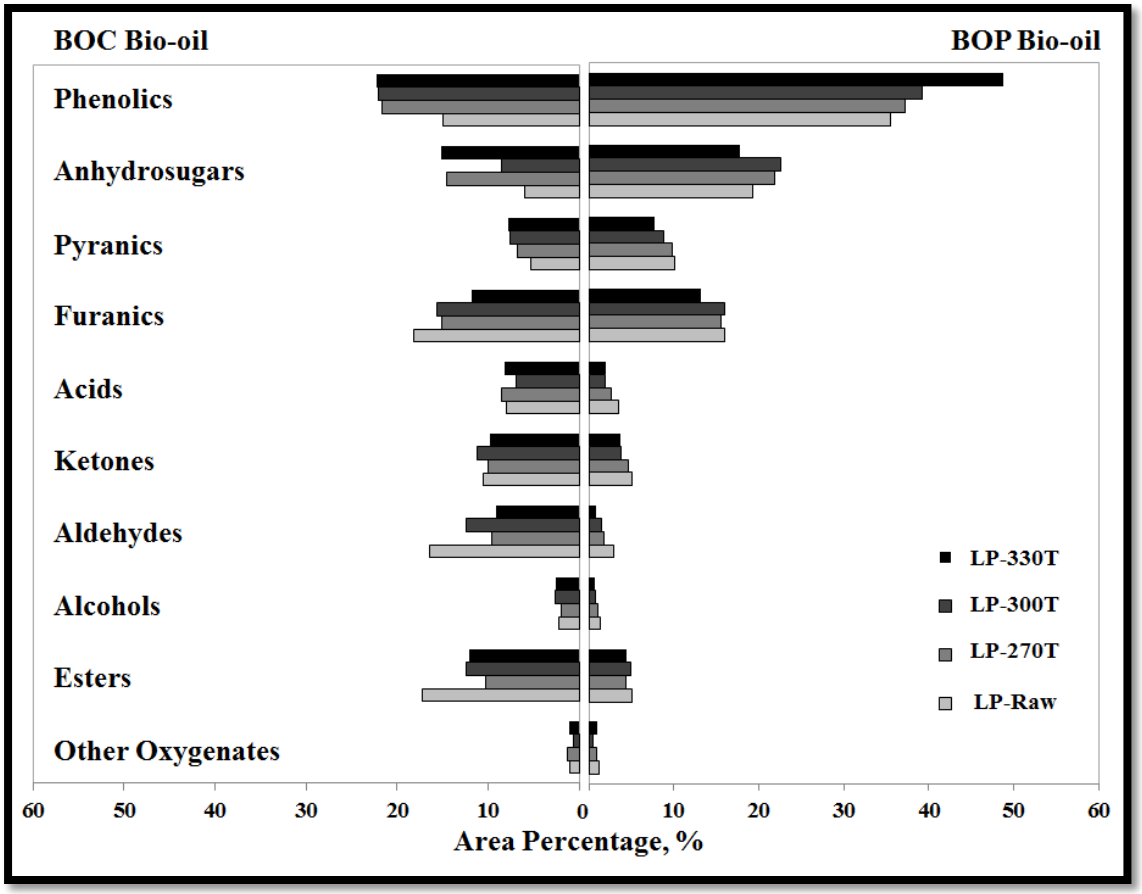

Figure 1.5 Summary of chemical compositions of bio-oils produced from raw wood, TW-270T, TW-300T and TW-330T (bottom to top within each chemical group) for BOC (left) and BOP (right).

Table 1.1 Total carbohydrate analyses of torrefied wood.

	Carbohydrate, %					Lignin, %			Extractives, %
	Glucan	Xylan	Galactan	A&M[a]	Total	AIR[b]	ASR[c]	Total	
Raw wood	36.1	6.4	2.3	10.0	54.8	30.1	1.6	31.7	2.1
TW-270T	34.4	4.2	1.0	7.0	46.6	41.0	1.8	42.8	5.8
TW-300T	32.0	3.0	0.7	5.4	41.1	48.1	1.8	49.9	6.0
TW-330T	18.0	0.4	0.0	0.6	19.0	74.2	2.6	76.8	10.4

a. A&M: arabinan and mannan

b. AIR: acid insoluble residue, usually termed as Klason lignin

c. ASR: acid soluble residue, usually termed as acid soluble lignin

Table 1.2 Proximate and ultimate analyses of torrefied wood.

	HHV[a], MJ/Kg	HVC[b], %	VM[c], %	FC[d], %	Ash, %	C, %	H, %	O, %	N, %	O/C[e]
Raw wood	20.0 (18.2)	9.3	84.6	14.8	0.56	50.5	6.3	43.2	0.09	0.64
TW-270T	22.7 (20.8)	8.1	78.6	20.8	0.62	55.0	5.9	39.0	0.11	0.53
TW-300T	24.0 (22.1)	8.0	76.4	22.8	0.78	57.3	5.8	36.7	0.14	0.48
TW-330T	26.3 (25.2)	4.2	59.9	38.6	1.45	65.8	4.9	29.0	0.28	0.33

a. HVV: high heating value based on dry wood (wet-based HHV in parentheses)

b. HVC: highly volatile compounds, which include moisture and light extractives generated by torrefaction

c. VM: volatile matter

d. FC: fixed carbon

e. O/C: oxygen to carbon atomic ratio

Table 1.3 Amount of pyrolysis bio-oil and bio-char produced from torrefied wood. The values are based on 100g of air-dry biomass introduced.

	Bio-oil, g			HHV[c], MJ/kg	Water in bio-oil, %		Biochar, g	Gas, g
	BOC[a]	BOP[b]	Total	MBO[d]	BOC[a]	BOP[b]		
Raw wood	44.3	22.9	67.2	21.0 (15.4)	44.4	14.3	9.7	23.1
TW-270T	37.1	17.4	54.5	21.2 (16.6)	36.7	8.5	22.2	23.3
TW-300T	33.5	18.6	52.1	23.5 (18.0)	41.3	9.0	27.0	20.9
TW-330T	17.9	15.6	33.5	28.7 (24.3)	35.7	6.3	43.3	23.2

a. BOC: bio-oil collected from first condenser

b. BOP: bio-oil collected from electrostatic precipitator

c. HHV: high heating value based on dry bio-oil (wet-based HHV in parentheses)

d. MBO: high heating value measured on mixed BOC and BOP

Table 1.4 Conversion yield of carbon and oxygen from biomass to pyrolysis products.

		Biomass	BOC[a]	BOP[b]	Bio-oil	Biochar	NCG[c]
C, %	**Raw wood**	100	30.1	27.8	57.9	17.5	24.6
	TW-270T	100	23.4	20.5	43.9	40.0	16.1
	TW-300T	100	15.9	26.0	41.9	45.1	13.0
	TW-330T	100	6.6	18.5	25.1	51.1	23.8
O, %	**Raw wood**	100	54.9	19.3	74.2	6.6	19.2
	TW-270T	100	47.7	17.0	64.7	7.2	28.1
	TW-300T	100	40.2	24.3	64.5	7.0	28.5
	TW-330T	100	20.3	20.2	40.5	21.0	38.5

a. BOC: bio-oil collected from first condenser

b. BOP: bio-oil collected from electrostatic precipitator

c. NCG: non-condensable gas

Table 1.5 Major chemical compounds in BOC as determined by GC/MS.

	BOC-LP-Raw		BOC-LP-270T	
	Chemicals	**Area, %**	**Chemicals**	**Area, %**
1	Glycolaldehyde	12.90	1,6-anhydro-β-D-glucopyranose	9.84
2	Acetyloxyacetaldehyde	12.80	Glycolaldehyde	6.78
3	Acetol	7.32	Acetol	5.70
4	Acetic Acid	6.56	Acetic acid	5.68
5	3,4-Furandiol, tetrahydro	5.82	Acetyloxyacetaldehyde	5.26
6	1,6-anhydro-β-D-glucopyranose	4.51	3,4-Furandiol, tetrahydro	2.71
7	Butanedial	2.90	Phenol, 2-methoxy-4-methyl-	2.57
8	Pyruvic acid methyl ester	2.63	Butanedial	2.28
9	2,5-dihydro-5-methylfuran-2-one	2.41	Guaiacol	2.05
10	Phenol, 2-methoxy-4-methyl-	1.99	2,5-dihydro-5-methylfuran-2-one	1.93
11	Furfural	1.92	Pyruvic acid methyl ester	1.91
12	Guaiacol	1.84	Furfural	1.89
13	5-hydroxymethyl-2-furaldehyde	1.70	Methyl-dihydro-(2H)-pyran-2-one	1.86
14	Methyl-dihydro-(2H)-pyran-2-one	1.56	5-hydroxymethyl-2-furaldehyde	1.83
15	2(5H)-Furanone	1.55	Phenol	1.58
16	Phenol	1.14	2(5H)-Furanone	1.35
17	p-Cresol & m-Cresol (overlapped)	1.11	1-acetyloxypropan-2-one	1.31
18			Unknown	1.31
19			Isoeugenol	1.28
20			o-cresol	1.21
21			1,2-Benzenediol	1.15
22			Formic acid	1.11
23				
Cumulative Area, %		**70.60**		**62.59**

Table 1.5 Continued.

	BOC-LP-300T		BOC-LP-330T	
	Chemicals	**Area, %**	**Chemicals**	**Area,%**
1	Glycolaldehyde	8.56	1,6-anhydro-β-D-glucopyranose	11.21
2	Acetyloxyacetaldehyde	8.03	Acetyloxyacetaldehyde	7.89
3	Acetol	6.19	Glycolaldehyde	6.88
4	1,6-anhydro-β-D-glucopyranose	5.68	Acetic acid	5.49
5	Acetic acid	5.14	Acetol	5.46
6	Phenol, 2-methoxy-4-methyl-	4.37	Phenol	3.18
7	3,4-Furandiol, tetrahydro	3.64	p-Cresol & m-Cresol (overlapped)	3.12
8	Butanedial	3.31	3,4-Furandiol, tetrahydro	3.00
9	2,5-dihydro-5-methylfuran-2-one	2.95	1,2-Benzenediol	2.93
10	Guaiacol	2.80	p-Ethylguaiacol	2.42
11	Methyl-dihydro-(2H)-pyran-2-one	2.42	Methyl-dihydro-(2H)-pyran-2-one	2.37
12	Pyruvic acid methyl ester	2.34	Butanedial	2.04
13	2-methoxy-4-vinylphenol	2.22	Unknown	1.63
14	1-acetyloxypropan-2-one	1.99	Pyruvic acid methyl ester	1.56
15	2(5H)-Furanone	1.64	1-acetyloxypropan-2-one	1.50
16	Furfural	1.52	Propanal, 2,3-dihydroxy-	1.42
17	Phenol	1.52	o-Cresol	1.36
18	p-Ethylguaiacol	1.51	Furfural	1.31
19	o-cresol	1.34	1,2-Benzenediol, 4-methyl-	1.29
20	Isoeugenol	1.22	2(5H)-Furanone	1.25
21	5-hydroxymethyl-2-furaldehyde	1.17	Phenol, 2,3-dimethyl	1.24
22	Unknown	1.12	Guaiacol	1.02
23	Propanal, 2,3-dihydroxy-	1.02	Unknown	1.01
Cumulative Area, %		**71.70**		**70.58**

Table 1.6 Major chemical compounds in BOP as determined by GC/MS.

	BOP-LP-Raw		BOP-LP-270T	
	Chemicals	**Area, %**	**Chemicals**	**Area, %**
1	1,6-anhydro-β-D-glucopyranose	13.91	1,6-anhydro-β-D-glucopyranose	14.74
2	5-hydroxymethyl-2-furaldehyde	3.28	Phenol, 2-methoxy-4-methyl-	4.19
3	Phenol, 2-methoxy-4-methyl-	2.80	Methyl-dihydro-(2H)-pyran-2-one	2.88
4	Isoeugenol	2.78	Isoeugenol	2.81
5	2,5-dihydro-5-methylfuran-2-one	2.38	Guaiacol	2.67
6	Acetol	2.36	2-methoxy-4-vinylphenol	2.59
7	Acetic acid	2.19	5-hydroxymethyl-2-furaldehyde	2.45
8	Guaiacol	2.18	m-Cresol & p-Cresol (overlapped)	2.41
9	Acetyloxyacetaldehyde	2.16	2,5-dihydro-5-methylfuran-2-one	2.33
10	Glycolaldehyde	2.08	5-hydroxymethyl-2-tetrahydro-furaldehyde-3-one	1.97
11	Vanilla	2.06	Acetic acid	1.89
12	Methyl-dihydro-(2H)-pyran-2-one	2.05	1,2-Benzenediol	1.87
13	p-Ethylguaiacol	1.94	Unknown	1.81
14	Tetrahydropyran-2-carbinol	1.70	Acetol	1.75
15	Furfural	1.69	Phenol	1.74
16	Unknown	1.48	Phenol, 2,3-dimethyl	1.69
17	Eugenol	1.44	Furfural	1.64
18	m-Cresol & p-Cresol (overlapped)	1.42	1,6-anhydro-β-D-galactofuranose	1.43
19	1,2-Benzenediol	1.37	Eugenol	1.33
20	2H-Pyran, 3,4-dihydro-2-methoxy-	1.35	Vanilla	1.26
21	1,6-anhydro-β-D-galactofuranose	1.34	2(5H)-Furanone	1.20
22	2(5H)-Furanone	1.29	Glycolaldehyde	1.16
23	Phenol, 2,3-dimethyl	1.19	o-Cresol	1.15
24	1-acetyloxypropan-2-one	1.13	Acetyloxyacetaldehyde	1.14
25	Phenol	1.11	Unknown	1.13
26	5-hydroxymethyl-2-tetrahydro-furaldehyde-3-one	1.04	(4)-methyltetrahydrofuran-3-one	1.10
27	Acetoguaiacone	1.03	p-Ethylguaiacol	1.09
Cumulative Area, %		**60.75**		**63.42**

Table 1.6 Continued.

	BOP-LP-300T		BOP-LP-330T	
	Chemicals	**Area, %**	**Chemicals**	**Area, %**
1	1,6-anhydro-β-D-glucopyranose	13.44	1,6-anhydro-β-D-glucopyranose	12.46
2	Phenol, 2-methoxy-4-methyl-	6.15	1,2-Benzenediol	4.87
3	2-methoxy-4-vinylphenol	3.76	m-Cresol & p-Cresol (overlapped)	4.43
4	Isoeugenol	3.64	1,2-Benzenediol, 3-methyl	3.80
5	Guaiacol	3.27	Phenol	3.10
6	Methyl-dihydro-(2H)-pyran-2-one	2.40	Methyl-dihydro-(2H)-pyran-2-one	2.69
7	5-hydroxymethyl-2-tetrahydro-furaldehyde-3-one	2.39	5-hydroxymethyl-2-tetrahydro-furaldehyde-3-one	2.64
8	2,5-dihydro-5-methylfuran-2-one	2.32	Phenol, 2,3-dimethyl	2.30
9	5-hydroxymethyl-2-furaldehyde	2.29	Phenol, 2-methoxy-4-methyl-	2.27
10	m-Cresol & p-Cresol (overlapped)	1.94	o-Cresol	1.83
11	Unknown	1.61	p-Ethylguaiacol	1.77
12	Acetol	1.46	Guaiacol	1.65
13	Furfural	1.44	5-hydroxymethyl-2-furaldehyde	1.56
14	1,6-anhydro-β-D-galactofuranose	1.42	Unknown	1.50
15	Phenol	1.41	Unknown	1.46
16	Acetic acid	1.39	Furfural	1.37
17	Acetyloxyacetaldehyde	1.38	Acetic acid	1.35
18	p-Ethylguaiacol	1.35	2,5-dihydro-5-methylfuran-2-one	1.29
19	Unknown	1.31	Acetol	1.09
20	1,2-Benzenediol	1.30	Acetyloxyacetaldehyde	1.08
21	Phenol, 2,3-dimethyl	1.29	2,3,5-Trimethyl phenol	1.01
22	Unknown	1.20		
23	2(5H)-Furanone	1.19		
24	Eugenol	1.19		
25	Vanilla	1.14		
26	1-acetyloxypropan-2-one	1.05		
27				
Cumulative Area, %		**62.73**		**55.52**

CHAPTER 2

Integrating Torrefaction Pretreatment into Biomass Fast Pyrolysis: Perspectives and Challenges

1. Introduction

Under elevated temperature (~500 °C) and oxygen free conditions, biomass fast pyrolysis converts solid lignocellulosic materials into liquid bio-oil (also known as bio-crude). The development of this simple conversion process is promoted by the fear of depletion of fossil fuel and deterioration of global warming. Shifting our main energy supply from crude oil to renewable energy is an inescapable decision that we have to make. Bio-oil is the only available liquid fuel among all the existing renewable energies, it is also considered as a potential candidate for replacing crude-oil as transportation fuel. Therefore, countless efforts have been made to develop various processes of making bio-oil competitive to conventional gasoline fuel [Hossain and Davies, 2013; Carlson et al., 2009; Melero et al., 2012].

Simulating a sophisticated conversion process (biomass to crude oil) that took nature millions of years to complete in a few seconds using fast pyrolysis is a great challenge. Pyrolysis bio-oil is very different from conventional mineral oil. Its high oxygen content (35-40 % on dry base) and low heating value (only half of that of the heavy fuel oil) [Mohan et al., 2006], greatly delayed the bio-oil application as transportation fuel. Also, this oxygen rich bio-oil has strong chemical reactivity: during the storage at room temperature, bio-oil viscosity increase and phase separation (termed as aging) often occurred [Diebold, 2000];

during the upgrading at high temperature (250-350 °C), bio-oil components polymerize and form coke on the catalyst. In addition, the existing oil upgrading infrastructures cannot accept crude bio-oil due to other poor oil properties, such as high acidity (pH~2) and high water content. Accordingly, crude bio-oil is not suitable for direct application without stabilization and elimination of oxygen; thus several upgrading technologies have been developed to settle these issues.

Hydroprocessing and hydrocracking are the most common bio-oil upgrading strategies. [Elliott and Hart, 2009] Hydroprocessing eliminates oxygen from bio-oil in the form of generating water by adding hydrogen into a reactor under high temperature and pressure along with the presence of catalyst (i.e. Ruthenium). Hydrocracking rejects the oxygen from bio-oil in the form of generating carbon dioxide, carbon monoxide and water by cracking them inside the pores of the catalyst (i.e. zeolite). After these two upgrading steps, the bio-oil oxygen content can be significantly reduced to an acceptable range (~1%) closing to that of petroleum oil. [Elliott, 2007] As a result, the upgraded bio-oil becomes stable because those reactive chemical components in the bio-oil have been converted into stable hydrocarbons. Unfortunately, successful case studies of catalytic upgrading of bio-oil are still limited to lab and pilot-scale operation. Barriers that retard this process development include high hydrogen consumption, catalyst deactivation and low production yield of hydrocarbons (20-30%). To addressing these difficulties, Vispute, et al., [Vispute et al., 2010] reported an integrated process, in which the above two catalytic upgrading processes are combined to convert bio-oil into industry commodity chemical feedstock. By carefully design the catalytic conditions and reactors, the overall conversion yields of light olefins and aromatic

hydrocarbons are three times higher than that contained in the original bio-oil. Other efforts [French and Czernik, 2010; Balagurumurthy 2013] using catalytic fast pyrolysis and hydropyrolysis attempt to integrate the bio-oil production and upgrading step together. Therefore, the overall process can be simplified and the operation cost can be reduced to obtain high quality bio-oil with low oxygen content.

The hydrotreating of bio-oil is an integrant part for making biofuel from biomass fast pyrolysis. To improve the bio-oil upgradability in hydroprocessing process, stable bio-oil intermediate with low-oxygen-content is needed which can be produced from catalytic fast pyrolysis process [Bridgwater, 1996; Mullen, 2011]. With achieving the same goal of obtaining stable low oxygen content bio-oil, we first proposed a catalyst-free process, torrefaction pretreatment, as an alternative to produce refinery-ready bio-oil with improved physical and chemical properties. In this process, raw wood materials were thermally pretreated (270-330 °C) under oxygen-free conditions and the resulting torrefied wood was used as a fast pyrolysis feedstock. A catalyst-free pretreatment process can reduce the cost and time spent on the catalyst and its regeneration. Compared to raw wood, pretreated biomass is easy to handle and transport due to its higher density and hydrophobicity and the friable torrefied wood can be easily grounded into even particle size while saving grinding energy. [Phanphanich and Mani, 2011] In addition, torrefaction pretreatment improves biomass quality in terms of altering wood chemical composition, reducing oxygen content, increasing energy density and removing acid volatiles and moistures. [Prins et al., 2006a; Prins et al., 2006b; Yan et al., 2010; Couhert 2009] All these effects are potentially beneficial to improvement the bio-oil properties. The author's previous publication [Meng et al., 2012]

showed promising results of reducing oxygen content and altering chemical composition of the bio-oil made from torrefied wood. Theoretically, reduced oxygen content in bio-oil could save hydrogen consumption in the hydroprocessing process and the simplified chemical composition with less reactive acids and aldehydes could make the bio-oil more stable and generate less coke in the upgrading process. Inspired by these great potentials, additional research work [Boateng and Mullen, 2013; Ren et al., 2013; Zheng et al., 2013] regarding on integrating torrefaction into fast pyrolysis has been investigated. However, questions on whether torrefaction is an effective pretreatment technology for producing high-quality bio-oil as a fuel intermediate have still not been answered because this pretreatment method also has negative effects on the pyrolysis process, i.e. reducing the overall yield of bio-oil. Based on our current understanding and results of integrated torrefaction-fast-pyrolysis process, this chapter try to answer the above question by analyzing both negative and positive effects of torrefaction on fast pyrolysis operation and bio-oil quality.

2. Materials and Methods

2.1 Torrefied biomass production

Loblolly pine chips containing bark were used as the raw material for torrefaction pretreatment. A pilot-scale torrefaction system was operated to produce torrefied wood at three different severities, which were treated under 270, 300, and 330°C for 2.5 minutes respectively and referred as TW-270T, TW-300T and TW-330T in this study. The wood sample without torrefaction pretreatment was named raw wood and the torrefaction severity increases in the series from TW-270T to TW-330T. The severity of torrefaction is quantified

by the weight loss of torrefied wood which is 16.5%, 24.1%, and 46.5% for TW-270T, TW-300T and TW-330T respectively, based on the original weight of non-torrefied dry wood. Characterizations of these torrefied wood samples were summarized in Table 2.1.

2.2 Bio-oil production via fast pyrolysis process

The bio-oil was produced from a lab-scale (150g/ hour) fluidizing bed reactor (O.D. 43mm) at 500 °C as described previously [Meng et al., 2012]. Bio-oils were collected by two water cooling condensers (0-4 °C) and one electrostatic precipitator. The collected bio-oils were thoroughly mixed and stored in a freezer (-4 °C) for further chemical and physical analyses. The yield of bio-oil and biochar was calculated by weight and the gas yield was calculated by difference. Bio-oil made from raw wood is named as LP-Raw (LP as liquid product) and bio-oils made from torrefied wood was labeled as LP-270T, LP-300T and LP-330T respectively. Characterizations of bio-oil properties are summarized in Table 2.2.

2.3 Characterizations of torrefied wood and bio-oil

Chemical Composition. Air dried wood samples (40-60 mesh) were extracted with benzene-ethanol mixture (v/v=2:1) according to Tappi Standard Method (T204cm-07) for 24 hours. The extractive amount was calculated by the gravimetric method of the extraction liquid after vacuum drying. The amounts of structural carbohydrates and lignin of wood were measured by Klason lignin analysis [Dence, 1992] followed by HPLC sugar analysis [Sluiter et al., 2008].

Ultimate and Proximate Analysis. Carbon, hydrogen, and nitrogen analyses of both the wood and bio-oil samples were performed according to ASTM-D5291 using a Perkin Elmer CHN Elemental Analyzer (2400 Series II). The oxygen contents were calculated by difference. The proximate analyses were performed with a muffle furnace according to ASTM-D1762-84. The trace metal content of torrefied wood was quantified by ICP-Optical Emission Spectrometer (Perkin Elmer – 2000 Dual View) and duplicate means are reported in Table 2.1.

Water content. The water content of the bio-oils was determined by Karl-Fischer titration according to ASTM E 203-08 using HYDRANAL Titrant 5E, HYDRANAL Solvent E and HYDRANAL Water Standard 10.0.

High Heating Value. The high heating value (HHV) of both wood and bio-oils was measured according to DIN 51900 with 1108 oxygen combustion bomb (Parr Instrument).

Acidity. The acidity of bio-oils was measured by both pH meter (Corning pH meter 430) and acid-base titration method. The total acid number (TAN) was measured according to ASTM D644-07 with Mettler-Toledo titrator (T50). Both inflection point and buffer potential (potential of buffer solution pH=11) method were employed to determine the end point of this acid-base titration. 0.1M KOH in isopropanol solution (Ricca Chemical 6257-32) used to titrate the bio-oil. The benzene and isopropanol were purchased from VWR international and used as received.

Viscosity and Solid Content. the dynamic viscosity of bio-oils was measured with a Rheometer (AR 2000, TA Instrument) at 40 ºC with a shear rate of 100 s^{-1}. Approximately 1 g of bio-oil was used for each test and 20 data points were collected for each sample to

calculate the average viscosity. The solid content of bio-oils was measured according to ASTM D7579 using dichloromethane and methanol (v:v=1:1).

Solvent Fractionation. The solvent fractionation of bio-oil was performed based on reference [Oasmaa and Kuoppala, 2003]. Dichloromethane (34856) and diethyl ether (346136) was purchased from Sigma-Aldrich and used as received. The solvent fractionation method employed here separates the bio-oil into water soluble (WS) and water insoluble fraction (WIS). The WS fraction was further separated into ether soluble (ES) and ether insoluble fraction (EIS). The WIS fraction was isolated into high-molecular-mass (HMM) lignin fraction and low-molecular-mass lignin fraction (LMM). Based on the GC/MS analysis and reference [Oasmaa and Kuoppala, 2003], the ES fraction contains aldehydes, ketones, acids and some lignin monomers; while the EIS fraction is composed of hydroxy acids, anhydrosugars, i.e. levoglucosan, and other anhydro-oligomer sugars. The HMM fraction has high molecular weight pyrolytic lignin and none of them are GC elutable; while LMM fraction is a low molecular weight lignin fraction and its GC visible compounds are mainly phenol, guaiacol and catechol.

GC/MS analysis. Gas chromatographic/mass spectrometric **(**GC/MS) analyses of bio-oils were performed on a Finnigan Polaris Q Plus system with DB-1701 column: 60m×0.25mm×0.25μm. The operational conditions of GC/MS can be found in previous publication. [Meng et al., 2012] The semi-quantification of the major chemical compounds in the bio-oils was achieved by generating calibration curves with standard chemicals and using internal standard - fluoranthene. All the standards (purity > 99.9%) are purchased from Sigma-Aldrich and VWR International.

^{1}H and ^{13}C NMR. ^{1}H and ^{13}C NMR of bio-oil samples were recorded in DMSO-d_6 solution (25% wt./wt.) with 5mm NMR tube using a Bruker Avance 700 MHz NMR spectrometer. All the NMR experiments were conducted with a cryoprobe maintained at 279K in order to increase the signal to noise ratio (S/N). ^{1}H spectrum was acquired with a single pulse sequence (zg) with 3.2s pulse delay time and a total of 32 scans at 25 ºC. ^{13}C spectrum was obtained by inverse gated decoupling pulse sequence (zgig), 90º pulse angle, 2.5s pulse delay time and a total of 18432 scans at 25 ºC. The phase/ base-line correction and integration of both ^{1}H and ^{13}C NMR spectra was analyzed with Topspin software (Bruker H9966S3) and the integration was selected based on the reference [Ingram et al.,2008].

3. Results and Discussions

3.1 Concept of Integrated torrefaction and fast pyrolysis process

The concept of improving bio-oil quality by adding a pretreatment step before biomass fast pyrolysis comes from a simple assumption, that is, high quality pyrolysis feedstock may generate bio-oils with improved physical and chemical properties. For example, under normal pyrolysis conditions, pretreated wood materials with reduced oxygen content may produce bio-oils with low oxygen content as well. In Scheme 2.1, this process starts with heat treatment of wet biomass. Biomass pre-drying and torrefaction pretreatment can be performed in a same reactor at different temperature and/or residence time producing torrefied wood with different torrefaction severities. These heat treated wood samples were further processed, i.e. grinding into small particles, and were pyrolyzed to make refinery-ready bio-oil with targeting oxygen content of 20% (dry base). The low-oxygen-content bio-

oil will then be transported to upgrading plant for further deoxygenation using hydrotreating and produce gasoline and diesel range fuel with targeting oxygen content of less than 1%. Due to the reduced oxygen content in the bio-oil intermediate, the hydrogen consumption and catalyst deactivation can be minimized in the upgrading process. Torrefaction volatiles and pyrolysis vent gas will be sent to a gas reforming plant to supply additional hydrogen for the upgrading plant. The pyrolysis char can be burned to provide heat for torrefaction pretreatment and gas reforming plant. Besides making transportation fuel, the torrefied wood can also be catalytic pyrolyzed to produce from torrefaction-pyrolysis process can also be further upgraded and purified making commodity chemicals, i.e. aromatics. For this purpose, torrefaction pretreatment is expected to simplify the oil composition and/or concentrating certain specialty chemical compounds in the bio-oil. In addition, coking formation during the upgrading process is expected to be reduced due to the removal of reactive bio-oil components, i.e. aldehydes by torrefaction pretreatment. The rest of this chapter will give detailed results and discussions on how torrefaction pretreatment can achieved this concept.

3.2 Effects of torrefaction pretreatment on bio-oil production

3.2.1 Bio-oil yield

Typical fast pyrolysis operation of woody biomass yields 65-70% liquid bio-oil. In this study, the loblolly pine without pretreatment (raw wood) gave a similar bio-oil yield (~67%) under optimal pyrolysis conditions. As shown in Table 2.3 (mass balance for single pyrolysis process), under same pyrolysis conditions, however, the torrefied wood (TW-270T, TW-300T and TW-330T) compared to raw wood, tends to give lower liquid yield but higher

char yield as increasing torrefaction severity. In case of severely torrefied wood sample (TW-330T), the bio-oil yield (33.5%) is only half of that for non-treated wood. A similar decreasing trend of bio-oil yield can be observed from the mass balance of integrated torrefaction- fast-pyrolysis process. In the integrated mass balance, the biochar yield slightly increased but the gas yield tended to decrease significantly due to the gas releasing during the pretreatment step.

The fact of reducing bio-oil yield with torrefaction pretreatment can be explained by the weight loss generated at the heat-treatment step (shown as TWL in Table 2.3). At torrefaction temperature range (270-330 °C), wood components starts to decompose. Volatile gas including permanent gas and light organics left the wood giving birth to the torrefaction weight loss while the residue char materials were locked in the torrefied wood. The chemical composition analyses of torrefied wood (see Table 2.1) supports that after torrefaction treatment, hemicellulose was extensively removed; cellulose content of the wood was also reduced, i.e. 50% reduction in case of TW-330T sample; but the amount of lignin and char residue increased significantly. Solid State NMR analysis [Park et al., 2013] found that the torrefied wood has more condensed PAH (poly-aromatic hydrocarbon) structure as increasing the torrefaction temperature. The residue char and lignin fraction of torrefied wood is likely to be the host of the PAH materials and their rigid structure is hard to decompose under pyrolysis conditions. Therefore, torrefied wood with high amount of torrefaction char and lignin residues would generate less liquid bio-oil because of the greater thermal resistance of these PAH materials compared to untreated wood. In addition, Table 2.1 also indicates that torrefied wood has higher ash content than the raw wood, known as

concentration effect [Phanphanich and Mani, 2011]. The concentrations of several ash-forming metal species were also listed in Table 2.1. These ash materials were found to be effective catalyst for reducing the bio-oil yield [Aho et al., 2013]. In summary, torrefaction weight loss, thermal resistance of torrefied wood components (torrefaction char and lignin residues) and catalytic effect of ash materials may well explain the bio-oil yield reduction caused by torrefaction pretreatment.

3.2.2 Carbon, oxygen and energy distribution

Reducing bio-oil oxygen content with increasing carbon retention from biomass into bio-oil is a key interest for pyrolysis oil production. However, removing oxygen from biomass in fast pyrolysis process usually consumes a large amount of carbon as oxygen is mainly removed as CO and CO_2. Fig. 2.1 presents the carbon, oxygen and energy balance in both single pyrolysis and integrated torrefaction-pyrolysis process. A decreasing trend of carbon flow into bio-oil but increasing carbon conversion into biochar can be observed in both Fig. 2.1-A-1 and 2.1-A-2. The carbon loss occurred in the torrefaction stage increased with higher torrefaction severity. For the oxygen conversion shown in Fig. 2.1-B-1 and 2.1-B-2, less oxygen was converted into bio-oil as increasing torrefaction severity. The low oxygen conversion into bio-oil was achieved by increasing oxygen flow into gas fraction and torrefaction weight loss. Additionally, for pyrolysis of severely torrefied wood (TW-330T), significantly amount of oxygen was retained in the biochar, suggesting this part of oxygen was locked in the condensed torrefied wood structure and cannot be released as gas or other volatile compounds in the pyrolysis stage resulting reduced oxygen conversion into the bio-

oil. Fig. 2.1-B-2 also suggests that, oxygen cannot be effectively removed during the torrefaction pretreatment unless higher pretreatment temperature was employed. The total energy distribution from biomass to bio-oil, biochar and gas fraction is shown in Fig. 2.1-C-1 and1C-2. Because of the reduced carbon conversion into the bio-oils, less total energy from biomass was transferred into bio-oil as a function of increasing torrefaction severity. More energy from starting biomass was retained in the biochar as it retains more carbon from the starting wood. The torrefaction step also consumes increasing amount of initial biomass energy from raw wood, but noticeable energy loss into torrefaction weight loss only occurred to severely torrefied wood sample (TW-330T). Recycling the energy in biochar, gas and torrefaction weight loss will be critical to the overall economics of this integrated process.

In summary, torrefaction pretreatment renders the integrated fast pyrolysis process with lower liquid yield, lower carbon, lower oxygen and energy conversion into the bio-oils. These effects may be attributed to torrefaction weight loss, thermal-recalcitrance of torrefied wood and also catalytic effect of concentrated ash content in the pretreated wood. The only positive effect of reducing oxygen conversion into bio-oil was achieved by making the above sacrifices to the integrated process and the question whether it is worth to make them depends on the quality improvement of the resulting bio-oil from torrefied wood.

3.3 Effects of torrefaction on bio-oil physical and chemical properties

3.3.1 Oxygen content in bio-oil made from torrefied wood

Reducing oxygen content in the bio-oil is the key interest for fast pyrolysis community. Under regular pyrolysis conditions, especially without using catalyst and/or

adding hydrogen, the oxygen content of the bio-oil largely depends on the oxygen content of the pyrolysis feedstock. Simply put, if the biomass has low oxygen content, the resulting bio-oil may also contain low oxygen as deoxygenation occurred in the pyrolysis process and no additional oxygen was introduced into the reaction system. As shown in Table 2.1, with higher torrefaction temperature, the oxygen content in the biomass reduced from 42.6% to 27.6% and accordingly the resulting bio-oils showed the same trend of reducing oxygen content from 32.2% to 21.7% (shown in Table 2.2). The lowest bio-oil oxygen content achieved in this study is slightly higher than 20% for LP-330T which approximately meets the target oxygen content as mentioned in the concept (section 3.1). In addition, Table 2.1 and 2 also show that the oxygen to carbon atomic ratio reduced as increasing torrefaction temperature for both torrefied wood and bio-oil samples. This reduced ratio indicates that the relative oxygen removal efficiency in the integrated process is higher than the carbon loss into char and torrefaction weight loss. As a result, the relative carbon concentration in the torrefied wood and bio-oil increases with efficient removal of the oxygen.

In the torrefaction and fast pyrolysis process, biomass mainly deoxygenates in the form of losing CO, CO_2 and H_2O. This means carbon and hydrogen in the wood are consumed as removing the oxygen. However, it is desired that more carbon which generates heating value can be retained in the bio-oil when oxygen is efficiently removed. To better understand this relationship, Fig. 2.2 presents the carbon retention versus oxygen content of both torrefied wood and bio-oil samples in the integrated process. In the torrefaction step, wood loss ~ 30% of carbon to achieve 15% oxygen removal from the raw wood. The resulting bio-oils follow a similar trend but consumed more carbon (39%) than wood with

reducing less amount of oxygen (10.5%), since a majority portion of carbon went to biochar rather than bio-oil in the fast pyrolysis step (see Fig. 2.1-A-1).

As discussed in the concept (section 3.1), bio-oil made from torrefied wood will be further upgraded though a catalytic hydrotreating process to make transportation fuel. Fig. 2.2, presents a comparative example of hydroprocessing the crude bio-oil made from pine wood (VTT) [Oasmaa et al., 2010] by Pacific Northwest National Laboratory (PNNL). In this process, the oxygen was removed by consuming added hydrogen and it can effectively retain carbon and remove most of the oxygen from the crude bio-oil. The process consumed 49.5 kg (669L) of hydrogen to upgraded one liter of crude bio-oil to oxygen content of 0.3% using Ru/C and NiMoS catalyst [Elliott et al., 2012]. If bio-oils made from severely torrefied wood go through the same hydrotreating process and assuming the hydrogen consumption is proportional to the oxygen content in the bio-oil (1.23kg/% oxygen), 23.1 kg of hydrogen maybe saved to upgraded one liter of LP-330T bio-oil, due to the low oxygen content in the bio-oil made from torrefied wood. A potential saving of hydrogen cost is around $85.5/L bio-oil (NREL estimated hydrogen production cost – $3.7/kg). In addition, based on our discussion with a refinery expert, the carbon recovery from bio-oil in the hydrotreating process could reach as high as 90%, because extensive decarboxylation already occurred in torrefaction and pyrolysis reaction and the left carbon in the bio-oil is stable under the hydroprocessing conditions. Therefore, the overall carbon retention after hydroprocessing of LP-330T bio-oil may be around 18%, about half of that of VTT upgraded bio-oil. The low carbon retention in the integrated process is due to extensive carbon loss in the torrefaction

and pyrolysis stage. In this sense, the integrated torrefaction-fast-pyrolysis process pays more renewable carbon penalty for saving expensive hydrogen.

3.3.2 Physical properties of bio-oil made from torrefied wood

Improving the physical properties of the crude bio-oil is another key interest for replacing petroleum based fuel using fast pyrolysis technology. When it comes to the oil quality, these improvements include reducing bio-oil water, solid content, acidity and viscosity as well as boosting the heating value of the bio-oil. As shown in Table 2.2, some of these properties can be improved by torrefaction pretreatment. Generally, the bio-oils produced from torrefied wood have lower water content and acidity and higher heating value than that from non-treated wood. However, these property improvements are accompanied by higher bio-oil viscosity and solid content.

3.3.2.1 Heating value of bio-oil

35-40% oxygen content (dry base) results in low heating value (~18MJ/kg) of woody biomass. If wood contains no oxygen, its heating value can be as high as ~45MJ/kg, similar to petroleum oil. Torrefaction was expected to achieve the goal of removing oxygen to get close to this ideal case. In Table 2.1 and 2.2, both torrefied wood and their resulting bio-oils have increased energy density (shown as HHV) as increasing the torrefaction temperature. However, this does not mean that the torrefaction process is making more energy from the starting wood to the bio-oil. It only concentrates the energy in the torrefied wood and bio-oil and the overall energy transferred from the starting wood to either torrefied wood or bio-oil

is actually decreasing. Fig. 2.3 presents the relationship of total heating energy change (calculated by wood and bio-oil energy density) as a function of torrefaction weight loss and pyrolysis yield when the process starts with 1kg of dry wood. As shown in Fig. 2.3, even though torrefied wood and bio-oil has increased energy density due to their low oxygen content, the total energy remained in wood and bio-oil decreased. In the torrefaction process, for example, TW-330T sample lost 30% energy due to ~46% weight loss. During pyrolysis process, because of the further energy loss into char and gas (see Fig. 2.1-C), the total energy preserved in bio-oil cannot exceed that contained in wood. The trend-line of bio-oil total energy shown in Fig. 2.3 lies underneath that of the torrefied wood. Also, when considering the negative effect of torrefaction on bio-oil yield, the total energy retained in bio-oils also reduced as increasing torrefaction severity. After the integrated torrefaction-fast-pyrolysis process, the bio-oils retain 46.5%, 34.9%, 32.6% and 20.1% of initial energy from wood for LP-Raw, LP-270T, LP-300T and LP-330T respectively. Therefore the energy densification of this integrated process was paid by the total energy loss in the final products, bio-oil.

3.3.2.2 Water content of bio-oil

Low water content in the bio-oil contributes to a smaller chance of phase separation. Bio-oil can be considered as a micro-emulsion with organic pyrolytic-lignin phase stabilized by aqueous phase composed of degradation products from holocellulose and small molecules from lignin degradation [Mohan et al., 2006]. Once the water content of bio-oil reaches a critical point, the stabilization of these two phases breaks, leading to separation of the aqueous phase from the organic phase. Additionally, lower water content also contributes to

higher heating value since water is not combustible. Therefore, reducing bio-oil water content is critical to its quality improvement.

Table 2.2 shows that the bio-oils made from torrefied wood have lower water content than that from non-treated wood. Water in bio-oil comes primarily from the moisture contained in wood and reaction water generated from thermo-degradation of the wood. The initial moisture in wood evaporated and was captured in the bio-oil under elevated temperature. As a result, decreased water content in torrefied wood (see Table 2.1 and 2.4) contributes to lower water content in the bio-oils. In addition, various dehydration reactions generate reaction water in both torrefaction and pyrolysis process. Some of the dehydration reaction occurred in torrefaction step and that reaction water was removed in the pretreatment step. Also, shown in Table 2.4, significantly reduced reaction water generated in the fast pyrolysis process can also lower water content in torrefaction-based bio-oils.

3.3.2.3 Solid content and viscosity of bio-oil

Pyrolysis oil contains a small amount of solid (determined as dichloromethane and methanol v;v=1:1 insoluble solids) originating from pyrolysis char retained in the gas stream or reaction solids comes from the secondary polymerization of bio-oil components. Thermally pretreated wood contains more fine particles that cannot be efficiently removed from pyrolysis aerosols using a cyclone. Therefore, shown in Table 2.2, the solid content in the torrefaction-based bio-oil increased with increasing torrefaction temperature. High amounts of residual char presented in the bio-oil will lead to a high possibility of secondary reaction since ash-containing char materials may perform as an effective catalyst for bio-oil

polymerization reactions. This may lead to viscosity increasing during the bio-oil shortage. Therefore, a more efficient char removal strategy, such as hot gas filtration may be needed to overcome this drawback.

As an intermediate for transportation fuel, bio-oil needs to be pumped in various processes, including transportation, upgrading, and combustion in engines. High bio-oil viscosity leads to expensive energy consumption during the transportation, therefore lowing bio-oil viscosity is also critical to bio-oil application. However, as shown in Table 2.2, bio-oils made from torrefied wood have increased dynamic viscosity compared to that from non-treated wood. With lower water and higher solid content in torrefaction-based bio-oils, viscosity increase is a predictable trend. In addition the increased viscosity may be also related to the different chemical composition of bio-oils made from torrefied wood, i.e. high amount of pyrolytic lignin fraction in bio-oil from severely torrefied wood (see Fig. 2.5). Fortunately, the increased viscosity of these bio-oils shown in Table 2.2 is still well under that of heavy crude bio-oil (10,000 cp) and they flow freely under room temperature, therefore, slightly increased viscosity caused by torrefaction is not a significant issue for their applications.

3.3.2.4 Acidity of bio-oil

High acidity of bio-oil causes potential corrosion to the storage and upgrading infrastructure. Acids in the bio-oil also catalyze various condensation reactions, i.e. aldol condensation and accelerate the aging rate of the bio-oil. Hence, reducing bio-oil acidity is crucial to its upgrading and stability. Chemical composition analysis of torrefaction volatiles

found various acids [Yan et al., 2010], mostly acetic acid was released during the heat treatment and this effect may rend the bio-oil made from pretreated wood with lower acidity.

pH measurement and acid-base titration are the two adopted methods for the bio-oil acidity characterization [Oasmaa and Meier, 2005; Oasmaa et al., 2010]. However, using pH measurement to estimate the acidity of bio-oil is not correct. Because this method is particularly designed for an aqueous system, mainly water, to measure the concentration of hydronium ion. Bio-oil does contain water, but also contain various other organic solvents and even solids; the ratio of these components often vary significantly from different samples. Developing a well-defined pH scale for this unstable complex mixture has not been reported and the determined pH value will be very sensitive to the water content in the bio-oil and the contact of pH probe with hydronium ion in the bio-oil as well. Secondly, in order to get an accurate pH value for the bio-oil, the pH meter has to be calibrated with pH standard dissolved in the same solvent system as bio-oil has; however pH meter is usually calibrate with buffer solution with water as solvent. This means that the pH value obtained from bio-oil measurement do not reflect its true value, because it is calibrated with a wrong solvent system. Therefore the pH measurement showed in Table 2.2 is only for comparison and they do not reflect the actual pH value of the bio-oils. For these concerns, the total acid number (TAN) obtained from the acid-base titration, adopted from petroleum industry is becoming more accepted index for bio-oil acidity characterization. In this titration method, inflection point is applied as an indicator of the end point of the titration. However, in some cases, such as aged bio-oil, absence of the inflection point often occurred; therefore the buffer potential

method (pH=11) is often used as a substitution. This work employed both inflection point and buffer potential method to determine the TAN value of the bio-oils.

In Table 2.2, according to the pH value and TAN value (determined by infection point), the bio-oils originated from torrefied wood becomes less acidic than that made from non-torrefied wood. This can be explained by the reduced amounts of acid components in the bio-oil due to pre-releasing of acids in the thermal pretreatment stage. However, TAN values determined by the buffer potential method indicate a reversed trend. The bio-oils made from torrefied wood have higher TAN value (determined by the buffer potential method) than that from non-treated feedstock. The gap of these TAN results is associated with the nature of two end-point determination methods. By correlating the potential readings with pH values using the Nernst equation, we found that the pH value of the inflection point resides in the range of 8-9. In this region, the possible dominant acid species in the bio-oil, carboxylic acids, have been titrated to their conjugated base form, due to their relatively low pKa value - 4.5. Therefore, it may be inferred that the inflection point can only be used to quantify the amount of weak carboxylic acids in the bio-oil. On the other hand, the TAN value determined by the buffer potential method, reflects not only the amount of carboxylic acids but also other weaker acids, such as phenolic compounds (pKa~10); because the buffer potential reading is obtained in a pH 11 environment where phenolic hydroxyl groups dissociated. In addition, in the alkaline condition, esters in the bio-oil may undergo a de-esterification reaction, releasing acids and consuming potassium hydroxide. The above inference can be well supported by investigating the titration curve in Fig. 2.4. It can be found that the initial slope of the titration curve was decreased from LP-Raw to LP-330T, indicating lower concentration of

weak acids in the torrefaction-based bio-oils. While the subsequent titration curve tends to be flat due to the depletion of weak carboxylic acids and the smaller signal change is resulted from the dissociation of much weaker acid groups - phenolic hydroxyl groups. In addition, all the titration profiles shown in Fig. 2.4 decreased slowly as increasing potassium hydroxide concentration and their inflection points occurred in basic range (pH 8-9) which fits the titration phenomenon of using strong base to titrate the weak acid. Accordingly, we may infer that bio-oil only contains weak acids and this also indicates that the bio-oil pH value shown in Table 2.2 is not reflecting its true value since pH of 2-3 indicates the presence of strong acids, such as HCl, in the bio-oil.

3.3.2.5 Chemical composition of bio-oil made from torrefied wood

The previous GC/MS analyses (summarized in Fig. 2.5-A) investigated the chemical compositional variance among bio-oils made from torrefaction-pretreated loblolly pine versus untreated pine wood. The results indicated higher amount of pyrolytic lignin and lower amount of light oxygenates presented in torrefaction based bio-oils. These results, however, only partially reveal the bio-oil composition due to the limitation of sample volatility. In this study, the solvent fractionation method was adopted to separate the bio-oil components according to their solubility in different solvents which illustrates the whole composition difference among these bio-oils.

There is a clear compositional variance between bio-oils produced from the torrefied wood and that from the raw wood. In Fig. 2.5-B, the pyrolytic lignin fraction, either HMM, LMM or their combination, shows clear increasing trend as torrefaction severity increased.

This is consistent with the increased phenolic content shown in Fig. 2.5-A. Both ES fraction and EIS fraction decreased. The reducing trend of ES fraction supports the data shown in Fig. 2.5-A as ES fraction contains mainly aldehydes, ketones, acids, alcohols and esters. Decreased EIS fraction is not consistent with the sugar fraction detected by GC/MS because only anhydrosugar, levoglucosan can be found using the GC/MS while EIS fraction quantifies the whole sugar fraction in the bio-oil. This composition variance caused by torrefaction pretreatment can be explained by different chemical composition of pyrolysis feedstock; because under identical pyrolysis conditions, the bio-oil composition directly depends on the composition of the wood materials. As shown in Table 2.1, torrefaction removes holocellulose from the biomass and renders the torrefied wood with concentrated lignin residues; therefore increased lignin fraction in bio-oil is predictable. As the ES fraction and EIS fraction are mainly derived from thermal degradation of cellulose and hemicellulose, their significant degradation at the torrefaction stage will certainly decrease the amount of light oxygenates and sugars in the bio-oil and therefore decreasing the amounts of ES and EIS fraction. From both GC/MS and solvent fractionation method, it can be conclude that bio-oil made from torrefied wood has different chemical composition to that from non-treated wood. Torrefaction-based bio-oil has high concentration of pyrolytic lignin and less degradation products from holocellulose. Concentrated pyrolytic lignin fraction indicates the potential of using these bio-oils as chemical raw materials for making value-added chemical products, i.e. replacing phenolic compounds in resin/wood adhesives production [Cheng et al., 2012; Stanzione 2013]. Reduced light oxygenates (ES) and sugar fraction (EIS), may contribute to the further upgrading process by generating less catalyst coke and improve the

catalyst stability, since these two fractions are often identified as the precursor for coking formation. [Gayubo et al., 2005; Wildschut et al., 2009] In fact, Hilten [Hilten et al., 2013a] found that upgrading bio-oil from torrefaction pretreated wood using zeolite catalyst generates less reactor char and less catalyst coke and tar. In addition, Hilten [Hilten et al., 2013b] also found that torrefaction improved the catalyst effectiveness for minimizing its property change after the upgrading process. These promising results may supports our hypothesis that the hydroprocessing performance of bio-oil made from torrefied wood can be enhanced.

3.3.3 ^{1}H and ^{13}C NMR characterization of bio-oil made from torrefied wood

To further confirm the chemical composition results of bio-oil obtained from GC/MS and solvent fraction method, ^{1}H and ^{13}C NMR characterization of bio-oil made from torrefied wood were also performed. The ^{13}C NMR spectra are very similar to those previously report [Zheng et al., 2012]. Table 2.5 summarizes the carbon distribution in the bio-oils made from torrefied wood. As increasing torrefaction temperature, the content of carbonyl carbon, methoxy and hydroxyl carbon decreased, while the aromatic and alkyl carbon content increased. This is consistent with the findings obtained from GC/MS and solvent fraction method, that torrefaction-based bio-oil contains lower amount of light oxygenates, i.e. aldehydes and acids (ES soluble fraction) but higher amount of phenolic compounds. ^{1}H NMR is less reliable than ^{13}C NMR for elucidating the chemical composition change in the bio-oils due to its narrow chemical shift range and significantly overlapped signals. Therefore, the integrated data summarized in Table 2.6 shows less pronounced trend of

hydrogen distribution among different samples than ^{13}C NMR does. However, results obtained from several distinctive narrow integration ranges are still informative. Table 2.6 tentatively supports the results from ^{13}C NMR that bio-oil made from torrefied wood contains less aldehydes, ketones and acids but more hydrocarbons as less carbonyl and carboxyl protons (8.0-10.0 ppm) but more aliphatic protons (0-1.6 ppm) were found as increasing torrefaction temperature. Also, the reduced proton signal (6.8-8.0 ppm) attached to aromatics may suggest more condensed pyrolytic lignin structure in the bio-oils. Overall, the carbon and proton distribution well supports the chemical composition results obtained from the GC/MS and solvent fraction method.

3.3.4 Quantification of major chemical compounds in bio-oil made from torrefied wood

Biomass pyrolysis can be considered as a sum of thermal degradation of holocellulose and lignin. These wood matrix-components have their distinct pyrolysis products. Therefore, investigating their appearance and concentration change in the bio-oil is beneficial to the understanding of how torrefaction affects the biomass pyrolysis chemistry.

Glycolaldehyde (hydroxyacetaldehyde), acetol (hydroxyacetone) and levoglucosan (1,6-anhydro-β-D-glucopyranose) are the major thermal degradation markers from cellulose pyrolysis [Shen and Gu, 2009]. The former two can also be generated from hemicellulose pyrolysis. Glycolaldehyde and acetol are believed to be the ring-opening products from active cellulose; while levoglucosan is the dehydration products from cellulose monomers in which the C6 ring was kept. In Fig. 2.6-A, it shows that glycolaldehyde and acetol generally decreased in the bio-oils from torrefaction treated wood as increasing torrefaction severity;

while the primary thermal degradation product, levoglucosan, increased. Since the holocellulose content decreased in the torrefied wood as increasing torrefaction severity, lower concentration of glycolaldehyde and acetol in the bio-oils is expected. However, an interesting observation is that levoglucosan disobey this expectation and detailed reason will be discussed in next chapter. As extensively identified, [Shen and Gu, 2009] acetic acid and furfural are the major thermal degradation products from hemicellulose. Acetic acid can also be thermally produced from cellulose degradation. Formic acid and hydroxymethylfurfural (HMF) are minor degradation products derived from cellulose. Similar to Liaw's finding [Liaw et al., 2013], due to gradually decreased holocellulose content in the torrefied wood, acetic acid, formic acid, HMF and furfural concentration shown in Fig. 2.6-B generally decreased in the bio-oils as increasing torrefaction temperature. Removing these reactive components may contribute to the improved bio-oil stability during storage and upgrading process.

Due to highly complex lignin structure, the mechanism of lignin pyrolysis is not well understood. One common reaction happened to lignin pyrolysis is the demethoxylation reaction. [Jiang et al., 2010] This reaction is believed to be a free radical reaction [Ben and Ragauskas, 2011] which may produce phenol and catechol or their derivatives depending on the reaction pathway. As show in Fig. 2.7-A and Fig. 2.7-B, the content of phenol, catechol and o-cresol significantly increased in the torrefaction based bio-oils; while the content of guaiacol, eugenol, isoeugenol, vanillin and 2-methoxy-4-methy-phenol first increased and then decreased. A well-developed explanation of these facts may not be able to drawn without deep understanding of the lignin pyrolysis mechanism and lignin structure. However,

a tentative inference can be projected as during the torrefaction pretreatment, lignin structure fragments, represented as homolysis of the lignin backbone and cleavage of the ether and C-C bonds, [Kuroda and Nakagawa-izumi, 2006; Evans et al., 1986; Bayerbach and Meier, 2009] creating more possible reaction site for the lignin monomer to be peeled off from the lignin main body in the following pyrolysis reaction; therefore the concentration of lignin monomers with/without methoxy-groups should increase as increasing torrefaction temperature. However due to the extensive demethoxylation occurred during torrefaction process, the torrefied wood lignin tends to have less available methoxy-groups than that of the raw wood [Park et al., 2013], therefore, less guaiacyl type lignin-pyrolysis-markers (with methoxy groups) are released during pyrolysis step. This explains why the content of guaiacyl type lignin decreased after high temperature torrefaction-treating. In addition, there is an inter-conversion between the precursors of guaiacyl type monomer to that of catechol and phenol precursor during torrefaction pretreatment as shown in Fig. 2.8. Such inter-conversion would yields less guaiacyl type lignin monomer but keeps increasing the concentration of catechol and phenol in the bio-oils as increasing the torrefaction severity (increasing demethoxylation degree).

3.4 Technical and economic barriers of torrefaction pretreatment

As discussed, torrefaction has positive effect on reducing bio-oil oxygen content as well as improving some of its physical and chemical properties and altering its chemical compositions. However, its negative effect on the bio-oil yield cannot be ignored. There are three types of deoxygenation mechanism for reducing bio-oil oxygen content in biomass

thermoconversion process, that is, decarboxylation, dehydration and hydrodeoxygenation. Torrefaction pretreatment reduce oxygen content in the bio-oil mainly by promoting the dehydration and decarboxylation reactions with wood at relatively low temperature. These two reactions consume carbon and hydrogen from the starting materials and generate torrefaction weight loss. The carbon consumption dominates the pretreatment process. After the torrefaction pretreatment, up to 30% carbon was lost as torrefaction weight loss to achieve 15% oxygen content reduction. How to design torrefaction conditions by selectively removing oxygen as CO_2 as consuming less carbon is critical to the process economics. Other than dry-torrefaction employed in this study, the effect of wet-torrefaction on bio-oil production has not investigated. This wet-torrefaction technology may be able to achieve same effect as improving bio-oil quality but reducing the carbon loss during the pretreatment. Also, effectively recycle the torrefaction weight loss as generating process heat and/or reforming it as syngas might be another strategy to compensate the negative impact on bio-oil yield. In the pyrolysis process, wood becomes more thermally recalcitrant to the pyrolysis conditions due to its highly condensed structure after heat pretreatment. Carbon and energy from starting wood are more favorably to be retained in the biochar rather than the bio-oil. This indicates that regular pyrolysis conditions are not favorable for the less reactive torrefied wood materials. How to optimize the pyrolysis conditions and reactor design targeting for the less reactive torrefied wood is needed. In fact, if these optimal conditions could not be found, changing the thermoconversion pathway to liquefaction may be another option. In summary, the main technical barrier for this integrated torrefaction-fast-pyrolysis process lies on the potential of increasing the production yield of high-quality bio-oil.

Except the negative impact on bio-oil yield, torrefaction pretreatment may also need an extra reactor to the existing pyrolysis infrastructure and this could increase the capital cost of the overall process. However, investing a torrefaction reactor may not be necessary; because this torrefaction reactor can be a combined with the drying reactor which is already equipped in the calculated pyrolysis production line. The torrefaction reactor can also be combined with a pyrolysis reactor, because the difference between torrefaction and fast pyrolysis is the residence time and temperature. Programming the pyrolysis reactor to perform both biomass torrefaction pretreatment and fast pyrolysis is possible and promising. In this sense, the capital cost on torrefaction reactor can be a minor issue. The torrefaction treatment also needs extra energy to heat the wood. In addition to the biomass drying energy, this amount of pretreatment energy can be supplied by burning the torrefaction volatile and/or char produced from the fast pyrolysis step. Therefore, energy cost on this pretreatment step may be self-sustained.

Decreased bio-oil yield and extra cost on pretreatment reactor and energy deteriorate the overall economics of this integrated process. However, by carefully design a fully integrated process, i.e. recycling the torrefaction weight loss, this negative effect may be minimized. Significant energy saving on grinding torrefied biomass is another potential plus to the process energy balance. In addition, the improved bio-oil quality may contributes to enhanced bio-oil upgrading performance, i.e. saving hydrogen and reducing coke formation; therefore it has a potential to cancel some of the negative effect as well. The final economic outcome of the integrated process lies between the extra cost generated by pretreatment process and the significance of the benefits that torrefaction can bring to the upgrading

process. Without additional hydrotreating results on bio-oils made from torrefied wood, a firm conclusion about the overall economics is not clear.

4. Conclusions

The overall effect of torrefaction pretreatment on bio-oil production via fast pyrolysis has been investigated. It is concluded that torrefaction pretreatment affect the chemical composition of pretreated wood by removing holocellulose and retaining lignin and char residues. As a result, the fuel properties of the pretreated wood were improved as oxygen content reduced. Further pyrolysis of this high quality feedstock produced bio-oil with reduced oxygen content as expected. In addition, the bio-oil physical and chemical properties (i.e. water content, acidity, energy density) were also improved as a consequence of torrefaction pretreatment. However, the torrefaction weight loss and the thermal recalcitrance of torrefied wood limit the production yield of the high quality bio-oil.

Confirmed by GC/MS, solvent fractionation and ^{13}C and ^{1}H NMR analyses, bio-oils made from torrefied wood contain lower amount of reactive oxygenates, i.e. acids and aldehydes, and sugars but rich in pyrolytic lignin. The concentration of certain pyrolysis marks from holocellulose (i.e. glycolaldehyde and acetic acid) decreased as torrefaction severity increased. However, the content of major cellulose pyrolysis product, levoglucosan increased as increasing torrefaction severity. The content of certain lignin pyrolysis monomers, i.e. catechol increased, while guaiacyl type monomer first increased and then decreased as increasing torrefaction severity. This can be explained by the extensive demethoxylation of native lignin in the pretreated wood.

5. Acknowledgements

This study was supported by Southeastern Sun Grant Center, the US Department of Transportation (Grant No. DTO559-07-G-00050) and the National Science Foundation (Grant No. 0832498). The author would like to thank Chris Hopkins at North Carolina State University for providing heat-treated wood samples, Dr. David Dayton and John Carpenter at RTI International for the help on measuring bio-oil TAN number.

References

Aho, A., DeMartini, N., Pranovich, A., Krogell, J., Kumar, N., Eränen, K., Holmbom, B., Salmi, T., Hupa, M., Murzin, D.Y. 2013. Pyrolysis of pine and gasification of pine chars – Influence of organically bound metals. Bioresource Technology, 128(0), 22-29.

Balagurumurthy, B., Oza, T., Bhaskar, T., Adhikari, D. 2013. Renewable hydrocarbons through biomass hydropyrolysis process: challenges and opportunities. Journal of Material Cycles and Waste Management, 15(1), 9-15.

Bayerbach, R., Meier, D. 2009. Characterization of the water-insoluble fraction from fast pyrolysis liquids (pyrolytic lignin). Part IV: Structure elucidation of oligomeric molecules. Journal of Analytical and Applied Pyrolysis, 85(1–2), 98-107.

Ben, H., Ragauskas, A.J. 2011. Heteronuclear Single-Quantum Correlation–Nuclear Magnetic Resonance (HSQC–NMR) Fingerprint Analysis of Pyrolysis Oils. Energy & Fuels, 25(12), 5791-5801.

Boateng, A.A., Mullen, C.A. 2013. Fast pyrolysis of biomass thermally pretreated by torrefaction. Journal of Analytical and Applied Pyrolysis, 100(0), 95-102.

Bridgwater, A.V. 1996. Production of high grade fuels and chemicals from catalytic pyrolysis of biomass. Catalysis Today, 29(1–4), 285-295.

Carlson, T., Tompsett, G., Conner, W., Huber, G. 2009. Aromatic Production from Catalytic Fast Pyrolysis of Biomass-Derived Feedstocks. Topics in Catalysis, 52(3), 241-252.

Cheng, S., Yuan, Z., Anderson, M., Leitch, M., Xu, C. 2012. Synthesis of biobased phenolic resins/adhesives with methylolated wood-derived bio-oil. Journal of Applied Polymer Science, 126(S1), E431-E441.

Couhert, C., Salvador, S., Commandré, J.M. 2009. Impact of torrefaction on syngas production from wood. Fuel, 88(11), 2286-2290.

Dence, C.W. 1992. The Determination of Lignin. in: Methods in Lignin Chemistry, (Eds.) S. Lin, C. Dence, Springer Berlin Heidelberg, pp. 33-61.

Diebold, J.P. 2002. A Review of the Chemical and Physical Mechanisms of the Storage Stability of Fast Pyrolysis Bio-Oils. in: Fast Pyrolysis of Biomass: A handbook, (Ed.) A.V. Bridgwater, CPL Press. Newbury, U.K., pp. 205-241.

Elliott, D.C. 2007. Historical Developments in Hydroprocessing Bio-oils. Energy & Fuels, 21(3), 1792-1815.

Elliott, D.C., Hart, T.R. 2008. Catalytic Hydroprocessing of Chemical Models for Bio-oil. Energy & Fuels, 23(2), 631-637.

Elliott, D.C., Hart, T.R., Neuenschwander, G.G., Rotness, L.J., Olarte, M.V., Zacher, A.H., Solantausta, Y. 2012. Catalytic Hydroprocessing of Fast Pyrolysis Bio-oil from Pine Sawdust. Energy & Fuels, 26(6), 3891-3896.

Evans, R.J., Milne, T.A., Soltys, M.N. 1986. Direct mass-spectrometric studies of the pyrolysis of carbonaceous fuels: III. Primary pyrolysis of lignin. Journal of Analytical and Applied Pyrolysis, 9(3), 207-236.

French, R., Czernik, S. 2010. Catalytic pyrolysis of biomass for biofuels production. Fuel Processing Technology, 91(1), 25-32.

Gayubo, A.G., Aguayo, A.T., Atutxa, A., Valle, B., Bilbao, J. 2005. Undesired components in the transformation of biomass pyrolysis oil into hydrocarbons on an HZSM-5 zeolite catalyst. Journal of Chemical Technology & Biotechnology, 80(11), 1244-1251.

Hilten, R.N., Speir, R.A., Kastner, J.R., Mani, S., Das, K.C. 2013. Effect of Torrefaction on Bio-oil Upgrading over HZSM-5. Part 1: Product Yield, Product Quality, and Catalyst Effectiveness for Benzene, Toluene, Ethylbenzene, and Xylene Production. Energy & Fuels, 27(2), 830-843.

Hilten, R.N., Speir, R.A., Kastner, J.R., Mani, S., Das, K.C. 2012. Effect of Torrefaction on Bio-oil Upgrading over HZSM-5. Part 2: Byproduct Formation and Catalyst Properties and Function. Energy & Fuels, 27(2), 844-856.

Hossain, A.K., Davies, P.A. 2013. Pyrolysis liquids and gases as alternative fuels in internal combustion engines – A review. Renewable and Sustainable Energy Reviews, 21(0), 165-189.

Ingram, L., Mohan, D., Bricka, M., Steele, P., Strobel, D., Crocker, D., Mitchell, B., Mohammad, J., Cantrell, K., Pittman, C.U. 2007. Pyrolysis of Wood and Bark in an Auger Reactor: Physical Properties and Chemical Analysis of the Produced Bio-oils. Energy & Fuels, 22(1), 614-625.

Jiang, G., Nowakowski, D.J., Bridgwater, A.V. 2010. Effect of the Temperature on the Composition of Lignin Pyrolysis Products. Energy & Fuels, 24(8), 4470-4475.

Kuroda, K.-i., Nakagawa-izumi, A. 2006. Analytical pyrolysis of lignin: Products stemming from β-5 substructures. Organic Geochemistry, 37(6), 665-673.

Liaw, S.-S., Zhou, S., Wu, H., Garcia-Perez, M. 2013. Effect of pretreatment temperature on the yield and properties of bio-oils obtained from the auger pyrolysis of Douglas fir wood. Fuel, 103(0), 672-682.

Melero, J.A., Iglesias, J., Garcia, A. 2012. Biomass as renewable feedstock in standard refinery units. Feasibility, opportunities and challenges. Energy & Environmental Science, 5(6), 7393-7420.

Meng, J., Park, J., Tilotta, D., Park, S. 2012. The effect of torrefaction on the chemistry of fast-pyrolysis bio-oil. Bioresource Technology, 111(0), 439-446.

Mohan, D., Pittman, C.U., Steele, P.H. 2006. Pyrolysis of Wood/Biomass for Bio-oil: A Critical Review. Energy & Fuels, 20(3), 848-889.

Mullen, C.A., Boateng, A.A., Mihalcik, D.J., Goldberg, N.M. 2011. Catalytic Fast Pyrolysis of White Oak Wood in a Bubbling Fluidized Bed. Energy & Fuels, 25(11), 5444-5451.

Oasmaa, A., Elliott, D.C., Korhonen, J. 2010. Acidity of Biomass Fast Pyrolysis Bio-oils. Energy & Fuels, 24(12), 6548-6554.

Oasmaa, A., Kuoppala, E. 2003. Fast Pyrolysis of Forestry Residue. 3. Storage Stability of Liquid Fuel. Energy & Fuels, 17(4), 1075-1084.

Oasmaa, A., Meier, D. 2005. Norms and standards for fast pyrolysis liquids: 1. Round robin test. Journal of Analytical and Applied Pyrolysis, 73(2), 323-334.

Oasmaa, A., Solantausta, Y., Arpiainen, V., Kuoppala, E., Sipilä, K. 2009. Fast Pyrolysis Bio-Oils from Wood and Agricultural Residues. Energy & Fuels, 24(2), 1380-1388.

Park, J., Meng, J., Lim, K.H., Rojas, O.J., Park, S. 2013. Transformation of lignocellulosic biomass during torrefaction. Journal of Analytical and Applied Pyrolysis, 100(0), 199-206.

Phanphanich, M., Mani, S. 2011. Impact of torrefaction on the grindability and fuel characteristics of forest biomass. Bioresource Technology, 102(2), 1246-1253.

Prins, M.J., Ptasinski, K.J., Janssen, F.J.J.G. 2006. More efficient biomass gasification via torrefaction. Energy, 31(15), 3458-3470.

Prins, M.J., Ptasinski, K.J., Janssen, F.J.J.G. 2006. Torrefaction of wood: Part 2. Analysis of products. Journal of Analytical and Applied Pyrolysis, 77(1), 35-40.

Ren, S., Lei, H., Wang, L., Bu, Q., Chen, S., Wu, J., Julson, J., Ruan, R. 2013. The effects of torrefaction on compositions of bio-oil and syngas from biomass pyrolysis by microwave heating. Bioresource Technology, 135(0), 659-664.

Sharma, R.K., Bakhshi, N.N. 1993. Catalytic upgrading of pyrolysis oil. Energy & Fuels, 7(2), 306-314.

Shen, D.K., Gu, S. 2009. The mechanism for thermal decomposition of cellulose and its main products. Bioresource Technology, 100(24), 6496-6504.

Sluiter, A., Hames, B., Ruiz, R., Scarlata, C., Sluiter, J., Templeton, D., Crocker, D. (2008). NREL Laboratory Analytical Procedure. NREL/TP-510-42618, 1-18. Retrieved from http://www.nrel.gov/biomass/pdfs/42618.pdf

Stanzione, J.F., Giangiulio, P.A., Sadler, J.M., La Scala, J.J., Wool, R.P. 2013. Lignin-Based Bio-Oil Mimic as Biobased Resin for Composite Applications. ACS Sustainable Chemistry & Engineering, 1(4), 419-426.

Vispute, T.P., Zhang, H., Sanna, A., Xiao, R., Huber, G.W. 2010. Renewable Chemical Commodity Feedstocks from Integrated Catalytic Processing of Pyrolysis Oils. Science, 330(6008), 1222-1227.

Wildschut, J., Mahfud, F.H., Venderbosch, R.H., Heeres, H.J. 2009. Hydrotreatment of Fast Pyrolysis Oil Using Heterogeneous Noble-Metal Catalysts. Industrial & Engineering Chemistry Research, 48(23), 10324-10334.

Yan, W., Hastings, J.T., Acharjee, T.C., Coronella, C.J., Vásquez, V.R. 2010. Mass and Energy Balances of Wet Torrefaction of Lignocellulosic Biomass†. Energy & Fuels, 24(9), 4738-4742.

Zheng, A., Zhao, Z., Chang, S., Huang, Z., He, F., Li, H. 2012. Effect of Torrefaction Temperature on Product Distribution from Two-Staged Pyrolysis of Biomass. Energy & Fuels, 26(5), 2968-2974.

Zheng, A., Zhao, Z., Chang, S., Huang, Z., Wang, X., He, F., Li, H. 2013. Effect of torrefaction on structure and fast pyrolysis behavior of corncobs. Bioresource Technology, 128(0), 370-377.

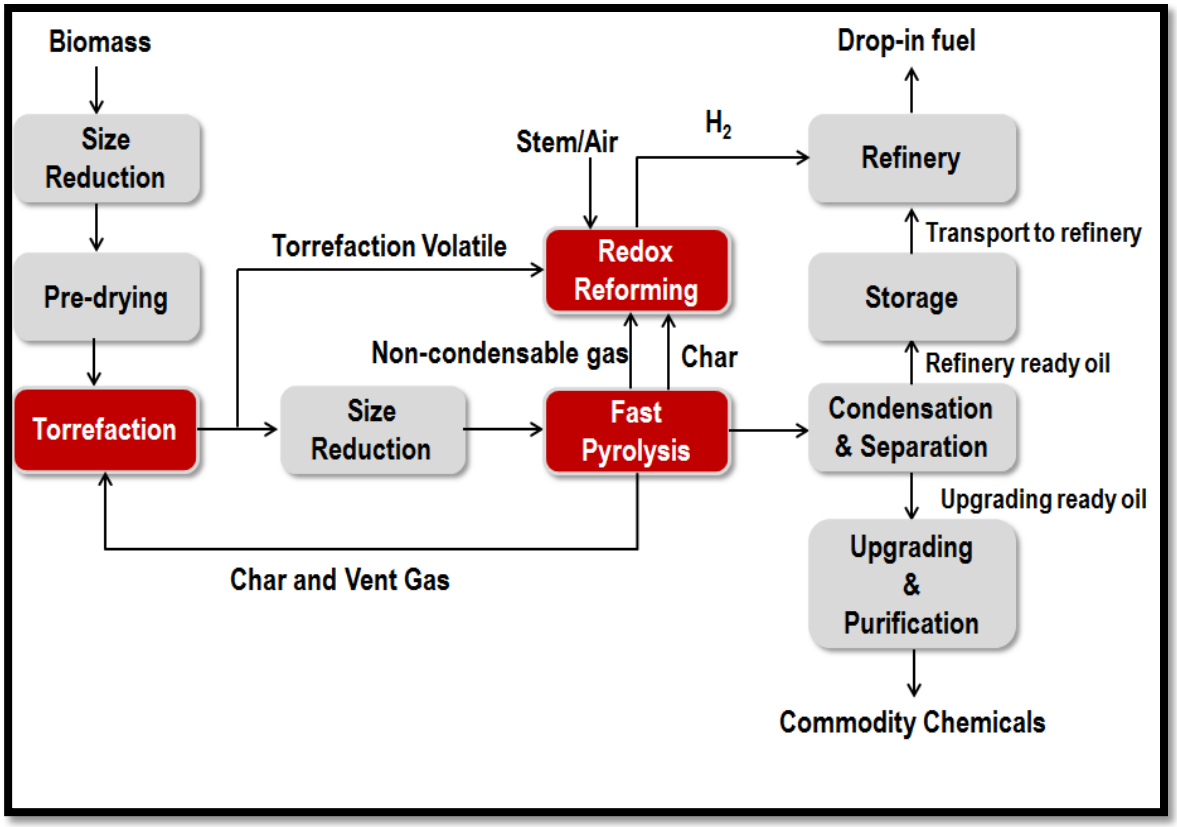

Scheme 2.1 Block diagram of integrated torrefaction-fast-pyrolysis concept.

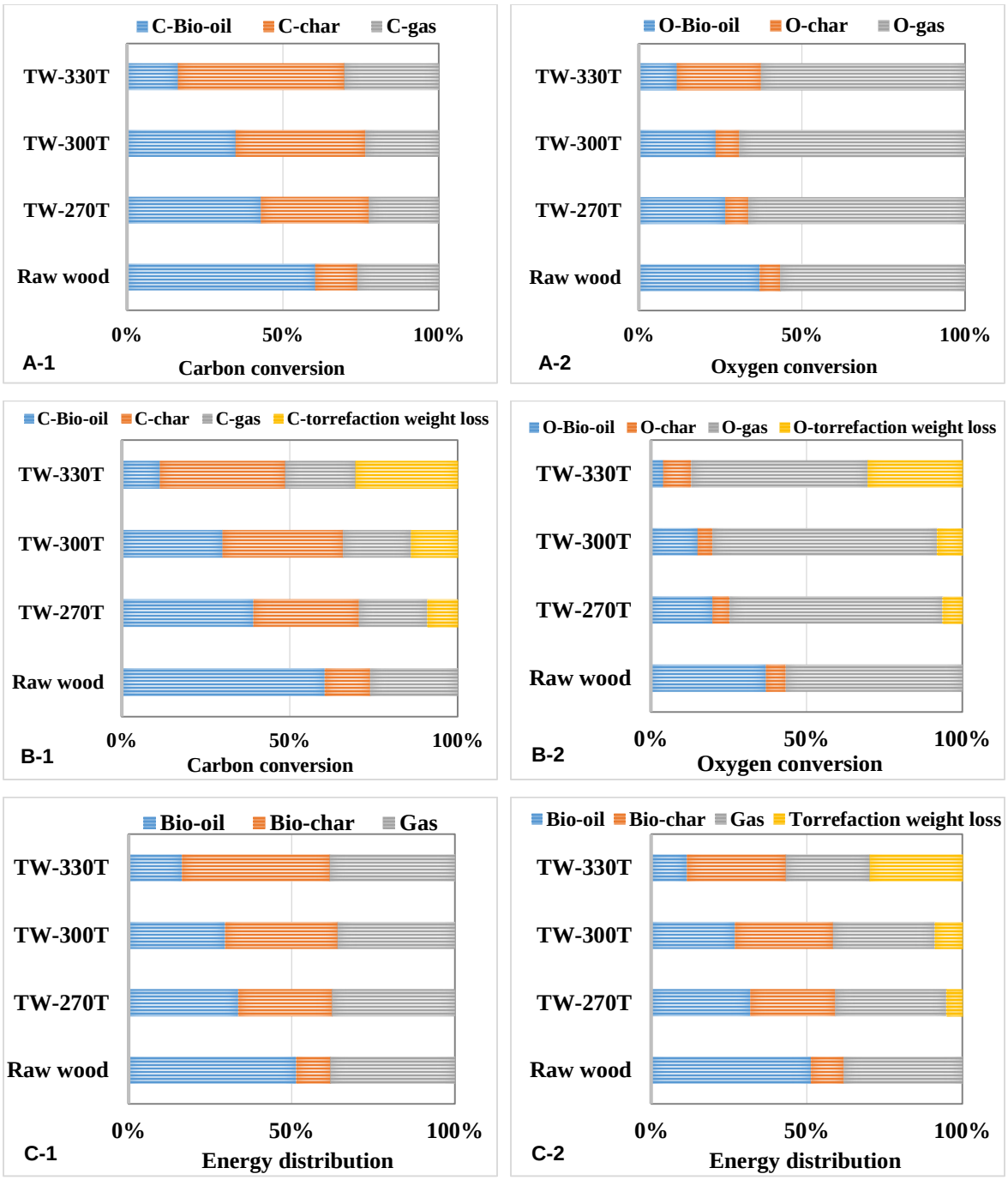

Figure 2.1 Carbon (A), oxygen (B) and energy (C) balance in fast pyrolysis step (A-1, B-1 and C-1) and integrated torrefaction-fast-pyrolysis process (A-2, B-2 and C-2).

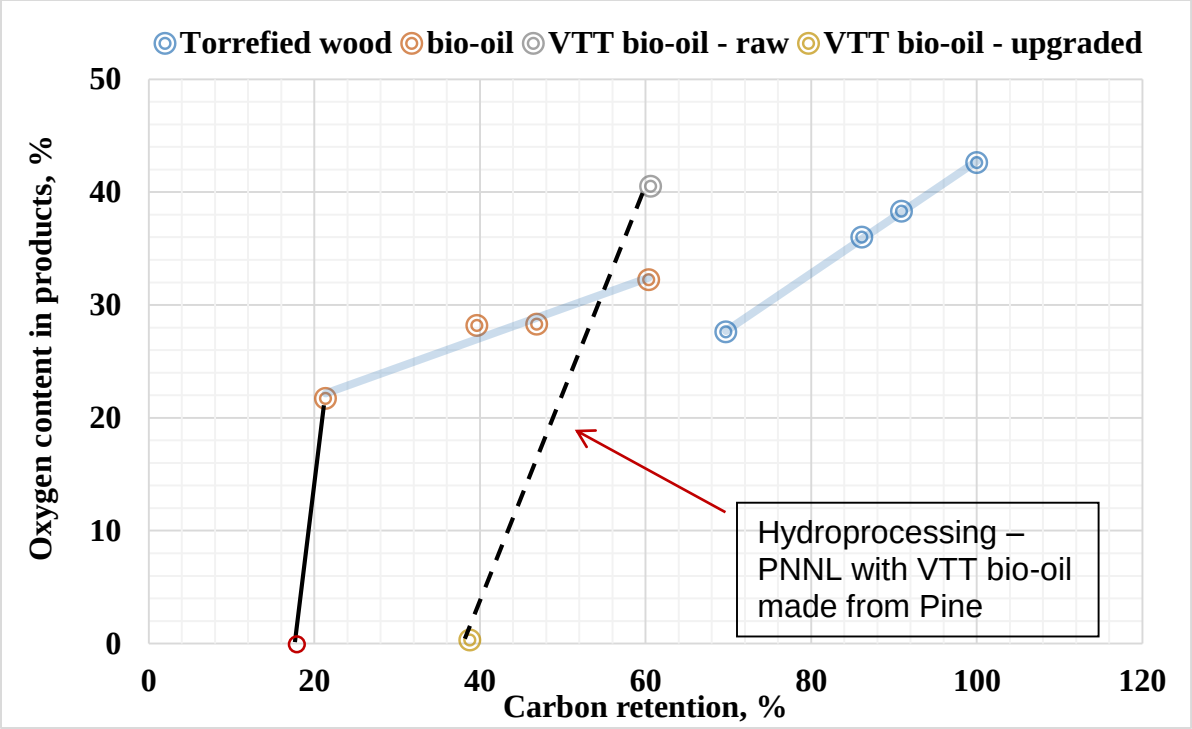

Figure 2.2 Carbon retention vs oxygen content in products. The long-dash-line (left) indicates the hydroprocessing process conducted by PNNL with VTT bio-oil made from pine wood and the black solid line (right) indicates the predicted hydroprocessing process with LP-330T bio-oil. VTT bio-oil production [Oasmaa et al., 2010]: fast pyrolysis of pine wood (50.5% carbon on dry base) was conducted with a PDU pyrolysis system at 520 ºC. The bio-oil yield is 74% (17% water) on dry biomass base; the bio-oil contained 45.7 % carbon on dry base. PNNL hydroprocessing [Elliott et al., 2012]: hydroprocessing tests were performed in a continuous-flow reactor with two catalytic beds, sulfide Ru/C and sulfide promoted Mo catalyst. The feed bio-oil from VTT contained 53.0% carbon and 40.5% oxygen on moisture free base and bio-oil hydroprocessing yield is 0.35 g/g dry feed with time on stream (TOS) of 4.5-20.6 hour. The hydroprocessing product contained 83.5% carbon and 0.3% oxygen on dry base.

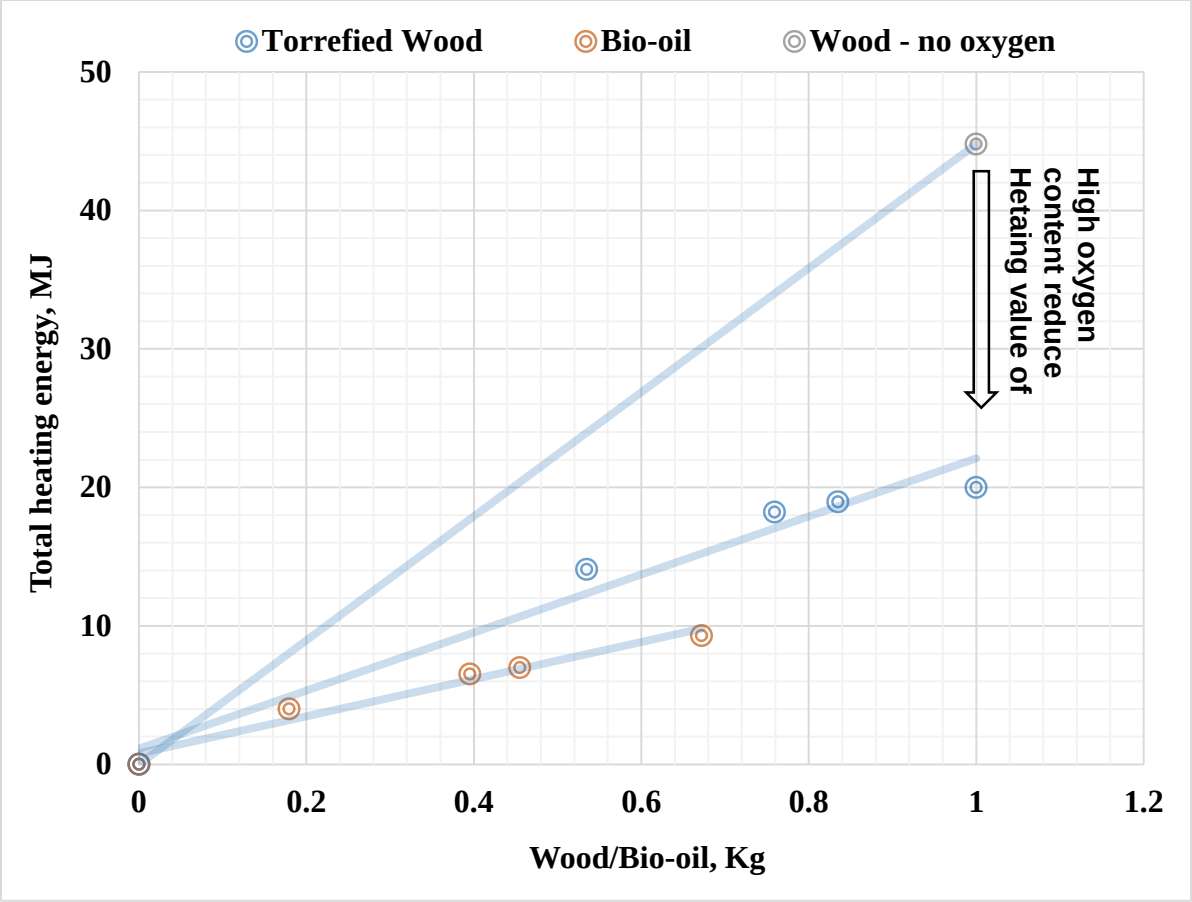

Figure 2.3 Total heating value of torrefied wood and resulting bio-oil.

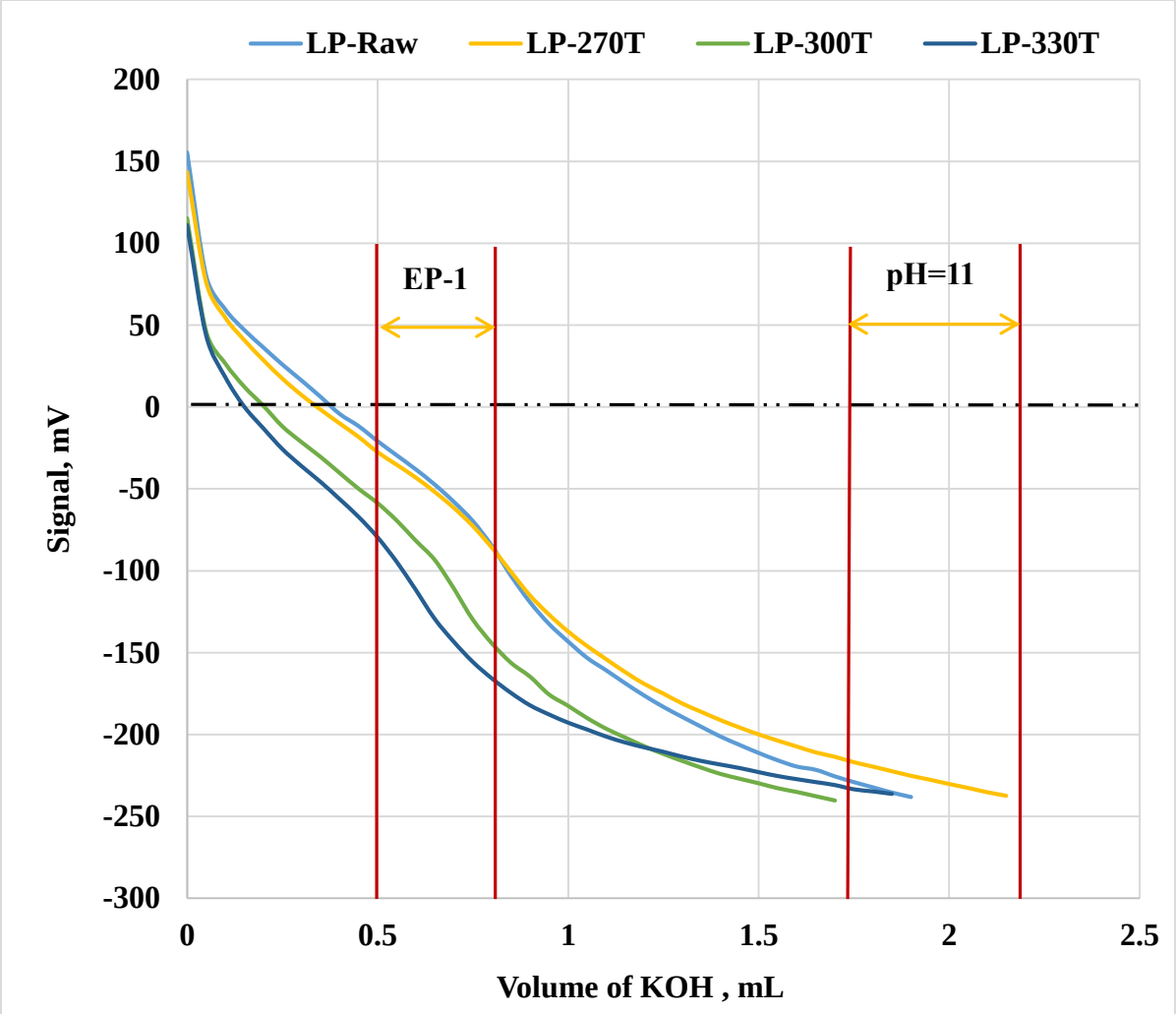

Figure 2.4 Acid-Base titration curve of bio-oils.

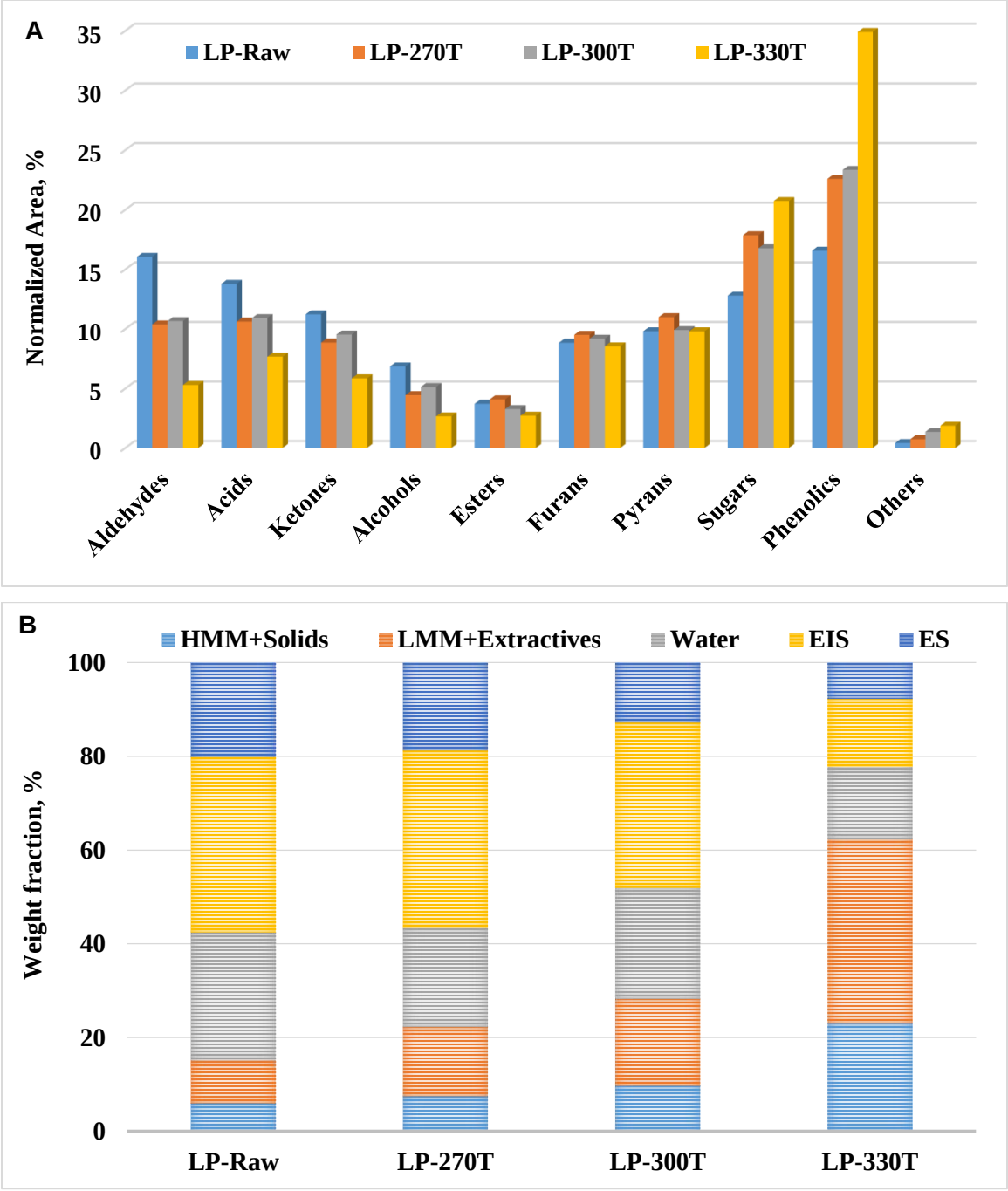

Figure 2.5 Chemical composition of bio-oils determined by (A) GC/MS method, data was normalized by the total detectable area in the GC chromatography; (B) solvent fractionation method.

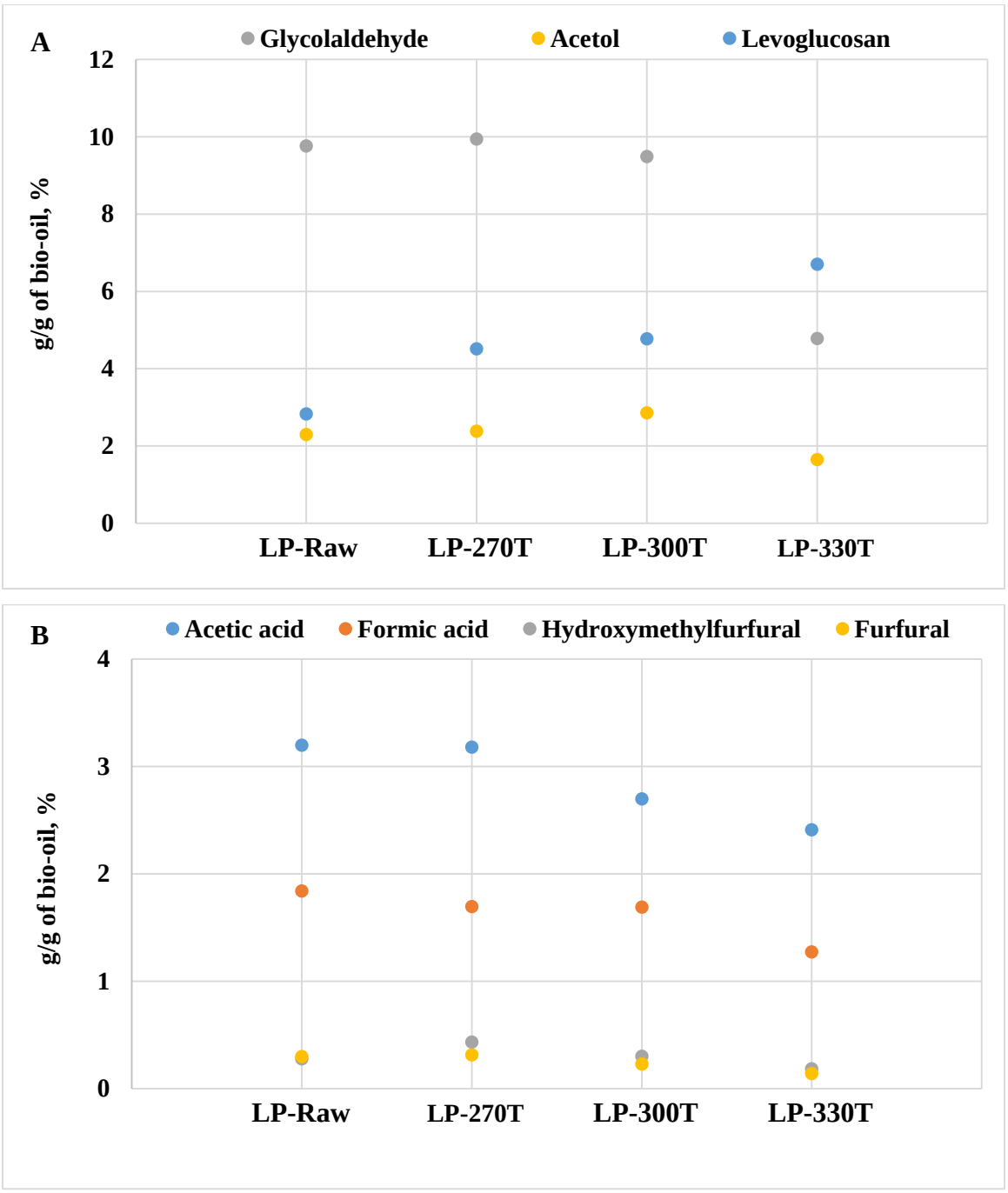

Figure 2.6 GC/MS quantification of major carbohydrate degradation products in bio-oils.

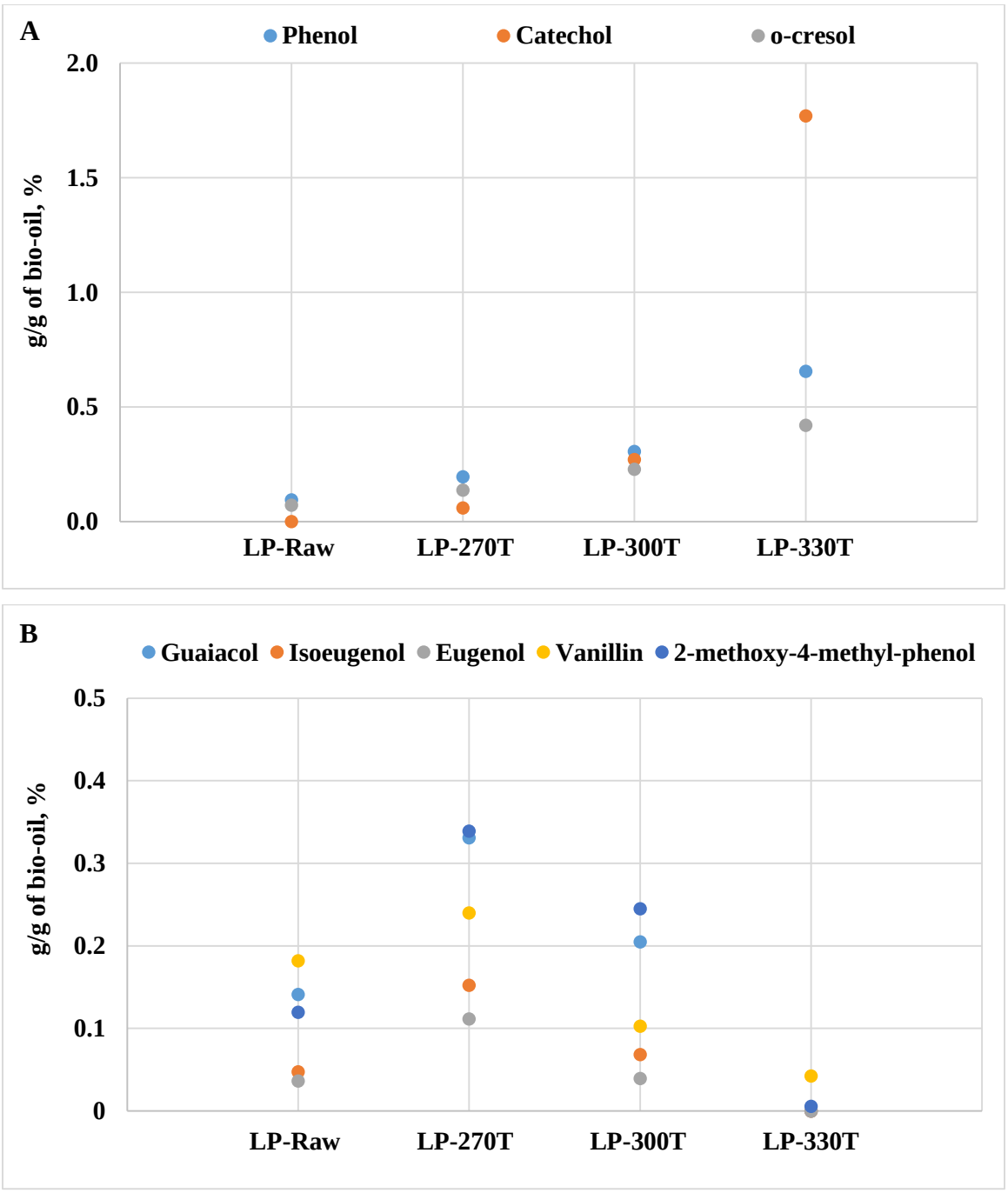

Figure 2.7 GC/MS quantification of major phenolic monomers (A. with methoxy groups and B. without methoxy groups) in bio-oils.

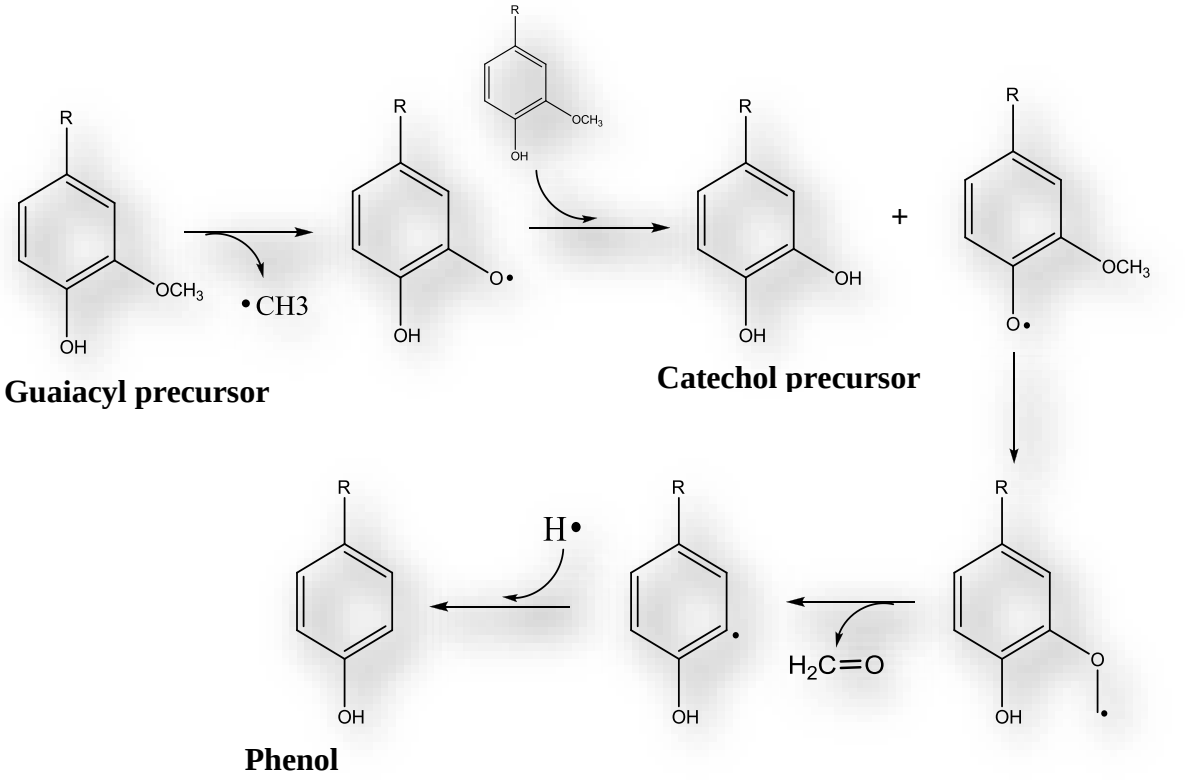

Figure 2.8 Demethoxylation pathway – inter-conversion between guaiacyl type to catechol and phenol precursor [Ben and Ragauskas, 2011].

Table 2.1 Characterization of torrefied wood (dry-base).

	Raw wood	TW-270T	TW-300T	TW-330T
Chemical Composition				
Carbohydrates, %				
Glucan	36.1	34.4	32.0	18.0
Xylan	6.4	3.2	3.0	0.4
Galactan	2.3	1.0	0.7	0.0
Arabinan & Mannan	10.0	7.0	5.4	0.6
Total sugar	54.8	46.6	41.1	19.0
Lignin+Residues[a], %				
Acid insoluble residues[b]	30.1	41.0	48.1	74.2
Acid soluble residues	1.6	1.8	1.8	2.6
Total lignin+char residues	31.7	42.8	49.9	76.8
Extractives[c], %	2.1	5.8	6.0	10.4
Ultimate and Proximate Analysis				
C, %	50.5	55.0	57.3	65.8
H, %	6.26	5.94	5.79	4.87
O, %	42.6	38.3	36.0	27.6
N, %	0.09	0.11	0.14	0.28
O/C atomic ratio	0.63	0.52	0.47	0.31
HVC[d], %	9.3	8.1	8.0	4.2
Volatile matter, %	84.6	78.6	76.4	59.9
Fix carbon, %	14.8	20.8	22.8	38.6
Ash, %	0.56	0.62	0.78	1.45
HHV[e], MJ/kg	20.0	22.7	24.0	26.3
Metal Content Analysis				
Na, ppm	45	32	93	191
K, ppm	171	115	225	468
Mg, ppm	207	303	368	788
Ca, ppm	622	1088	1252	2082

a. Lignin + Residue: contain conventional lignin and char made from torrefaction process.

b. Acid insoluble residue: Klason lignin and char made from cellulose, hemicellulose and lignin heat treatment.

c. Extractives: contain conventional wood extractives and other organics, i.e. levoglucosan produced from torrefaction treatment.

d. HVC: highly volatile compounds, including water and other light organics absorbed on the torrefied wood surface.

e. HHV: high heating value.

Table 2.2 Characterization of bio-oils properties.

	LP-Raw	LP-270T	LP-300T	LP-330T
Elemental Analysis[a]				
C, %	62.4	65.8	66.3	72.0
H, %	5.1	5.6	5.3	5.7
O, %	32.2	28.3	28.2	21.7
N, %	0.29	0.26	0.24	0.54
O/C atomic ratio	0.39	0.32	0.32	0.23
Physicochemical Properties				
Water content, %	27.2	21.0	23.7	15.5
Viscosity, cp	4.4	6.4	5.4	50.1
Solid content, %	0.04	0.46	0.70	1.35
pH	2.3	2.5	2.6	3.2
TAN[b], mg KOH/g	78.0	74.9	67.7	55.7
TAN[c], mg KOH/g	161.9	167.5	181.9	182.3
HHV[d], MJ/Kg	20.0	22.7	24.0	26.3

a. Data calculated based on dry bio-oil.

b. TAN: total acid number based on inflection point method; wet oil based.

c. TAN: total acid number based on buffer potential at pH~11 method; wet oil based.

d. HHV: high heating value.

Table 2.3 Mass balance of single pyrolysis and integrated torrefaction-fast-pyrolysis process.

	Pyrolysis Mass Balance[a], %			**Integrated Pyrolysis Mass Balance[b], %**			
	Bio-oil	Biochar	Gas[c]	Bio-oil	Biochar	Gas[c]	TWL[d]
Raw wood	67.2	9.7	23.1	67.2	9.7	23.1	0.0
TW-270T	54.5	22.2	23.3	45.5	18.5	19.5	16.5
TW-300T	52.1	27.0	20.9	39.5	20.5	15.9	24.1
TW-330T	33.5	43.3	23.2	17.9	23.2	12.4	46.5

a. Pyrolysis mass balance: calculated starting with torrefied wood.

b. Pyrolysis mass balance: calculated starting with raw wood without torrefaction pretreatment.

c. Gas: gas yield was calculated by difference.

d. TWL: torrefaction weight loss.

Table 2.4 Mass balance of water generated in fast pyrolysis of torrefied wood[a].

	Water[b] - bio-oil, g	Water[c] - wood, g	Water[d] – Pyrolysis, g
Raw wood	18.3	9.3	9.0
TW-270T	14.4	8.1	3.3
TW-300T	12.3	8.0	4.3
TW-330T	5.5	4.2	1.3

a. Calculation based on with 100g of biomass input; assumptions: water loss in the gas flow is negligible; char is moisture free.

b. Water amount contained in bio-oils.

c. Water amount contained in wood.

d. Water amount generated from fast pyrolysis of wood.

Table 2.5 ^{13}C NMR integration of bio-oils made from torrefied wood.

Type of carbon	δ region[a] ppm	Carbon content, %			
		LP-Raw	LP-270T	LP-300T	LP-330T
Carbonyl	215-163	6.4	5.7	5.1	3.8
Aromatic	163-110	26.7	29.2	30.7	31.9
Carbohydrate	110-84	20.6	21.8	21.2	20.2
Methoxy/hydroxy	84-54	28.4	25.9	25.7	24.6
Alkyl carbons	54-1	17.9	17.4	17.3	19.5

a. Integration range was selected based on reference [Ingram et al., 2008].

Table 2.6 ^{1}H NMR integration of bio-oils made from torrefied wood.

Type of Proton	δ region[a], ppm	Proton content, %			
		LP-Raw	LP-270T	LP-300T	LP-330T
-CHO, -COOH, downfield ArH	10.0-8.0	6.6	6.0	4.4	4.0
ArH, HC=C (conjugated)	8.0-6.8	5.1	4.8	4.1	3.3
HC=C (nonconjugated)	6.8-6.4	9.7	10.6	8.4	7.1
>CHO, ArOH, HC=C (nonconjugated)	6.4-4.2	27.2	29.6	21.9	18.3
CH_3O-, -CH_2O-, CHO	4.2-3.0	25.0	23.8	33.2	32.7
$CH_3C(=O)$-, CH_3-Ar, -CH_2Ar	3.0-2.2	7.8	8.6	16.6	10.9
-CH_2-, aliphatic OH	2.2-1.6	12.4	12.5	5.3	13.5
-CH_3, -CH_2-	1.6-0.0	6.2	4.1	6.1	10.2

a. Integration range was selected based on reference [Ingram et al., 2008]

CHAPTER 3

Unraveling the Levoglucosan Increase in Pyrolysis Bio-oil Produced from Heat-treated Biomass

1. Introduction

Bio-oil as a potential fuel intermediate can be produced from thermal degradation of woody biomass and has also been recognized as a potential chemical source. The current synthetic route of bio-oil to commercial chemicals uses catalysts (e.g. HZSM-5, Pt, Ru) to convert bio-oil components into aromatics. [Vispute et al., 2010] In this process, one of the major bio-oil compounds, levoglucosan (1,6-anhydro-β-D-glucopyranose, LG) produced from cellulose degradation, is also converted to an aromatic compound. Levoglucosan is an attractive precursor for synthesis due to its chiral synthon possessing features and its applications include pharmaceutical and pesticide syntheses, chiral ligands, and glucoside surfactants. [Witczak, 1994] Therefore, the separation of LG is worthwhile and it can be easily separated from bio-oil using water extraction, while the rest of the bio-oil (mostly pyrolytic lignin) can be upgraded to make aromatics using the abovementioned route.

Unfortunately, the yield of LG in the bio-oil from biomass (~1-2%) is low under conventional fast pyrolysis conditions. Further, the extraction of LG from bio-oil for chemical production, via water extraction, will only be practical if the LG concentration in the bio-oil can be maximized. Pioneering work by Shafizadeh and coworkers [Shafizadeh et al., 1979; Shafizadeh and Stevenson, 1982] found low temperature vacuum pyrolysis and demineralization of wood by acid pretreatment can achieve high LG production. In addition,

Piskorz [Piskorz et al., 2000] made efforts to produce anhydro-oligomers from flash pyrolysis of purified cellulose (Avicel PH-102) using additives and heating, and achieved a higher yield of LG. However, the substrate they used, which has high crystallinity and short DP, is very different from native cellulose in biomass. Also, other biomass constituents, not presented in purified cellulose, especially inorganic salts, would have a significant impact on the cellulose pyrolysis pathway and vary the product composition.

Preheating the woody biomass under oxygen-free conditions for making high quality bio-oil via pyrolysis was first reported previously by our group. [Meng et al., 2012] The intention of using preheated biomass as fast pyrolysis feedstock is that the preheating step can reduce the oxygen content of biomass by partially removing hemicellulose and cellulose. Therefore, the resulting oxygen content of the bio-oil can be reduced as well as the carbohydrate degradation products, i.e. acetic acid and LG. However, when analyzing the bio-oil composition using GC/MS, we found LG concentration did not decrease with increasing heating severity as expected. Therefore, to explain this experimental result, this letter discloses our recent findings that the yield of LG in pyrolysis bio-oil can be increased two-fold by pretreating the feedstock biomass at mild temperatures (270-330 °C) under oxygen-free conditions. To the best of our knowledge, this is the first experimental verification of such an increase in bio-oil made from pretreated wood. Also, this letter first presents a tentative mechanism for this LG yield enhancement based on the cellulose conversion chemistry and this LG yield enhancement may be a direct evidence for the understanding of cellulose pyrolysis pathway.

2. Materials and Methods

2.1 Materials and Chemicals

Fast pyrolysis feedstock (the heat treated wood, loblolly pine with bark) with three different treatment severities was produced from a pilot scale reactor at 270 °C, 300 °C and 330 °C for 2.5 mins and referred as TW-270T, TW-300T and TW-330T in this study. The wood without pretreatment was labeled as raw wood. Levoglucosan, glycolaldehyde dimer, and fluoranthene were purchased from Sigma-Aldrich and acetol (AAAL15008-22) was purchased from VWR international. All chemicals were used as received.

2.2 Bio-oil Generation

The method for bio-oil generation has been previously reported. [Meng et al., 2012] After production, the bio-oils from condensers and ESP were mixed with a vortex mixer for 30 mins and stored at -5 °C until use. Prior to analysis, the bio-oils were homogenized with the vortex mixer for 30 mins to ensure uniformity.

2.3 Py-GC/MS of Woody Materials

Py-GC/MS experiments were carried out on a CDS Analytical Pyroprobe Model 5150. For each analysis, 50 μg of wood powder was loaded in the quartz tube and the pyrolysis temperature was set at 600 ºC to compensate for the temperature lag (about 100 ºC) caused by the heat transfer from heating coil to wood powder. Triplicate tests were conducted for each wood sample and averaged data are plotted in Fig. 3.1.

2.4 Wood and Bio-oil Characterization

Determination of wood composition has been described in detail in a previous publication. [Park et al., 2013] GC/MS quantification of bio-oil compounds were performed on a Thermo Fisher Polaris Q Plus system. The quantification of the major chemicals in the bio-oils was achieved by the generation of calibration curves with standard chemicals and the use of fluoranthene as an internal standard. Triplicate tests were conducted for each bio-oil sample and averaged data are plotted in Fig. 3.1.

3. Results and Discussions

The chemical composition of pyrolysis bio-oil largely depends on the chemical properties of its feedstock, and cellulose is the only source of LG in the biomass pyrolysis process. Therefore, if cellulose in heat treated wood reacts at the same efficiency as that in raw wood, the LG yield should decrease due to the decreased amount of cellulose (36.1% in raw wood vs. 18.0% in TW-330T, Table 3.1-c). However, Fig. 3.1 shows a contrary trend in that the LG concentration is higher in bio-oils made from heat treated wood versus that made from raw wood. In addition, results from py-GC/MS experiments show the same trend as those shown in Fig. 3.1. Table 3.1 summarizes the mass balance of LG produced from fast pyrolysis of heat-treated biomass. Note that, although the majority of the LG in the bio-oil originates from the pyrolysis of the heat treated wood, a small amount arises from the heat treated wood itself (Table 3.1-d). Specifically, the heat treatment produces a small amount of LG that is adsorbed on the surface of the wood. This LG was quantified by benzene-ethanol extraction followed by GC/MS analysis (Table 3.1-d). Based on a pyroprobe experiment

using an LG standard, the amount of degradation products from LG is insignificant since it is quickly volatilized from the reaction zone. Therefore, the difference between the LG in the pyrolysis bio-oil (Table 3.1-e) and that generated from the pretreatment step (Table 3.1-d) represents the amount of the LG produced from the pyrolysis (Table 3.1-f).

In comparing the absolute amount of LG produced solely from fast pyrolysis, TW-270T and TW-300T generated more than the raw wood, while TW-330T produced less. However, it is not appropriate to compare the absolute values because the starting cellulose content in the samples is different. Thus, the index of LG conversion efficiency is employed here to demonstrate how thermal pretreatment enhances LG production. Using this index, Table 3.1-g indicates that less cellulose content in the heat treated wood (e.g. 50% less in the TW-330T sample) results in the LG conversion efficiency increasing significantly (from 5.3% for raw wood to 9.6% for TW-330T). Also, it has been reported that some metal species can reduce the LG yield in bio-oil. [Patwardhan et al., 2010] Thermally treated wood was found to have a much higher inorganic content than non-thermally treated wood as inorganic species are not volatilized during the thermal treatment. As a result, if treated wood has the same degree of metal content as the non-treated wood, then LG conversion efficiency should be much higher than that shown in Table 3.1. Based on these considerations, it is clear that heat treatment boosts the conversion of cellulose to LG.

Treating cellulose with heat has been reported to reduce its degree of polymerization (DP) [Piskorz et al., 1989] mainly through cleavage of cellulose's β-1,4-glycosidic linkages. Additionally, it is believed that the effective cleavage of the β-1,4-glycosidic linkage is the key step that determines the rate of LG formation from fast pyrolysis, regardless of the type

of reaction mechanism hypothesized [Mayes and Broadbelt, 2012; Zhang et al., 2011; Shen and Gu, 2009]. The number of chain ends also determines the rate of LG formation because LG is released from them, and once this process starts, it is more likely to proceed sequentially along the chain [Mamleev et al., 2007]. As shown in Fig. 3.2, after thermal treatment, two modified cellulose chains ("b" and "c") can be formed from the native cellulose ("a"). [Lin et al., 2009] By generating these shorter cellulose chains via heat treatment, the chances of producing LG from cellulose are enhanced in the subsequent pyrolysis process as these cellulose chains undergo the same pyrolysis reaction to its parent chain. More importantly, the new cellulose chain possesses a 1,6-anhydro-linkage at the reducing end ("b" and "d"), in which a molecule of LG can be quickly released for each subsequent scission of the glycosidic bond [Vinu and Broadbelt, 2012].

Heat treatment also alters cellulose crystallinity by breaking the hydrogen bonds which distinguish between its crystalline and amorphous structures. It was found that low temperature heat treatment can effectively break the intra-molecular hydrogen bonding (e.g. 2OH···6O and 3OH···5O) in cellulose. [Agarwal et al., 2011] In addition, the presence of a short-lived liquid phase [Mettler et al., 2012a] during the pyrolysis of cellulose was observed as amorphous cellulose and a change from its chair to boat formation might be necessary for forming LG. [Seshadri et al., 2012] Heat treatment applied in this study was expected to have the similar effect on cellulose structure modification by breaking hydrogen bonds and increasing the amorphous proportion. As a result, it would facilitate the conformational change of the cellulose macromolecules required to form LG.

Another consideration in understanding the LG conversion is illustrated through three cellulose pyrolysis pathways shown in Fig. 3.2. When LG is produced via the fast pyrolysis process (Pathway 1), ring opening products such as glycolaldehyde and acetol can also be formed (Pathway 2). In addition, LG may serve as an intermediate for the formation of glycolaldehyde and acetol presented as Pathway 3. [Kawamoto et al., 2009] However, at typical fast pyrolysis conditions, a short residence time of ~1.0 s may not be enough for LG to undergo significant degradation before its removal from the hot reactor zone. From the viewpoint of reaction kinetics, the formation of LG from glucose requires fewer carbon-carbon bond cleavages and molecular rearrangements than the formation of glycolaldehyde and acetol.[Mettler et al., 2012b] That is, the activation energy required to form LG is much lower than that required forming glycolaldehyde and acetol; therefore the formation of LG from cellulose is a kinetically favorable reaction. In addition, the heat treatment discussed above may facilitate the formation of LG by producing cellulose with reduced DP and crystallinity which, in turn, may further reduce the activation energy of LG formation. This reduction may enhance the reaction favorability towards Pathway 1 leading to higher LG yields in bio-oil. The experimental results in Fig. 3.1 support this explanation in that glycolaldehyde and acetol content in both bio-oil and py-GC/MS products generally decrease, while the LG content increases with increased heat treatment intensities. When comparing LP-Raw to LP-330T bio-oil samples, the relative ratio of glycolaldehyde-to-LG decreased from 3.4 to 0.7 and the same trend was observed for the ratio of acetol-to-LG from 0.8 to 0.2. In other words, the heat treatment enhances the cellulose pyrolysis reaction to favor the formation of LG instead of glycolaldehyde or acetol.

4. Conclusions

In summary, this chapter presents rationale for the unexpected phenomenon that heating biomass prior to its fast pyrolysis results in bio-oil with higher concentrations of LG. Specifically, this phenomenon is likely explained by the DP reduction of the cellulose chain and decrystallization effect caused by the thermal treatment. In addition, the kinetic favorability of LG formation may be enhanced by thermal treatment. Finally, removing inorganic species in heat treated wood by acid washing may be another strategy in increasing the LG formation.

5. Acknowledgements

This study was supported by Southeastern Sun Grant Center, the US Department of Transportation (Grant No. DTO559-07-G-00050) and the National Science Foundation (Grant No. 0832498). The author would like to thank Chris Hopkins at North Carolina State University for providing heat-treated wood samples.

References

Agarwal, V., Huber, G.W., Conner, J.W.C., Auerbach, S.M. 2011. Simulating infrared spectra and hydrogen bonding in cellulose I beta at elevated temperatures. The Journal of Chemical Physics, 135(13), 134506-13.

Kawamoto, H., Morisaki, H., Saka, S. 2009. Secondary decomposition of levoglucosan in pyrolytic production from cellulosic biomass. Journal of Analytical and Applied Pyrolysis, 85(1–2), 247-251.

Lin, Y.-C., Cho, J., Tompsett, G.A., Westmoreland, P.R., Huber, G.W. 2009. Kinetics and Mechanism of Cellulose Pyrolysis. The Journal of Physical Chemistry C, 113(46), 20097-20107.

Mamleev, V., Bourbigot, S., Yvon, J. 2007. Kinetic analysis of the thermal decomposition of cellulose: The main step of mass loss. Journal of Analytical and Applied Pyrolysis, 80(1), 151-165.

Mayes, H.B., Broadbelt, L.J. 2012. Unraveling the Reactions that Unravel Cellulose. The Journal of Physical Chemistry A, 116(26), 7098-7106.

Meng, J., Park, J., Tilotta, D., Park, S. 2012. The effect of torrefaction on the chemistry of fast-pyrolysis bio-oil. Bioresource Technology, 111(0), 439-446.

Mettler, M.S., Mushrif, S.H., Paulsen, A.D., Javadekar, A.D., Vlachos, D.G., Dauenhauer, P.J. 2012. Revealing pyrolysis chemistry for biofuels production: Conversion of cellulose to furans and small oxygenates. Energy & Environmental Science, 5(1), 5414-5424.

Mettler, M.S., Paulsen, A.D., Vlachos, D.G., Dauenhauer, P.J. 2012. Pyrolytic conversion of cellulose to fuels: levoglucosan deoxygenation via elimination and cyclization within molten biomass. Energy & Environmental Science, 5(7), 7864-7868.

Park, J., Meng, J., Lim, K.H., Rojas, O.J., Park, S. 2013. Transformation of lignocellulosic biomass during torrefaction. Journal of Analytical and Applied Pyrolysis, 100(0), 199-206.

Patwardhan, P.R., Satrio, J.A., Brown, R.C., Shanks, B.H. 2010. Influence of inorganic salts on the primary pyrolysis products of cellulose. Bioresource Technology, 101(12), 4646-4655.

Piskorz, J., Majerski, P., Radlein, D., Vladars-Usas, A., Scott, D.S. 2000. Flash pyrolysis of cellulose for production of anhydro-oligomers. Journal of Analytical and Applied Pyrolysis, 56(2), 145-166.

Piskorz, J., Radlein, D.S.A.G., Scott, D.S., Czernik, S. 1989. Pretreatment of wood and cellulose for production of sugars by fast pyrolysis. Journal of Analytical and Applied Pyrolysis, 16(2), 127-142.

Seshadri, V., Westmoreland, P.R. 2012. Concerted Reactions and Mechanism of Glucose Pyrolysis and Implications for Cellulose Kinetics. The Journal of Physical Chemistry A, 116(49), 11997-12013.

Shafizadeh, F., Furneaux, R.H., Cochran, T.G., Schott, J.P., Sakai, Y. 1979. Production of levolgucosan and glucose from pyrolysis of cellulosic materials. Journal of Applied Polymer Science, 23, 3525-3539.

Shafizadeh, F., Stevenson, T.T. 1982. Saccharification of douglas-fir wood by a combination of prehydrolysis and pyrolysis. Journal of Applied Polymer Science, 27, 4577-4585.

Shen, D.K., Gu, S. 2009. The mechanism for thermal decomposition of cellulose and its main products. Bioresource Technology, 100(24), 6496-6504.

Vinu, R., Broadbelt, L.J. 2012. A mechanistic model of fast pyrolysis of glucose-based carbohydrates to predict bio-oil composition. Energy & Environmental Science, 5(12), 9808-9826.

Vispute, T.P., Zhang, H., Sanna, A., Xiao, R., Huber, G.W. 2010. Renewable Chemical Commodity Feedstocks from Integrated Catalytic Processing of Pyrolysis Oils. Science, 330(6008), 1222-1227.

Witczak, Z.J. 1994. Levoglucosenone and Levoglucosans: Chemistry and Applications. in: Production of Levoglucosan as an Industrial Chemical, (Ed.) Z.J. Witczak, ATL Pr Scientific Publisher. Washington, D.C, pp. 179-188.

Zhang, X., Li, J., Yang, W., Blasiak, W. 2011. Formation Mechanism of Levoglucosan and Formaldehyde during Cellulose Pyrolysis. Energy & Fuels, 25(8), 3739-3746.

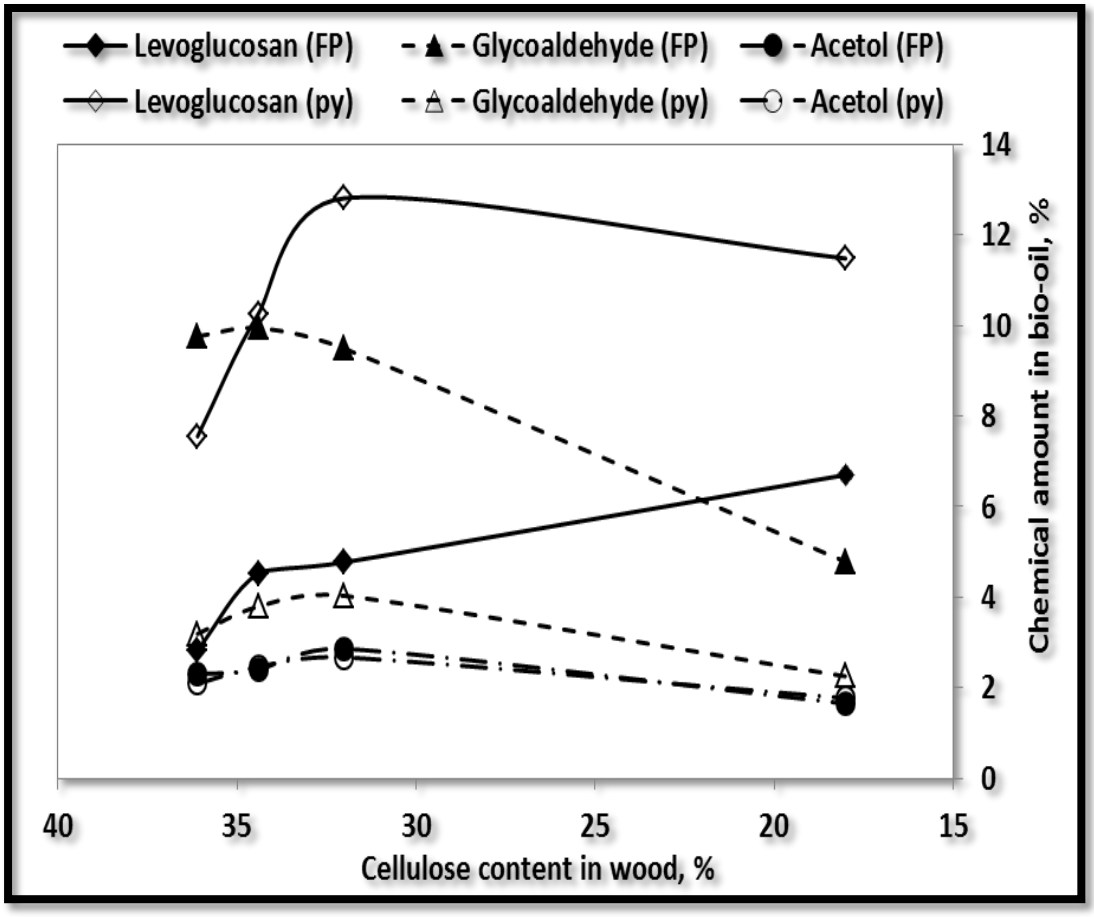

Figure 3.1 Major cellulose degradation products in bio-oil (Levoglucosan, Glycolaldehyde, and Acetol) determined by GC/MS. Cellulose content in wood samples is 36.1%, 34.3%, 32.0%, and 18.0% for raw wood, TW-270T, TW-300T and TW-330T. Filled markers ("FP") represent the analysis of bio-oil produced from a bench-scale fast pyrolysis reactor (150 g/hr feed fluidized-bed), while opened markers ("py") represent simulated pyrolysis using a pyroprobe reactor connected to a GC/MS.

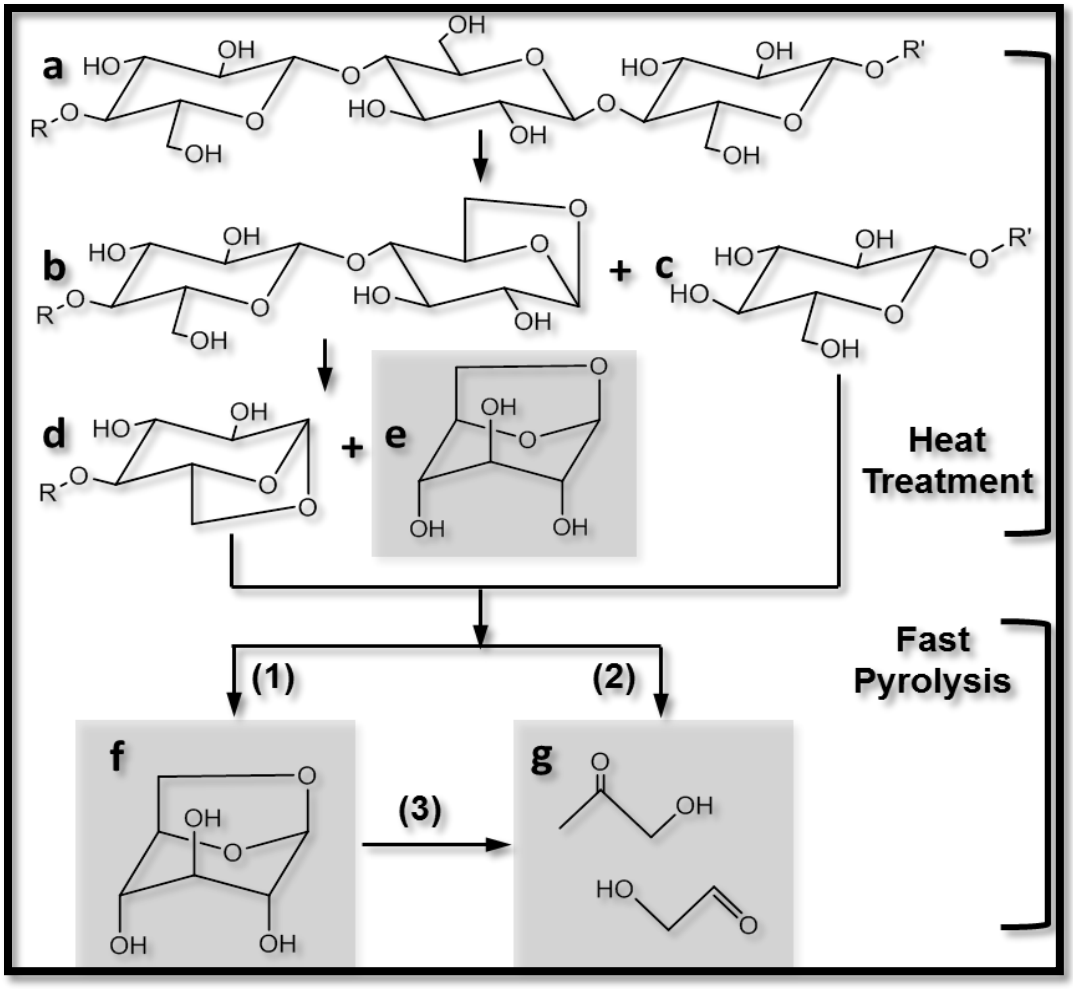

Figure 3.2 Proposed mechanisms for the production of glycolaldehyde and acetol (g) and levoglucosan (e, f) from heat treated native cellulose (a), modified cellulose with anhydro-linkage at the end (b, d), and short-chain cellulose (c). Three reaction pathways during fast pyrolysis are presented as (1) Pathway 1: Low DP cellulose to anhydrosugars and sugar oligomers, (2) Pathway 2: Low DP cellulose to ring-opening products, and (3) Pathway 3: Levoglucosan to ring-opening product.

Table 3.1 Mass balance of levoglucosan produced in the fast pyrolysis process.

[a] Sample ID	[b] Bio-oil, g/ 100g	[c] LG_{max}, g/ 100g	[d] LG_{ex}, g/ 100g	[e] LG_{oil}, g/ 100g	[f] LG_{py}, g/ 100g	[g] ICE_{LG}, %
Raw wood	67.2	36.1	0.00	1.90	1.90	5.3
TW-270T	54.5	34.4	0.25	2.46	2.22	6.4
TW-300T	52.1	32.0	0.27	2.49	2.22	6.9
TW-330T	33.5	18.0	0.51	2.24	1.74	9.6

a. Pyrolysis feedstock, raw wood is loblolly pine without heat treatment; TW-270T, TW-300T and TW-330T indicate pine wood pretreated at 270, 300 and 330 °C for 2.5 min.

b. Amount of bio-oil produced from 100g of starting biomass.

c. Maximum amount of LG that can be converted from cellulose, which is the same as cellulose content in biomass.

d. Amount of LG adsorbed on the treated wood, analyzed by solvent extraction followed by GC/MS.

e. Amount of LG in the bio-oils.

f. Amount of LG produced from fast pyrolysis process, assuming LG adsorbed on the surface of treated wood does not decompose in the fast pyrolysis process.

g. Index of conversion efficiency of LG from cellulose during the fast pyrolysis process.

h. $ICE_{LG} = (LG_{oil} - LG_{ex}) / LG_{max} \times 100$ %.

CHAPTER 4

The Effect of Torrefaction on the Thermal and Storage Stability of Pyrolysis Oil

1. Introduction

Bio-oil produced from biomass pyrolysis using elevated temperature (~500 °C) and oxygen-free conditions can be upgraded into hydrocarbons and potentially used as transportation fuel. However, crude bio-oil is neither chemically nor thermally stable. During the storage and transportation, oil phase separation and viscosity increase, termed as aging, obstruct its further refining. Severe aging reactions also occur when bio-oil is heated for processing and upgrading purpose. Direct injecting raw bio-oil into combustion engine results in serious clogging problems; therefore the stability of bio-oil has to be improved before its commercial use as transportation fuel.

Instability of bio-oil could be explained by polymerization, esterification, acetalization, oxidization and dimerization of bio-oil components; the bio-oil oxygen-rich aldehydes and carboxylic acids contribute significantly to these proposed aging reactions. [Diebold, 2002] Adding methanol with acid catalyst [Moens et al., 2009] could give relatively stable bio-oil by sealing the reaction sites of carboxyl and carbonyl compounds. Filtrating bio-oil char particles could also significantly slow down the bio-oil viscosity increase after aging [Naske et al., 2011; Baldwin et al., 2013], suggesting a catalytic effect of char containing minerals on bio-oil condensation reactions [Diebold, 2002; Diebold and Czernik, 1997]. However, because of the complexity of bio-oil composition, the aging reaction mechanism has not been experimentally verified.

Though no standard method has been established for bio-oil stability test, accelerated aging of bio-oil in a sealed bottle at 80 ºC for 24 hours and long-term storage aging at room-temperature are often adopted for bio-oil stability evaluation. The accelerated avenue saves a large amount of time when compared to the long-term storage method. In addition, at confined testing conditions, the viscosity of accelerated aged bio-oil can be correlated to that of one-year room-temperature aged bio-oil [Oasmaa, et al., 2011]. Therefore, accelerated aging procedure is often considered as a simulation process of bio-oil aging at room-temperature for a one-year period.

Crude bio-oil needs to be upgraded before using as transportation fuel; its initial oil properties also need to be maintained during the storage, handling and shipping. Recent process design tends to integrate the pyrolysis and upgrading operations together by in-situ vapor upgrading [Biddy et al., 2013]. The resulting bio-oil with low-oxygen-content from this process could be very stable making storage stability a minor issue. Also, unlike crude oil, the bio-oil productivity may be limited by available biomass supply and the fresh-made oil can be upgraded instantaneously after it was produced from the pyrolysis plant. In this sense, long-term bio-oil storage seems to be unnecessary. However, the author tends to envision that the bio-oil industry, once established, has to adopt a similar operation scheme to the petroleum industry by producing bio-oil onsite where biomass is abundant, and the bio-oils will then be shipped through existing petroleum piping system to existing refinery plants. This operation mode could significantly reduce biomass shipping costs and take advantage of existing oil-transportation and refinery infrastructures. Accordingly, the importance of bio-oil long-term storage stability for at least three months stands out. In addition, polymerization

reactions that occur under accelerated aging conditions could be very different to those that occur at room-temperature. It will be very risky to estimate bio-oil storage stability using accelerated aging method. Therefore, both accelerated aging and long-term room temperature aging methods were adopted in this study to access the torrefaction effect on bio-oil stability.

A number of studies [Mante and Agblevor, 2012; Song et al., 2010; Kim et al., 2012] indicated that oxygen-rich species in the bio-oil are the major causes for its stability issue, suggesting a correlation between oxygen content and bio-oil stability may exist. Torrefaction pretreatment, performed at low-temperature (200~350 °C) pyrolysis condition is an effective biomass upgrading technology. The author's previous study [Meng et al., 2012], found that using torrefied wood as pyrolysis feedstock can effectively reduce the oxygen content of the resulting bio-oil. In addition, certain reactive components, i.e. glycolaldehyde and acetic acid, can also be extensively removed from bio-oil. Therefore, bio-oil made from heat pretreated wood may have improved stability when comparing to the bio-oil made from non-treated wood. To our knowledge, this hypothesis has not yet been investigated; hence the goal of this study is to evaluate the torrefaction effect on the bio-oil thermal and storage stability. Experimentally, bio-oils made from torrefied wood with different treatment severity were aged in accelerated aging and regular storage conditions; the bio-oil stability was evaluated by comparing the physicochemical and compositional variation of aged torrefaction bio-oils to that of aged raw bio-oil.

2. Materials and Methods

2.1 Torrefied biomass and bio-oil production

Loblolly pine was used as a raw material for torrefaction pretreatment and small chips (~ 15 mm × 6 mm) were introduced into a pilot-scale torrefaction system [Meng et al., 2012]. It was operated in oxygen-free conditions to produce torrefied wood at three different severities, which were treated under 280, 310, and 330 °C for 2.5 minutes respectively. The samples are referred as TW-280T, TW-310T, and TW-330T in this study. The torrefaction severity is quantified by the weight loss of torrefied wood, which is 17.0%, 25.4%, and 46.5% for TW-280T, TW-310T, and TW-330T respectively, based on the original weight of non-torrefied dry wood. Typical characteristics of these materials are summarized in Table 4.1.

The bio-oils for aging study were produced from a fluidized bed reactor (O.D. 43mm) at 500 °C as described previously [Meng et al., 2012]. Pyrolysis vapor was collected by two condensers (~4 °C) and an electrostatic precipitator. The collected bio-oils were thoroughly mixed with a vortex mixer and stored in a freezer (-4 °C) for further analyses. The bio-oil made from non-treated wood is named as LP-Raw (LP as liquid product) and the bio-oils made from torrefied wood are labeled as LP-280T, LP-310T and LP-330T respectively. The initial bio-oil oxygen content is 42.7, 39.1, 37.7 and 30.9% for LP-Raw, LP-280T, LP-310T and LP-330T respectively.

2.2 Bio-oil Aging

Accelerated aging. Approximately 10 g of bio-oils were aged at 80±1 °C for 24 hours in a convection oven according to a reference method [Elliott et al., 2012]. The weight loss after accelerated aging was under 0.1 %. The starting bio-oil before aging is denoted as FH (fresh) bio-oil and the accelerated aged sample is named as AA (e.g. LP-Raw-AA, accelerated aged bio-oil from untorrefied biomass). Aged bio-oil water content, viscosity, solid content, average molecular weight, and acidity were recorded and the aging index for each property was calculated based on Equation 1, where P stands for particular property. Accelerated aging experiments were repeated at least twice and averaged values were reported.

$$\text{Aging index, \%} = (P_{Aged} - P_{Initial}) / P_{Initial} \times 100 \quad [1]$$

Long-term room-temperature aging. Approximately 60 g of bio-oils sealed in a clear glass bottle were stored in a light-free dark cabinet under 25±1 °C for 1, 3, 6, 9, and 12 months to evaluate the effect of natural aging. The physicochemical properties and chemical composition of aged bio-oil were measured in fresh state and after 1, 3, 6, 9, 12 months storage from the starting date.

2.3 Characterization of torrefied wood and bio-oil

Ultimate analysis. Carbon, hydrogen, and nitrogen analyses of bio-oil were performed according to ASTM-D5291 using a Perkin Elmer CHN Elemental Analyzer (2400 Series II). The oxygen contents were calculated by difference. The analyses were repeated three times and the average data were reported.

Water content. The water content of the bio-oil was determined by Karl-Fischer titration according to ASTM E 203-08 using HYDRANAL Composite 5 (Sigma-Aldrich 34805), HYDRANAL Medium K (Sigma-Aldrich 34698). The titrant concentration was determined by HYDRANAL Water Standard 10.0 (Sigma-Aldrich 34849). The titration was repeated three times and the average water content was reported.

Viscosity. The kinematic viscosity of bio-oil was measured according to ASTM D445 using Cannon-Fenske viscometer (size 150, 200, 350). The analyses were repeated twice and the average viscosity was reported.

Acidity. The total acid number (TAN) of bio-oil was measured according to ASTM D644-07 with an automatic titrator (Mettler-Toledo, T50). Inflection point was employed as a titration end point. The titration reagent, 0.1M KOH dissolved in isopropanol solution (Ricca Chemical 6257-32) was purchased from Fisher Scientific. The benzene and isopropanol were purchased from VWR international and used as received.

Solvent fractionation. The solvent fractionation of bio-oil was performed based on the procedure described in a previous study [Oasmaa and Meier, 2005]. The bio-oil was first extracted with excess DI water (1:30 by weight) and separated into water soluble (WS) and water insoluble (WIS) fraction. The WS fraction was further extracted with diethyl ether (1:1 by volume) and fractionated into ether soluble (ES) and ether insoluble (EIS) fraction. The WIS fraction was extracted with dichloromethane (1:1 by volume) and fractionated into low molecular mass lignin (LMM) and high molecular mass (HMM) lignin fraction. Dichloromethane (34856) and diethyl ether (346136) were purchased from Sigma-Aldrich and used as received. The analyses were repeated twice and the averaged result was reported.

GC/MS analysis. Gas chromatographic/mass spectrometric analyses of bio-oil were performed on a Finnigan Polaris Q Plus system. The operational conditions can be found in previous publication [Meng et al., 2012]. The semi-quantification of bio-oil major chemical compounds was achieved by generating calibration curves with standard chemicals and using internal standard - fluoranthene. Calibration standards (purity > 99.9%) were purchased from Sigma-Aldrich and VWR International. The quantification was repeated two times and the averaged concentration was reported.

GPC analysis. Gel Permeation Chromatography (GPC) characterization of the bio-oil was carried out on a Shimadzu HPLC system (LC-20AD) with an RI detector (RID-10A) and a UV detector (SPD-20A) at 254 nm. Two columns (WatersStyragel HR-1 and HR-5E) are connected for the separation of bio-oil components. The column oven temperature was set at 35 ºC. Tetrahydrofuran (THF, Sigma 401757) was used as the mobile phase flowing at 0.7 mL/min. Bio-oil sample was dissolved in THF to approximately 2 w.t. % and then filtered through a 0.25 μm PTEF filter. Twelve polystyrene standards with molecular weight ranging from 162 to 3,520,000 were used to generate the calibration curve.

NMR analysis. ^{1}H and ^{13}C NMR characterization of bio-oil were recorded in DMSO-d6 (Cambridge Isotope Laboratories, DLM-10TB) solution (25% wt./wt.) with 5mm NMR tube (Wilmad, 528-PP-7) using a Bruker Avance 700MHz NMR spectrometer. The NMR experiments were conducted with a cryoprobe maintained at 279K in order to increase the signal to noise ratio (S/N). ^{1}H spectrum was acquired with a single pulse sequence (zg) with 3.2s pulse delay time and a total of 32 scans at 25 ºC. ^{13}C spectrum was obtained by inverse-gated decoupling pulse sequence (zgig), 90º pulse angle, 2.5s pulse delay time and a total of

20000 scans at 25 ºC. The phase, base-line correction and integration of ^{1}H and ^{13}C NMR spectra were conducted with Topspin software 3.2 (Bruker H9966S3).

3. Results and Discussions

3.1 Torrefaction effect on stability of accelerated aged bio-oil

3.1.1 Physicochemical properties of accelerated aged bio-oil

After accelerated aging, four bio-oil samples, including LP-Raw, LP-280T, LP-310T and LP-330T were able to maintain a relative uniform phase with minor weight loss; no irreversible phase separation (determined as forming a liquid phase flowing on the top of a gum-solid phase) occurred to any of these aged bio-oils. However, after bio-oil homogenization with a vortex mixer, as shown in Fig. 4.1, sticky bio-oil gum can be found on the inner-wall of the aging bottles. Visual judgment suggested more sever gum formation for LP-Raw than that for aged bio-oils made from torrefied wood.

The comparison of physicochemical properties of aged bio-oils is summarized in Table 4.2. The elemental composition of bio-oils remains unchanged after accelerated aging, indicating a proper aging process without oxidation occurred to bio-oil components. Compare to that of initial bio-oil, aged bio-oil water content, viscosity, TAN number, solid content and average molecular weight increased to different extents. This similar aging phenomenon may suggest a shared reaction mechanism for bio-oils made from raw and torrefied wood. Various aging reactions produced water as by-product, therefore aged bio-oil was found to contain more water than that of fresh bio-oil. As shown in Fig. 4.4-A, similar aging indexes for water content increase suggests torrefaction pretreatment cannot inhibit the

moisture accumulation in the aged bio-oil. Although Oasmaa [Oasmaa and Kuoppala, 2003; Oasmaa et al., 2010] reported no bio-oil acidity change after accelerated aging, the author observed a consistent TAN number increase on accelerated aged bio-oils. A similar result has also been published as Ortega found a pH reduction associated with aged pyrolysis oil [Ortega et al., 2011]. In addition, in-situ NMR characterization of aged softwood bio-oil showed increased carboxyl-proton signal during accelerated aging [Ben and Ragauskas, 2012]. These results suggest that organic acids could be produced from the aging reactions. Pyrolytic sugar fraction contained in bio-oil may be a precursor for these acids production, as formic and acetic acids are major sugar degradation products. Similar to water content change, torrefaction did not show significant effect on maintaining a stable acid concentration in aged bio-oils (see Fig. 4.4-A).

As shown in Fig. 4.4-A, viscosity of aged torrefaction bio-oils had more significant increase than that of raw bio-oil. This particular aging phenomenon is considered to be a result of bio-oil polymerization. Theoretically, water/solid content and molecular weight can be correlated to bio-oil intrinsic viscosity. As shown in Table 4.2, the water contents of all aged bio-oils were similar but the solid contents were much higher with aged torrefaction bio-oils. Ortega concluded that bio-oil with a char-free characteristic could have slow tendency towards viscosity increase [Ortega et al., 2011] which may explain the varied viscosity rising degree between these bio-oils. In addition, high amounts of water insoluble lignin fraction (WIS) associated with torrefaction bio-oils (see Fig. 4.3) may also contribute significantly to their viscosity increase. The molecular weights of starting bio-oils were very similar before aging; after accelerated aging, the torrefaction bio-oils were expected to have

larger molecular weight than the raw bio-oil due to their higher viscosity. However, a reversed trend was observed in Table 4.2 and the aging indexes shown in Fig. 4.4-A also support a slower rate of molecular weight increase associated with torrefaction bio-oils. The molecular weight distribution shown in Fig. 4.2 further illustrated that this unexpected phenomenon is accomplished by a slower growth of large-molecular-weight fraction in aged torrefaction bio-oils, especially for LP-330T, than the raw bio-oil. This contradicted viscosity and molecular weight correlation between torrefaction and raw bio-oils may be explained by the varied solid content, different molecular shape and chemical composition presented in the bio-oils. Previously, such disagreement between bio-oil viscosity and molecular weight has also been reported as unchanged viscosity with significantly increased molecular weight has been observed with accelerated aged bio-oil. [Hoekstra et al., 2009]

In summary, as evaluated by accelerated aging method, torrefaction did not improve physicochemical properties of aged bio-oil in terms of reducing water and acid accumulation. The significant viscosity increase with torrefaction bio-oil is clearly a negative factor for its further processing but the bio-oil gum formation can be well controlled by torrefaction treatment.

3.1.2 Chemical composition of accelerated aged bio-oil

GC/MS quantification of several bio-oil components before and after aging is presented in Table 4.3. Most of these bio-oil components identified in this study had reduced concentration after accelerated aging indicating their reactive role in bio-oil condensation reactions. With less concentration change, phenol, catechol, levoglucosan, HMF,

glycolaldehyde and acetol appeared to be relatively more stable in torrefaction bio-oils. In addition, slightly increased acetic acid, acetol and guaiacol content had also been observed after aging which may indicate the existence of two completing aging reactions. One of these reactions consumes a particular type of bio-oil components and the other one produce it. For example, acetic acid can react with alcohols forming esters, but it could also be produced from degradation of bio-oil sugar components.

In order to investigate the whole composition variance after accelerated aging, the results of solvent fraction of aged bio-oil is summarized in Fig. 4.3. After aging, bio-oil water soluble fraction (WS) decreased and water insoluble fraction (WIS) increased. Within WS fraction, both ether soluble fraction (ES) and ether insoluble fraction (EIS) decreased. ES fraction decreased more significantly than EIS fraction as it contains highly reactive oxygenated components, i.e. aldehydes, while EIS fraction is mainly composed of pyrolytic sugars. Within WIS fraction, both HMM and LMM fraction increased suggesting the formation of hydrophobic polymers in aged bio-oils. This WIS fraction is usually termed as pyrolytic lignin, however, after aging reaction, the increase of HMM and LMM does not necessarily mean that more lignin was produced. The increased lignin fraction could result from the condensation of the WS fraction with the lignin fraction producing modified lignin-polymers or it may represent newly formed water-insoluble solids formed between or within the EIS and ES fraction. When comparing the chemical composition of aged raw bio-oil to torrefaction bio-oil, the latter is considered to be more stable than the former, because as shown in Fig. 4.4-B, raw bio-oil had a sharp increase of WIS fraction (197.7%) after aging. The rapid increase of WIS fraction may explain why aged raw bio-oil had higher molecular

weight than aged torrefaction oil. For torrefaction bio-oil, the increase of WIS was only 96.9%, 85.0% and 36.3% for LP-280T, LP-310T and LP-330T respectively. According to the information presented in Table 4.3, Fig. 4.3 and 4.4-B, torrefaction pretreatment has a clear effect on minimizing bio-oil compositional alternation after accelerated aging.

3.1.3 NMR characterization of accelerated aged bio-oil

Quantitative ^{1}H NMR integration of accelerated aged bio-oils is summarized in Table 4.4. Similar to Ben's finding [Ben and Ragauskas, 2012], the number of carbonyl and carboxyl protons slightly increased after accelerated aging for the four bio-oil samples. This result can be correlated with the increased TAN value presented in Table 4.2. The aged torrefaction bio-oils, especially LP-330T tended to show a less pronounced increase of carbonyl/carboxyl protons. The number of aliphatic protons increased substantially for LP-Raw after aging, indicating a possible formation of aliphatic protons from alkene protons. In contrast, the aged torrefaction bio-oils did not show such sharp increase and it may indicate their more stable nature. The number of protons (3.0-6.0 ppm) in which the attached carbon is directly connected to an oxygen atom decreased significantly for LP-Raw, while the same proton content increased for aged LP-280T and LP-330T and slightly decreased for LP-310T. This change of proton content can be achieved by acetalization, dehydroxylation and decomposition of ether compounds in the bio-oil. For aromatic proton content, torrefaction bio-oils showed more significant decreases than that of raw bio-oil. Since torrefaction bio-oils contain high amounts of pyrolytic lignin, it can be inferred that aromatic substitution is

one of the major aging reactions which could lead to significantly increased viscosity of aged bio-oils due to the formation of bulky polymers.

Quantitative ^{13}C NMR integration of accelerated aged bio-oils is summarized in Table 4.5. The content of carbonyl, carbohydrate and methoxy/hydroxy carbon decreased after accelerated aging. The aged torrefaction bio-oils, especially LP-330T showed less pronounced decreases than aged raw bio-oil. Carbonyl carbons, such as aldehyde carbon can engage in different condensation reactions, i.e. aldol-condensation, and forming alkene carbon. Under acidic and high temperature conditions, the carbohydrates in bio-oil could decompose into various light-oxygenates, i.e. HMF, formic acid. Ben [Ben and Ragauskas, 2012] suggested that the dropped signal at 54-84 ppm can be explained by demethoxylation of lignin units. However, methoxy groups on lignin molecules are very stable and the author believes that they may not be effectively cleaved from the aromatic ring under mild aging conditions. Instead, the decreased carbon signal at 54-84 ppm is probably due to the overlapping signal from hydroxyl carbons in sugar fraction and lignin side chains (α-hydroxyl group). The carbon content of aromatic/C=C increased after accelerated aging and torrefaction bio-oils had less pronounced increases when compared to the raw bio-oil. Aromatic carbon is considered to be stable and may not be destructed or produced under aging conditions. In addition, aromatic condensation with aldehydes forming tertiary carbons occurred in bio-oil aging and could increase the carbon relaxation time and reduce the signal for these condensed carbons. Therefore, after accelerated aging, it is expected that the aromatic carbon signals would decrease or at least remain at the same level as it was for the fresh bio-oil. The author believes that the increased signal at 110-163 ppm is more associated

with the production of bio-oil aging components which have non-aromatic double bonds, i.e. furfural, or olefins [Xu et al., 2011] and they can be formed by sugar decomposition and dehydration reactions under acidic conditions. Similar to ^{1}H NMR results, the aliphatic carbon increased after accelerated aging for raw bio-oil; the increase was less significant for LP-280T and LP-310T and a reversed trend was observed for LP-330T.

In summary, by comparing ^{1}H and ^{13}C NMR integration of fresh and aged bio-oils from torrefied and raw wood, aged torrefaction bio-oils tend to have less pronounced signal change therefore their chemical composition can be considered as more stable than raw bio-oil.

3.2 Torrefaction effect on stability of long-term room-temperature aged bio-oil

3.2.1 Bio-oil phase behavior during room-temperature storage

During storage, bio-oil phase separation forming sticky gum is often observed. Fratini [Fratini et al., 2006] studied the microstructure characterization of aged bio-oil using a small-angle neutron scattering technique and concluded that the aggregation and polymerization of pyrolytic lignin is the main reason for the formation of viscous oil sludge. Bio-oil made from torrefied wood contains gradually increased pyrolytic lignin content with increasing treatment temperature and this high lignin concentration may affect the bio-oil phase stability. Table 4.6 records the bio-oil phase property during the twelve-month-storage. Both raw and torrefaction bio-oils have a uniform phase property when freshly made. This uniform phase could be maintained after one month storage for all the bio-oils. At third month, raw bio-oil and LP-310T start to have small amounts of gum formed in the bottom of the storage

bottle and it can be observed by flipping the aging bottle over. After vortex mixing, the gum-oil could be essentially mixed into the bulky liquid phase and this bio-oil was considered in a pseudo-uniform phase. After six-month storage, extensive amount of gum-oil was formed in the raw bio-oil and LP-310T. This time, vortex mixing was less effective for aged raw bio-oil than LP-310T. In contrast, the LP-280T and LP-330T were still in a uniform phase. After nine-month storage, aged raw bio-oil completely phase-separated (see Fig. 4.5) forming a large amount of gum in the storage bottle and vortex mixing was no longer useful to homogenize the separated two phases. In addition, attempts to vortex-mix the aged raw bio-oil moved the gum-oil phase with plenty of air bubbles from the bottom to the top of the storage bottle. The nine-month-aged LP-310T oil started to have similar phase behavior to the six-month-aged raw bio-oil (see Fig. 4.5). After passing designated twelve-month storage time, the LP-310T oil was completely phase separated as occurred to raw bio-oil at nine month. On the other hand, as stated in Table 4.6 and Fig. 4.5, the aged LP-280T and LP-330T were able to maintain a uniform phase during the whole-course of twelve-month storage; however these aged bio-oils became more viscous as they flowed slower than that in a fresh state.

3.2.2 Bio-oil physicochemical properties during room-temperature storage

As stated in the introduction, the aged bio-oil property was initially plan to be measured on the first, third, sixth, ninth and twelfth month after the bio-oils were made. However, as discussed in 3.2.1 raw bio-oil and LP-310T completely phase-separated after six-month and nine-month standing in room-temperature; therefore their property

measurement was not continued after six and nine month storage. Accordingly, the comparison of torrefaction bio-oil to raw bio-oil is limited to six-month storage as shown in Fig. 4.7. This rule is also applied to the composition change of aged bio-oil discussed in Fig 4.11.

Fig. 4.6 records the water content, viscosity, TAN number and molecular weight change of aged bio-oil during the long-term storage. In general, except for viscosity, raw bio-oil had much faster property changes than torrefaction bio-oil during the storage. For example, as shown in Fig. 4.6, the TAN number of aged raw bio-oil increased linearly during six-month storage; in contrast, the aged torrefaction bio-oils (LP-310T and LP-330T) did not show such a continuous increase and they can reach a fast acid-concentration equilibrium after one-month storage. In addition, a reversed molecular weight ranking has also been observed in room-temperature aged bio-oils. In the beginning of the storage, raw bio-oil had slightly lower Mw than the torrefaction bio-oils'; however, it increased exponentially in the first three-month and exceeded the Mw of torrefaction bio-oils. Similar to the results presented for accelerated aged bio-oils, torrefaction bio-oils, especially LP-330T also had a more significant viscosity increase during storage.

For a better comparison of aged raw bio-oil to torrefaction bio-oils in the first half-year storage, a daily averaged property change was plotted in three storage periods (first month, first-to-third month and third-to-sixth month). As shown in Fig. 4.7, during the first month storage, the bio-oil water content increased rapidly (0.13%/day) for LP-Raw, while other torrefaction bio-oils had 10X lower water content increasing rate in the same period; the raw bio-oil also had a more rapid molecular weight increase but slightly slower TAN

increasing rate than that of torrefaction bio-oils. As noted above, the viscosity of LP-330T increased very fast in the initial storage. It increased 1.97 cSt/day in the first month while the raw bio-oil viscosity only had 0.1 cSt increase per day. In the following two storage periods (1-3 month and 3-6 month), the increasing rate of bio-oil water content, viscosity, and molecular weight decreased significantly. Between raw and torrefaction bio-oils, the raw bio-oil still had a more noticeable water content increase than torrefaction bio-oils did during 1-3 month storage. In the 3-6 month storage, torrefaction bio-oils started to show slightly faster water content and molecular weight increases than raw bio-oil. On the other hand, after the initial one month storage, raw bio-oil TAN number started to increase much faster than torrefaction bio-oils. Similar to the first month storage, torrefaction bio-oils, especially LP-330T, still have a much faster viscosity increase during these two storage periods. Overall two torrefaction bio-oils (LP-280T and LP-310T) are considered to be more stable in physicochemical property than raw bio-oil. LP-330T made from severely treated wood showed a must rapid viscosity increase during the storage, however, its other physicochemical properties changed less significantly than the other torrefaction and raw bio-oils.

3.2.3 Correlation between bio-oil viscosity and other physicochemical properties

Typically, bio-oil viscosity can be correlated with its molecular weight and water content. As indicated by Table 4.2 and Fig. 4.6, after aging, torrefaction bio-oil with much higher viscosity showed lower molecular weight than that of raw bio-oil. This is not an expected result since high molecular weight usually leads to high viscosity. Using the

collected data during the long-term storage, Fig. 4.8 and Fig. 4.9 reveal the correlation between bio-oil viscosity and other physicochemical properties which may give some clues on understanding the conflict mentioned above.

As shown in Fig. 4.8, when plotting the observed viscosity (logarithmic scale) with Mw for each bio-oil sample during the available aging period, a good linear correlation ($R^2>0.82$) between Mw and viscosity can be observed. A similar correlation can also be established between viscosity and water content for raw bio-oil. As for torrefaction bio-oils, they showed some correlation during the first six-month storage between water content and viscosity, but not during the entire storage period (especially for LP-280T and LP-330T at six-to-nine month storage). This observation might suggest that bio-oil viscosity is controlled by both molecular weight and water content in the initial six-month storage. Another important factor that can affect the bio-oil viscosity is its chemical composition. As stated earlier, bio-oil can be separated into WS and WIS fractions. The WIS fraction is very viscous and its weight fraction also gradually increased during the storage. This may imply a causal relationship exists between the amount of bio-oil WIS fraction and viscosity. Indeed, as indicated in Fig. 4.8, the bio-oil viscosity showed better correlation ($R^2>0.88$) with the amount of WIS fraction than that between viscosity and Mw. The amount of WIS fraction also showed some correlation with Mw as well, however the R^2 is not as satisfied as that between WIS and viscosity.

Although for a particular bio-oil sample either made from raw wood or torrefied wood, bio-oil viscosity can be correlated to its Mw and WIS content; such a correlation may not exist between raw and torrefaction bio-oils at a particular aging time, as otherwise

torrefaction bio-oil with higher viscosity should have higher molecular weight than that of raw bio-oil. Hoekstra [Hoekstra et al., 2011] found that measuring bio-oil molecular weight using size exclusion chromatography calibrated by polystyrene could bring substantial errors to the predicted bio-oil molecular weight and the RI detector also respond differently to different chemical compounds in the bio-oil. Therefore, if bio-oil contains different chemical compositions, their molecular weight obtained from GPC analysis may not be comparable. Accordingly, these inaccurate molecular weights cannot be correlated to bio-oil viscosity; however a strong correlation between bio-oil viscosity to its chemical composition, especially the viscous fraction may still exist. In Fig. 4.9, the viscosity for the raw bio-oil and three torrefaction bio-oils were plotted against their Mw and WIS content at four different time-points during the initial half-year storage. In this way, the viscosity to Mw/WIS correlation can be accessed between bio-oils with different origin. As expected and shown in Fig. 4.9, viscosity did not show good correlation to its Mw between bio-oils made from different feedstock, especially in the initial fresh state and after one month storage; however similar to Fig. 4.8, a strong correlation between viscosity and WIS content still exists even between different bio-oil samples. Therefore, the viscosity of bio-oil made from raw and torrefied wood maybe dominated by the amount of WIS fraction rather than its average molecular weight, as the determined Mw from GPC does not reflect its absolute value. These results also suggest that using Mw obtained from size exclusion chromatography to estimate bio-oil aging severity may not be accurate if bio-oils have different chemical composition.

3.2.4 Bio-oil chemical composition during room-temperature storage

The GC/MS quantification of aged bio-oil components over a long-term storage was summarized in Table 4.3. Among these bio-oil components, glycolaldehyde, levoglucosan, catechol and HMF exhibited more stable natures when contained in torrefaction bio-oil (particularly for LP-330T) as its concentration changes within the first six month were less significant than that of raw bio-oil. The content of acetic acid, acetol and phenol did not vary significantly during storage. Interestingly, guaiacol and p-cresol, 4-methoxy showed significantly increased concentration in aged LP-280T which suggests that lignin-monomer formation via fragmentation of lignin-oligomers or inter-conversion between lignin monomers may have occurred in the aging process of torrefaction bio-oils.

There is also a clear chemical composition change for raw and torrefaction bio-oils during the twelve-month-storage as revealed by solvent fractionation of aged bio-oils shown in Fig. 4.10. Similar to the composition change after accelerated aging, the room-temperature aged bio-oils also showed the same variation tendency. Aged bio-oil WS/ES/EIS fractions generally decreased while WIS/HMM fraction increased during the available aging period. The bio-oil LMM fraction showed a less predictable nature as it alternated between an increasing and decreasing trend has been observed for LP-Raw, LP-310T and LP-330T.

For a better compositional stability comparison between raw and torrefaction bio-oils, a daily averaged fraction change divided into three periods on a six-month storage basis was calculated in Fig. 4.11. In the first month storage, LP-Raw and LP-280T showed smaller WS/WIS and LMM/HMM fraction variation than LP-310T and LP-330T. The ES and EIS fraction were more reactive in LP-310T and LP-330T respectively. In 1-3 month storage, the

changing rate of WS/WIS/ES/LMM/HMM fractions of aged raw bio-oil accelerated while torrefaction bio-oils started to become more stable, especially for LP-330T. In 3-6 month storage, only LP-280T showed noticeable changes on WS/WIS/ES/HMM fractions and LP-Raw also have a similar increasing rate for the HMM fraction. In addition, the EIS fraction of LP-330T increased significantly during 3-6 month storage and it may indicate condensation reactions occurred between pyrolytic sugar and other bio-oil constituents. As suggested by Oasmaa, water-soluble sugar-lignin-complex may be presented in the EIS fraction [Oasmaa and Kuoppala, 2003], hence, the lignin moieties in the sugar fraction may condense with bio-oil ES or WIS components forming complex water-soluble polymers and cause the increased EIS fraction in LP-330T. Overall, during the six-month room-temperature storage, LP-Raw and LP-280T are considered to be slightly more stable than other two torrefaction bio-oils in the first month storage, while torrefaction bio-oils, especially LP-330T had less composition change during the next five month storage.

4. Conclusions

The effect of biomass torrefaction on bio-oil stability has been compared with accelerated aging and long-term room-temperature aging methods. Mixed effects have been observed on the physicochemical and compositional property of aged bio-oils. Torrefaction pretreatment cannot inhibit water and acid accumulation in accelerated aged bio-oils and it also has a negative effect on maintaining bio-oil initial viscosity especially for bio-oils (LP-330T) made from high temperature tread wood. During the storage, however, the physical properties of torrefaction bio-oils (especially LP-330T) could reach a fast equilibration in the

initial storage period and they also had less significant molecular weight increase after aging. In addition, a stable bio-oil phase could be achieved by torrefaction pretreatment as less severe gum formation and no phase separation has been observed on certain torrefaction bio-oils, i.e LP-280T. Bio-oils made from torrefied wood also have relatively more stable chemical compositions than raw bio-oil as the latter had rapid accumulation of water insoluble solids after accelerated aging and during the 1-3 month storage. By considering the overall effects on aged bio-oil physicochemical and compositional properties, bio-oil made from mild-torrefaction treated wood, LP-280T, exhibited the most stable and predictable nature after aging and has a good potential to be processed in bio-oil application as transportation fuel.

5. Acknowledgements

This study was supported by Southeastern Sun Grant Center, the US Department of Transportation (Grant No. DTO559-07-G-00050) and the National Science Foundation (Grant No. 0832498). The author would like to thank Chris Hopkins at North Carolina State University for providing heat-treated wood, Dr. David Dayton and Dr. John Carpenter at RTI International for the help on measuring bio-oil TAN number.

References

Ben, H., Ragauskas, A.J. 2012. In Situ NMR Characterization of Pyrolysis Oil during Accelerated Aging. ChemSusChem, 5(9), 1687-1693.

Biddy, M., Dutta, A., Jones, S., Meyer, A. 2013. In-situ catalytic fast pyrolysis technology pathway. Technical Report NREL/TP-5100-58056, PNNL-22320, pp. 1-6. Retrieved from http://www.nrel.gov/docs/fy13osti/58056.pdf

Baldwin, R.M., Feik, C.J. 2013. Bio-oil Stabilization and Upgrading by Hot Gas Filtration. Energy & Fuels, 27(6), 3224-3238.

Diebold, J.P. 2002. A Review of the Chemical and Physical Mechanisms of the Storage Stability of Fast Pyrolysis Bio-Oils. in: Fast Pyrolysis of Biomass: A handbook, (Ed.) A.V. Bridgwater, CPL Press. Newbury, U.K., pp. 205-241.

Diebold, J.P., Czernik, S. 1997. Additives To Lower and Stabilize the Viscosity of Pyrolysis Oils during Storage. Energy & Fuels, 11(5), 1081-1091.

Elliott, D.C., Oasmaa, A., Preto, F., Meier, D., Bridgwater, A.V. 2012. Results of the IEA Round Robin on Viscosity and Stability of Fast Pyrolysis Bio-oils. Energy & Fuels, 26(6), 3769-3776.

Fratini, E., Bonini, M., Oasmaa, A., Solantausta, Y., Teixeira, J., Baglioni, P. 2005. SANS Analysis of the Microstructural Evolution during the Aging of Pyrolysis Oils from Biomass. Langmuir, 22(1), 306-312.

Hoekstra, E., Hogendoorn, K.J.A., Wang, X., Westerhof, R.J.M., Kersten, S.R.A., van Swaaij, W.P.M., Groeneveld, M.J. 2009. Fast Pyrolysis of Biomass in a Fluidized Bed

Reactor: In Situ Filtering of the Vapors. Industrial & Engineering Chemistry Research, 48(10), 4744-4756.

Hoekstra, E., Kersten, S.R.A., Tudos, A., Meier, D., Hogendoorn, K.J.A. 2011. Possibilities and pitfalls in analyzing (upgraded) pyrolysis oil by size exclusion chromatography (SEC). Journal of Analytical and Applied Pyrolysis, 91(1), 76-88.

Ingram, L., Mohan, D., Bricka, M., Steele, P., Strobel, D., Crocker, D., Mitchell, B., Mohammad, J., Cantrell, K., Pittman, C.U. 2007. Pyrolysis of Wood and Bark in an Auger Reactor: Physical Properties and Chemical Analysis of the Produced Bio-oils. Energy & Fuels, 22(1), 614-625.

Kim, T.-S., Kim, J.-Y., Kim, K.-H., Lee, S., Choi, D., Choi, I.-G., Choi, J.W. 2012. The effect of storage duration on bio-oil properties. Journal of Analytical and Applied Pyrolysis, 95(0), 118-125.

Mante, O.D., Agblevor, F.A. 2012. Storage stability of biocrude oils from fast pyrolysis of poultry litter. Waste Management, 32(1), 67-76.

Meng, J., Park, J., Tilotta, D., Park, S. 2012. The effect of torrefaction on the chemistry of fast-pyrolysis bio-oil. Bioresource Technology, 111(0), 439-446.

Moens, L., Black, S.K., Myers, M.D., Czernik, S. 2009. Study of the Neutralization and Stabilization of a Mixed Hardwood Bio-Oil. Energy & Fuels, 23(5), 2695-2699.

Naske, C.D., Polk, P., Wynne, P.Z., Speed, J., Holmes, W.E., Walters, K.B. 2011. Postcondensation Filtration of Pine and Cottonwood Pyrolysis Oil and Impacts on Accelerated Aging Reactions. Energy & Fuels, 26(2), 1284-1297.

Oasmaa, A., Elliott, D.C., Korhonen, J. 2010. Acidity of Biomass Fast Pyrolysis Bio-oils. Energy & Fuels, 24(12), 6548-6554.

Oasmaa, A., Korhonen, J., Kuoppala, E. 2011. An Approach for Stability Measurement of Wood-Based Fast Pyrolysis Bio-Oils. Energy & Fuels, 25(7), 3307-3313.

Oasmaa, A., Kuoppala, E. 2003. Fast Pyrolysis of Forestry Residue. 3. Storage Stability of Liquid Fuel. Energy & Fuels, 17(4), 1075-1084.

Oasmaa, A., Meier, D. 2005. Characterization, Analysis, Norms and Standards. CPL Scientific Publishing, Newbury, UK.

Ortega, J.V., Renehan, A.M., Liberatore, M.W., Herring, A.M. 2011. Physical and chemical characteristics of aging pyrolysis oils produced from hardwood and softwood feedstocks. Journal of Analytical and Applied Pyrolysis, 91(1), 190-198.

Song, M., Zhong, Z., Dai, J. 2010. Different solid acid catalysts influence on properties and chemical composition change of upgrading bio-oil. Journal of Analytical and Applied Pyrolysis, 89(2), 166-170.

Xu, F., Xu, Y., Lu, R., Sheng, G.-P., Yu, H.-Q. 2011. Elucidation of the Thermal Deterioration Mechanism of Bio-oil Pyrolyzed from Rice Husk Using Fourier Transform Infrared Spectroscopy. Journal of Agricultural and Food Chemistry, 59(17), 9243-9249.

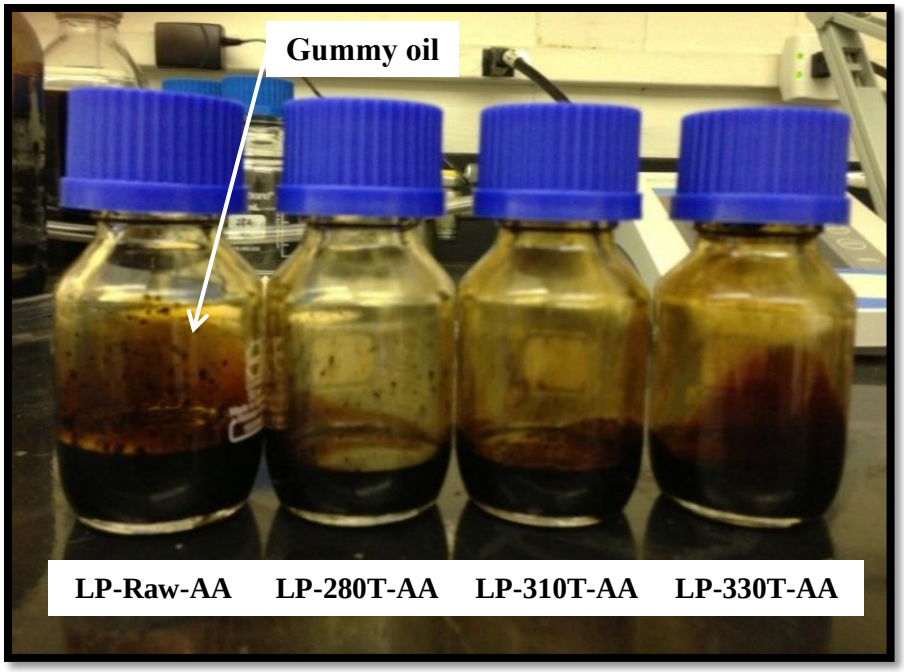

Figure 4.1 Accelerated-aged bio-oils. LP-Raw-AA contains significant amount of gummy oil after accelerated aging, while the other aged bio-oil from torrefied wood are visually-free of such sticky oil.

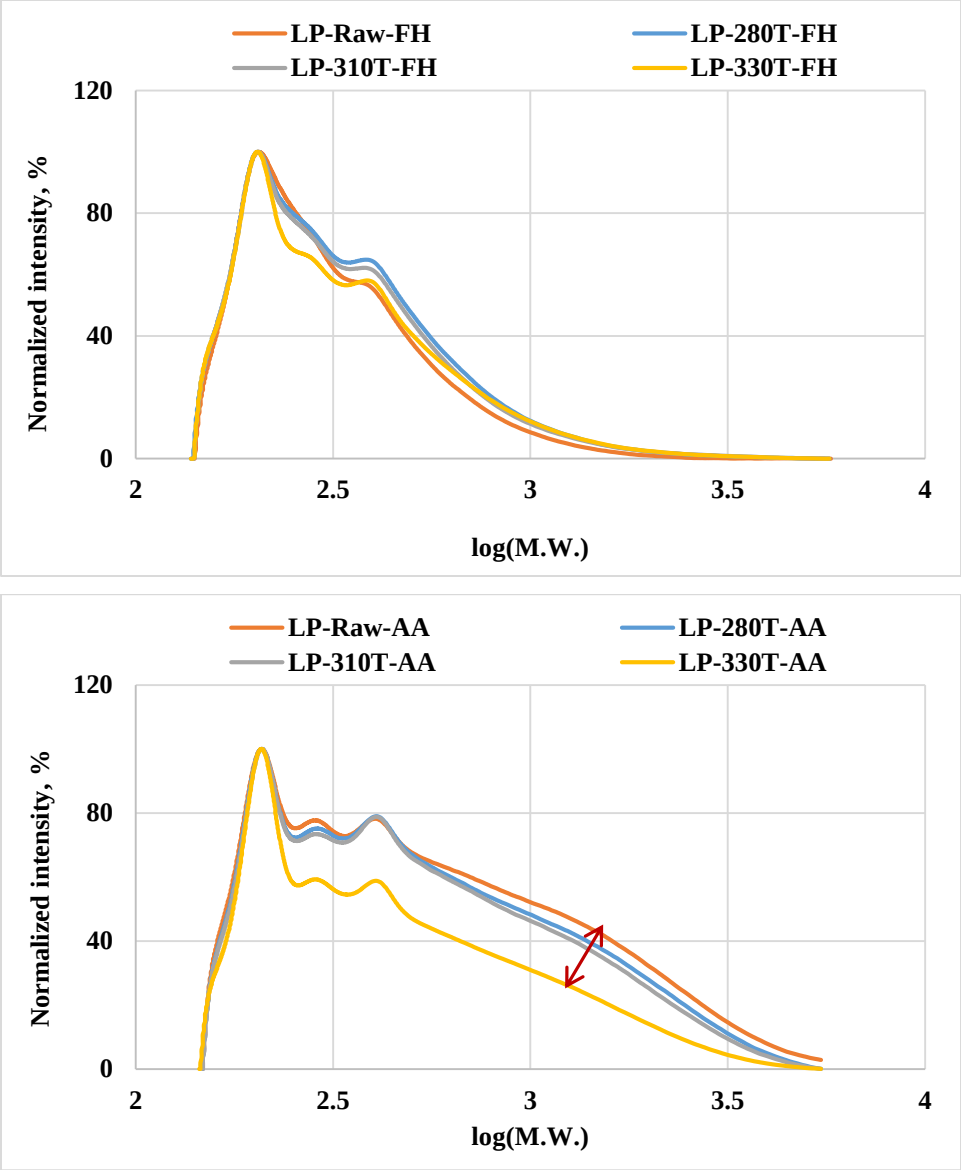

Figure 4.2 Molecular weight distribution (Mw) of accelerated aged bio-oil determined by RI detector. Top one is molecular weight distribution for fresh bio-oils and bottom one is molecular weight distribution for accelerated aged bio-oils.

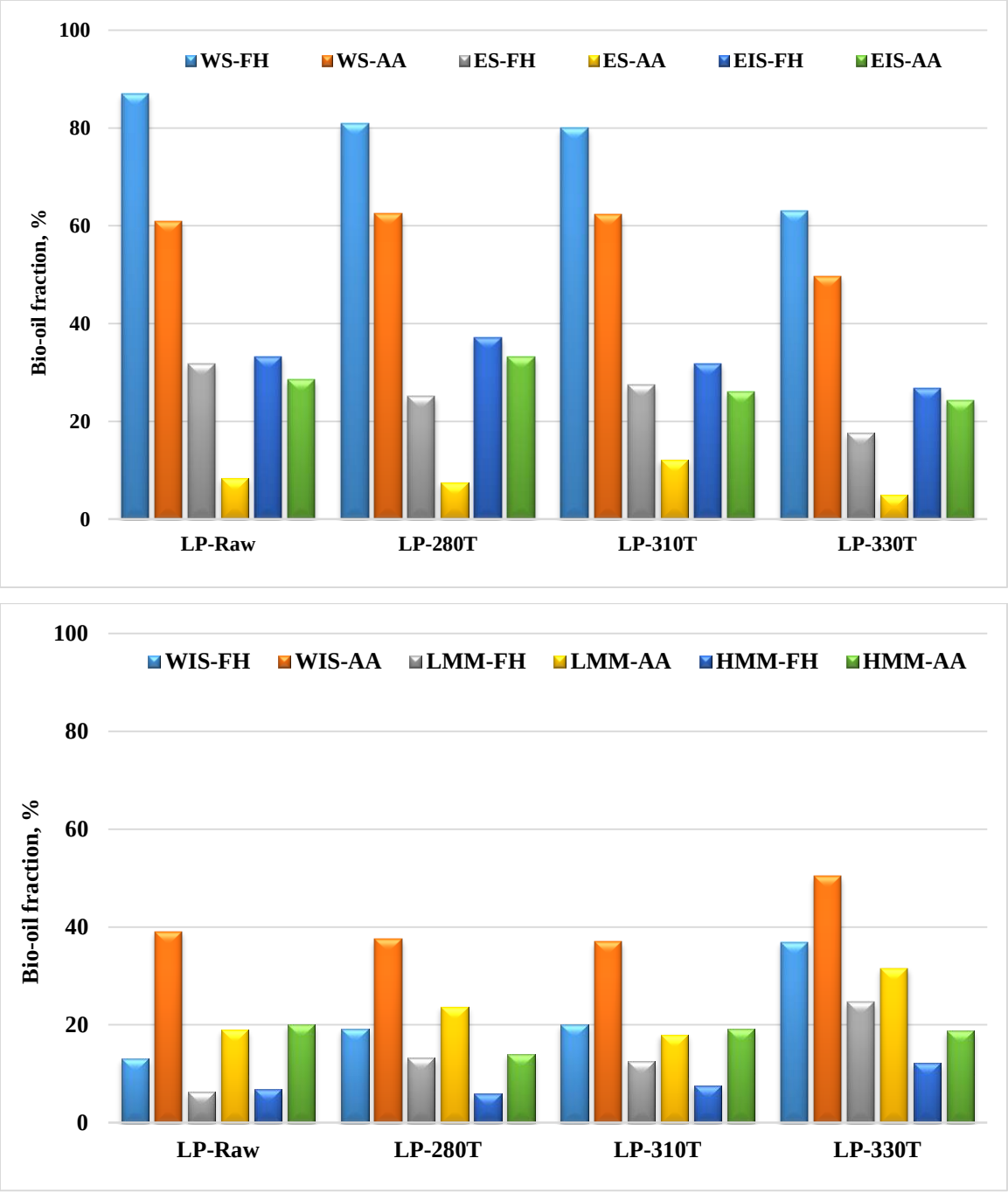

Figure 4.3 Comparison of chemical composition between fresh and accelerated aged bio-oils determined by solvent fractionation method.

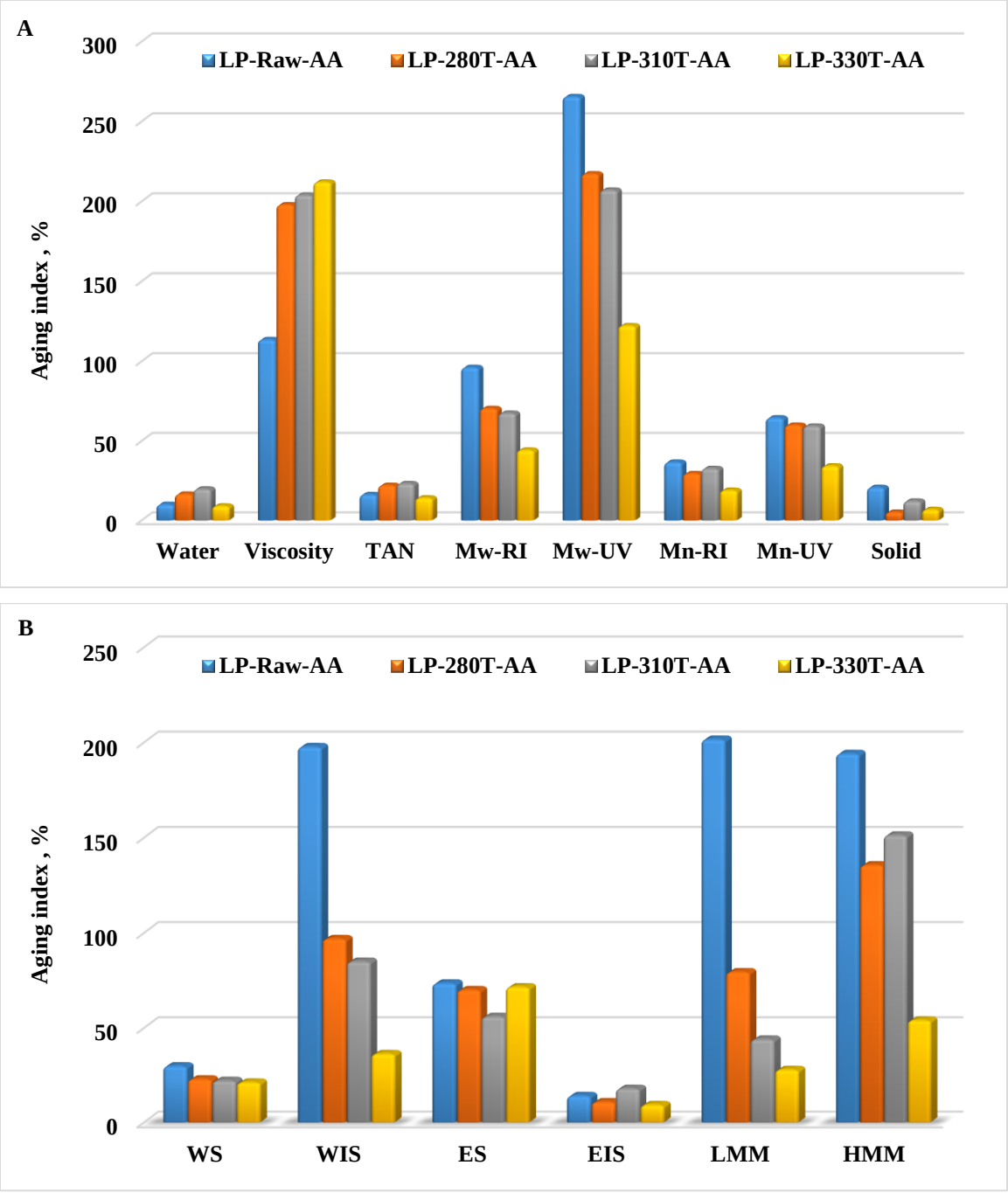

Figure 4.4 Aging index of physicochemical properties (A) and chemical composition (B) of accelerated aged bio-oil.

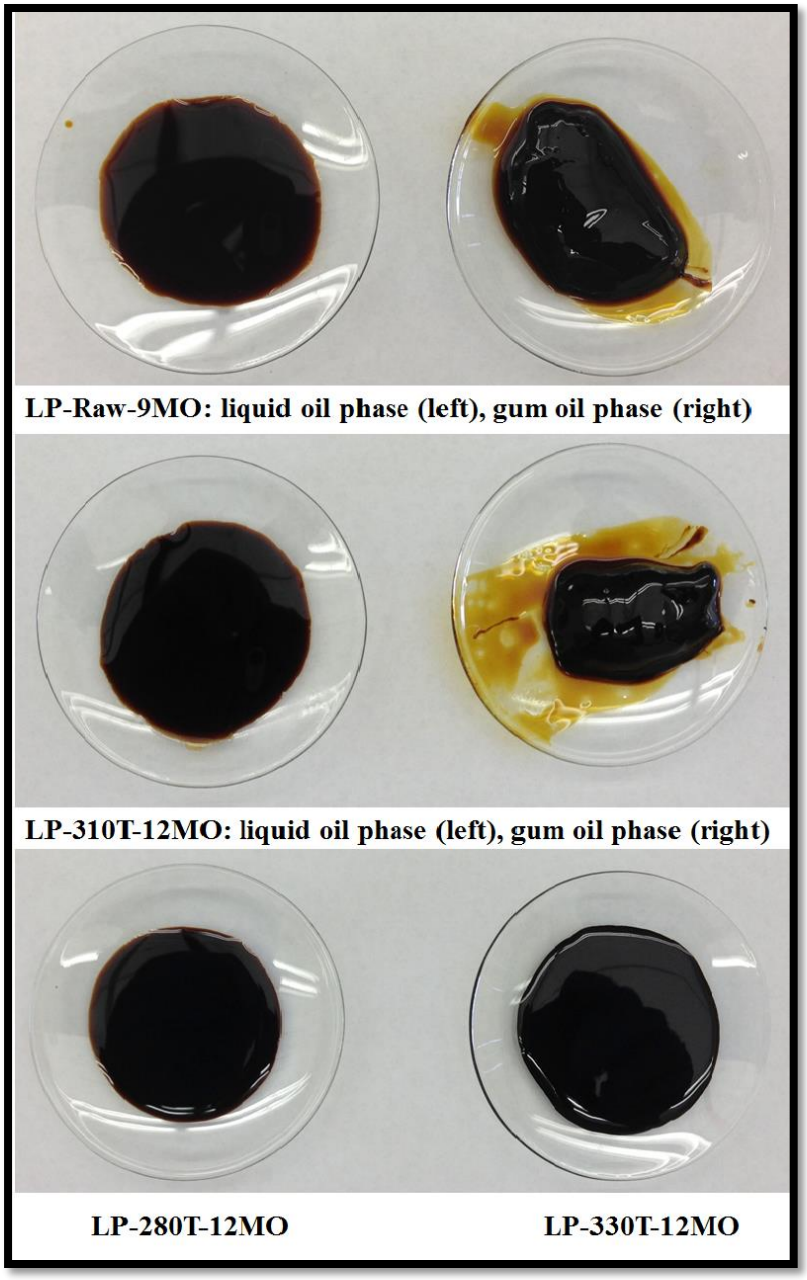

Figure 4.5 Phase behavior of aged bio-oils. LP-Raw and LP-310T phase separated at nine and twelve month storage; LP-280T and LP-330T can maintain one phase after twelve month storage.

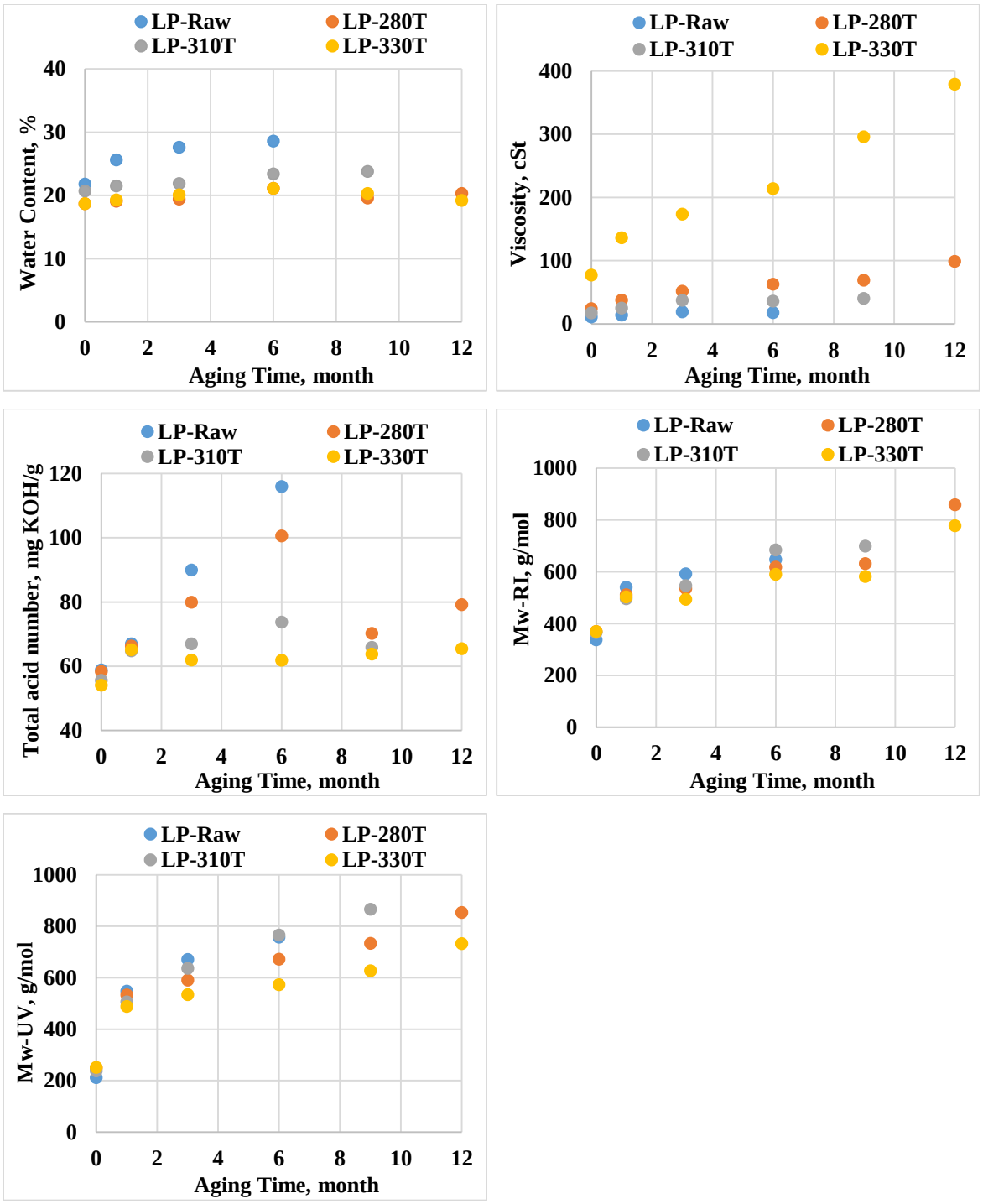

Figure 4.6 Physicochemical property change of aged bio-oil during twelve-month room-temperature storage.

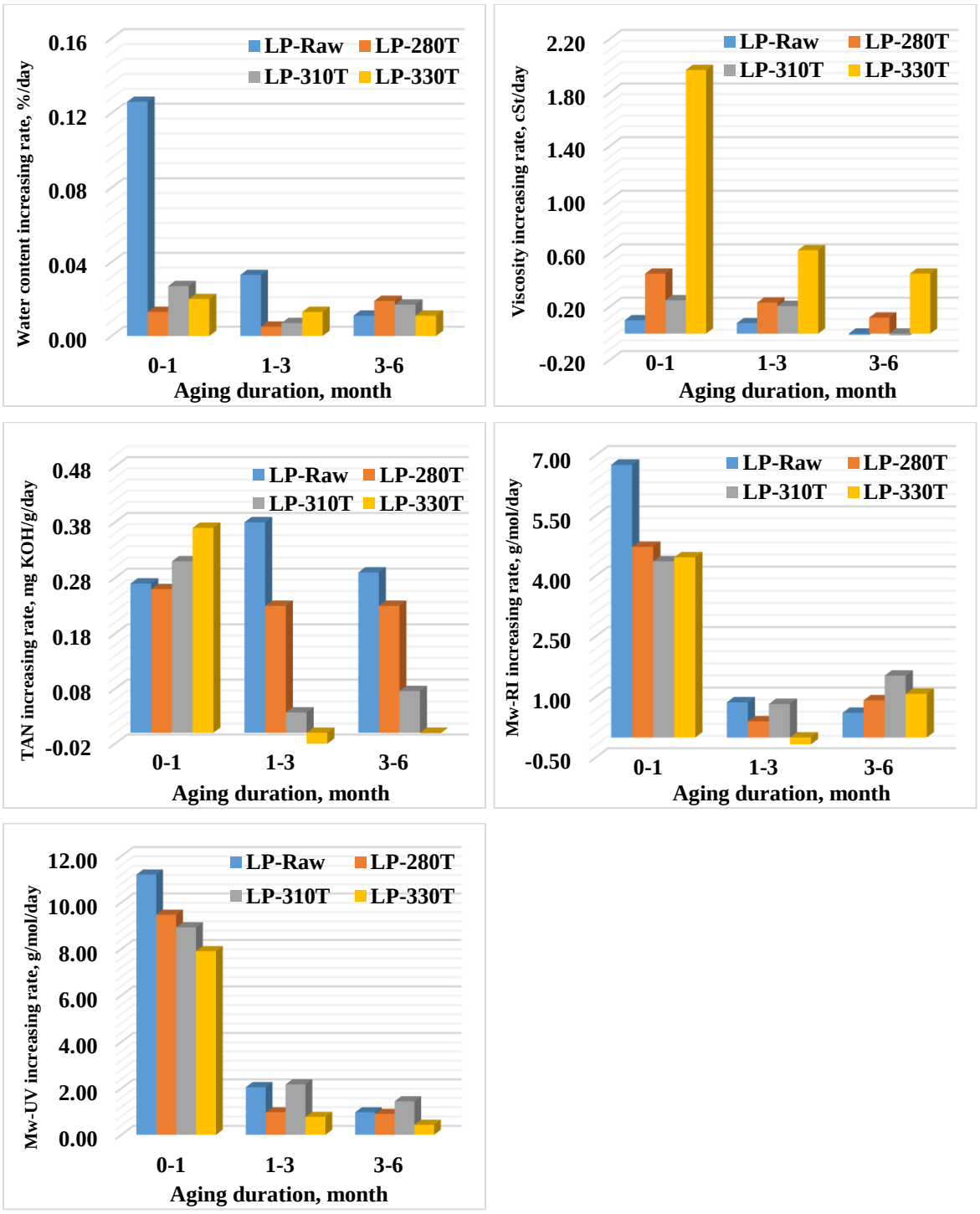

Figure 4.7 Physicochemical property changing rate of accelerated aged bio-oil in six-month storage.

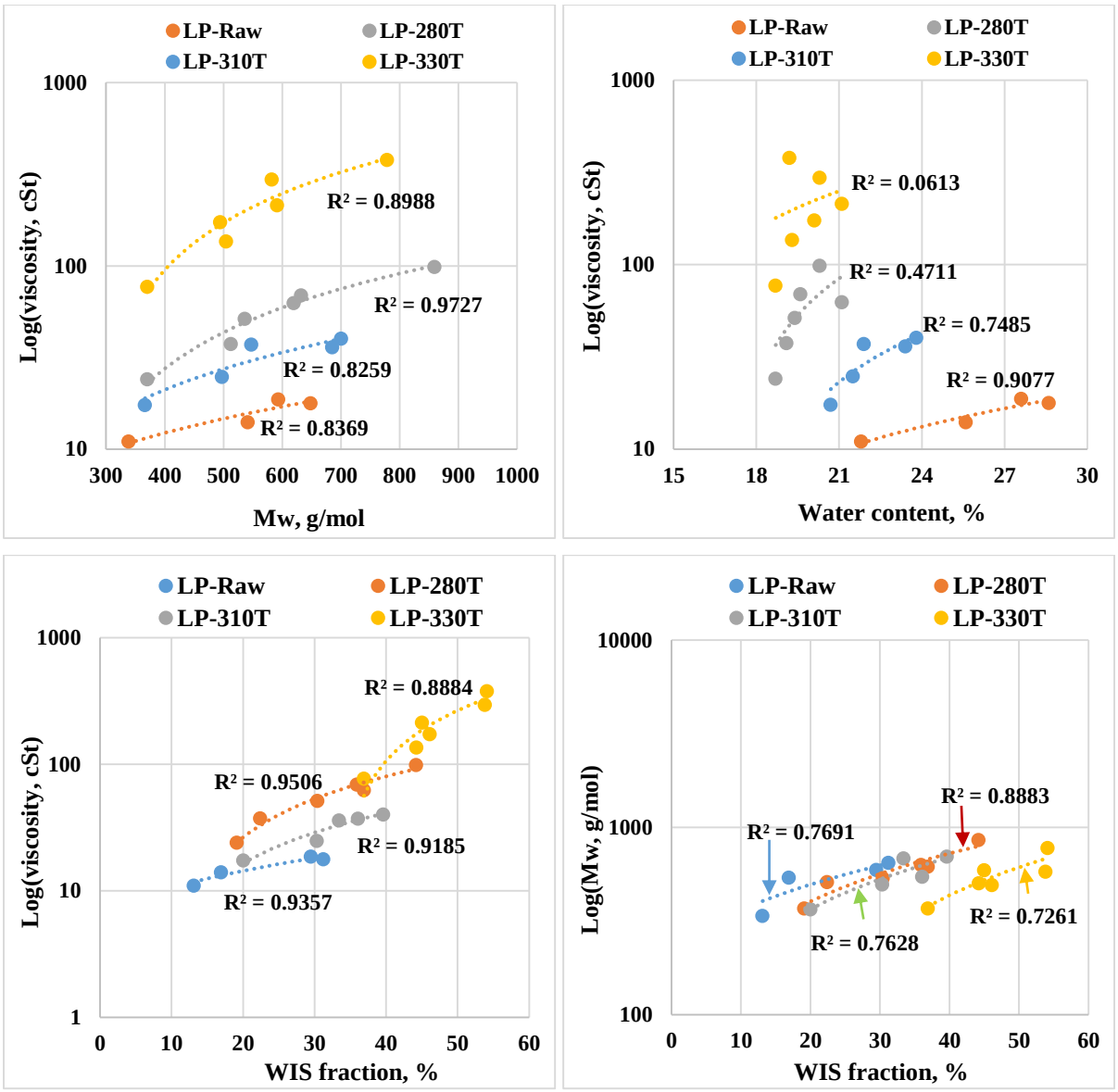

Figure 4.8 Correlation between viscosity and molecular weight/water content for the bio-oils during entire storage (top two figures) and correlation between viscosity/Mw and WIS fraction of the bio-oils during entire storage (bottom two figures).

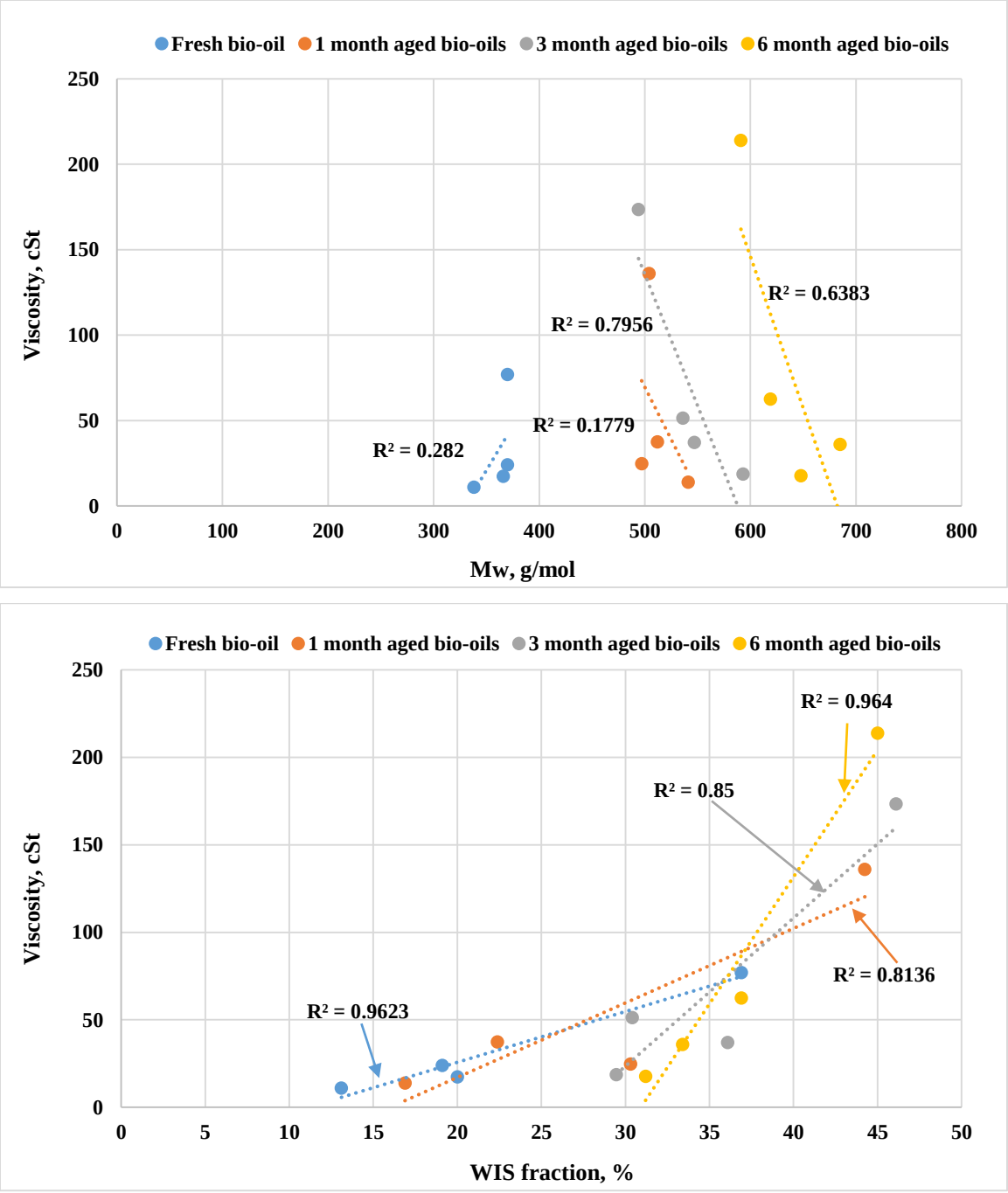

Figure 4.9 Correlation between viscosity and WIS/Mw for raw and torrefaction bio-oils at same aging time within first six-month storage.

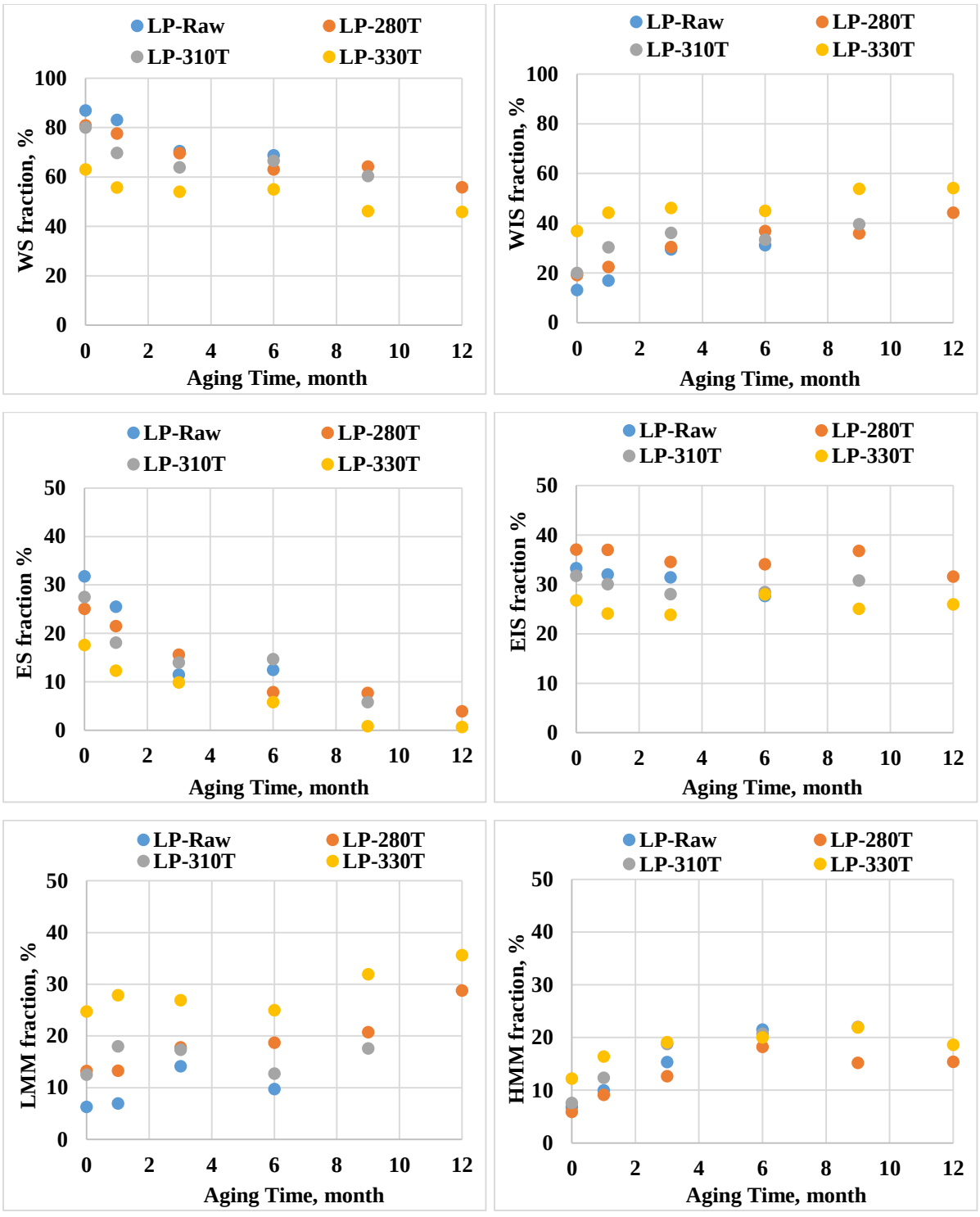

Figure 4.10 Chemical composition change of aged bio-oil during twelve-month room-temperature aging.

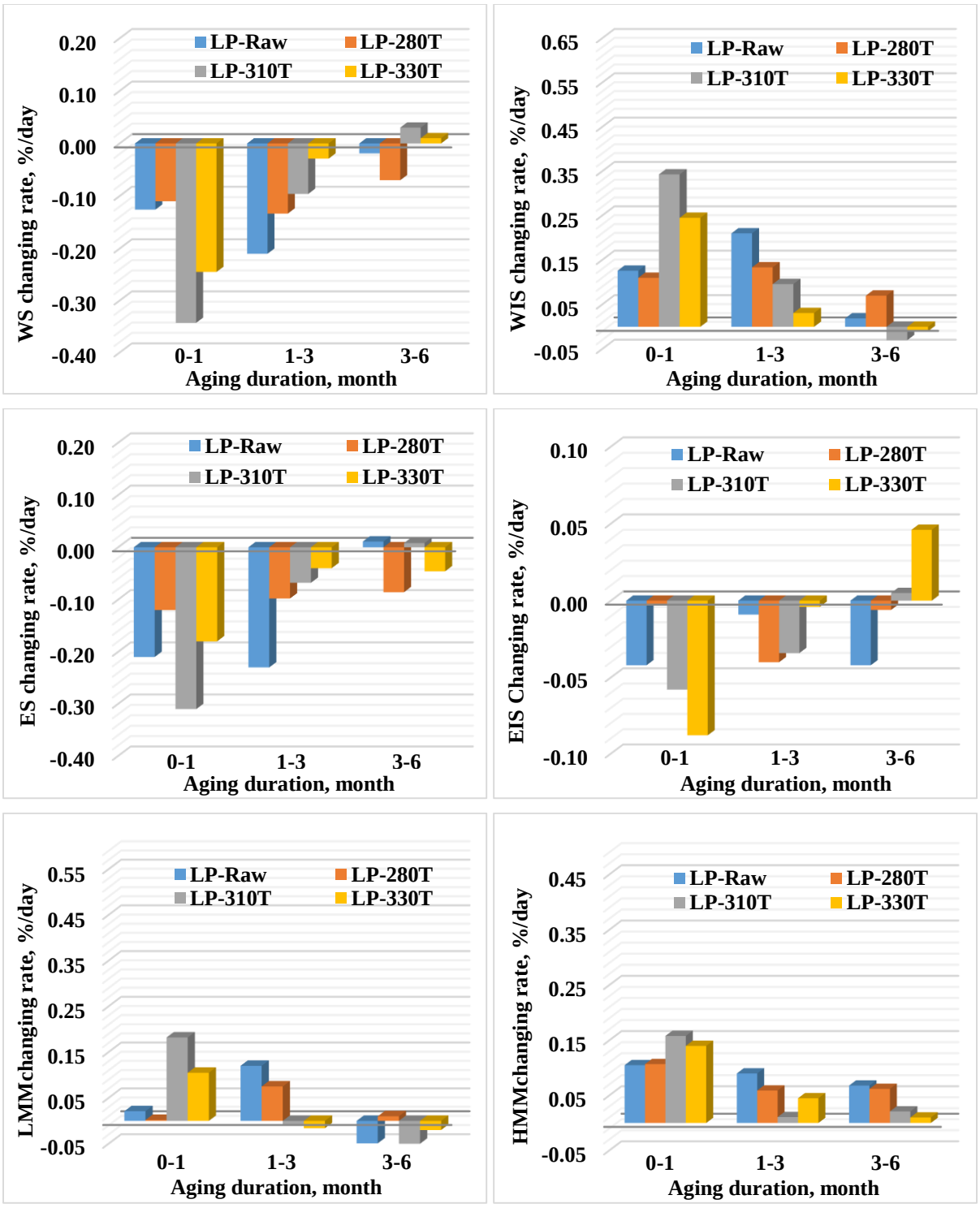

Figure 4.11 Chemical composition changing rate of aged bio-oil during six-month aging.

Table 4.1 Characterization of torrefied wood (dry base).

Wood sample	Raw wood	TW-280T	TW-310T	TW-330T
Chemical Composition				
Carbohydrates, %				
Glucan	40.8	37.1	28.9	18.0
Xylan	6.8	3.8	2.3	0.4
Galactan	2.3	1.2	0.8	0.0
Arabinan & Mannan	11.1	6.8	4.2	0.6
Total sugar, %	61.0	48.9	36.2	19.0
Lignin+Residues[a], %				
Acid insoluble residues[b]	30.0	42.0	55.5	74.2
Acid soluble residues	1.0	1.1	1.0	2.6
Total lignin+char residues	31.0	43.1	56.5	76.8
Extractives[c], %	1.5	4.0	6.2	10.4
Ultimate and Proximate Analysis				
C, %	49.3	54.3	59.4	65.8
H, %	6.64	5.96	5.48	4.87
O, %	44.0	39.6	35.0	27.6
N, %	0.07	0.09	0.11	0.28
O/C atomic ratio	0.67	0.55	0.44	0.31
HVC[d], %	6.5	3.9	3.9	4.2
Volatile matter, %	88.4	79.5	73.5	59.9
Fix carbon, %	11.1	19.4	25.2	38.6
Ash, %	0.52	1.10	1.26	1.45
HHV[e], MJ/kg	19.7	21.1	22.8	26.3

a. Lignin + Residue: contain conventional lignin and char residue made from torrefaction process.

b. Acid insoluble residue: Klason lignin and char made from cellulose, hemicellulose and lignin heat treatment.

c. Extractives: contain conventional wood extractives and other organics, i.e. levoglucosan produced from torrefaction treatment.

d. HVC: highly volatile compounds, including water and other light organics absorbed on the torrefied wood surface.

e. HHV: high heating value.

Table 4.2 Physicochemical properties of accelerated aged bio-oils.

	LP-Raw	LP-280T	LP-310T	LP-330T
Physicochemical Properties				
Water content - FH, %	21.8	18.7	20.7	18.7
Water content - AA, %	24.0	21.8	24.8	20.4
Viscosity - FH, cSt	11.0	24.1	17.4	77.0
Viscosity - AA, cSt	23.5	71.8	52.9	240.3
TAN - FH, mg KOH/g	58.9	58.4	55.6	54.1
TAN - AA, mg KOH/g	68.5	71.3	68.5	61.8
Mw[a] - FH, g/mol	338 (212)	370 (249)	366 (238)	370 (251)
Mw[a] - AA, g/mol	663 (775)	631 (790)	613 (731)	534 (558)
Mn[a] - FH, g/mol	267 (65)	278 (70)	275 (69)	274 (70)
Mn[a] - AA, g/mol	365 (107)	360 (112)	356 (110)	326 (94)
Solids - FH, %	0.24	0.58	0.74	1.16
Solids - AA, %	0.29	0.61	0.83	1.24
Elemental Composition (dry base)				
C - FH, %	50.1	54.1	55.6	62.8
C - AA, %	51.1	56.7	58.5	65.0
H - FH, %	6.7	6.4	6.2	5.6
H - AA, %	6.3	6.4	6.1	6.0
O - FH, %	42.7	39.1	37.7	30.9
O - AA, %	42.0	36.5	35.0	28.3
N - FH, %	0.53	0.44	0.47	0.67
N - AA, %	0.63	0.40	0.41	0.70

a. Mw and Mn are determined by RI detector and UV detector at 254 nm; data shown in parentheses represents the average molecular determined by UV detector.

Table 4.3 GC/MS quantification of bio-oil compounds after natural and accelerated aging.

Aging Time	0 month	1 month	3 month	6 month	9 month	12 month	AA
			Glycolaldehyde				
LP-Raw	12.4	8.1	8.9	9.2	-	-	6.4
LP-280T	11.9	9.2	10.2	9.7	7.2	7.1	6.5
LP-310T	9.8	8.9	10.1	9.1	8.2	-	6.3
LP-330T	5.8	6.4	5.8	5.2	4.2	3.7	2.4
			Acetic Acid				
LP-Raw	2.8	2.5	2.7	2.6	-	-	2.4
LP-280T	2.6	2.3	2.4	2.3	2.4	2.5	2.5
LP-310T	2.7	2.5	3.1	2.7	2.6	-	2.5
LP-330T	2.1	1.8	1.7	2.2	1.8	2.3	2.4
			Acetol				
LP-Raw	2.8	3.1	2.8	2.3	-	-	1.9
LP-280T	2.5	2.7	2.5	2.1	1.3	1.2	2.0
LP-310T	2.4	2.8	2.8	2.2	1.5	-	1.9
LP-330T	1.1	1.6	1.6	1.4	1.1	1.0	1.4
			Levoglucosan				
LP-Raw	3.7	3.2	3.1	3.0	-	-	2.7
LP-280T	4.6	4.1	4.0	4.1	2.5	2.5	3.6
LP-310T	5.1	4.8	4.8	4.4	3.9	-	3.9
LP-330T	6.1	6.4	5.6	6.1	5.7	4.6	5.8
			HMF				
LP-Raw	0.42	0.39	0.36	0.29	-	-	0.30
LP-280T	0.42	0.42	0.43	0.36	N.D.	0.46	0.34
LP-310T	0.43	0.36	0.37	0.30	N.D.	-	0.31
LP-330T	0.27	0.26	0.21	0.24	N.D.	0.40	0.25
			Phenol				
LP-Raw	0.20	0.16	0.20	0.13	-	-	N.D.
LP-280T	0.22	0.19	0.21	0.16	0.15	0.20	0.01
LP-310T	0.25	0.32	0.38	0.30	0.31	-	0.06
LP-330T	0.33	0.39	0.45	0.38	0.37	0.41	0.08
			Catechol				
LP-Raw	0.92	0.87	0.81	0.76	-	-	0.44
LP-280T	1.01	0.49	0.56	0.72	N.D.	N.D.	0.42
LP-310T	1.06	1.49	1.27	0.96	N.D.	-	0.35
LP-330T	1.09	1.82	1.51	0.90	N.D.	N.D.	0.57
			Guaiacol				
LP-Raw	N.D.	N.D.	N.D.	N.D.	-	-	N.D.
LP-280T	0.01	0.31	0.31	0.21	0.24	0.28	0.05
LP-310T	0.06	N.D.	N.D.	N.D.	0.02	-	0.08
LP-330T	0.08	0.10	0.10	0.05	0.13	0.15	0.13
			p-Cresol, 4-methoxy				
LP-Raw	N.D.	N.D.	N.D.	N.D.	-	-	N.D.
LP-280T	0.02	0.38	0.40	0.32	0.35	0.38	0.06
LP-310T	0.06	N.D.	N.D.	N.D.	0.10	-	0.08
LP-330T	0.09	0.10	0.13	0.07	0.16	0.10	0.15

N.D. – Not Detected.

Table 4.4 Quantitative ^{1}H NMR characterization of accelerated aged bio-oil.

Type of Proton	δ[a], ppm	LP-Raw		LP-280T		LP-310T		LP-330T	
		FH %	AA %	FH %	AA %	FH %	AA %	FH %	AA %
-CHO, -COOH	10.0-9.6	0.97	1.11	0.71	0.82	0.54	0.62	0.32	0.35
ArH, HC=C-	8.2-6.0	14.8	10.1	21.9	8.6	17.9	7.8	14.2	5.8
CH_3O-, -CH_2O-, -CHO-	6.0-3.0	62.7	55.3	47.2	55.6	47.2	45.1	41.8	49.9
-CH_3, -CH_2-	0.5-3.0	21.5	33.3	34.1	34.0	34.9	39.9	43.6	44.0

a. Integration range was selected based on reference [Ben and Ragauskas., 2012]

Table 4.5 Quantitative ^{13}C NMR characterization of accelerated aged bio-oil.

Type of carbon	δ[a], ppm	LP-Raw		LP-280T		LP-310T		LP-330T	
		FH	AA	FH	AA	FH	AA	FH	AA
		%	%	%	%	%	%	%	%
Carbonyl	215-163	6.4	5.4	5.7	5.5	5.1	5.1	3.8	3.7
Aromatic & C=C	163-110	26.7	31.0	29.2	33.4	30.7	33.8	31.9	35.8
Carbohydrate	110-84	20.6	19.1	21.8	17.9	21.2	19.9	20.2	20.0
Methoxy/hydroxy	84-54	28.4	24.9	25.9	24.7	25.7	23.4	24.6	23.3
Alkyl carbons	54-1	17.9	19.6	17.4	18.5	17.3	17.8	19.5	17.2

a. Integration range was selected based on reference [Ingram et al., 2008]

Table 4.6 Phase behavior during long-term room temperature aging.

	Storage duration, month					
	0	1	3	6	9	12
LP-Raw	Y	Y	X	X	N	N
LP-280T	Y	Y	Y	Y	Y	Y
LP-310T	Y	Y	X	X	X	N
LP-330T	Y	Y	Y	Y	Y	Y

a. Y: one uniform bio-oil phase.

b. X: pseudo-uniform bio-oil phase determined as small amount of gum formed in the bottom of storage bottle but it can be mixed with other portion of bio-oil using vortex mixer for 30mins.

c. N: completely phases-separation – liquid phase in the top and gum phase in the bottom; the gum oil phase cannot be mixed with the liquid phase and a vortex mixing on this phase separated bio-oil lead to the gum phase move up to the top with a lot of air-bubble formed in the oil.

CHAPTER 5

Towards Understanding on Bio-oil Aging Mechanism: Accelerated Aging of Bio-oil and Bio-oil Sub-Fractions

1. Introduction

Bio-oil condensed from biomass pyrolysis vapor is a dark-brown viscous liquid and has economic potential to be upgraded into transportation fuel using current refinery infrastructure. Because of its apparent close to crude oil, bio-oil is also commonly known as bio-crude; however, it shares no similarities with natural fossil oil in terms of fuel property. Typical bio-oil liquids contain high oxygen, water and acid content. Also, due to the presence of oxygen-rich compounds, e.g. aldehydes, bio-oil is neither chemically nor thermally stable. The unstable nature of pyrolysis oil make it unprocessable in the storage and further upgrading stage, as aged bio-oil typically shows increased water content, viscosity, and phase separation. In addition, the catalyst coke-formation may also be blamed to the bio-oil poor stability under high temperature upgrading conditions. [Bertero et al., 2011]

The bio-oil aging phenomena can be explained by polymerization of bio-oil components under acidic and thermal conditions catalyzed by the mineral compounds contained in the bio-oil char particles [Naske et al., 2011; Baldwin and Feik, 2013]. Diebold [Diebold, 2000] proposed that diverse aging reactions could occur in bio-oil. These possible reactions include: esterification of organic acids with alcohols; homo-polymerization of aldehydes; hydration of aldehydes or ketones with water; formation of hemiacetals or acetals from aldehydes and alcohols; resin formation from aldehydes and phenols; olefinic

condensation; and air oxidation of alcohols and aldehydes forming carboxylic acids. However, none of these proposed reactions have been experientially verified in a chemical environment similar to that of bio-oil.

The extreme complexity of bio-oil composition adds great difficulties on bio-oil aging mechanism study. Current aging research mainly focused on characterizing its bulky physicochemical and compositional property change together with seeking methods to slow down the aging rate. [Diebold and Czernik, 1997; Xu, et al., 2011; He et al., 2009; Xu et al., 2008; Chaala et al., 2004] Studies on molecular-level bio-oil polymerization mechanism has rarely been published. Hu and his co-workers [Hu et al., 2013] reported a bio-oil polymerization study by heating the bio-oil model compounds under gradually increased temperature and concluded that sugars, acids, phenolics and furfural may contribute significantly to the bio-oil polymerization. These results are of great importance to the understanding of bio-oil aging reactions, however the model compounds used in the study did not represent the whole bio-oil composition as the oligomers were not included; in addition, the complicated bio-oil chemical environment was not simulated in the study. To make it more representative to actual reactions occurred in bio-oil, isolated bio-oil fractions may be used.

In this chapter, investigation on the bio-oil aging reactions has been performed in a step-wised strategy. First, accelerated aging of the whole bio-oil produced from loblolly pine was performed with varied conditions to gain an overall understanding on its aging characteristics. Further, to suppress the interference of complicated bio-oil composition on actual aging reactions, isolated bio-oil fractions were accelerated aged under different

temperature and pH environment. The aging severities were evaluated with characterizing the molecular weight and carbon distributions of the aged bio-oil fractions. This particular aging study, for its first time, studied the aging behavior of individual bio-oil fractions. Finally, one of the most possible aging interactions between aldehydes and pyrolytic lignin has been carried with model compounds study and reacting various aldehydes identified in bio-oil with the isolated pyrolytic lignin. The reaction products were characterized with GPC and ^{13}C NMR. Based on the results obtained from the above experimental design, a preliminary bio-oil aging model has been proposed to help future research on related bio-oil aging mechanism study.

2. Materials and Methods

2.1 Bio-oil production

Loblolly pine chips (properties summarized in Table 5.1) were grinded and sieved into small particles (<0.5 mm) with a Wiley mill and were further air dried for fast pyrolysis operation. The bio-oil was produced from a fluidized bed reactor (O.D. 43mm, 150 g/hour feed capacity) at 500±10°C with ~1s residence time as described previously [Meng et al., 2012]. The bio-oils were collected by two condensers (0-4 °C) and an electro-static precipitator. One liter of raw bio-oils were produced for the aging study with an average liquid yield ~65%. These oils were thoroughly homogenized and stored in a freezer (-4 °C) for further aging experiments. The characterization of typical bio-oil properties are summarized in Table 5.2.

2.2 Bio-oil accelerated aging

Unless otherwise specified, approximately 10 g of bio-oil were aged in a reaction tube (ACE 8648-04-15 mL) under 80 °C for 24 hours in an convection oven [Elliott et al., 2012]; different aging time and temperature were also employed in specific studies. The bio-oil aging index (absolute value) was calculated according to equation 1, where P stands for a particular bio-oil property. Accelerated aging was denoted as AA in this chapter.

$$\text{Aging index} = (P_{\text{Aged bio-oil}} - P_{\text{Initial bio-oil}})/P_{\text{Initial bio-oil}} * 100\% \quad [1]$$

For the accelerated aging of bio-oil fractions, approximated 10 g of bio-oil water soluble (WS) fraction (~90% water, pH-2.5) and ether insoluble (EIS) sugar fraction (~80 % water, pH-2.6) were aged in individual reaction tubes under 80 °C and 110 °C for 24 hours. To investigate the pH effect on bio-oil aging severity, sodium hydroxide neutralized WS and EIS fractions were also aged at 80 °C. The aged water soluble fraction were dissolved in THF and dried with anhydrous sodium sulfate (Fisher, 7757-82-6) for GPC analyses and the aged ether insoluble fraction were rotatory-vacuum dried for further ^{13}C NMR and GPC characterization. Accelerated aging of bio-oil water insoluble (WIS) lignin fraction (~3% water, ~1g loading) were performed in a ACE tube with/without adding carboxylic acids (acetic acid and formic acid) under 80 or 110 °C for 24 hours. The aged lignin samples were rotatory-vacuum dried to remove the moisture and acids for further GPC and ^{13}C NMR characterization.

2.3 Characterization of bio-oil

2.3.1 Physicochemical properties

Bio-oil ultimate analysis was performed according to ASTM-D5291 using a Perkin Elmer CHN Elemental Analyzer (2400 Series II). The oxygen content was calculated by difference. The water content of the bio-oil was determined by Karl-Fischer titration according to ASTM E 203-08 using HYDRANAL Composite 5 (Sigma-Aldrich 34805) and HYDRANAL Medium K (Sigma-Aldrich 34698). The total acid number (TAN) of bio-oil was measured according to ASTM D644-07 using an automatic titrator (Mettler-Toledo, T50). Inflection point was employed to determine the titration end point. The titration reagent, 0.1M KOH in isopropanol solution (RICCA 6257-32) was purchased from Fisher Scientific. The bio-oil kinematic viscosity was measured according to ASTM D445 using the Cannon-Fenske viscometer (size 150 and 200). The bio-oil average molecular weight was analyzed by Gel Permeation Chromatography (GPC) carried out on a Shimadzu HPLC system (LC-20AD) with an UV detector (254 nm) and an RI detector. Two columns (WatersStyragel, HR-1 and HR-5E) were connected for the bio-oil components separation. The column oven temperature was set at 35 ºC. Tetrahydrofuran (THF, Sigma 401757) was used as the mobile phase flowing at 0.7 mL/min. The bio-oil samples was dissolved in THF to approximately 2 mg/mL (0.5 mg/mL for pyrolytic lignin) and then filtered through a 0.25μm filter for the analysis. Twelve polystyrene standards with the molecular weight ranging from 162-3520000 were used to generate the calibration curve.

2.3.2 Chemical composition

The bio-oil solvent fractionation was performed according to a method described in a reference [Oasmaa and Meier, 2005]. Simply, the bio-oil was first extracted with excess DI water (bio-oil:water=1:30 w.t. ratio) and separated into water soluble (WS) and water insoluble (WIS) fraction. The water soluble fraction was further extracted with diethyl ether (v:v=1:1) and fractionated into an ether soluble (ES) and an ether insoluble (EIS) fraction. The water insoluble fraction was extracted with dichloromethane (v:v=1:1) and fractionated into a low molecular mass lignin (LMM) fraction and a high molecular mass (HMM) lignin fraction. Dichloromethane (34856) and diethyl ether (346136) was purchased from Sigma-Aldrich and used as received.

Gas chromatographic/mass spectrometric (GC/MS) analyses of the bio-oil were performed on a Finnigan Polaris Q Plus system. The operational conditions of GC/MS can be found in author's previous publication [Meng et al., 2012]. The semi-quantification of the major bio-oil compounds was achieved by generating calibration curves with standard chemicals and using internal standard - fluoranthene. All the standards (purity > 99.9%) were purchased from Sigma-Aldrich and VWR International and used without further purification.

2.3.3 ^{1}H and ^{13}C NMR characterization of bio-oil

^{1}H and ^{13}C NMR characterization of bio-oils were recorded in DMSO-d6 (Cambridge Isotope Laboratories, DLM-10TB) solution (25% wt./wt.) with 5mm NMR tube (Wilmad, 528-PP-7) using a Bruker Avance 700 MHz NMR spectrometer. The NMR experiments were conducted with a cryoprobe at 279K. ^{1}H spectrum was acquired by a single pulse sequence

(zg) with 3.2s pulse delay time and a total of 32 scans at 25 ºC. ^{13}C spectrum was obtained by inverse gated decoupling pulse sequence (zgig), 90º pulse angle, 2.5s pulse delay time and a total of ~20000 scans at 25 ºC. The spectra phase and base-line correction and integration of the ^{1}H and ^{13}C NMR spectra was conducted with a Topspin software 3.2 (Bruker H9966S3).

2.4 Phenol-glycolaldehyde reaction

Glycolaldehyde was produced when heating the glycolaldehyde dimmer (Sigma Aldrich, G6805) solution above 70 °C [Yaylayan, et al., 1998] during the reaction. In three reaction vials (45 mL), 0.1 mole of phenol and 0.05 mole of glycolaldehyde dimer (moral ratio phenol to glycolaldehyde = 1:1) was prepared in each vial along with three different acid catalysts: (a) 3 ml of acetic acid (b) 3 ml of formic acid and (c) 3 ml of HCl (0.5 mol/ml) respectively. 1 ml of DI water was also added into the reaction vials when acetic acid and formic acid were used. A control vial with 0.05 mole of glycolaldehyde and 3 ml of HCl without phenol addition was also included. After mixing with a vortex mixer, the four vials with acetic acid, formic acid, HCl and the control were placed in a silicone oil bath at 90 °C for 24 hours, 12 hours, 5 hours and 2 hours respectively. The cooled reaction products were rotatory-vacuum dried to remove the water and acids for ^{13}C NMR characterization according to the method described in section 2.3.3. All the reaction chemicals (ACS reagent) used in this experiment were purchased from Sigma-Aldrich and used as received.

2.5 Pyrolytic-lignin-aldehydes reaction

Approximately 60 g of pyrolytic lignin (PL) was isolated from 500 ml of bio-oil using ice-water precipitation method as described in a reference [Scholze et al., 2001]. Rather than collecting the lignin through filtration, isolated lignin was collected by centrifuging the suspended oil-water solution at 5300 rpm for 30 mins. After centrifuging, the liquid phase was decanted and the residue lignin was washed with DI water until the water becomes colorless. The collected wet lignin was vacuumed dried at 30 ° for 24 hours. After vacuum drying, the pyrolytic lignin was in a sticky gum shape, similar to plasticene, and contained ~3% of moisture.

Several kinds of aldehydes identified in the bio-oil, including formaldehyde [Tessini et al., 2012], glycolaldehyde, furfural, HMF, vanillin were reacted with PL under 80 °C for 24 hours in a convection oven. Approximately, 1g of PL along with the aldehydes and acid catalyst (acetic acid or formic acid) were added into a 15 mL reaction tube (ACE, 864804). The weight ratio between pyrolytic lignin to aldehydes and acid was kept at 6:1:6. In addition, ~0.3 ml of DI water was also added into the reaction tubes except the one containing formaldehyde, as formaldehyde was already added as a water solution (37 wt.%). The carboxylic acids could fully dissolve the lignin and forming a uniform reaction media for the potential reaction between PL and aldehydes. After the reaction, the solutions were cooled to room-temperature and transferred to a pear-shape flask for rotatory-vacuum drying removing the residue acids and water. In case of solid resin formed in the reaction tube, the reaction products were dissolved in acetone and then vacuum dried. The vacuum-dried final reaction products were brown to dark lignin solids and were characterized by GPC and ^{13}C

NMR technique. ^{13}C NMR analyses of the lignin-aldehyde reaction products were conducted according to the same method as described in 2.3.3 but using a Bruker Avance DRX 500 MHz NMR spectrometer. All the reaction chemicals (ACS grade) were purchased from Sigma-Aldrich and used as received.

3. Results and Discussions

3.1 Characterization of physicochemical properties and chemical composition of aged bio-oil

The physicochemical properties of accelerated aged bio-oil are presented in Table 5.2. The elemental composition of aged bio-oil was essentially the same to that for raw bio-oil. The bio-oil water content, viscosity, average molecular weight (represented as Mw and Mn) and total acid number (TAN) increased after accelerated aging.

Various condensation reactions, generating by-product water, could take place in the bio-oil aging process leading to increased water content in aged bio-oil. Recently, reduced water content has also been reported on the accelerated aged bio-oil [Elliott et al., 2012] and the reason of this opposite trend could due to a leaking of water vapor during the heating process which can be avoided by using better sealed aging bottle, e.g. ACE pressure tube. Moreover, heterogeneous phase property of aged bio-oil may also affect the water content determination. For example, water condensates could build up on the inner wall of the storage bottle after aging and they may not be mixed well with the bio-oil bulky phase. In addition, inappropriate solvent choice for bio-oil Karl-Fischer (KF) titration could also contribute to the low water content. The raw bio-oil contains high amount of aldehydes and

ketones which can react with the alcohol-based KF solvent producing reaction water and giving misleadingly high initial water content. After aging, the aldehydes and ketones were consumed; when the aged bio-oil was tested with the same solvent, a lower water content may be obtained as less by-product water would be generated during the titration. The author has seen 5-10% (absolute value) water content difference by using ethanol based KF solvent verse chloroform based one. Therefore, avoid using the alcohol-based KF solvent is critical to correct water content determination on the aged bio-oil.

The viscosity increase of aged bio-oil is well supported by its increased average molecular weight and expanded molecular weight distribution. Fig. 5.1 presents an Mw distribution comparison between the fresh and aged bio-oil. After aging, a significant growth of bio-oil high molecular weight fraction can be observed. By an even closer examination on the molecular weight aging index shown in Table 5.2, the number averaged molecular weight (Mn) changed less significantly than the weight average molecular weight (Mw); this may suggests that only a low-degree polymerization, e.g. dimerization occurred in the bio-oil aging process. In addition, the UV detector discovered a more significant change in the bio-oil molecular weight variation than the RI detector did suggesting the active role of UV-visible compounds in the bio-oil aging reactions.

The bio-oil chemical composition change was determined by solvent fractionation and GC/MS quantification method. As shown in Fig. 5.2, the bio-oil water soluble (WS) fraction decreased; as a result, the water insoluble (WIS) fraction increased indicating more hydrophobic solids were generated after aging. The WS fraction can be further separated into an ether soluble (ES) and an ether insoluble (EIS) fraction. The ES fraction, containing

carboxylic acids, aldehydes and lignin monomers is highly reactive and it decreased rapidly after accelerated aging. Accordingly, as shown in Fig. 5.3, the content of glycolaldehyde, acetol, acetic acid, HMF, phenol and catechol decreased after aging. On the other hand, the EIS fraction, also known as the sugar fraction only decreased slightly after aging. The pyrolytic sugar fragments contained in the bio-oil has been previously determined by Lomax [Lomax et al., 1991]. Under acidic and high temperature conditions, these sugar products could go further decomposition reactions producing aldehydes and carboxylic acids which may explain the TAN increase associated with aged bio-oil. As an example, it was found that levoglucosan, one of the most abundant anhydrosugars in the bio-oil, can be hydrolyzed to glucose [Bennett et al., 2009] and further degraded to formic acid and furfural. Therefore, as shown in the Fig. 5.3, levoglucosan concentration decreased after accelerated aging as it was either converted into glucose or further degraded into other light oxygenates. However, severe sugar degradation only take place at high temperature; while the accelerated aging temperature at 80 °C cannot initiate a massive losing of the pyrolytic sugar components; therefore, compared to the ES fraction, the EIS fraction was relatively stable. The WIS fraction is typically referred as a pyrolytic-lignin fraction containing various phenolic oligomers derived primarily from lignin pyrolysis. This fraction can be further separated into a low molecular mass (LMM) and a high molecular mass (HMM) lignin fraction using dichloromethane extraction. After aging, the LMM and HMM fractions increased in a same manner. The newly generated WIS lignin fraction must originate from the WS fraction; however, aromatic lignin fraction is not likely to be produced solely from the bio-oil water-soluble components. This increase may be fulfilled by potential condensation occurred

between the lignin fraction and the ES or EIS fractions. In addition, since solvent fraction method is solely based on the solubility of bio-oil components, this increase may also come from the formation of hydrophobic solids formed in WS fraction alone.

3.2 The effect of aging temperature and duration on bio-oil properties

The physicochemical property of aged bio-oil with varied aging temperature and time are summarized in Table 5.3. As gradually increasing these two parameters, the bio-oil water content, viscosity, TAN number and average molecular weight increased accordingly. At the low heating temperature (40 and 60 °C), the aged bio-oil did not show considerable property change after 24 hours heating. A severe bio-oil property alternation could only be observed after aging temperature reached 80 °C. Further promoting the temperature to 110 °C lead to severe phase separation observed as sticky gum-oil aggregates with high Mw precipitated from the bio-oil liquid-phase. In the case of varied aging time at 80 °C, the properties of aged bio-oil, increased more steadily over the 24 hours heating. These results suggest that bio-oil aging involves temperature and time dependent condensation reactions.

The bio-oil composition dependence on aging temperature and time is presented in Table 5.4 and Fig. 5.4. As indicated in Table 5.4, the content of glycolaldehyde, acetic acid, acetol, HMF, levoglucosan, phenol and catechol generally decreased as increasing the aging severity. The glycolaldehyde showed most significant concentration decrease after aging. The gum-oil aggregates generated from aged bio-oil at 110 °C contained no GC-elutable compounds except the acetic acid. Fig. 5.4 presents the whole bio-oil composition change with varied aging time and temperature. Generally, the WS fraction including the ES and EIS

fractions decreased while the WIS fraction including the HMM and LMM fractions increased as increasing the aging severity. Similar to its physicochemical property change, the bio-oil composition showed less sensitivity to the low temperature heating but changed linearly as increasing the heating time at a constant temperature. The chemical composition of bio-oil aged at 110 °C was not quantified due to the difficulty of extracting gum oil with water.

3.3 Individual aging of the bio-oil fractions

Complicated bio-oil composition (over 300 different chemicals) poses significant difficulties on its molecular-level aging mechanism study and simple characterization of aged bio-oil properties, as discussed above, could not provide enough information to reveal the fuzzy reaction pathway. In author's opinion, one breakthrough on bio-oil aging study can be made by fractionating the whole bio-oil followed by individual aging of these fractions under accelerated aging conditions. As each bio-oil fraction contains similar chemical species, their reaction patterns in the aging process may be shared. In fact, bio-oil is not a uniform single-phase liquid as it was previously found to be a micro-emulsion with an organic pyrolytic-lignin phase stabilized by an aqueous phase [Fratini et al, 2006]. Due to this heterogeneous nature, the bio-oil aging reactions may primarily occur in each individual bio-oil fraction, i.e. WS and WIS fractions. However, it cannot be excluded that mutual reactions between the bio-oil fractions could also occur especially under high temperature. In this section, the bio-oil WS, EIS and WIS fractions were aged under accelerated aging conditions with different temperature and pH environment.

3.3.1 Accelerated aging of water soluble fraction and pyrolytic sugar fraction

It is previously suggested that the aldehydes, acids and sugars are the main villains causing bio-oil aging and catalyst coking [Diebold, 2002; Wildschut et al., 2009; Gayubo et al., 2010; Lu et al., 2010]; the bio-oil WS fraction is the main host of these three aging suspects. Therefore, understanding the aging behavior of the WS fraction could be critical to piecing together overall bio-oil aging mechanism. In addition, as part of the WS fraction, ether insoluble sugar fraction may also participate actively in the aging reactions as these sugars are typically reactive under acidic heating conditions.

The initial WS and EIS fractions were light-yellow clear liquids; after accelerated aging at 80 °C, there were a small amount of brown solid formed inside the aging tubes; the liquid color of aged WS and EIS remain unchanged. At a higher heating temperature - 110 °C, as shown in Fig. 5.5, a significant amount of dark-brown solid, especially for the sugar fraction, were accumulated inside the reaction tubes. The liquid color of the aged sugar-fraction turned into dark-brown after the high temperature heating. Obviously, after solvent fractionation of an aged bio-oil sample, these brown solids generated after aging of WS and EIS fraction could be miscalculated as pyrolytic lignin.

The average molecular weight of accelerated aged bio-oil fractions are summarized in Table 5.5 and the Mw aging indexes were plotted in Fig. 5.6. After heating treatment under acidic condition (pH=2.5) at 80 °C, no apparent Mw change was observed for the liquid phase of aged WS and EIS fractions as indicated by the aging index shown in Fig. 5.6-A and B; however the precipitated brown-solids showed significant Mw increase when compared to

their starting liquid fractions. Similar but more pronounced effect, especially for the WS fraction, has been found when aging temperature was adjusted to 110 °C for and EIS.

The exact sugar polymerization mechanism is not clearly demonstrated by literatures, but the author believes that it is initiated by acid-catalyzed sugar decomposition forming reactive compounds which possess hydroxyl, carbonyl groups and conjugated double bonds, e.g. HMF and then followed by re-polymerization of these degradation products. In the abovementioned reaction pathway, acid catalyst plays an important role on promoting the initial sugar depolymerization and the secondary re-polymerization reactions. Therefore, it is expected that the reaction rate would be significantly decreased if the acids could be removed from the bio-oil fractions. To test this hypothesis, the pH value of WS and EIS sugar fraction was slowly adjusted to 7 using dry sodium hydroxide and the resulting neutral fractions were accelerated aged under 80 °C for 24 hours. After aging, as shown in Fig. 5.6-C and D, the aged WS and EIS fraction, especially the solids part, showed significantly less molecular weight increase than that aged under acidic conditions. Therefore, the condensation reactions of WS and EIS fractions which generate water-insoluble solids are acid catalyzed reactions.

To further elucidate the pyrolytic sugar aging reaction, ^{13}C NMR integration of the fresh and aged EIS fraction was calculated. As shown in Table 5.6, the carbonyl carbon decreased while the amount of C=C carbon increased significantly after aging. The reduced carbonyl signal could be achieved by condensation reactions similar to aldol-condensation for polymerizing sugar compounds or sugar degradation products containing aldehyde groups. The increased C=C carbon may support the abovementioned sugar degradation and repolymerization path as the typical sugar degradation products, i.e. furfural, contain such

conjugated carbon double bonds. In addition, the aldol condensation products also contain such π bond system. For the six-carbon sugar ring structure, the number of C_1 end carbon and C_1-O-C_4 carbon decreased while the aliphatic carbon increased. The content of $C_{2,3,4,5,6}$ carbon remain unchanged. The reduced C_1 end carbon and C_1-O-C_4 carbon suggest that the sugar fragmentation may occurred at sugar ring structure on the C_1-O-C_5 bond and sugar chain structure at the β-1,4 linkage. The increased aliphatic carbon may originate from the sugar condensation products, e.g. the brown solid. In all, these NMR results support the two stage sugar decomposition and re-polymerization mechanism.

3.3.2 Accelerated aging of pyrolytic lignin fraction

Phase separation and sticky gum formation are often observed after bio-oil aging especially at high heating temperature. As the WS and EIS sugar fraction did not produce such gum after aging, the author believes that these gum aggregates are mainly formed from the condensation and aggregation of bio-oil lignin fraction.

The average molecular weight of aged pyrolytic lignin with/without acid addition is presented in Table 5.7. As indicated by the aging index shown in Fig. 5.6-E, the molecular weight of aged pyrolytic lignin increased significantly in an acid-free environment. Adding acetic acid could further promote the lignin condensation, however more pronounced effect was not shown until formic acid was added. In addition, more severe Mw increase was observed when aging temperature was raised from 80 to 110 °C. It is well known that the acid-catalyzed lignin condensation could take place between the electron-rich aromatic-ring and the cationic site from benzyl alcohol and benzyl ether at α-carbon [Shimada et al., 1997].

As shown in Fig. 5.7, such condensation will increase the amount of aromatic C-C linkage in condensed lignin structure. Interestingly, pyrolytic lignin also polymerized under acid-free condition and it may be explained by a free radical reaction mechanism shown in Fig. 5.7. As suggested by Britt and Kibert [Britt et al., 1995; Kibet, et al., 2012], free radicals were generated during the lignin pyrolysis and the presence of these radicals in nature and kraft lignin has also been observed [Steelink, 1966]. In fact, the author has already confirmed the presence of radicals in pyrolytic lignin using EPR characterization and it will be discussed in the next chapter. Depending on where the radical locates, the condensed lignin structure from radical initiated reactions would feature increased amount of aromatic C-O and C-C bond.

The ^{13}C NMR integration of the aged lignin spectra (see Fig. 5.8) are summarized in Table 5.8. The results shown in this table support the above inference as the content of aromatic C-O and C-C bond increased after aging when compared to that of starting lignin. On the contrary, the aromatic C-H bond decreased. The aged lignin with acetic acid showed less significant change on the aromatic carbon distribution when compared to that with formic acid, suggesting the latter is more effective on crosslinking the lignin structure. The carbon signals at 54-58 ppm which often assigned to methoxy groups also decreased after aging. Ben [Ben and Ragauskas, 2012] published similar results and suggested that lignin demethoxylation could happen during the aging process. However, methoxy groups may not be easily cleaved from aromatic ring unless strong acid, i.e. HI, or high temperature is employed. Under mild aging conditions, the demethoxylation is less likely to happen and this signal drop may be more associated with the reduction of other overlapped signals, e.g. the hydroxyl-group attached β carbon in the lignin side chain.

3.4 Pyrolytic-lignin aldehyde reaction

In addition to the separate aging reactions within individual bio-oil fractions, mutual aging reactions between these fractions may also exist. One of the most important interactions involves the condensation between phenolic compounds in WIS fraction and aldehydes in ES fraction which may condense in a same fashion to that for classic phenol-formaldehyde reaction.

3.4.1 Model compounds study of phenol-glycolaldehyde reaction

Glycolaldehyde is the most abundant aldehyde identified in the bio-oil made from loblolly pine. After accelerated aging, the content of glycolaldehyde decreased by a factor of two. Many reactions may occur to this bi-functional chemical during the aging. For example, it may react with the pyrolytic lignin and cause the gum formation in the aged bio-oil. However, no reference has been found on reporting phenol-glycolaldehyde condensation; therefore this part of the chapter attempts to disclose glycolaldehyde reactivity towards condensing pyrolytic lignin. In order to verify the potential reaction between them, glycolaldehyde and phenol (n:n=1:1) were reacted with three different acid catalysts (acetic acid, formic acid and HCl) for different length of reaction time. The choice of using different reaction time is based on the concern of not forming DMSO insoluble resin which prevents the characterization of reaction product using NMR.

Before heating, as shown in Fig. 5.9-A, the reaction liquid was a clear solution with un-dissolved phenol deposited in the bottom of glass tube. After five hours heating at 90 °C, a free-flow dark-oil phase (see Fig. 5.9-D) was formed in the vial containing HCl. After,

twelve hours heating, a black liquid solution (see Fig. 5.9-C) was formed when formic acid was used. Acetic acid may have the least ability to catalyze the phenol-glycolaldehyde reaction as the liquid product only showed slightly color change (see Fig. 5.9-B) after 24 hours heating at 90 °C. As a control, the glycolaldehyde was also heated without adding phenol under acidic condition (see Fig. 5.9-E); after 2 hours heating at 90 °C, many soil-brown solids were found in the reaction tube suggesting that glycolaldehyde could undergo self-polymerization via possibly an aldol-condensation pathway.

^{13}C NMR analyses were performed to further characterize the above reaction product. It is expected that if the condensation between glycolaldehyde and phenol does occur in the applied aging conditions, a similar reaction pathway which generates phenol-formaldehyde resin may be applied. Specifically, the reaction would start with aromatic electrophilic substitution (ortho or para) and followed by a condensation step leading to crosslinking. However, compared to formaldehyde, glycolaldehyde has a bulky group (-CH2-OH) attached to its aldehyde group which may have steric hindrance for the crosslinking reactions to take place and it also has high tendency towards its self-polymerization. Therefore, the condensation, if does exist, may only occur at a limited extent i.e. dimerization of phenol and glycolaldehyde. In addition, due to the dual-functionality of glycolaldehyde (aldehyde and alcohol), various side-reactions could occur between the glycolaldehyde and the carboxylic acid catalysts.

As indicated in Fig. 5.10, all the reaction products contained significantly high amount of residual phenol suggesting its low reactivity towards glycolaldehyde. The NMR spectra of the oil phase (see Fig. 5.10-D) from hydrochloric acid catalyzed reaction have a

featured C_1 and C_4 aromatic substitution pattern. The aromatic C_1 shifted from 157.5 to 155.6 ppm (C_1') and C_2 shifted from 115.5 to 127.2 ppm (C_2') after ortho substitution. For the para substitution, the aromatic C_4 carbon signal shifted from 119.0 to 133.4 ppm (C_4') and a similar C_1 carbon shifting was also observed. These chemical shifting patterns were confirmed with carbon-shift predications on the proposed substitution structures shown in Fig. 5.10 using ACD/NMR Processor 10.0 software and a satisfactory matching can be obtained within ~0.3 ppm error. When formic acid was applied as the reaction catalyst, a similar ortho and para aromatic substitution can also be observed as C_1 shifted to C_1' from157.2 to155.8 ppm, C_2 shifted to C_2' from 115.2 to 127.4 ppm and C_4 shifted to C_4' from 118.8 to132.0 ppm. For acetic acid, however, such substitution pattern has not been detected indicating no reaction between phenol and glycolaldehyde in a weak-acid reaction medium.

In addition to the aromatic carbons discussed above, the NMR spectra of Fig. 5.10-B and C were found to be more complicated than that shown in Fig. 5.10-D. A strong signal assigned to a carbonyl ester carbon (~163 ppm) can be easily identified for formic acid catalyzed reaction indicating the esterification between formic acid and glycolaldehyde. Acetic acid, as shown in Fig. 5.10-B, can also react with glycolaldehyde forming acetyloxyacetaldehyde. In Fig. 5.10-B and C, the weak carbonyl carbon (aldehyde type) signal at 200-210 ppm indicates the presence of residual aldehyde in the final reaction product. In addition, a series of oxygen attached carbon signals were also found between 60 to 110 ppm which may originate from the hydroxyl carbons in self-polymerized

glycolaldehyde polymers as similar carbon signals (see Fig 5.9-E) have also been detected in the control reaction.

In summary, phenol-glycolaldehyde reaction could potentially occur with limited condensation degree (dimerization without further condensation reaction) when strong acid catalyst (HCl) are used. Similar reaction could also be catalyzed with formic acid. This implies that glycolaldehyde could potentially reacted with pyrolytic lignin under strong acidic environment in the bio-oil (pH=2.5). However, the reaction degree between glycolaldehyde and lignin may be limited and other side-reactions, i.e. esterification with carboxylic acids and self-polymerization may greatly inhibit the reaction rate; therefore glycolaldehyde may not be able to crosslinking the pyrolytic lignin.

3.4.2 Accelerated aging of pyrolytic lignin with aldehydes under acidic conditions

Formaldehyde, furfural and HMF are well-known aldehydes that could react with phenol making phenolic resins. [Knop and Pilato, 1985] Glycolaldehyde as disclosed above also has limited reactivity with phenol. To test the potential condensation between aldehydes and pyrolytic lignin, five different aldehydes previously identified in bio-oil, including formaldehyde, glycolaldehyde, furfural, HMF and vanillin were directly reacted with lignin extracted from bio-oil at accelerated aging conditions. Acetic and formic acid commonly found in the bio-oil were able to completely dissolve the pyrolytic lignin and used as reaction catalysts. Two pyrolytic lignin controls (without adding aldehydes) dissolved in acetic acid or formic acid were also included.

Before the reaction, the lignin-aldehyde mixtures were well dissolved in acids as a uniform liquid solution. After heating under acetic acid condition, the lignin-formaldehyde solution turned into solid, but the control and other lignin-aldehyde samples were still in a viscous liquid form. In the case of formic acid, lignin-aldehyde and lignin control solution turned into black chunks after aging suggesting higher lignin condensation degree as compared to that in acetic acid. Moreover, the aged lignin-formaldehyde products (formic acid catalyst) cannot fully dissolve in THF indicating a resin formation; therefore, only the THF soluble fraction was characterized with GPC and ^{13}C NMR.

Fig. 5.11 compared the averaged molecular weight (Mw) of lignin-aldehyde reaction products from two different acid environments. The Mw of aged pyrolytic lignin (control sample) increased gradually in acetic and formic acid solution. Formic acid showed more pronounced effect on condensing the lignin units due to its stronger acidity (pKa=3.75) than that of acetic acid (pKa=4.75). For lignin-aldehyde reaction in acetic acid solution, only formaldehyde cross-linked the lignin units as the Mw of aged lignin increased 8X when compared to that of starting lignin. A ^{13}C NMR characterization of this condensed lignin also howed a strong methylene bridge at ~30 ppm [Werstel, 1985] indicating an ortho-ortho or ortho-para linkage between the two phenolic units connected by substituted formaldehyde. Other aldehydes, including glycolaldehyde, furfural, HMF and vanillin did not show such effect. Particularly, the glycolaldehyde, as investigated above cannot effectively condense the lignin model compound - phenol in acetic acid, therefore no severe condensation with pyrolytic lignin is expected.

In contrary, as revealed by increased lignin molecular weight, when formic acid was used to catalyze the lignin-aldehyde reaction, most of the aldehydes used in this study were able to promote the lignin condensation. However, vanillin showed no reactivity on condensing pyrolytic lignin as the Mw of the reacted lignin-vanillin mixture was almost identical to that of aged lignin control. Also, the ^{13}C NMR characterization of the reaction product did not show any evidence on the linkage between vanillin aldehydes and lignin aromatic rings, instead only fingerprinted vanillin carbon signals were observed indicating its inert nature reacting with pyrolytic lignin in applied aging condition. Among other aldehydes, formaldehyde showed highest reactivity towards crosslinking the pyrolytic lignin due to the formation of THF insoluble resin. Although, aged pyrolytic lignin with glycolaldehyde, furfural and HMF addition also showed higher Mw than that of aged control lignin, no solid resins were obtained after the reaction indicating their low reactivity towards lignin condensation. In addition, the ^{13}C NMR characterization of these reacted lignin samples showed a featured glycolaldehyde self-condensation pattern similar to that shown in Fig. 5.9-E and excessive amount of residual furfural and HMF. This may imply that glycolaldehyde, HMF and furfural did not effectively promoting the lignin condensation and the increased Mw may largely due to aldehyde self-condensation or other side condensation reactions, e.g. esterification with acid catalyst. In fact, when reacting furfural or HMF to phenolic compounds, special synthesis technics, such as, slowly adding furfural into phenol solution is needed to enhance the reaction rate. In addition, the presence of water was also found to have a negative effect on the reaction rate. [Brown, 1952] Therefore, low reactivity of this two aldehydes to pyrolytic lignin is not surprised.

3.5 Proposed bio-oil aging pattern

Based on the above results, the author proposed a bio-oil aging model shown in Fig. 5.12. The bio-oil is composed of the WS fraction, including the ES and EIS fractions and the WIS fraction. Each of these fractions undergo different aging reactions forming aged bio-oil polymers. The WIS fraction (pyrolytic lignin) condensed after aging and as a result it may separate itself from the bio-oil microstructure and forming sticky-gum aggregates. The WS fraction and its sub-fraction - EIS (pyrolytic sugar) formed brown-solids after aging. The sugar fraction may first decompose into aldehydes and acids and then re-polymerize though unidentified reaction pathway. The ES fraction was not directly aged in this study, however its high reactivity can be measured as it contains highly reactive components; esterification, acetalization, aldol-condensation could occur in this fraction. These proposed reaction patterns can be catalyzed by acids and they are termed as individual aging model shown in the bottom side of Fig. 5.12.

In addition, each bio-oil fraction could have synergistic effect on promoting the bio-oil condensation degree. For example, the acids in ether soluble fraction could promote the condensation of lignin fraction and decomposition of sugar fraction. As a focus in this study, the aldehydes, especially formaldehyde in ether soluble fraction, could effectively crosslink the pyrolytic lignin even with weak acetic acid catalyst. These interactions were termed as a mutual aging model and the bio-oil would be much more stable if such synergistic effect does not exist. For instance, if acids could be removed from WS fraction, then acid condensation of lignin and lignin-aldehyde reaction would not take place and sticky gum aggregates may not be formed in the aged bio-oil. To further develop and understand the bio-

oil aging mechanism, the proposed pattern shown in Fig. 5.12 may serve as a ground for more detailed study on bio-oil aging reactions.

4. Conclusions

The aged bio-oil after accelerated aging had very different physicochemical property and chemical composition to the starting raw bio-oil. Specifically, the bio-oil water content, viscosity, acidity and molecular weight increased after aging and the aged bio-oil contained more water insoluble components than that of the raw bio-oil. These aging phenomena can be explained by bio-oil condensation reactions which have time and temperature dependence.

The bio-oil fractions, including the WS, EIS and WIS fraction aged in a different manner. The WS and EIS fraction generated high molecular weight solids after aging. The acids presented in the bio-oil significantly promoted the condensation of these two fractions. The WIS lignin fraction condensed after heating treatment and formic acid can enhance the condensation degree of pyrolytic lignin.

Model compounds study of phenol-glycolaldehyde reaction showed that the most abundant bio-oil aldehyde, glycolaldehyde can potentially react with phenol to a limited extent (dimerization) with proper acid catalyst (HCl and formic acid) presence. Various aldehydes identified in the bio-oil, especially formaldehyde can promote the condensation degree of pyrolytic lignin. However, such effect was not achieved with most of bio-oil aldehydes except for formaldehyde when using acetic acid as the catalyst. The results presented in this study suggest that bio-oil aging model can be constructed based on an individual aging and a mutual aging pattern within or between bio-oil fractions.

5. Acknowledgements

This study was supported by Southeastern Sun Grant Center, the US Department of Transportation (Grant No. DTO559-07-G-00050) and the National Science Foundation (Grant No. 0832498). The author would like to thank Chris Hopkins at North Carolina State University for providing heat-treated wood samples, Dr. David Dayton and John Carpenter at RTI International for the help on measuring bio-oil TAN number.

References

Baldwin, R.M., Feik, C.J. 2013. Bio-oil Stabilization and Upgrading by Hot Gas Filtration. Energy & Fuels, 27(6), 3224-3238.

Ben, H., Ragauskas, A.J. 2012. In Situ NMR Characterization of Pyrolysis Oil during Accelerated Aging. ChemSusChem, 5(9), 1687-1693.

Bennett, N.M., Helle, S.S., Duff, S.J.B. 2009. Extraction and hydrolysis of levoglucosan from pyrolysis oil. Bioresource Technology, 100(23), 6059-6063.

Bertero, M., de la Puente, G., Sedran, U. 2011. Effect of Pyrolysis Temperature and Thermal Conditioning on the Coke-Forming Potential of Bio-oils. Energy & Fuels, 25(3), 1267-1275.

Britt, P.F., Buchanan Iii, A.C., Thomas, K.B., Lee, S.-K. 1995. Pyrolysis mechanisms of lignin: surface-immobilized model compound investigation of acid-catalyzed and free-radical reaction pathways. Journal of Analytical and Applied Pyrolysis, 33(0), 1-19.

Brown, L.H. 1952. Resin Forming Reactions of Furfural and Phenol. Industrial & Engineering Chemistry, 44(11), 2673-2675.

Centeno, A., Laurent, E., Delmon, B. 1995. Influence of the Support of CoMo Sulfide Catalysts and of the Addition of Potassium and Platinum on the Catalytic Performances for the Hydrodeoxygenation of Carbonyl, Carboxyl, and Guaiacol-Type Molecules. Journal of Catalysis, 154(2), 288-298.

Chaala, A., Ba, T., Garcia-Perez, M., Roy, C. 2004. Colloidal Properties of Bio-oils Obtained by Vacuum Pyrolysis of Softwood Bark: Aging and Thermal Stability. Energy & Fuels, 18(5), 1535-1542.

Czernik, S., Johnson, D.K., Black, S. 1994. Stability of wood fast pyrolysis oil. Biomass and Bioenergy, 7(1–6), 187-192.

Dence, C.W. 1992. The Determination of Lignin. in: Methods in Lignin Chemistry, (Eds.) S. Lin, C. Dence, Springer Berlin Heidelberg, pp. 33-61.

Diebold, J.P. 2002. A Review of the Chemical and Physical Mechanisms of the Storage Stability of Fast Pyrolysis Bio-Oils. in: Fast Pyrolysis of Biomass: A handbook, (Ed.) A.V. Bridgwater, CPL Press. Newbury, U.K., pp. 205-241.

Diebold, J.P., Czernik, S. 1997. Additives To Lower and Stabilize the Viscosity of Pyrolysis Oils during Storage. Energy & Fuels, 11(5), 1081-1091.

Elliott, D.C., Oasmaa, A., Preto, F., Meier, D., Bridgwater, A.V. 2012. Results of the IEA Round Robin on Viscosity and Stability of Fast Pyrolysis Bio-oils. Energy & Fuels, 26(6), 3769-3776.

Fratini, E., Bonini, M., Oasmaa, A., Solantausta, Y., Teixeira, J., Baglioni, P. 2005. SANS Analysis of the Microstructural Evolution during the Aging of Pyrolysis Oils from Biomass. Langmuir, 22(1), 306-312.

Gayubo, A.G., Valle, B., Aguayo, A.T., Olazar, M., Bilbao, J. 2010. Pyrolytic lignin removal for the valorization of biomass pyrolysis crude bio-oil by catalytic transformation. Journal of Chemical Technology & Biotechnology, 85(1), 132-144.

He, R., Ye, X.P., Harte, F., English, B. 2009. Effects of high-pressure homogenization on physicochemical properties and storage stability of switchgrass bio-oil. Fuel Processing Technology, 90(3), 415-421.

Hu, X., Wang, Y., Mourant, D., Gunawan, R., Lievens, C., Chaiwat, W., Gholizadeh, M., Wu, L., Li, X., Li, C.-Z. 2013. Polymerization on heating up of bio-oil: A model compound study. AIChE Journal, 59(3), 888-900.

Ingram, L., Mohan, D., Bricka, M., Steele, P., Strobel, D., Crocker, D., Mitchell, B., Mohammad, J., Cantrell, K., Pittman, C.U. 2007. Pyrolysis of Wood and Bark in an Auger Reactor: Physical Properties and Chemical Analysis of the Produced Bio-oils. Energy & Fuels, 22(1), 614-625.

Junming, X., Jianchun, J., Yunjuan, S., Yanju, L. 2008. Bio-oil upgrading by means of ethyl ester production in reactive distillation to remove water and to improve storage and fuel characteristics. Biomass and Bioenergy, 32(11), 1056-1061.

Kibet, J., Khachatryan, L., Dellinger, B. 2012. Molecular Products and Radicals from Pyrolysis of Lignin. Environmental Science & Technology, 46(23), 12994-13001.

Knop, A., Pilato, L.A. 1985. Phenolic Resins Chemistry, Applications and Performance Future Directions. Springer-Verlag, Berlin Heidelberg, 14-22.

Lomax, J.A., Commandeur, J.M., Arisz, P.W., Boon, J.J. 1991. Characterisation of oligomers and sugar ring-cleavage products in the pyrolysate of cellulose. Journal of Analytical and Applied Pyrolysis, 19(0), 65-79.

Lu, Q., Zhang, Y., Tang, Z., Li, W.-z., Zhu, X.-f. 2010. Catalytic upgrading of biomass fast pyrolysis vapors with titania and zirconia/titania based catalysts. Fuel, 89(8), 2096-2103.

Meng, J., Park, J., Tilotta, D., Park, S. 2012. The effect of torrefaction on the chemistry of fast-pyrolysis bio-oil. Bioresource Technology, 111(0), 439-446.

Naske, C.D., Polk, P., Wynne, P.Z., Speed, J., Holmes, W.E., Walters, K.B. 2011. Postcondensation Filtration of Pine and Cottonwood Pyrolysis Oil and Impacts on Accelerated Aging Reactions. Energy & Fuels, 26(2), 1284-1297.

Oasmaa, A., Kuoppala, E. 2003. Fast Pyrolysis of Forestry Residue. 3. Storage Stability of Liquid Fuel. Energy & Fuels, 17(4), 1075-1084.

Oasmaa, A., Kuoppala, E., Ardiyanti, A., Venderbosch, R.H., Heeres, H.J. 2010. Characterization of Hydrotreated Fast Pyrolysis Liquids. Energy & Fuels, 24(9), 5264-5272.

Oasmaa, A., Meier, D. 2005. Norms and standards for fast pyrolysis liquids: 1. Round robin test. Journal of Analytical and Applied Pyrolysis, 73(2), 323-334.

Scholze, B., Hanser, C., Meier, D. 2001. Characterization of the water-insoluble fraction from fast pyrolysis liquids (pyrolytic lignin): Part II. GPC, carbonyl groups, and ^{13}C-NMR. Journal of Analytical and Applied Pyrolysis, 58–59(0), 387-400.

Shimada, K., Hosoya, S., Ikeda, T. 1997. Condensation Reactions of Softwood and Hardwood Lignin Model Compounds Under Organic Acid Cooking Conditions. Journal of Wood Chemistry and Technology, 17(1-2), 57-72.

Sluiter A., Hames, B., Ruiz, R., Scarlata, C., Sluiter. J., Templeton, D., Crocker, D. 2008. NREL Laboratory Analytical Procedure. NREL/TP-510-42618, 1-18. Retrieved from http://www.nrel.gov/biomass/pdfs/42618.pdf.

Steelink, C. 1966. Stable Free Radicals in Lignin and Lignin Oxidation Products. in: Lignin Structure and Reactions, Vol. 59, AMERICAN CHEMICAL SOCIETY, pp. 51-64.

Tessini, C., Müller, N., Mardones, C., Meier, D., Berg, A., von Baer, D. 2012. Chromatographic approaches for determination of low-molecular mass aldehydes in bio-oil. Journal of Chromatography A, 1219(0), 154-160.

Werstler, D.D. 1986. Quantitative ^{13}C n.m.r. characterization of aqueous formaldehyde resins: 1. Phenol-formaldehyde resins. Polymer, 27(5), 750-756.

Wildschut, J., Mahfud, F.H., Venderbosch, R.H., Heeres, H.J. 2009. Hydrotreatment of Fast Pyrolysis Oil Using Heterogeneous Noble-Metal Catalysts. Industrial & Engineering Chemistry Research, 48(23), 10324-10334.

Xu, F., Xu, Y., Lu, R., Sheng, G.-P., Yu, H.-Q. 2011. Elucidation of the Thermal Deterioration Mechanism of Bio-oil Pyrolyzed from Rice Husk Using Fourier Transform Infrared Spectroscopy. Journal of Agricultural and Food Chemistry, 59(17), 9243-9249.

Yaylayan, V.A., Harty-Majors, S., Ismail, A.A. 1998. Investigation of the mechanism of dissociation of glycolaldehyde dimer (2,5-dihydroxy-1,4-dioxane) by FTIR spectroscopy. Carbohydrate Research, 309(1), 31-38.

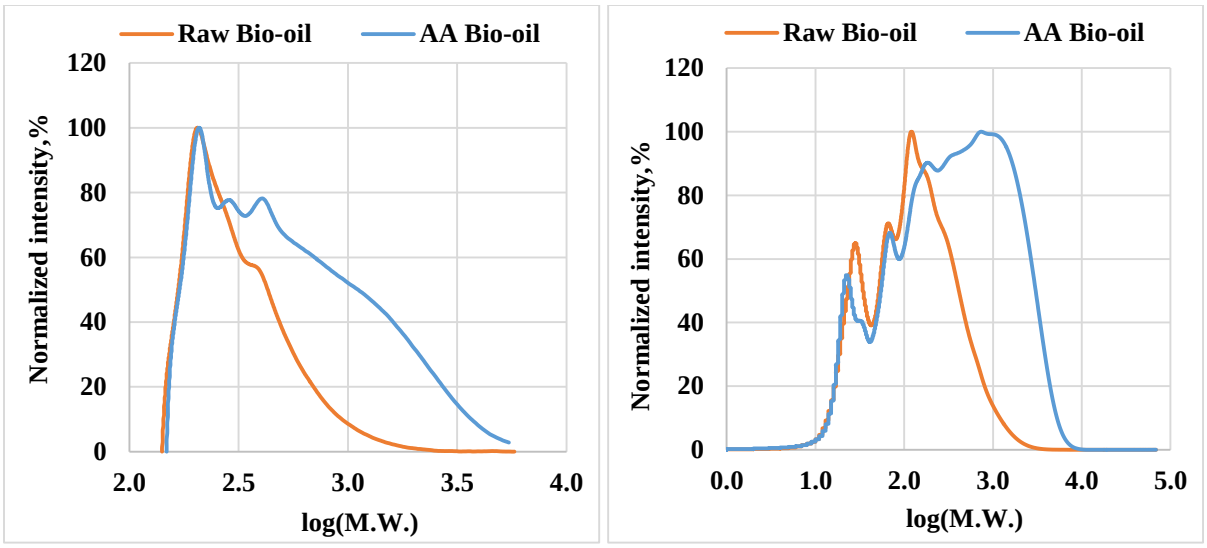

Figure 5.1 Molecular weight distribution of fresh and aged bio-oil from RI detector (left one) and UV detector (right one).

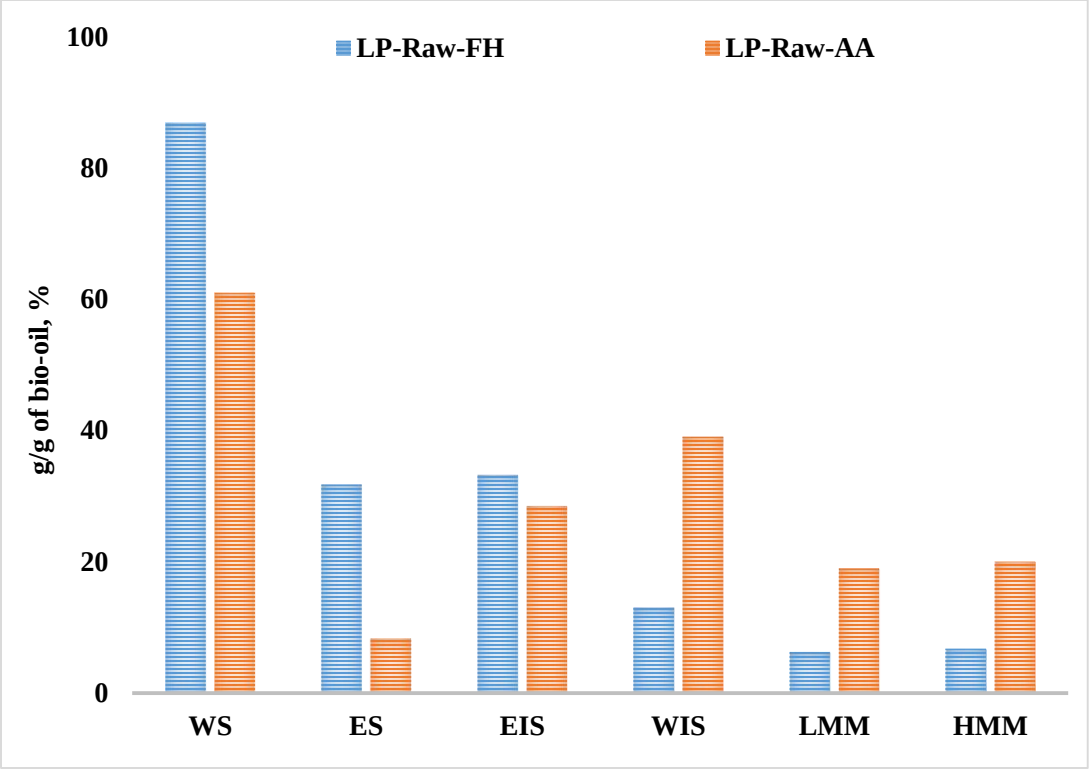

Figure 5.2 Composition variance between fresh and accelerated aged bio-oil. WS – water soluble fraction, WIS – water insoluble fraction, ES – ether soluble fraction, EIS – ether insoluble fraction, LMM – low molecular mass lignin fraction, HMM – high molecular mass lignin fraction.

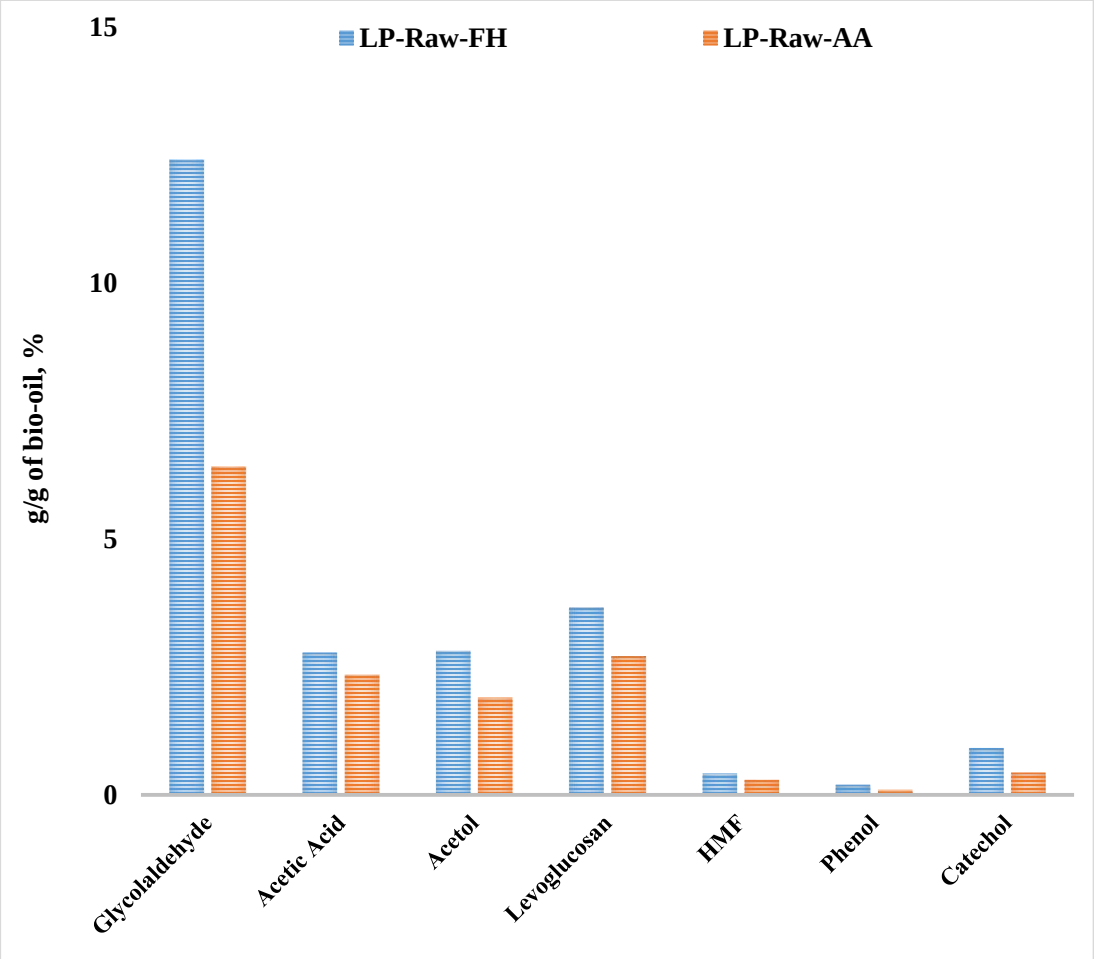

Figure 5.3 GC/MS characterization of compositional fresh and aged bio-oil.

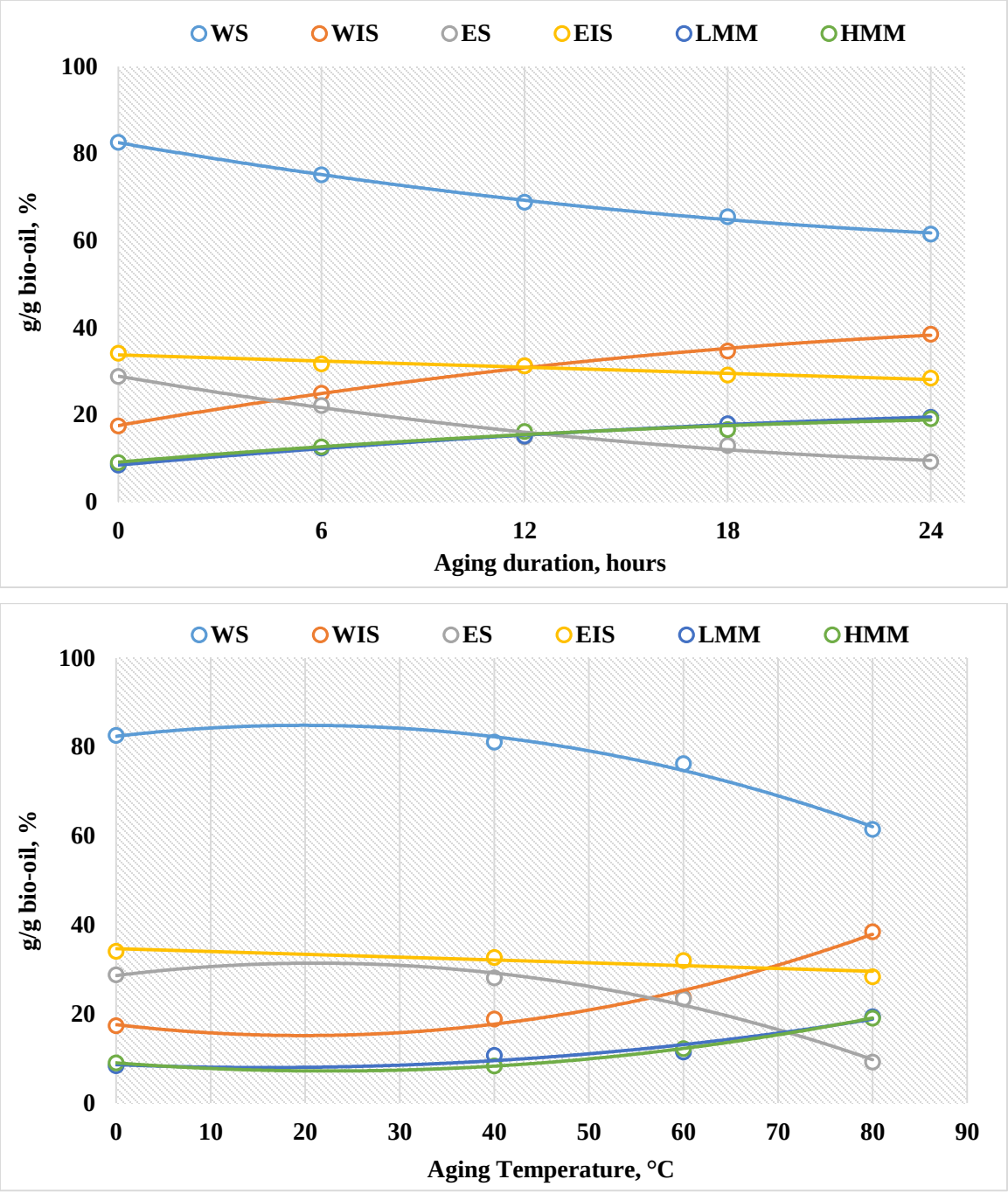

Figure 5.4 Chemical composition of aged bio-oil with varied aging time and temperature.

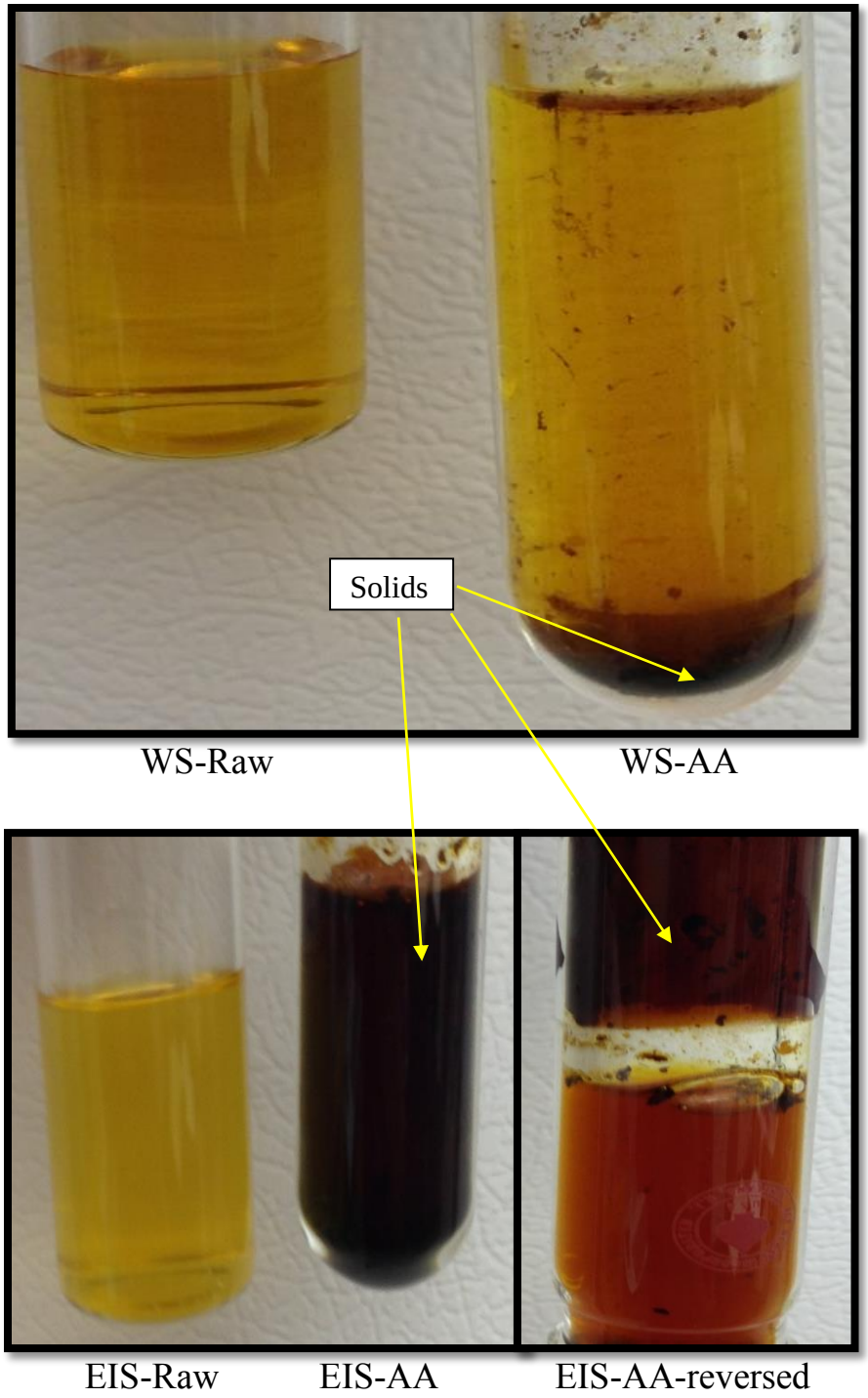

Figure 5.5 Visual appearance of bio-oil WS and EIS fraction after accelerated aging at 110 °C.

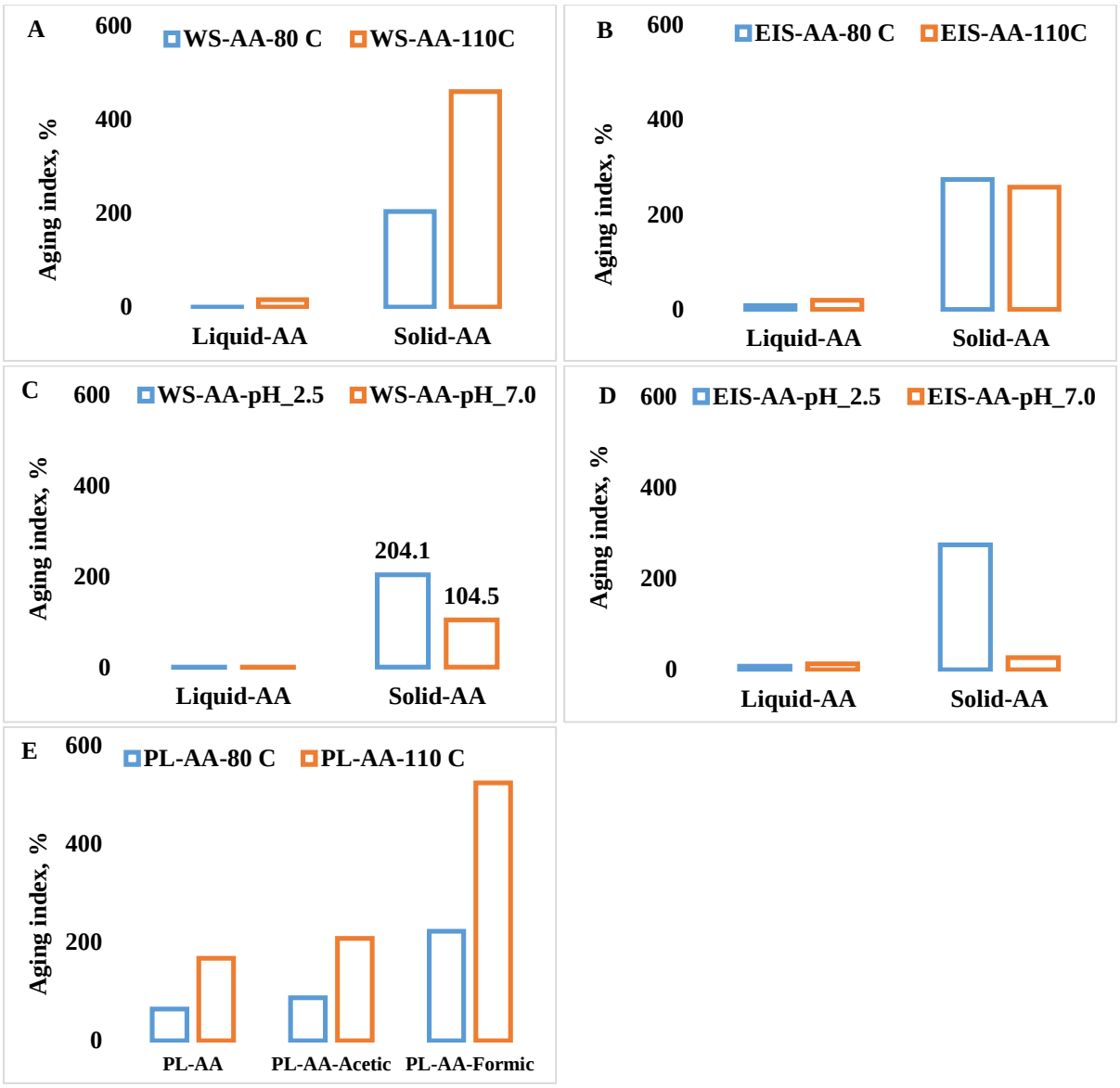

Figure 5.6 Mw aging index of bio-oil fractions after accelerated aging. A, B: the aging indexes were obtain with aged WS and EIS fractions heated under pH-2.5 and aging temperature at 80 and 110 °C; C and D: the aging indexes were obtained with aged WS and EIS fractions heated under pH-2.5 and 7.0 and aging temperature at 80 °C; E: the aging indexes were obtained with aged WIS lignin fraction with or without acid catalyst under 80 and 110 °C.

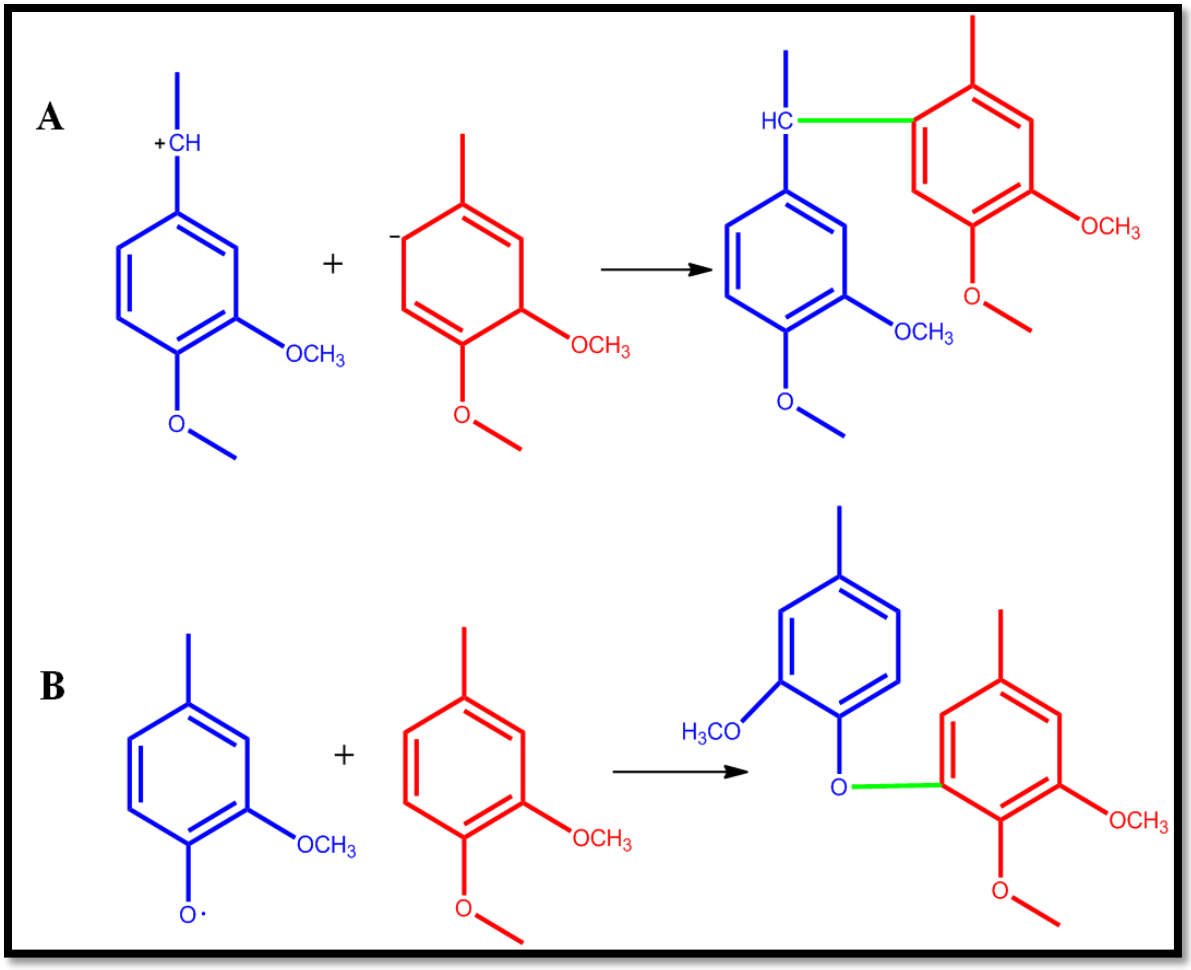

Figure 5.7 Acid condensation (A) and free radical condensation (B) of pyrolytic lignin.

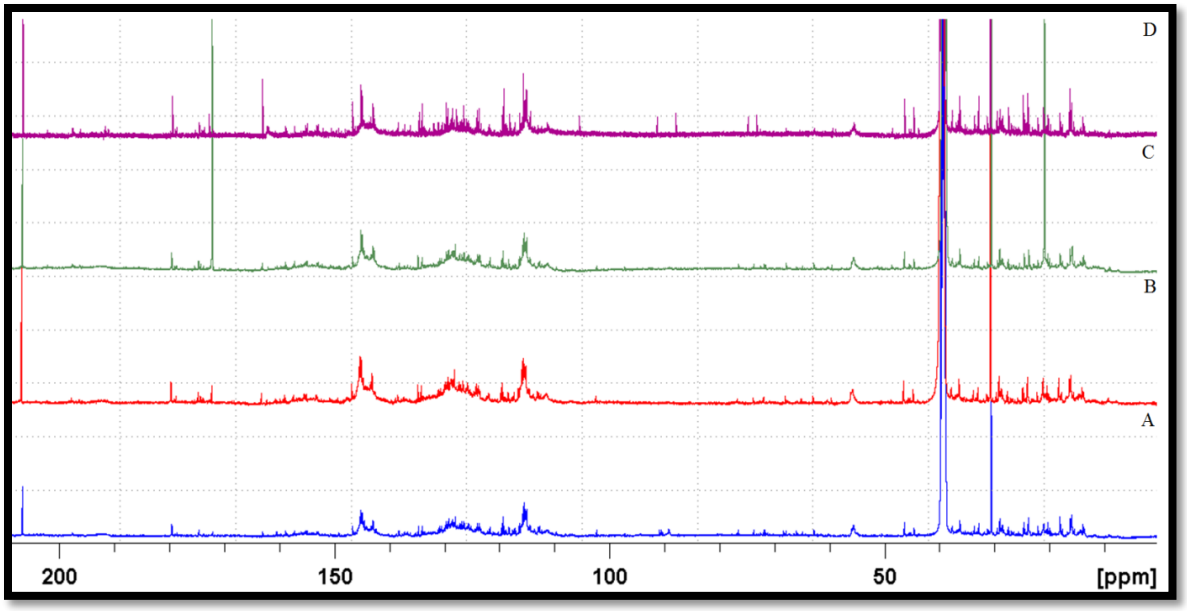

Figure 5.8 ^{13}C NMR characterization of pyrolytic lignin. A:starting pyrolytic lignin; B: accelerated aged pyrolytic lignin without addition of acid; C: accelerated aged pyrolytic lignin with adding acetic acid, the carbon signal at 163 and 21 ppm in the spectra came from hard to remove residual acetic acid; D. accelerated aged pyrolytic lignin with adding formic acid.

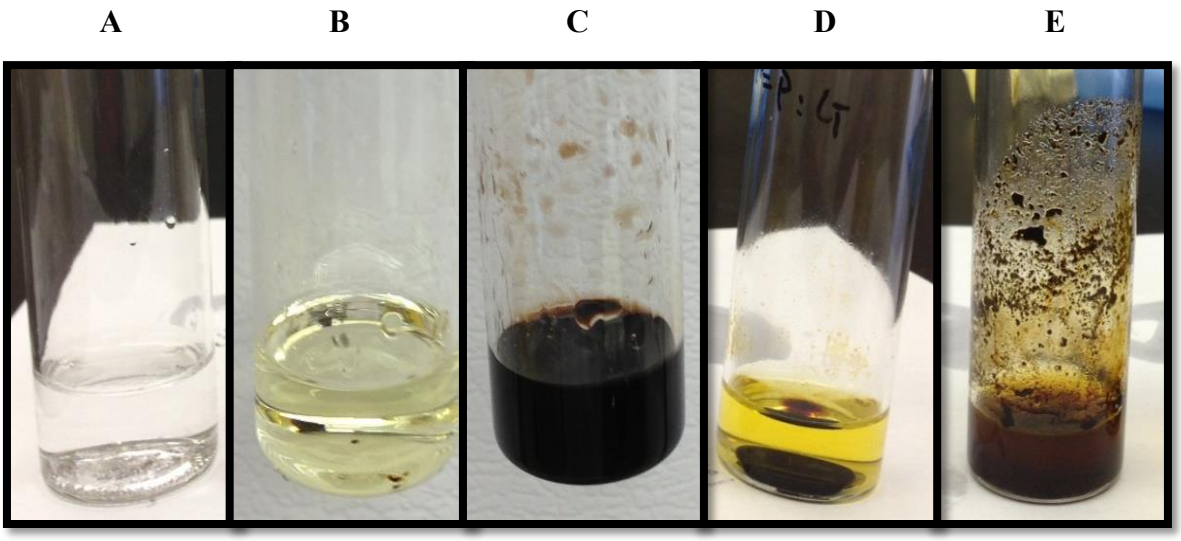

Figure 5.9 Phenol-glycolaldehyde reaction solutions with three different acid catalysts. A: phenol-glycolaldehyde mixture before reaction; B: phenol-glycolaldehyde reaction solution formed with acetic acid, 24 hours heating at 90 °C; C: phenol-glycolaldehyde reaction solution formed with formic acid, 12 hours heating at 90 °C; D: phenol-glycolaldehyde reaction solution formed with HCl, 5 hours heating at 90 °C; E: glycolaldehyde reaction control without addition of phenol formed with HCl, 2 hours heating at 90 °C.

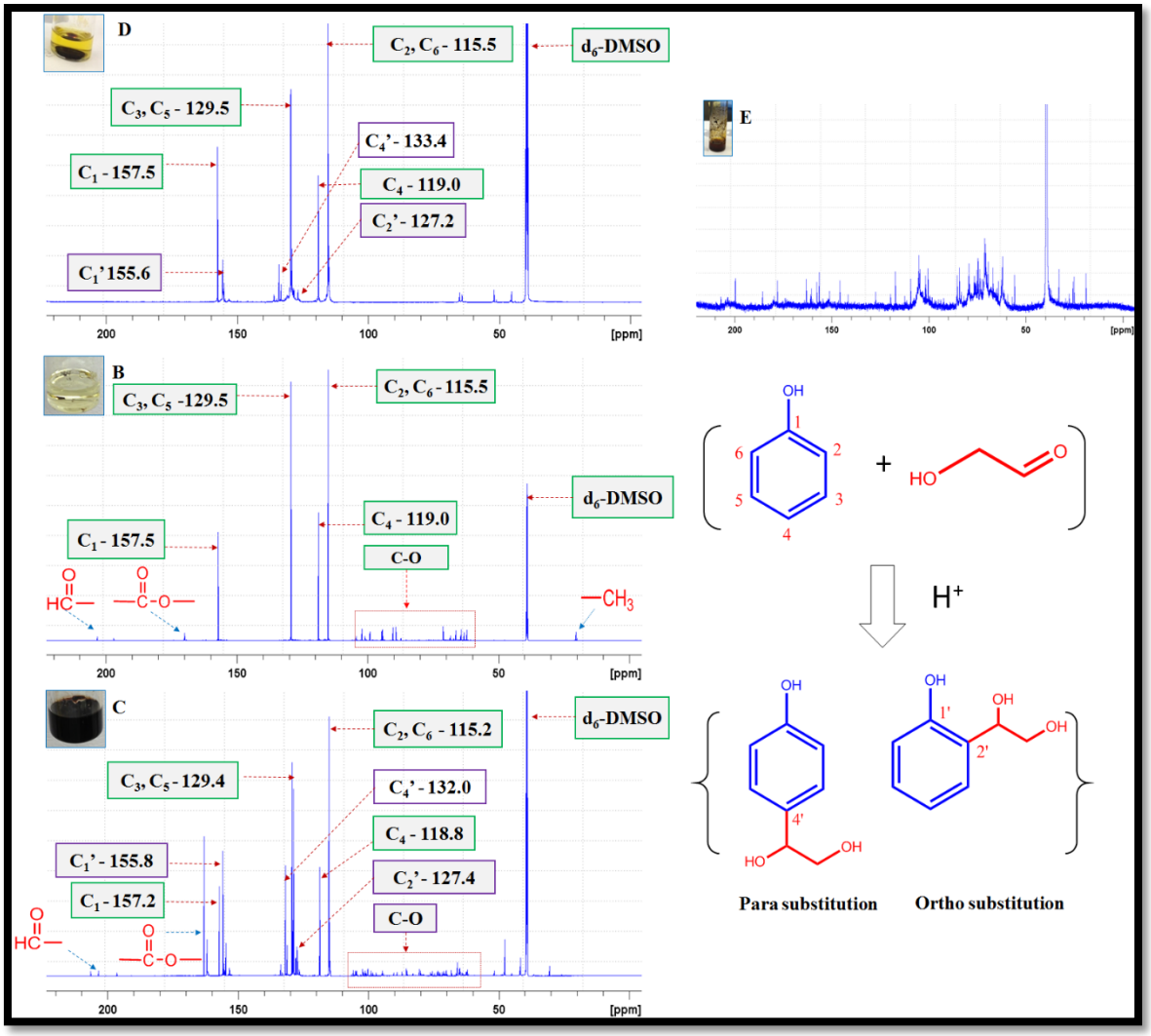

Figure 5.10 ^{13}C NMR characterization of phenol-glycolaldehyde reaction products. B: phenol-glycolaldehyde reaction product formed with acetic acid, 24 hours heating 90 °C; C: phenol-glycolaldehyde reaction product formed with formic acid, 12 hours heating at 90 °C; D: phenol-glycolaldehyde reaction product formed with HCl, 5 hours heating at 90 °C; E: glycolaldehyde reaction control without addition of phenol formed with HCl acid, 2 hours heating at 90 °C. Aromatic carbon showed as C_1', C_2' and C_4' after glycolaldehyde substitution.

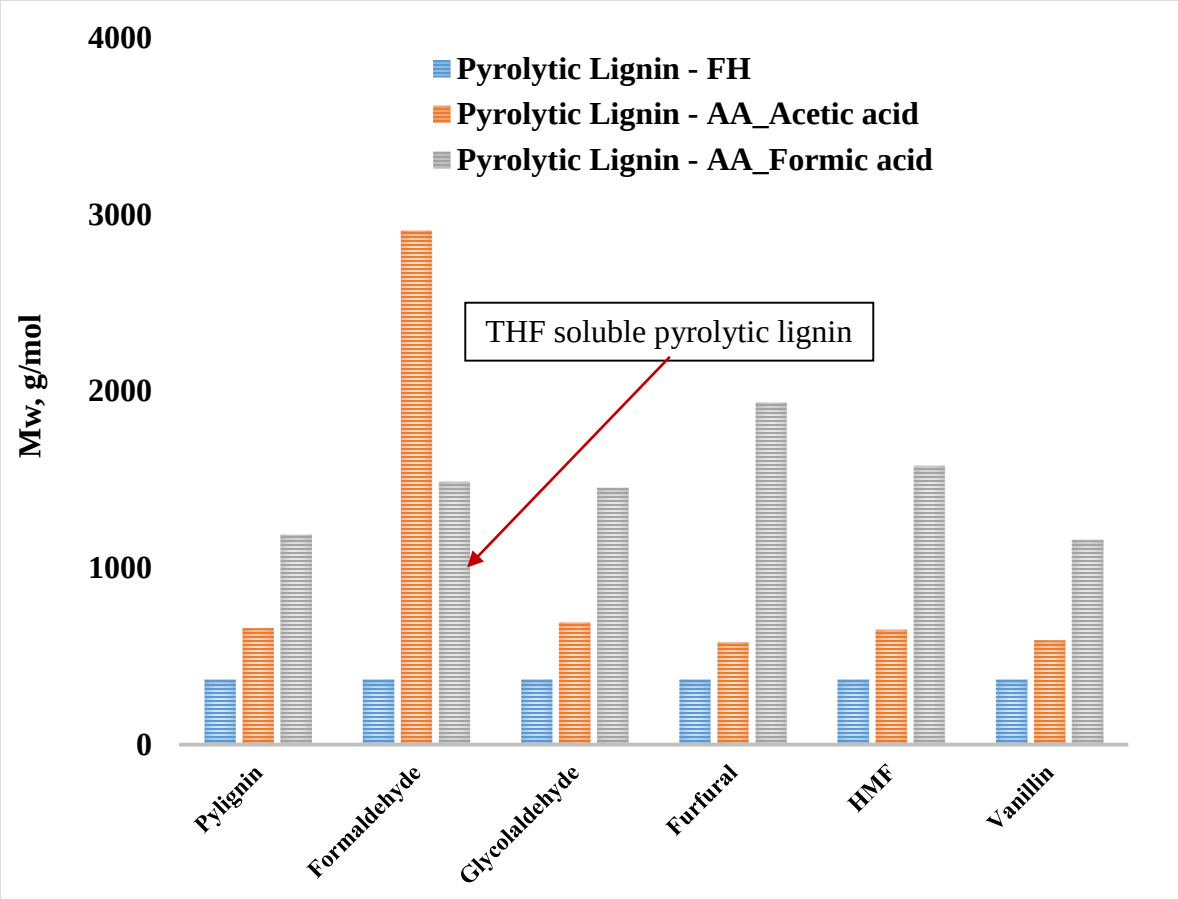

Figure 5.11 Molecular weights of the pyrolytic-lignin-aldehydes reaction products with different acid catalysts. The average molecular weight of pyrolytic-lignin-formaldehyde product catalyzed by formic acid represents only the THF soluble polymer; the majority of reaction products from this particular reaction were insoluble in THF.

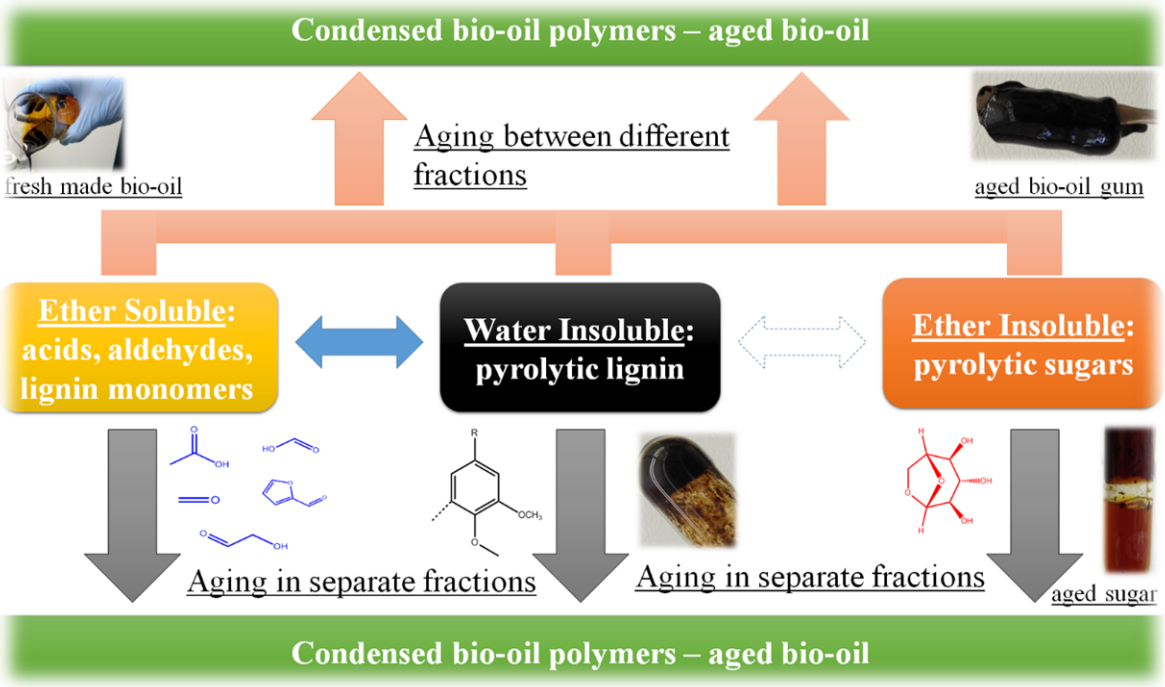

Figure 5.12 Proposed bio-oil aging mechanism.

Table 5.1 Characterization of pyrolysis feedstock loblolly pine (dry base).

Ultimate Analysis	
C, %	49.3
H, %	6.64
O, %	44.0
N, %	0.07
O/C atomic ratio	0.67
Proximate Analysis	
Moisture, %	6.5
Volatile matter, %	88.4
Fix carbon, %	11.1
Ash, %	0.52
High heating value, MJ/kg	19.7

Table 5.2 Characterization of pyrolysis bio-oil from loblolly pine (dry base).

	Raw Bio-oil	Aged Bio-oil	
Elemental Analysis (dry base)			
C, %	50.1	51.1	
H, %	6.65	6.31	
O, %	42.7	42.0	
N, %	0.53	0.63	
O/C atomic ratio	0.64	0.62	
Physicochemical Properties			**Aging Index, %**
Water content, %	19.8	23.9	20.7
Viscosity, cp	16.4	55.7	239.6
Mw[a], g/mol	338	663	96.2
Mn[a], g/mol	267	365	36.7
TAN[b], mg KOH/g	58.9	68.5	16.3

a. Mw and Mn are determined by an RI detector.

Table 5.3 The effect of aging temperature and duration on aged bio-oil properties.

	Water Content %	Viscosity cSt	TAN mg KOH/g	Mw[a] g/mol	Mn[a] g/mol
Raw Bio-oil	19.8	16.4	58.9	338	267
Accelerated Aged Bio-oil					
Aging Temperature[b], °C					
40	20.3	20.0	60.1	465	321
60	20.9	24.6	58.8	569	358
80	23.9	55.7	68.5	688	367
110[c]	25.7	N/A	64.2	1616 (G) 487 (L)	597 (G) 332 (L)
Aging Duration[d], hours					
6	21.4	27.3	61.5	529	337
12	22.7	40.7	62.0	634	367
18	23.5	45.0	62.8	664	373
24	23.9	55.7	68.5	663	365

a. Mw, Mn determined by an RI detector.

b. Accelerated aging was performed with different temperature for 24 hours.

c. Aged bio-oil phase separated after accelerated aging at 110 °C; the water content and TAN number of two fractions were reported on weight-averaged value; the viscosity is not measured due to the phase separation and the average molecular weight is expressed separately for the liquid (L) and gum (G) phase.

d. Accelerated aging was performed at 80 °C for varied length of aging time.

Table 5.4 GC/MS characterization of aged bio-oil with varied aging time and temperature.

	GA %	AA %	Acetol %	HMF %	LG %	Phenol %	Catechol %
Raw bio-oil	12.4	2.8	2.8	0.42	3.7	0.20	0.92
Accelerated Aged Bio-oil							
Aging Temperature[a], °C							
40	10.1	2.4	2.2	0.36	3.0	0.19	0.75
60	9.8	2.6	2.3	0.36	2.9	0.18	0.76
80	6.4	2.4	1.8	0.30	2.7	0.15	0.90
110[b]	N.D. (G) 0.1 (L)	4.5 (G) 3.7 (L)	N.D. (G) 1.7 (L)	N.D. (G) 0.18 (L)	N.D. (G) 2.1 (L)	N.D. (G) 0.08 (L)	N.D. (G) N.D. (L)
Aging Duration[c], hours							
6	10.7	2.9	2.5	0.39	3.3	0.19	0.84
12	8.5	2.8	2.4	0.37	3.2	0.21	0.84
18	8.7	2.8	2.5	0.35	3.1	0.18	0.94
24	6.4	2.4	1.9	0.30	2.7	0.15	0.90

a. Accelerated aging was performed with different temperature for 24 hours

b. Aged bio-oil phase separated after accelerated aging at 110 °C forming a liquid (L) and a gum (G) phase

c. Accelerated aging was performed at 80 °C with varied length of aging time

Table 5.5 Molecular weight of accelerated aged water soluble and ether insoluble fraction under different aging temperature and pH.

	Mw,g/mol	Mn, g/mol
pH=2.5		
WS-Raw	296	237
EIS-Raw	328	268
Accelerated aged at 80 °C for 24 hours		
WS-Liquid-AA[a]	291	227
WS-Solid-AA[b]	900	649
EIS-Liquid-AA[a]	354	280
EIS-Solid-AA[b]	1228	516
Accelerated aged at 110 °C for 24 hours		
WS-Liquid-AA[a]	343	262
WS-Solid-AA[b]	1657	969
EIS-Liquid-AA[a]	391	296
EIS-Solid-AA[b]	1174	649
pH=7.0		
WS-Raw	310	244
EIS-Raw	252	203
Accelerated aged at 80 °C for 24 hours		
WS-Liquid-AA[a]	303	250
WS-Solid-AA[b]	634	449
EIS-Liquid-AA[a]	284	222
EIS-Solid-AA[b]	319	208

a. Aged liquid phase of WS and EIS fraction.

b. Solids formed after accelerated aging of WS and EIS fraction.

Table 5.6 ^{13}C NMR Characterization of aged pyrolytic-sugar[a].

	210-166 ppm Carbonyl	**166-110 ppm C=C**	**100-105 ppm C_1-O-C_4**	**88-100 ppm C_1 end**	**88-60 ppm $C_{2,3,4,5,6}$**	**38-0 ppm Aliphatic**
Pyrolytic-Sugar-Raw	6.8	4.7	11.5	20.0	45.8	11.2
Pyrolytic-Sugar-AA[b]	4.9	8.1	10.6	16.7	45.7	14.0

a. The integration range was determined based on carbon chemical shifts of a cellobiose model

b. Aging condition at 80 °C for 24 hours

Table 5.7 Molecular weight (determined by a UV detector) of accelerated aged pyrolytic-lignin (PL) with different acid catalysts and aging temperature.

	Mw, g/mol	Mn, g/mol
PL-Raw	369	61
Aging at 80 °C for 24 hours		
PL-AA[a]	606	81
PL-AA-Acetic Acid[b]	690	80
PL-AA-Formic Acid[c]	1188	167
Aging at 110 °C for 24 hours		
PL-AA[a]	986	203
PL-AA-Acetic Acid[b]	1135	224
PL-AA-Formic Acid[c]	2302	213

a. Aging without acid catalyst

b. Aging with equal amount of acetic acid to pyrolytic lignin

c. Aging with equal amount of formic acid to pyrolytic lignin

Table 5.8 ^{13}C NMR Characterization of aged pyrolytic lignin.

	PL-Raw	PL-AA[a]	PL-AA-Acetic[b]	PL –AA-Formic[c]
210-166 ppm, carbonyl	3.7	5.8	6.2	6.9
166-142 ppm, aromatic C-O	15.1	20.4	20.2	23.6
142-125 ppm, aromatic C-C	22.6	25.0	23.9	27.2
125-102 ppm, aromatic C-H	25	22.4	21.6	17.8
90-58 ppm aliphatic C-O	6.6	1.6	1.5	1.7
58-54 ppm, methoxyl/hydroxyl	2.4	2.1	2.3	1.3
37-10 ppm, aliphatic side chain	24.5	23.1	24.4	21.5

a. Aging without acid catalyst

b. Aging with adding equal amount of acetic acid to pyrolytic lignin

c. Aging with adding equal amount of formic acid to pyrolytic lignin

CHAPTER 6

Identification of Free Radicals in Pyrolysis Oil and Their Impact on Bio-oil Aging

1. Introduction

Bio-oil, also known as bio-crude, is a promising fuel intermediate produced from biomass pyrolysis at elevated temperature (~500 °C) and oxygen-free conditions. Typical bio-oil has poor physicochemical properties, as it contains 35-40% oxygen, ~25% water and over 300 different chemical species; the crude bio-oil needs to be hydrodeoxygenated before its projected use as drop-in transportation fuel. Freshly-prepared bio-oil shares some similarities to crude petroleum-based oil with regards to handling and processing: both are stored and then shipped to a processing facility for upgrading and/or refining. Bio-oil, however, is not stable under regular storage condition at room-temperature and atmospheric pressure [Elliott et al., 2012], not to mention under high-temperatures often employed in the upgrading steps. The instability of bio-oil, often called aging, has been identified as one of the most important hurdles that prevent its commercialization. Common adverse behaviors of bio-oil aging include a viscosity increase and an oil phase separation (a sticky gum-phase separated out from the liquid oil phase). In addition to bio-oil storage stability, catalyst coking during its upgrading is also closely related to the high reactivity of bio-oil components towards polymerization. Some studies suggested that the sugar fraction in the bio-oil is mainly responsible for the aging reaction [Wildschut et al., 2009]; others proposed that aldehydes, acids, ketones, and pyrolytic lignin are the main participants for the bio-oil

polymerization [Diebold, 2002; Gayubo et al., 2010]. However, due to the complicated bio-oil composition, a molecular-level bio-oil polymerization mechanism is still unclear.

The previous chapter investigated a bio-oil aging mechanism through an acid-catalyzed condensation pathway. In addition to that, the author also believes that the bio-oil aging could be achieved by radical coupling reactions and the presence of free radicals in the bio-oil will be a direct evidence to support such hypothesis. However, the existence of reactive radicals in the pyrolysis oil has rarely been published before. Some relevant knowledge about the radical presence in biomass constituents and pyrolysis process was summarized as follows: first, free radicals were found to exist in living plants and extracted lignin; fungal attack and chemical/physical treatment could increase the radical concentration in biomass constituents [Steelink, 1966; Hu et al., 2013; Chu et al., 2013; Britt et al., 1995; Kringstad et al., 1969; Steelink, 1964; Banby et al., 1969]; second, free radicals were found to be generated from lignin and tobacco pyrolysis process using in-situ and spin-trapping EPR technology [Khachatryan et al., 2012; Maskos et al., 2005]; in addition, free radicals has also been observed in solid products, i.e. torrefied wood and char, from torrefaction, pyrolysis and combustion of biomass and carbohydrates [Melkior et al., 2012; Bardet et al., 2007; Smirnova et al., 1994; Chatterjee et al., 2012]; however, to the best of author's knowledge, no detailed work has been reported on the verification of radical existence in liquid oil collected from biomass pyrolysis process.

The author's initial thoughts on the presence of free radicals in the bio-oil are ambiguous as the radicals are often by nature extremely unstable. It is commonly agreed that they can be generated during the biomass pyrolysis, especially with the presence of metal

catalyst; however, reactive radicals may be quickly quenched by re-polymerization forming stable secondary bio-oil constituents. Therefore, even if they do exist in the initial pyrolysis vapor, its life-time may be too short for them to be observed after bio-oil condensation and collection which could take a few hours to complete. To settle these doubts, this chapter employed electron paramagnetic resonance (EPR) spectrometry, a technique for studying materials with unpaired electrons, for the first time, on characterizing the raw bio-oil and its sub-fractions. After confirming radical presence in fresh bio-oil, the rest of this chapter preliminarily estimated the relationship between radical presence and bio-oil aging severity using accelerated aging method with addition of radical scavengers and methanol.

2. Materials and Methods

Bio-oil production. The bio-oil used in this study was produced from pyrolysis of loblolly pine wood (clean chips) using a 150 g/hour capacity fluidized bed reactor (O.D. 43mm) at 500 °C with approximate 1s residence time as described previously [Meng et al., 2012]. The raw bio-oil contains 63.1 wt. % carbon, 6.4 wt. % hydrogen, 0.17 wt. % nitrogen, and 30.3 wt. % oxygen in dry base. The freshly-prepared bio-oil is referred as raw bio-oil.

Solvent fractionation. The bio-oil fractions, water soluble fraction (WS), ether soluble fraction (ES), ether insoluble fraction (EIS) and water insoluble fraction (WIS) were prepared using solvent fractionation method according to a reference method [Oasmaa et al., 2012]. Simply, the whole bio-oil was first extracted with excess DI water and separated into WS and WIS (pyrolytic lignin) fraction. The WS fraction was further separated using diethyl ether (Sigma Aldrich 296082) extraction into ES and EIS (pyrolytic sugar) fraction. The

pyrolytic lignin (PL) was prepared using ice-water precipitation method as described in a reference [Scholze et al., 2001]. The bio-oil used in this study contains, 82.6 wt. % WS (including water, ES and EIS), 17.4 wt. % WIS, 28.8 wt. % ES and 34.1 wt. % EIS.

Accelerated aging. Approximately 5 g of bio-oil, 1 g of pyrolytic lignin with/without addition of organic acids were directly aged in a reaction tube (ACE 8648-04-15 mL) under 80 °C for 24 hours in a convection oven. These employed aging conditions are suggested by International Energy Agency (IEA) [Elliott et al., 2012] and widely adopted in bio-oil aging study. The use of ACE reaction tube prevents leaking of volatile compounds during the heating process and no weight loss was observed after bio-oil aging. As a comparison to regular aging without purging, bio-oils were also treated with 1.5 hour nitrogen and air purging before aging. The purging gas outlet was inserted below the bio-oil surface in order to replace the gas dissolve in the bio-oil as well as the gas in the headspace of the aging tube. In some aging studies, 1 wt. % (based on pyrolytic lignin) of radical scavengers, including eugenol, isoeugenol, guaiacol, ascorbic acid (Vc), 2,6-di-tert-butylphenol (DTBP) and butylated hydroxytoluene (BHT) were added into pyrolytic lignin acid solution (lignin:acid=1:1 wt. ratio) before aging. Methanol diluted lignin solution (~30 wt.%) were also aged in accelerated aging conditions. The radical scavengers and acetic/formic acids were purchased from Sigma Aldrich and used as received. The accelerated aged bio-oils were labeled as AA bio-oil.

Bio-oil characterization. The water content of the bio-oil was determined by Karl-Fischer titration method according to ASTM E 203-08 using HYDRANAL Composite 5 (Sigma-Aldrich 34805), HYDRANAL Medium K (Sigma-Aldrich 34698). Gel Permeation

Chromatography (GPC) characterization of bio-oil and pyrolytic lignin was carried out on a Shimadzu HPLC system (LC-20AD) with an UV detector (SPD-20A) at frequency 254 nm and a RI detector (RID-10A). Two Styragel columns from WatersStyragel (HR-1 and HR-5E) were connected for the separation of bio-oil components. The column oven temperature was set at 35 ºC. Tetrahydrofuran (THF, Sigma Aldrich 401757) was used as the mobile phase flowing at 0.7 mL/min. Bio-oil sample was dissolved in THF to approximately 2 mg/mL (0.5 mg/mL for pyrolytic lignin) and then filtered through a 0.25μm filter for the analysis. Twelve polystyrene standards (molecular weight ranging from 162-3520000) were used to generate the calibration curve. ^{13}C NMR analyses of pyrolytic lignin were recorded in DMSO-d_6 solution (~25% wt./wt.) with 5 mm NMR tube using a Bruker Avance DRX 500 MHz NMR spectrometer. ^{13}C NMR spectrum was obtained by inverse-gated decoupling pulse sequence (zgig), 90º pulse angle, 2.5 s pulse delay time and a total of ~20000 scans at 25 ºC. The spectra were analyzed with Topspin software 3.2 (Bruker H9966S3).

Electron Paramagnetic Resonance analyses of bio-oil. The raw bio-oil, bio-oil fractions (WS, ES, EIS and WIS) and accelerated aged bio-oils were characterized with a Bruker ELEXSYS-II 500 CW EPR spectrometer at room-temperature (25 °C). In a typical experiment, raw/aged bio-oils and bio-oil fractions were drawn into a glass capillary (smi-micro/petto 1057-C for bio-oil; Drummond Microcaps 1-000-0250 for bio-oil fractions) and placed into a standard quartz EPR tube (Wilmad-LabGlass, Vineland, NJ) for EPR characterization. The pyrolytic lignin was pre-diluted in methanol (0.38 g/mL) for the EPR characterization. The data acquisition parameters were set as follows: modulation amplitude, 1 G; microwave power, 2 mW; scan width, 100 G; sweep time, 30 s; time constant, 32 ms.

Conducting EPR experiments under air and nitrogen has been compared and no signal difference has been noticed, therefore all the spectra reported in this studies were based on EPR measurement under air atmosphere. Since none of the EPR signals fit Gauss, Lorentzian and their combined line-shape, the peak-to-peak width (ΔHp-p) was manually selected from the spectra using Bruker Xepr software. The relative concentration of free radicals for the raw and aged bio-oil was estimated by comparing the double integration of bio-oil EPR signal to that of standard TEMPO radical.

3. Results and Discussions

3.1 Verification of free radicals in the bio-oil

In the biomass pyrolysis, radicals are often liberated by homolytic cleavage of weak covalent bonds as a result of high-temperature heating. Zhang's finding [Zhang, 2011] indicated that the cellulose favors a radical decomposition pathway forming levoglucosan via homolytic cleavage of a β-1,4-linkage. In-situ EPR characterization on the lignin pyrolysis also found the presence of free-radicals in pyrolysis vapor phase [Kibert et al., 2012]. These results identified potential sources that could deliver radicals into pyrolysis final products. In fact, the solid biochar obtained from biomass pyrolysis process has already been found to contain stable radicals [Bardet et al., 2007]. Accordingly, as a major liquid product from the same process, the bio-oil components may also contain un-paired electrons.

In order to confirm the above hypothesis, a fresh-made bio-oil sample (12 hour storage under -4 °C) was examined with EPR spectroscopy. As shown in Fig. 6.1, a broad but symmetric EPR signal was observed for the whole bio-oil with a line-width (ΔHp-p) of

5.12 G and a g-factor of 2.0019. No hyperfine splitting feature was observed with this EPR peak. After one month storage in a refrigerator (-4 °C), the bio-oil still showed a similar EPR signal indicating the radicals' stable nature. This observation as for its first time confirmed the presence of unpaired electrons in the pyrolysis oil.

The bio-oil can be separated into different fractions based on its solubility in water and organic solvents. The WS fraction of bio-oil contains water, pyrolytic sugar fraction (EIS) and ether soluble fraction (ES, containing light oxygenates, i.e. aldehydes, acids). The WIS fraction contains mainly lignin oligomers and is typically referred as pyrolytic lignin (PL). An EPR characterization of these bio-oil sub-fractions can help further understanding on which of these bio-oil fractions is hosting the detected free-radicals. Among them, WIS lignin fraction is of prime suspect as other kinds of isolated lignin, i.e. Kraft lignin has already been confirmed to have EPR response [Rex, 1960] and the lignin radicals were suggested to have stable semiquinone architecture. [Khachatryan et al., 2010].

In Fig. 6.1, the bio-oil WS fraction and its sub-fractions, ES and EIS fraction, produced no detectable EPR signal. In contrast, an unstructured EPR peak has been detected as expected for the pyrolytic lignin. Its peak width of 5.15 G and g-factor of 2.0019 are essentially the same as that for raw bio-oil suggesting its primary role in stabilizing the bio-oil radical species. These radicals lived in pyrolytic lignin fraction could be generated from hydrogen abstraction at the phenolic O-H and Cα-H during lignin pyrolysis [Watanabe et al., 2009] and they were further stabilized by highly conjugated lignin aromatic system. Similar to the EPR signal obtained from chemically isolated lignin, no hyperfine EPR structure was observed for the pyrolytic lignin. This hyperfine-absent peak-shape maybe caused by

averaged EPR signals from a group of highly complex free-radical species or a similar chemical environment surrounding the unpaired free electrons within the lignin macrostructure. In addition, the g-factor of 2.0019 obtained for pyrolytic lignin is much lower than reported value for the pine lignin of 2.0037 [Czechowski et al., 2003] and the lignin pyrolysis vapor of 2.0072 [Kibet et al., 2012]. This may suggests that free radicals in pyrolytic lignin are mainly attached to carbon atoms, because the g-factor of carbon-centered radical (g-factor close to 2.0023) is usually lower than that of oxygen-centered radical (g-factor close to 2.0040) [Tian et al., 2009]. In addition, the low g-factor value could also result from the orbital interaction between free electrons with metal species contained in the bio-oil [Czechowski et al., 2003].

3.2 Characterization of free radicals in the accelerated aged bio-oil

The bio-oil viscosity and molecular weight increased significantly after heat treatment. This aging phenomenon may be explained by acid-catalyzed polymerization of bio-oil components. As an alternative, a free radical mechanism was also proposed to explain how hydrogen donor solvent – tetralin stabilizing liquefaction bio-oil [Adjaye et al., 1992]. Due to the radical presence in the pyrolysis oil, its aging phenomenon may also be caused by radical initiated condensation reactions. This reaction would ideally decrease the radical concentration in the aged bio-oil as a result of radical annihilation and the physicochemical property of the aged bio-oil would change accordingly. Therefore, measuring bio-oil radical concentration variation and its corresponding property change after the aging would give a rough estimate on how important these radicals are contributing to the bio-oil aging severity.

In this section, accelerated aged bio-oil was quantitatively characterized with EPR spectroscopy. In addition, the effect of aging environment on the aged bio-oil molecular weight and EPR response was investigated with pre-purging the raw bio-oil with nitrogen and air.

Fig. 6.2 presents the EPR spectra comparison between raw and aged bio-oils. As shown in the caption of Fig. 6.2, the g-factor and peak-to-peak width of raw and aged bio-oil remain unchanged after aging suggesting same radical species lived in the raw and aged bio-oil. The aged bio-oils without purging treatment and with nitrogen purging showed slightly weaker EPR signal than the raw bio-oil indicating minor radical annihilation occurred in the aging process. The estimated radical concentration reduced from 185.3 μM (raw bio-oil) to 150.8 μM (AA-unpurged) and 157.0 μM (AA-N_2). Significantly reduced radical concentration (60.3 μM for AA-Air) was found for the aged bio-oil with air pre-purging. This pronounced effect may indicate that air played an important oxidation role on quenching free radicals in the pyrolysis oil. A similar radical content decay has also been found on cellulose pyrolysis char when exposed to air. [Feng et al., 2004]

Table 6.1 presents the physicochemical properties of the bio-oils after aging. The water content of aged bio-oil without purging (AA-unpurged) increased from 19.8 % to 23.3 %; in contrast, the aged bio-oils with gas purging (AA-N_2 and AA-Air) showed reduced water content. This may be caused by the losing of volatile compounds during the gas purging operation, which can potentially produce reaction water during the heating treatment. More importantly, although the radical content of accelerated aged bio-oils decreased to different extents, its molecular weight, which indicating the bio-oil condensation degree did

not vary from each sample. For the air purged bio-oil after aging, its radical concentration decreased significantly but its molecular weight was essentially the same to that of the other aged bio-oils that only had minor radical content reduction. Since the bio-oil aging was performed in an environment that acid-catalyzed condensation could easily occur, these results seem to suggest that radical initiated condensation does not contributed significantly to bio-oil aging severity and the aged bio-oil physicochemical property is mainly dominated by acid-catalyzed condensation reactions.

3.3 ^{13}C NMR characterization of accelerated aged pyrolytic lignin

It is well-known that severe condensation could occur to the lignin between its electron-rich aromatic-ring and the cationic site from benzyl alcohol and benzyl ether at α-carbon under acidic conditions [Shimada et al., 1997]. The pyrolytic lignin contained in the bio-oil may condense in a similar manner during accelerated aging under proper acidic environment in pyrolysis oil (pH~2), However, after careful isolation, organic acids contained in the pyrolytic lignin should be extensively removed, providing no catalyst for such condensation to occur. Under this acid-free environment, the pyrolytic lignin may primarily condense through a radical initiated reaction pathway as the radical presence has already been confirmed in the previous section.

The ^{13}C NMR spectra of raw and aged pyrolytic lignin shown in Fig. 6.3 reveal the lignin structure change after radical condensation. Since the two spectra looked very similar, a quantitative integration on their carbon distribution was summarized. As shown in Table 6.2, the number of carbonyl carbon increased while the amount of methoxyl/hydroxyl and

aliphatic carbon slightly decreased after aging. Similar results have also been acquired by Ben [Ben and Ragauskas, 2012] on pyrolysis oil made from lignin. The amount of aliphatic C-O carbon typically assigned to lignin propyl side chain named Cα, Cβ and Cγ (see Fig. 6.4), [Scholze et al., 2001] reduced significantly after aging indicating their reactive role on lignin aging reactions. For aromatic carbon, the content of aromatic C-O and C-C carbon increased significantly while the aromatic C-H carbon decreased suggesting extensive condensation occurred to the aromatic ring structure. Due to the absence of acid catalyst, this aromatic condensation is primarily initiated by the free radicals and the proposed reaction mechanisms are shown in Fig. 6.4. Depending on the type of radical species, either oxygen-centered phenoxyl radicals or its resonated carbon-centered radicals (see Fig. 6.4), the aged lignin structure would feature increased amount of aromatic C-O and C-C carbon linkage, i.e. C_5-O and C_5-C_5 as shown in Fig 6.4, while the aromatic C-H carbon content would decrease.

3.4 Accelerated aging of pyrolytic lignin with addition of radical scavengers and methanol

One way to access the effect of free radicals on bio-oil aging can be performed by using radical scavenger. Radical scavenger or antioxidant, remove and stabilize free radicals by being oxidized itself. If radicals contained in the bio-oil can be stabilized by the scavenger, the bio-oil aging severity represented by an increase of molecular weight may be controlled. In addition, using organic solvents, i.e. methanol to dilute the radical concentration could also reduce the radical coupling potential and achieve the same goal on relaxing the bio-oil aging degree.

Since radicals were only found in the bio-oil lignin fraction, accelerated aging with direct adding radical scavengers or methanol into this fraction was studied. In addition, using pyrolytic lignin rather than the whole bio-oil excludes the interference of bio-oil WS fraction on reacting with the added additives. For example, methanol could react with acids and carbonyl compounds in the bio-oil WS fraction blocking their reactive condensation sites. As a result, the potential methanol stabilization effect on bio-oil radicals may misleadingly result from its ability on stabilizing bio-oil WS fraction.

To build a good contact between scavengers and lignin radicals during aging, acetic acid was used to fully dissolve the pyrolytic lignin and the scavengers. Although, lignin can condense under acidic condition, as shown in Table 6.3, acetic acid did not effectively catalyze such condensation as similar Mw for aged lignin with and without addition of acetic acid was observed. The major functionality for acetic acid addition is to provide a uniform reaction media. In addition to acetic acid, formic acid was also used to dissolve the pyrolytic lignin. Different from the acetic acid, the formic acid was found to be an effective catalyst on condensing the pyrolytic lignin as the Mw of aged lignin increased by 405.9 % when compared to the starting lignin. Therefore, with the presence of formic acid, radical scavenger capability on inhibiting lignin condensation can be accessed under a background that acid condensation could also occur. In addition, when comparing the aging index shown in Table 6.2, the aged lignin with formic acid addition showed more pronounced effect on lignin condensation than that for the aged lignin without acid addition or with acetic acid addition. As stated earlier, mainly radical initiated condensation occurred to the pyrolytic lignin in the acid-free and weak-acid conditions, this result may suggest that lignin

condensation is primarily governed by acid-catalyzed condensation rather than radical condensation.

The average molecular weight of aged pyrolytic lignin with the presence of radical scavengers under acidic condition is summarized in Table 6.3. According to the aging index, only eugenol, guaiacol and vitamin C showed minor effect on controlling the lignin condensation in acetic acid solution. Under this weak acid condition, activated radicals may be the only driving force to crosslink lignin units; however using radical scavengers did not show distinct effect on stabilizing them. This may suggest that the radicals contained in pyrolytic lignin are already in a stable state; therefore the scavengers cannot provide further stabilization. This is particularly true as pyrolytic lignin has already been found an effective scavenger targeting DPPH and ABTS radicals [Nsimba et al., 2012].

In contrast to acetic acid, the aging indexes for aged lignin with addition of radical scavengers and formic acid is about half of that without scavenger addition. Obviously, this suggests that the scavengers can inhibit lignin crosslinking reaction when added with formic acid. However, it is not clear if such effect can be solely attributed to their radical stabilization capability as they did not show similar inhibition efficiency when added with acetic acid. With formic acid, radical scavengers may have participated in the acid-catalyzed condensation reactions and interrupted severe condensation between lignin macromolecules. For example, the aromatic ring of phenolic radical scavengers could attack the α-carbocation in lignin side chain and seal this reaction site for its further condensation with other lignin molecules.

In addition to using radical scavengers, pyrolytic lignin may also be stabilized when its radical concentration can be effectively diluted with organic solvent. As shown in Table 6.3, the aging index for aged lignin with methanol dilution is only half of that for the aged raw lignin. Besides, compared to stabilizing radicals using scavengers, especially in acetic acid solution where acid-catalyzed lignin condensation is inhibited, diluting the radical concentration showed more pronounced effect on controlling the lignin condensation severity.

4. Conclusions

The characterization of pyrolysis oil made from loblolly pine wood using electron paramagnetic resonance technique confirmed the presence of free radicals in this bio-derived liquid. In addition, these radicals were found to be all located in the bio-oil water insoluble lignin fraction. The observed g-factor of 2.0019 for the pyrolytic lignin radical is particularly lower than that of other isolated lignin. After accelerated aging, the bio-oil radical concentration decreased but it did not show close relationship to the bio-oil aging severity. Using radical scavengers or methanol dilution could inhibit the lignin radical condensation to different extent. However, when compared to the acid-catalyzed condensation, the lignin radical assisted reaction may only play a second role in determining bio-oil aging severity.

5. Acknowledgements

This study was supported by Southeastern Sun Grant Center, the US Department of Transportation (Grant No. DTO559-07-G-00050) and the National Science Foundation (Grant No. 0832498). The author would like to thank Chris Hopkins at North Carolina State University for providing heat-treated wood samples.

References

Adjaye, J.D., R.K. Sharma, and N.N. Bakhshi. "Characterization and Stability Analysis of Wood-derived Bio-oil." Fuel Process. Technol. 31(1992): 241-256.

Bardet, M., S. Hediger, G. Gerbaud, S. Gambarelli, J.F. Jacquot, M.F. Foray, and A. Gadelle. "Investigation with ^{13}C NMR, EPR and Magnetic Susceptibility Measurements of Char Residues Obtained by Pyrolysis of Biomass." Fuel 86(2007): 1966-1976.

Britt, P.F., A.C. Buchanan, K.B. Thomas, and S.K. Lee. "Pyrolysis Mechanisms of Lignin: Surface-immobilized Model Compound Investigation of Acid-catalyzed and Free Radical Reaction Pathways." J. Anal. Appl. Pyrolysis 33(1995): 1-19.

Chatterjee, S., F. Santos, S. Abiven, B. Itin, R.E. Stark, and J.A. Bird. "Elucidating the Chemical Structure of Pyrogenic Organic Matter by Combining Magnetic Resonance, Mid-infrared Spectroscopy and Mass Spectrometry." Org. Geochem. 51(2012): 35-44.

Chu, S., A.V. Subrahmanyam, and G.W. Hubert. "The Pyrolysis Chemistry of a β-O-4 Type Oligomeric Lignin Model Compound." Green Chem. 15(2013): 125-136.

Czechowski, F., I. Golonka, and A. Jezierski. "Organic Matter Transformation in the Environment Investigated by Quantitative Electron Paramagnetic Resonance Spectroscopy: Studies on Lignins." Spectrochim. Acta, Part A 60(2004): 1387-1394.

Diebold, P.J., 2002. A review of the chemical and physical mechanisms of the storage stability of fast pyrolysis bio-oils. In: Bridgwater, A.V. (Ed.), Fast Pyrolysis of Biomass: A handbook. CPL Press, Newbury, U.K., pp. 205–241.

Elliott, D.C., Oasmaa, A., Preto, F., Meier, D., Bridgwater, A.V. 2012. Results of the IEA Round Robin on Viscosity and Stability of Fast Pyrolysis Bio-oils. Energy & Fuels, 26(6), 3769-3776.

Elliott, D.C., Oasmaa, A., Meier, D., Preto, F., Bridgwater, A.V. 2012. Results of the IEA Round Robin on Viscosity and Aging of Fast Pyrolysis Bio-oils: Long-Term Tests and Repeatability. Energy & Fuels, 26(12), 7362-7366.

Feng, J.W., S. Zheng, and G.E. Maciel. "EPR Investigations of the Effects of Inorganic Additives on the Charring and Cha/air Interactions of Cellulose." Energy Fuels 18(2004): 1049-1065.

Gayubo, A.; Valle, B.; Aguayo, A.; Olazar, M.; Bilbao, J. Pyrolytic lignin removal for the valorization of biomass pyrolysis crude bio-oil by catalytic transformation. J. Chem. Technol. Biotechnol. 2010, 85, 132-144.

Hu, Jun, Dekui Shen, Rui Xiao, Shiliang Wu, and Huiyan Zhang. "Free-radical Analysis on Thermochemical Transformation of Lignin to Phenolic Compounds." Energy Fuels 27(2013): 285-293.

J. Meng, J. Park, D. Tilotta, S. Park, The effect of torrefaction on the chemistry of fast-pyrolysis bio-oil, Bioresour. Technol. 111 (2012) 439-446.

Kibet, J., L. Khachatryan, and B. Dellinger. "Molecular Products and Radicals from Pyrolysis of Lignin." Environ. Sci. Technol. 46(2012): 12994-13001.

Kringstad, K., E.B. Cowling, and S.Y. Lin. "The Free Radical Content in Wood and Lingins." Acta Chem. Scand. 23(1969): 3257-3275.

Maskos, Z., L. Khachatryan, R. Cueto, W.A. Pryor, and B. Dellinger. "Radicals from the Pyrolysis of Tobacco." Energy Fuels 19(2005): 791-799.

Melkior, T., S. Jacob, G. Gerbaud, S. Hediger, L.L. Pape, L. Bonnefois, and M. Bardet. "NMR Analysis of the Transformation of Wood Constituents by Torrefaction." Fuel 92(2012): 271-280.

Nsimba, R.Y., N. West, and A.A. Boateng. "Structure and Radical Scavenging Activity Relationships of Pyrolytic Lignins." J. Agric. Food Chem. 60(2012): 12525-12530.

Oasmaa, A., E. Kuoppala, and D.C. Elliott. "Development of the Basis for an Analytical Protocol for Feeds and Products of Bio-oil Hydrotreatment." Energy Fuels 26(2012): 2454-2460.

Ranby, B., K. Kringstad, E.B. Cowling, and S.Y. Lin. "The Free Radical Content in Wood and Lignin." Acta Chem. Scand. 23(1969): 3257-3275.

Rex, R.W.. "Electron Paramagnetic Resonance Studies of Stable Free Radicals in Lignins and Humic Acids." Nature 188(1960): 1185-1186.

Scholze, B., C. Hanser, and D. Meier. "Characterization of the Water-insoluble Fraction from Fast Pyrolysis Liquids (pyrolytic Lignin) Part II. GPC, Carbonyl Goups, and C-13-NMR." J. Anal. Appl. Pyrolysis 58-59(2001): 387-400.

Shimada, K., Hosoya, S., Ikeda, T. 1997. Condensation Reactions of Softwood and Hardwood Lignin Model Compounds Under Organic Acid Cooking Conditions. Journal of Wood Chemistry and Technology, 17(1-2), 57-72.

Smirnova, T.I., A.I. Smirnova, R.B. Clarkson, and R.L. Belford. "Half-field EPR Transitions in Synthetic Carbohydrate Chars." Solid State Commun. 91(1994): 319-323.

Steelink, C. (1966). Stable free radicals in lignin and lignin oxidation products. In Lignin structure and reactions (pp. 51-64). Washington: Advances In Chemistry.

Tian, L., C.P. Koshland, J. Yano, V.K. Yachandra, I.T.S. Yu, S.C. Lee, and D. Lacus. "Carbon-Centered Free Radicals in Particulate Matter Emissions from Wood and Coal Combustion." Energy Fuels 23(2009): 2523-2526.

Watanabe, T., H. Kawamoto, and S. Saka. "Radical Chain Reactions in Pyrolytic Cleavage of the Ether Linkages of Lignin Model Dimers and a Trimer." Holzforschung 63(2009): 424-430

Wildschut, J.; Mahfud, F.; Venderbosch, R.; Heeres, H. Hydrotreatment of fast pyrolysis oil using heterogeneous noble metal catalysts. Ind. Eng. Chem. Res. 2009, 48, 10324-10334.

Zhang, X., Li, J., Yang, W., Blasiak, W., 2011. Formation mechanism of levoglucosan and formaldehyde during cellulose pyrolysis. Energy Fuels 25, 3739-3746.

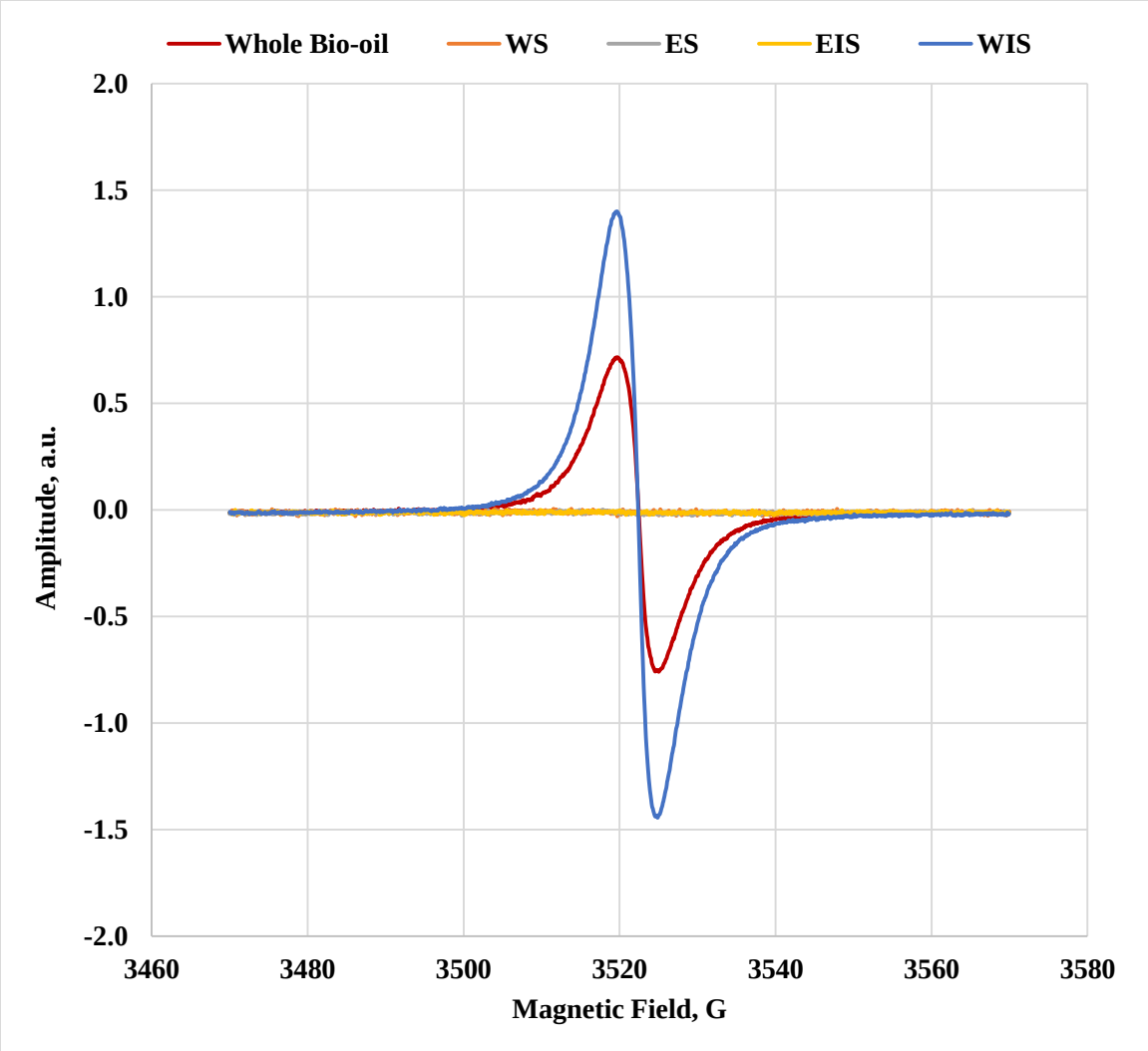

Figure 6.1 EPR spectra of whole bio-oil and its sub-fractions. EPR signals for bio-oil WS, ES and EIS fractions are overlapped on the x-axis. The WIS fraction was dissolved in methanol (30 wt. %). The peak to peak line width for whole bio-oil and bio-oil WIS fraction were 5.33 G and 5.15 G respectively; the g-value of EPR signals for whole bio-oil and bio-oil WIS fraction were same at 2.0019.

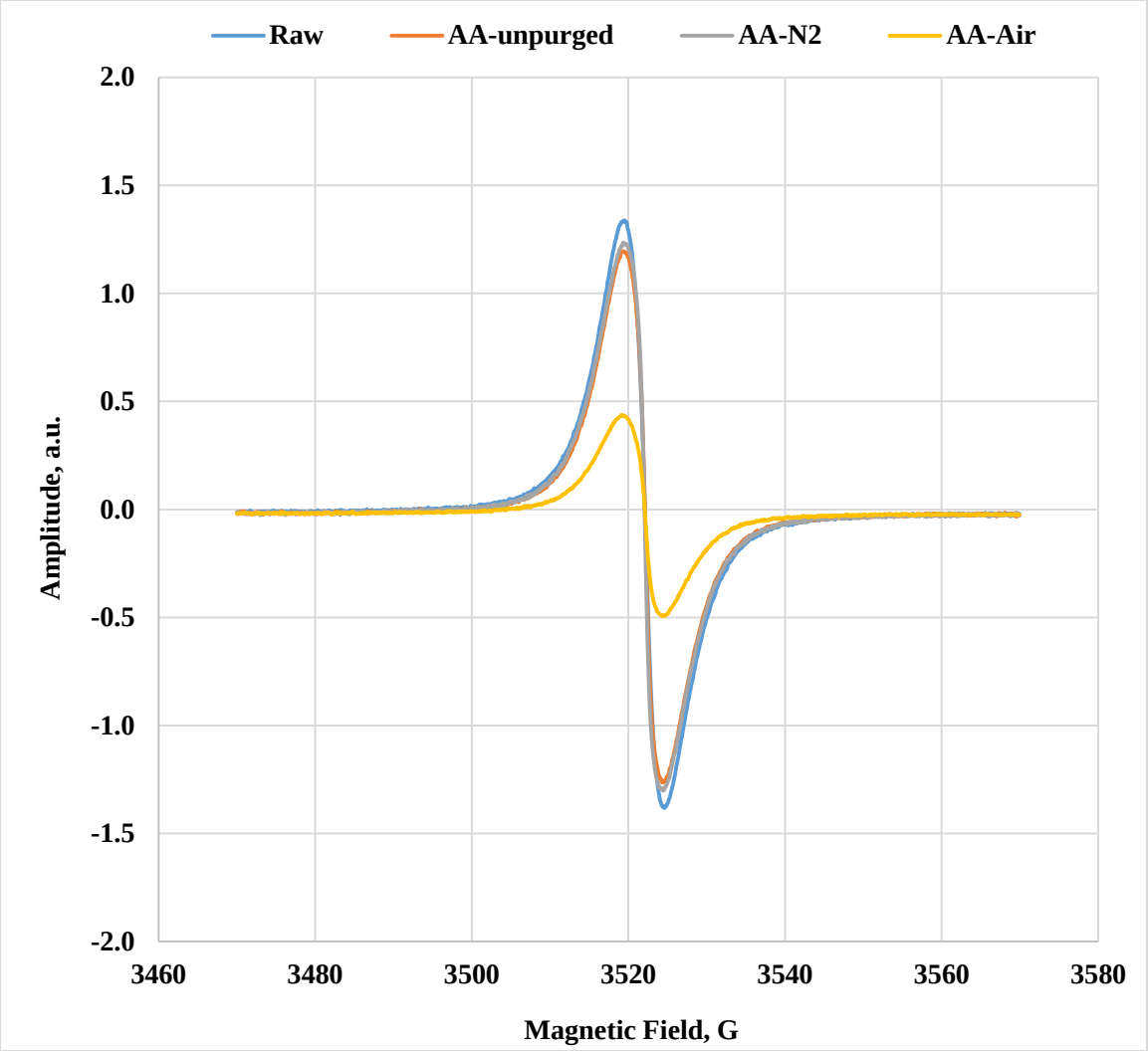

Figure 6.2 EPR spectra of accelerated aged bio-oils. Raw stands for fresh bio-oil; AA-unpurged stands for aged bio-oil without pre-purging; AA-N_2 stands for aged bio-oil with nitrogen pre-purging; AA-Air stands for aged bio-oil with air pre-purging. The peak to peak line width of EPR signals for Raw, AA-unpurged, AA-N_2 and AA-Air were 5.12 G, 5.18 G, 5.01 G and 5.22 G respectively; the g-values for Raw, AA-unpurged, AA-N_2 and AA-Air were same at 2.0019.

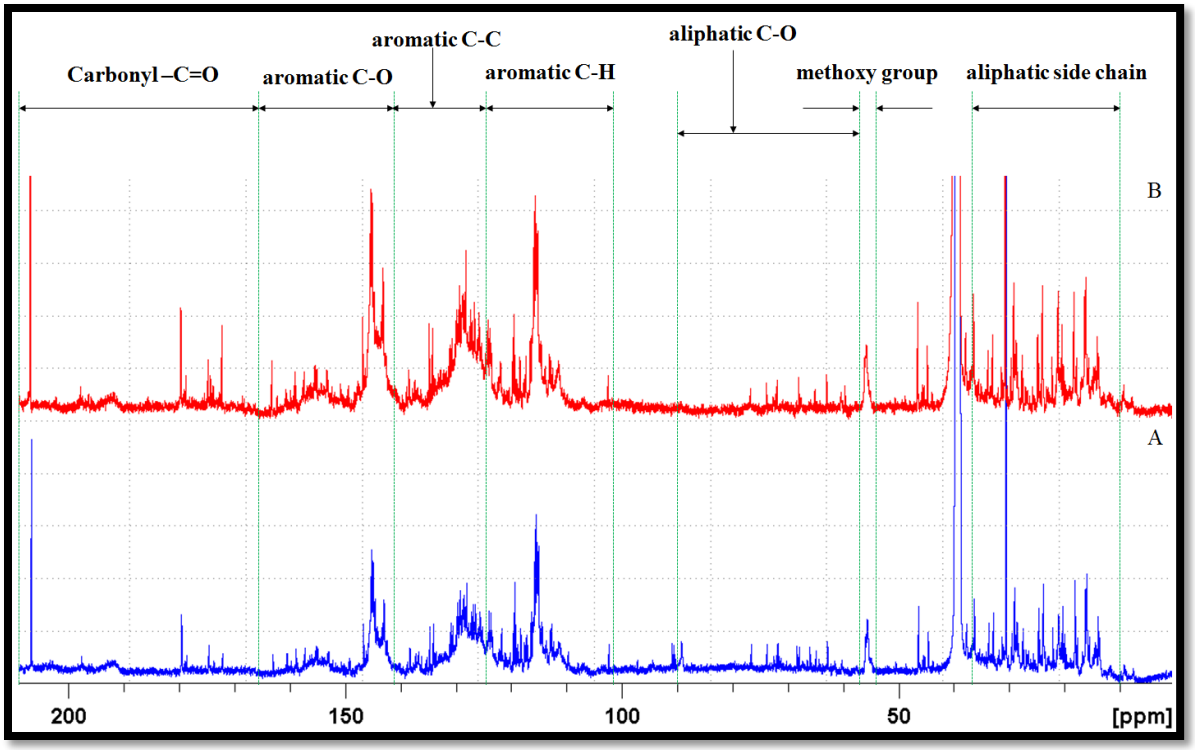

Figure 6.3 ^{13}C NMR characterization of fresh and accelerated aged lignin. A. raw pyrolytic lignin; B. accelerated aged pyrolytic lignin.

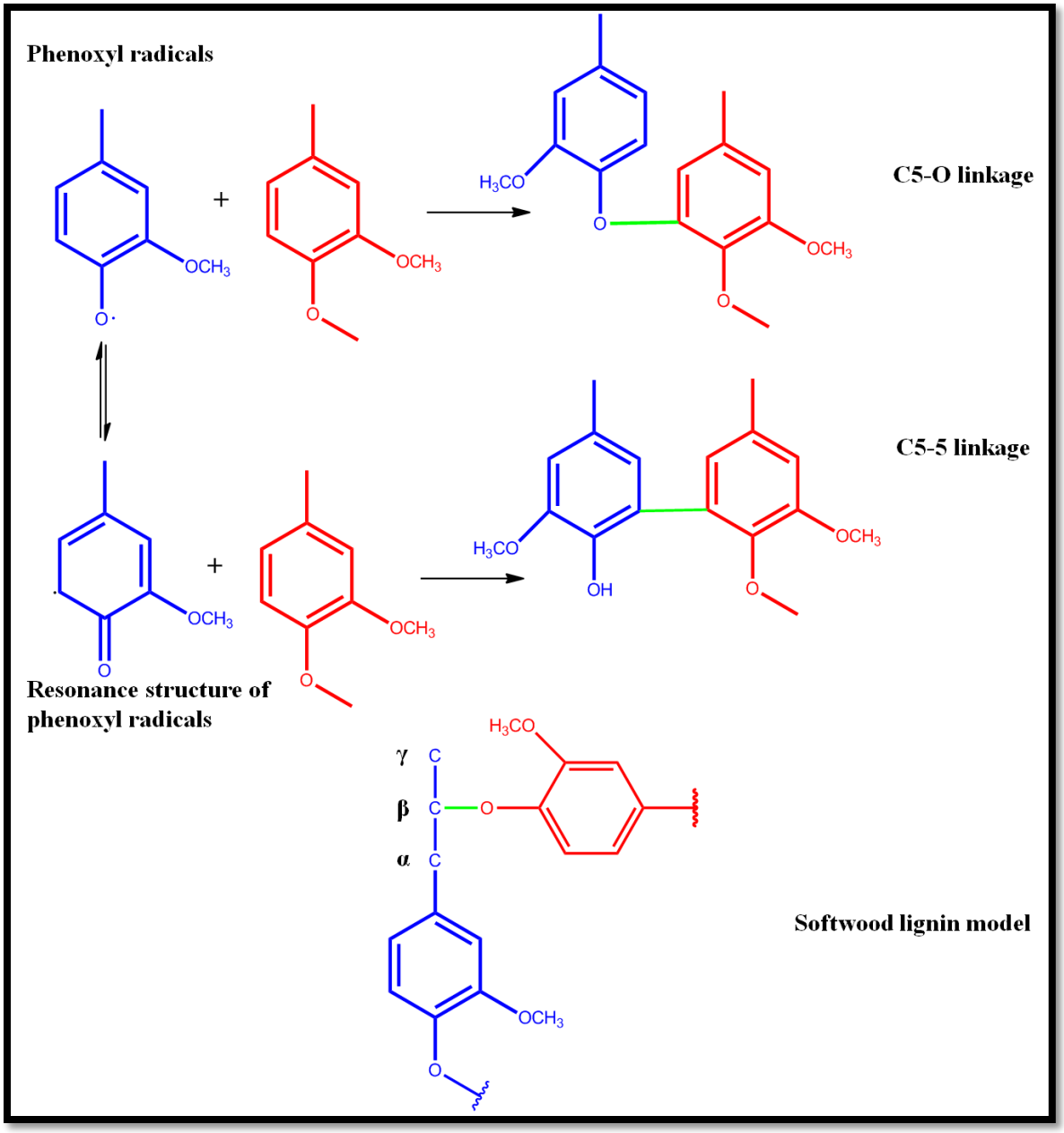

Figure 6.4 Proposed mechanism of pyrolytic lignin free radical condensation.

Table 6.1 Water content and average molecular weight of accelerated aged bio-oil.

	Raw	**AA-unpurged**	**AA-N_2**	**AA-Air**
Water content, %	19.8	23.3	16.4	14.5
Mw - RI, g/mol	352	705	707	711
Mw - UV, g/mol	357	831	841	836

Table 6.2 ^{13}C NMR Characterization of accelerated aged pyrolytic lignin (PL).

	PL-Raw	PL-AA
210-166 ppm, carbonyl	3.7	5.8
166-142 ppm, aromatic C-O	15.1	20.4
142-125 ppm, aromatic C-C	22.6	25.0
125-102 ppm, aromatic C-H	25	22.4
90-58 ppm, aliphatic C-O	6.6	1.6
58-54 ppm, methoxyl/hydroxyl	2.4	2.1
37-10 ppm, aliphatic	24.5	23.1

Table 6.3 Average molecular weight of accelerated aged pyrolytic lignin (PL) with addition of radical scavengers and methanol.

	Mw, g/mole	Aging index[a], %	Mw, g/mole	Aging index[a], %
PL-Raw	455			
PL-AA[b]	688	51.2		
PL-Raw-MeOH	428			
PL-AA-MeOH[c]	516	20.6		
	Acetic acid		**Formic acid**	
PL-AA-Acid-control[d]	781	71.6	2302	405.9
PL-AA-Acid-Eugenol	717	57.6	1630	258.2
PL-AA-Acid-Isoeugenol	779	71.2	1577	246.6
PL-AA-Acid-Guaiacol	715	57.1	1786	292.5
PL-AA-Acid-Vc[e]	722	58.7	1578	246.8
PL-AA-Acid-DTBP[f]	810	78.0	1532	236.7
PL-AA-Acid-BHT[g]	792	74.1	1592	249.9

a. Aging index was calculated according to $(Mw_{aged}-Mw_{initial})/Mw_{initial}*100\%$

b. Aged pyrolytic lignin without addition acid, radical scavenger and methanol

c. Aged pyrolytic lignin with addition of methanol but without addition of radical scavenger and acid

d. Aged pyrolytic lignin with addition of carboxylic acid but without radical scavenger

e. Vc – vitamin c, ascorbic acid

f. DTBP – 2,6-Di-tert-butylphenol

g. BHT - Butylated hydroxytoluene

CHAPTER 7

Suggested Future Research

The current investigation studied the effect of torrefaction on bio-oil physicochemical property and stability. In addition, the bio-oil polymerization mechanisms are proposed to be acid-catalyzed condensation of bio-oil components and free radical condensation of pyrolytic lignin. To further understand torrefaction potential in bio-fuel and bio-chemical production, future research may focus on (1) hydrotreating performance of bio-oil made from torrefied wood, (2) utilization of torrefaction bio-oil as platform chemicals, especially in resin production and (3) bio-oil polymerization mechanism under high-temperature and high-pressure upgrading conditions.

Torrefaction effect on bio-oil hydrotreating performance

Although bio-oil made from torrefied wood featured reduced oxygen content and other improved physicochemical properties, its overall fuel property is still very different from petroleum based oil. 20% more oxygen needs to be removed from bio-oil using hydrotreating technology. It has recently been reported that bio-oil made from torrefied wood could reduce zeolite catalyst coke formation [Hilten et al., 2012], however hydrotreating with noble metal catalyst on torrefaction bio-oil has not been reported. It is expected with low-oxygen-content, hydrogen consumption could be significantly saved in the bio-oil upgrading process. The stability of the bio-oil could potentially be improved with less coke generated on the catalyst surface and the catalyst activity may also be improved accordingly. To verify

these potential benefits, different catalysts need to be screened; detailed mass balance, product distribution and property on hydrotreating of bio-oil made from torrefied wood needs to be investigated. In addition, utilization of torrefaction volatiles using gas reforming technology is desired to make a fully integrated torrefaction-pyrolysis process. After accumulating all these understandings, a detailed economic model on integrated torrefaction-pyrolysis-hydrotreating process can be built to determine its feasibility as a successful industry production.

Utilizing bio-oil as platform chemicals

Bio-oil is often projected as an intermediate to produce transportation fuel, however, it also has great potential to be used as bio-based chemicals. Bio-oil contains several groups of chemical compounds, including, acids, aldehydes, ketones, furans, pyrans, sugars and phenolics. These bio-oil components can be fractioned or further converted into different value-added chemicals. For example, sugar fraction in bio-oil can be fermented into bio-ethanol [Bennett et al, 2009]. For torrefaction based bio-oil, its phenolic compounds can account for 50 wt. % of the overall bio-oil composition suggesting a great potential for its application in phenolic based resin production. As reviewed by Effendi [Effendi et al., 2007], considerable amount of work has been done on producing renewable phenolic resin by thermochemical conversion of biomass. The bio-oil lignin fraction is of the great interest to replace the phenol for PF resin production. However, one challenge of using bio-oil for PF resin production is that its non-phenolic water-soluble-fraction inhibit the reactivity of pyrolytic lignin with formaldehyde. Fractionation of the bio-oil, rejecting unfavorable

reaction participants could increase the substitution. Methyl isobutyl ketone has been found one of the most efficient organic solvent to extracting phenolics from bio-oil [Žilnik and Jazbinšek, 2012]; however the production cost and the complexity of the overall process increased significantly if organic extraction is involved. Bio-oil made from torrefied wood, on the contrary, has significantly reduced water soluble fraction but concentrated phenolics which may be a better candidate for economic renewable resin production than raw bio-oil.

Aging mechanism study under high temperature hydrotreating conditions

The current research proposed acid-catalyzed condensation and radical condensation mechanism for bio-oil aging reactions and investigated these reaction mechanism with accelerated aging of bio-oil fractions and model compounds. In order to maintain a uniform oil phase for characterization of the whole bio-oil property, low temperature heating at 80 °C are typically used in this study. However, when bio-oil is processed in a hydrotreating reactor, heating temperature above 250 °C are often applied. The polymerization of bio-oil compounds are considered to be more severe as large amount of coke is formed in the reactor and the surface of the catalyst. On the other hand, at low heating temperature, radical condensation mechanism of pyrolytic lignin does not show pronounced effect on bio-oil aging severity. However, at high hydrotreating temperature, these stable radicals may be reactivated and start to play an important role on bio-oil aging reactions, especially in the vapor phase. Therefore, further research on bio-oil aging mechanism study could focus on aging reactions under upgrading temperature and pressure.

References

Bennett, N.M., Helle, S.S., Duff, S.J.B. 2009. Extraction and hydrolysis of levoglucosan from pyrolysis oil. Bioresource Technology, 100(23), 6059-6063.

Effendi, A., Gerhauser, H., Bridgwater, A.V. 2008. Production of renewable phenolic resins by thermochemical conversion of biomass: A review. Renewable and Sustainable Energy Reviews, 12(8), 2092-2116.

Fele Žilnik, L., Jazbinšek, A. 2012. Recovery of renewable phenolic fraction from pyrolysis oil. Separation and Purification Technology, 86(0), 157-170.

Hilten, R.N., Speir, R.A., Kastner, J.R., Mani, S., Das, K.C. 2012. Effect of Torrefaction on Bio-oil Upgrading over HZSM-5. Part 2: Byproduct Formation and Catalyst Properties and Function. Energy & Fuels, 27(2), 844-856.